



## Durham E-Theses

---

### *Photoconducting cdse powder for flat panel displays*

Fellows, Andrew T.

#### **How to cite:**

---

Fellows, Andrew T. (1984) *Photoconducting cdse powder for flat panel displays*, Durham theses, Durham University. Available at Durham E-Theses Online: <http://etheses.dur.ac.uk/7187/>

#### **Use policy**

---

The full-text may be used and/or reproduced, and given to third parties in any format or medium, without prior permission or charge, for personal research or study, educational, or not-for-profit purposes provided that:

- a full bibliographic reference is made to the original source
- a [link](#) is made to the metadata record in Durham E-Theses
- the full-text is not changed in any way

The full-text must not be sold in any format or medium without the formal permission of the copyright holders.

Please consult the [full Durham E-Theses policy](#) for further details.

Photoconducting CdSe Powder for Flat Panel Displays

by

Andrew T. Fellows, B.Sc.

A thesis submitted in accordance  
with the regulations for the  
degree of Doctor of Philosophy  
in the University of Durham.

17th June 1984

---

The copyright of this thesis rests with the author.  
No quotation from it should be published without  
his prior written consent and information derived  
from it should be acknowledged.

---



-1. MAY 1985

Thesis  
1984 / FEB

## ABSTRACT

The initial aim of this work was the preparation of sensitized photoconductor layers for use in conjunction with d.c. electroluminescent panels to develop an optically triggered bistable system for sustaining pixel states during the frame time of dynamically addressed flat panel displays. More than 200 CdSe powder samples and devices were prepared in attempts to achieve the required response speed of approximately 1 millisecond and photocurrent density of at least  $10\text{mA cm}^{-2}$  under expected operating conditions. Powder samples were sensitized by various dopant incorporation and heat treatment processes. Copper and halogen ions were introduced in the form of dilute solutions. Correlations between preparation conditions and photoelectronic behaviour were sought, additional information being obtained from various physical and chemical analytical techniques. Devices were prepared from sensitized powder samples by compression, sintering or mixing with a nitrocellulose binder. A screen printing process was employed to deposit powder-binder layers 40-70 microns in thickness.

Although an optically triggered bistable element was not experimentally demonstrated, sensitized powder characteristics were successively improved to within an order of magnitude of those required. Response times of 2 - 10 milliseconds were recorded, and photo-response in a sandwich type powder-binder device was finally achieved with photocurrent density of approximately  $100\text{mA cm}^{-2}$ . Simple power law relationships between conductivity and applied voltage, pressure and photoexcitation intensity were experimentally established. Prolonged ball milling of CdSe powder was found to cause a wurtzite to sphalerite phase transition which was reversible by firing in air for 2 hours at  $500^\circ\text{C}$ . The estimated sphalerite lattice parameter was  $6.051\text{\AA}$ . Long term variations in sample conductivities and photosensitivities were attributed primarily to oxygen adsorption in the presence of water vapour during storage. Photoelectronic characteristics indicative of both oxygen photoadsorption and photodesorption were observed, and explained in terms of dopant levels. Photoconductive processes in sensitized CdSe powder were shown to be dictated principally by surface chemistry and inter particle contacts.

## ACKNOWLEDGEMENTS

I would like to thank my supervisor, Dr. Woods, for his guidance and encouragement during the course of this research. I am also indebted to Dr. Brinkman, Dr. Russell and many other friends and colleagues for their helpful contributions and discussions. I also want to express my gratitude to Bill Mounsey, Peter Richardson, Frank Spence and all the other technical staff for assistance with equipment and car repairs! I am particularly grateful to Margaret Leese for typing this thesis, and to Norman Thompson for preparing the diagrams. Finally I would like to thank my parents and all my friends who have supported and encouraged me during the difficult months of writing up while in full time employment.

## CONTENTS

## Pages

i	Abstract
ii	Acknowledgements
5-18	Chapter 1. Introduction
5-7	1.1 Introduction
7-9	1.2 Flat Panel Displays
9-15	1.3 Use of Photoconductors in Active Displays
16-18	References
19-44	Chapter 2. Preliminary Theory
19-21	2.1 Introduction
21-25	2.2 Phenomenological Photoconductivity Theory
25-27	2.3 Sensitization by Impurity Incorporation
27-29	2.4 Speed of Response
29-31	2.5 Spectral Distribution of Photosensitivity
31-33	2.6 Electrode Requirements
33-34	2.7 Limits to Photoconductor Performance
34-38	2.8 Photoconductivity in Powders
39-44	References
45-62	Chapter 3. Powder Preparation
45-46	3.1 Introduction
46-47	3.2 Laboratory Manufacture of CdSe Powder
47-55	3.3 Powder Sensitization
55-60	3.4 Individual Sample Preparation
61-62	References

63-75	Chapter 4.	Device Fabrication
63-64	4.1	Introduction
64-66	4.2	Formation of Compressed Pellets
66-67	4.3	Formation of Sintered Layers
67-69	4.4	Formation of Prototype Powder - Binder Layers
69-72	4.5	Formation of Screen Printed Powder-Binder Layers
73-75		References
76-90	Chapter 5.	Experimental Work
76-77	5.1	Introduction
77-78	5.2	Investigation of Topography
78-80	5.3	Crystallographic Analysis
80-81	5.4	Chemical Analysis
81-86	5.5	Powder Test Cell Construction
86-89	5.6	Electrical and Optical Apparatus
90		References
91-108	Chapter 6.	Result of Physical Analysis
91	6.1	Introduction
91-95	6.2	Results of Topographic Analysis
95-100	6.3	Results of Crystallographic Analysis
100-104	6.4	Results of Chemical Analysis
104-105	6.5	Miscellaneous Physical Observations
106-108		References

109-146	Chapter 7.	Results of Electronic Measurements
109-111	7.1	Introduction
111-120	7.2	Powder Samples: Statistical Observations
121-130	7.3	Powder Samples: Individual Results
130-136	7.4	Performance of Devices
136-143	7.5	Discussion
144-147		References
147-i53	Chapter 8.	Conclusion

## CHAPTER 1: INTRODUCTION

### 1.1 INTRODUCTION

This investigation into the photoconducting properties of CdSe powder was initially prompted by a requirement of International Computers Ltd to design and commercially manufacture d.c. electroluminescent dynamic flat panel displays. A potentially simple and inexpensive method of achieving inherent picture element (pixel) memory capability by the use of a photoconductive layer adjacent to the electroluminescent material was proposed. It was thus intended to create a matrix of optically triggered bistables.

CdSe powder was selected as a suitable material for investigation for several reasons. As with other II-VI compounds, sensitized CdSe is characterized by a high photosensitivity to visible light, peak sensitivity occurring in the visible red to near infra-red region. More importantly, it has been shown possible to prepare photosensitive CdSe with a high speed of response (less than 1 ms). Most of the published literature describing studies of photoconductivity in CdSe, however, deals with samples in the form of single crystals and, to a lesser extent, evaporated layers. Investigation of the electrical properties of a powdered semiconductor is complicated by the large surface area to volume ratio, inter-particle contact phenomena and the problem of making suitable electrodes.



The experimental work described in this report consists of attempts to establish a reproducible procedure for the preparation of sensitized CdSe powder to produce devices suitable for use in conjunction with electroluminescent displays. High purity CdSe powder from several sources was sensitized by the incorporation of controlled impurities. Copper ions were used as activators to enhance photosensitivity and speed of response, while halogen (chlorine or iodine) ions were employed as co-activators to increase overall conductivity. These were introduced in the form of dilute solutions of various compounds; once the solvents had evaporated, samples were fired to promote diffusion of the dopants into the powder particles. Measurements were made on powder samples placed between indium coated copper electrodes and on a variety of devices produced by compression, sintering or mixing the sensitized powder with a nitrocellulose binder. The total number of such samples and devices produced exceeded 200. Electronic measurements were therefore necessarily limited in scope to those operational parameters of direct relevance to the proposed application. These included conductivity as a function of applied voltage, photoexcitation, or compression, transient response to change of photoexcitation, and longer term changes of conductivity levels due to photochemical processes. Complementary to these investigations of photoelectronic behaviour were a topographical analysis of powder particles using scanning electron microscopy, crystallographic analysis using X-ray powder photography and diffractometry and RHEED analysis, and chemical analysis using a quadrupole mass spectrometer.

The problem of interpreting data obtained for so many samples and correlating this with preparation which involved numerous successive processes was tackled by breaking down results on a statistical basis. In this way trends derived from comparisons between groups of samples emerged. Individual samples, however, sometimes exhibited anomalous behaviour increasing the scatter of results. It was concluded that the treatment of samples after preparation, and the timing of measurements, could profoundly affect observed behaviour.

## 1.2 FLAT PANEL DISPLAYS

Since the mid 1950's research into various types of "solid state" flat panel display has been steadily increasing. Concurrently there have been continued refinements and innovations in cathode ray tube (CRT) technology (1). The dominance of the CRT for displaying continuously moving pictorial images (e.g. domestic television) remains unchallenged; as yet no other display technology can combine the speed of response, polychromatic output and grey scale capabilities of the CRT. These features combined with the economic advantages of mass production seem certain to ensure a long future for CRT technology. Such devices, however, suffer the disadvantages of being bulky, heavy, fragile and having relatively high power consumption. For these reasons flat panel display technology is beginning to make an impact where the generation of less complex images such as alphanumeric or vectorgraphic displays is required. As products such as microcomputers become increasingly compact the need for a

comparably compact output display system becomes more obvious. For several years now flat panel displays have been produced which can successfully compete with the CRT for this type of application.

Published reviews of this area of technology (2,3) describe the development of many different types of display device. These can be broadly divided into active (i.e. light-emitting) displays, and passive displays which produce contrast ratios visible in ambient light. Included in the former category are electroluminescent devices (4-8), plasma discharge panels and cathodo-luminescent devices (9). Passive displays include liquid crystal devices (10-12) and electrochromics (13). Pixel addressing presents problems in both categories of display, and active displays are faced with the additional hurdle of achieving adequate luminous efficiency.

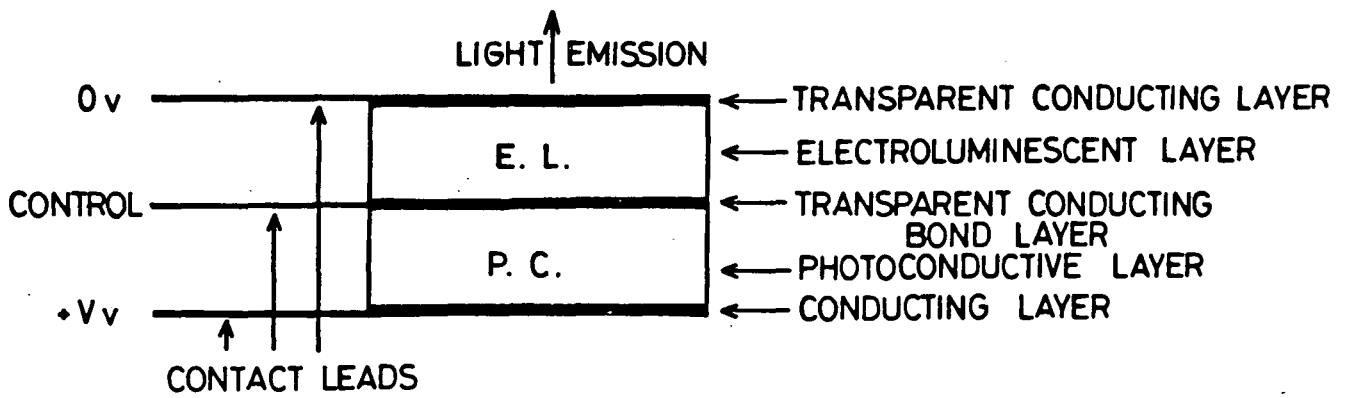
DC electroluminescent displays have been successfully produced for several years. However, the addressing circuitry required for dynamic displays has been complex and expensive, typically contributing more to the cost of the complete device than the electroluminescent panel itself. The problem of addressing in a dynamic display is twofold. Each pixel must be uniquely identified and controlled in turn during the frame time. This frame time is the equivalent of a single raster scan in a CRT, and if it entails addressing  $n$  pixels in  $t$  seconds it is immediately apparent that the longest time that the state of a single pixel can be directly controlled is  $t/n$  seconds. Since a

large value of  $n$  is required to achieve acceptable image resolution, it is essential for each pixel to possess some form of inherent memory capability enabling the directly controlled state to be sustained from one frame to the next.

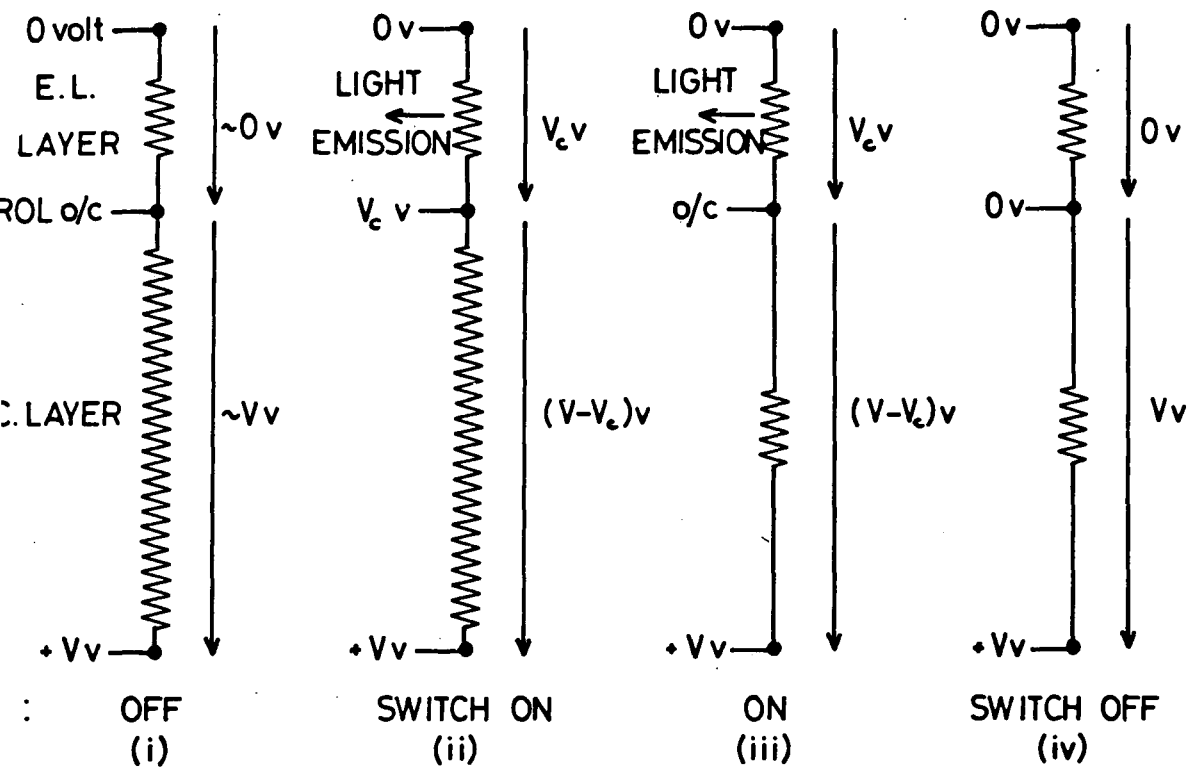
A widely adopted method of storing control information in this way is the use of a network of transistors and/or capacitors associated with each pixel. A constituent layer in displays of this kind is a large area matrix of thin film devices. The current cost of a sheet of thin film transistors with good yield is around \$10 per square inch. These films are even more expensive to produce in very large areas and become prone to element and line defects resulting in visible flaws in the display output.

### 1.3 USE OF PHOTOCONDUCTORS IN ACTIVE DISPLAYS

A proposed alternative system for maintaining a light-emitting pixel state between successive address instructions by the use of a photoconductor will now be discussed in terms of a dynamic d.c. electroluminescent display panel. Fig. 1.1(a) shows a simplified representation of a single pixel having inherent memory capability. Such an arrangement can be considered as an optically triggered bistable. The hypothetical operation of such a pixel can be understood with reference to Fig. 1.1(b). Assuming that the pixel is initially in the "off" state, the electroluminescent (E.L.) layer emits no light and



(a)



(b)

FIG. 1.1 a) SCHEMATIC DIAGRAM OF SIMPLE OPTICAL LOGIC PIXEL  
 b) REPRESENTATION OF BISTABLE MECHANISM OF SIMPLE OPTICAL LOGIC PIXEL

thus the photoconductive (P.C.) layer has an extremely high resistance (much higher than that of the E.L. layer). The proportion of the constant drive bias  $V$  (which is applied across every pixel) across the E.L. layer is below the threshold required for light output so the pixel will remain indefinitely in the "off" state under such conditions.

If a control pulse  $V_c$  ( $0 < V_c < V$ ) is applied to the control electrode for sufficient time to allow the E.L. layer to start emitting light, the resistance of the P.C. layer will be reduced by several orders of magnitude. The pixel has been switched into the 'on' state and light output will be maintained by the constant drive voltage, enough of which now appears across the E.L. layer. This stable state may be reversed by applying  $0v$  to the control electrode (i.e. short circuit across the E.L. layer) which interrupts light output causing the photoconductor to return to its high resistance state. This type of pixel may be considered as a variable potential divider comprising one approximately constant resistance (E.L. layer) and a variable resistance (P.C. layer) in series. Stable states are defined by the constant drive voltage and P.C. layer resistance.

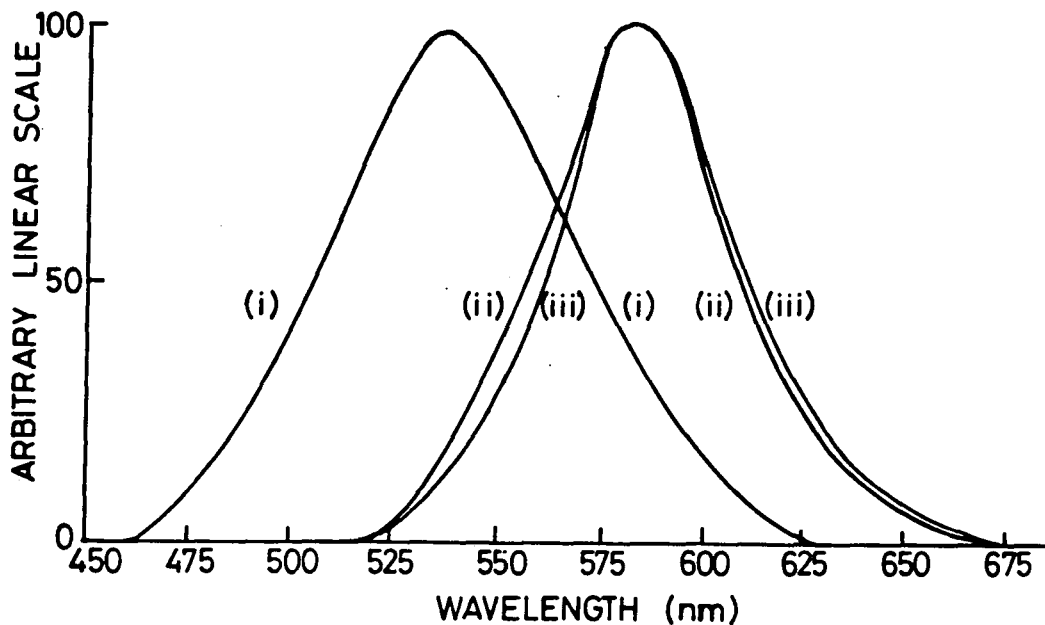
This model simply illustrates the principle of optical bistable operation; a practical device would certainly be more complex. For example, a separate addressing light source would be required since light emission from two opposite surfaces is not characteristic of D.C.E.L. panels. Thus the P.C. layer might be sandwiched between two E.L. layers. A more complex

arrangement using two E.L. layers and a photoconductor addressed by a 1mW He - Ne laser has been demonstrated in the form of a 400 element matrix (14). The photoconductor used in this device was a CdS:Cu,Cl thin film. Other applications of interaction between electroluminescent and photoconductive layers include infra-red and X-ray image converters (15,16), both of which used doped CdSe powder as the photoconducting material. These devices gave acceptable brightness and resolution but suffered from slow response of between 10ms and several seconds.

The characteristics of three electroluminescent panels were experimentally evaluated. These were an a.c. panel produced commercially by Saunders-Roe for use in aircraft, a d.c. driven Mn and CuS doped ZnS panel constructed by Alan Thomas in this Department, and a similar device obtained from RSRE (Malvern). Fig. 1.2 shows measured spectral distributions of light emission for each panel and also lists their operating characteristics. It should be mentioned that the radiant emittance for each device was deduced from the photometric brightness which was estimated using an S.E.I. photometer (18,19).

These measured values (in particular those for the R.S.R.E. d.c. panel) will now be considered in conjunction with the proposed photoconductor application described earlier in order to outline performance criteria for the photoconductor material as follows:

i) The physical form of the photoconductor should be appropriate for mass fabrication of large area pixel arrays. The advantages



a) SPECTRAL DISTRIBUTION OF LIGHT EMISSION FROM THREE ELECTROLUMINESCENT PANELS (i) a.c. ( SAUNDERS-ROE )  
(ii) d.c. ( A.THOMAS )  
(iii) d.c. ( R.S.RE. , MALVERN )  
PLOTS NORMALISED TO ALLOW FOR NON-LINEAR PHOTOMULTIPLIER SENSITIVITY.

	UNITS	D.C.(ii)	D.C.(iii)	A.C.(i)
AREA	cm <sup>2</sup>	0.2	0.2	50
DRIVE VOLTAGE	V	60 d.c.	60 d.c.	240 a.c.
CURRENT	mA	3.5	0.85	1.76rms
RESISTANCE	k.Ω	20	70	136
POWER CONSUMPTION	mW	210	51	422
POWER DENSITY	mW cm <sup>-2</sup>	1050	255	8.44
CURRENT DENSITY	mA cm <sup>-2</sup>	17.5	4.25	0.035rms
RADIANT EMITTANCE	μW cm <sup>-2</sup>	201.7	207.1	8.2
EMISSION BANDWIDTH	μm	0.51-0.67	0.51-0.67	0.46-0.63
PEAK EMISSION WAVELENGTH	μm	0.573	0.579	0.533
EFFICIENCY	x 10 <sup>-4</sup>	1.92	8.12	9.72

b) SUMMARY OF MEASURED ELECTROLUMINESCENT PANEL CHARACTERISTICS.

FIG. 1.2 ELECTROLUMINESCENT PANEL CHARACTERISTICS

of using a photoconducting layer instead of a thin-film transistor matrix to achieve inherent pixel memory would increase with the size of display, thus anticipated areas would be 10-100cm<sup>2</sup> upwards. Clearly this precludes the use of single crystal devices; a powder layer, probably mixed with a suitable binder, would be preferable to an evaporated or sputtered thin film since deposition of these becomes increasingly difficult over large areas.

ii) The spectral distributions of photoconductor layer response and E.L. layer emission should be compatible. Maximum photosensitivity in CdSe occurs in the 0.6 - 0.9 $\mu$ m wavelength region yet the peak emission wavelength of the RSRE d.c. panel is approximately 0.58 $\mu$ m. However, the E.L. layer used for addressing need not emit the same wavelength as the visible display E.L. layer and could be designed to have increased longer wavelength output to improve compatibility.

iii) The series resistance of the photoconductor layer in the pixel 'on' state (Fig.1.1) should be sufficiently low for an acceptable ( $\leq 100$ v) overall drive voltage (V) to be employed. Assuming E.L. panel operating characteristics similar to those of the RSRE d.c. panel ( $V_c=60$ v, current density  $\approx 5$ mAcm<sup>-2</sup>) and a photoconductor layer thickness of 50  $\mu$ m, the minimum acceptable photoconductor material conductivity under illumination may be estimated as  $6.25 \times 10^{-7} \Omega^{-1}\text{cm}^{-1}$ . In view of the non-linear I-V characteristics of many powder systems it should be noted that the applied field under these conditions is  $8 \times 10^3 \text{Vcm}^{-1}$ .

iv) The series resistance of the photoconductor layer in the pixel 'off' state should be sufficiently high to ensure negligible light output from the E.L. layer. The most successful empirical relation describing the increase in brightness  $B$  with voltage  $V$  of an E.L. cell containing ZnS is

$$B = B_0 \exp(-c/V^{\frac{1}{2}})$$

in which  $B_0$  and  $c$  are constants (Zalm (17)). Even allowing for the sub-linear dependence of photoconductivity on light intensity (e.g. Fig.7.12 shows that  $I_L \propto B^{0.4}$  approximately), a residual field of at least 10v across the E.L. layer is estimated to be acceptable. Therefore the maximum acceptable dark conductivity of the photoconductor material (based on the same numerical estimates used in iii)) is around  $2 \times 10^{-9} \Omega^{-1} \text{cm}^{-1}$  (with an applied field of approx.  $1.8 \times 10^4 \text{Vcm}^{-1}$ ). Thus the conductivity of the P.C. layer is required to be at least 2 orders of magnitude higher under photoexcitation than in darkness.

v) The speed of response of the photoconductor should be as fast as possible as this will determine the time required to address each pixel and hence the overall frame time. Assuming that the display will contain at least 1,000 pixels and that the longest acceptable frame time is around 1 second it is immediately apparent that the response time of the P.C. layer must be lms or less. It is worth noting in this context that the measured rise and decay times for the ZnS; MnCu d.c. EL panel (5) are both approximately 0.5ms, so greatly reduced P.C. layer response times below lms would be of little benefit even if feasible.

vi) Photoconductor performance should be reproducible and stable

over prolonged periods of time (>1000 hrs operating life) and over a range of working environment conditions e.g. 0-40°C ambient temperature.

Construction of a manually switched prototype bistable element was envisaged once a reproducible technique for preparing CdSe powder with required characteristics was achieved. This device is shown schematically in Fig.1.3. However, preparation of suitable powder was found to be so difficult that the emphasis of the research moved towards an investigation of the factors governing photoelectronic behaviour of CdSe powder and devices. It should be remembered, therefore, that although the principal objective of this work was to prepare a photoconducting layer and to use it in conjunction with an electroluminescent panel, this was not achieved. However, the improved understanding of photoconductor sensitization resulting from the analysis of measured electrical behaviour as a function of powder preparation conditions may yet enable this application to be successfully developed.

The numerous results obtained in the course of this work were analysed statistically to reveal general trends, and results for individual samples were also studied in more detail. From these investigations simple power law relationships between conductivity and applied voltage, pressure and photoexcitation intensity were derived both for powder samples and fabricated devices. Studies of the time dependence of current levels both in the dark and under illumination revealed the extensive effects of CdSe surface chemistry phenomena, especially oxygen sorption,

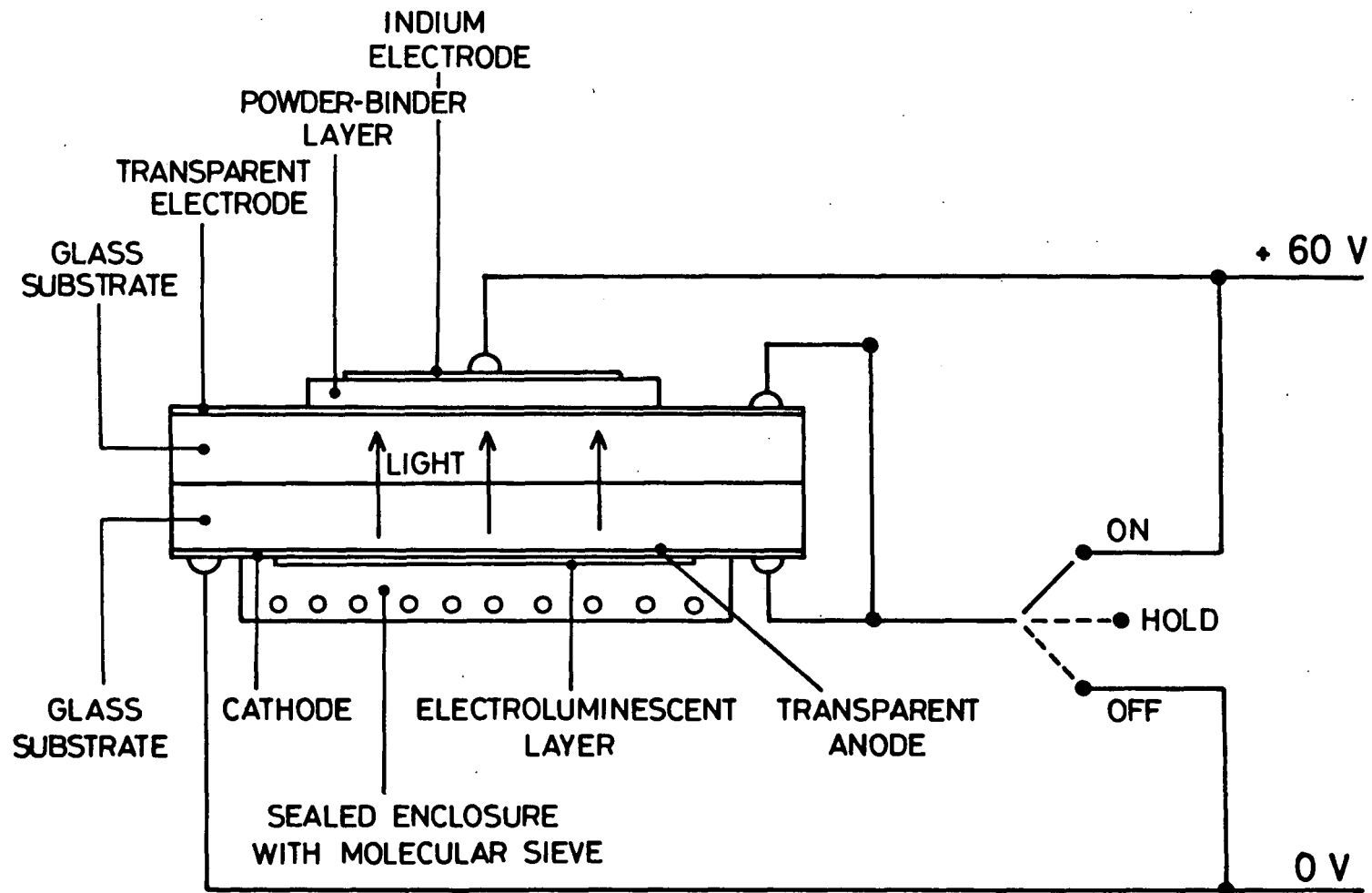


FIG. 1-3 SIMPLE PROTOTYPE BISTABLE ELEMENT (MANUALLY SWITCHED)

upon electronic behaviour.

Screen printing of sensitized powder binder mixture produced mechanically stable layers 40-70  $\mu\text{m}$  in thickness. By depositing these on transparent conducting glass substrates appreciable photoresponse in a sandwich type structure was finally achieved. It was concluded that dark conductivity of these layers needed to be reduced by several orders of magnitude, possibly by increasing the copper doping levels, in order to produce electronic characteristics suitable for use in flat panel displays. Powders having these required characteristics were produced before the screen printing technique was developed.

Crystallographic analysis indicated that a reversible transition from the normal wurtzite structure to a sphalerite modification occurred as a result of prolonged ball milling.

## CHAPTER 1: REFERENCES

- 1) ANON: "Laboratory Demonstrates the Feasibility of Flat Cathode-Ray Tube for TV Sets" Electronics, 68-70 (20th July 1978).
- 2) TANNAS L. and GOEDE W.F. "Flat Panel Displays: A Critique" IEEE Spectrum, 26-32 (July 1978)
- 3) VARIOUS: "Journées de Visualisation par Ecrans Plats" (Workshop on Flat Screen Displays). Vide les Couches Minces (France) 37, 214 (Nov.-Dec. 1982)
- 4) ROUSE R.L. "New Electroluminescent Panels for Displays" GEC Journal of Science and Technology 40, No. 4 (1973)
- 5) VECHT A. "DC Electroluminescence in Zinc Sulphide and Related Compounds "Journal of Luminescence 7, 213-27 (1973)
- 6) BRODY T.P. et al "Electroluminescent Display Panel" Proc. Conf. on Display Devices and Systems. New York City. (11 Oct. 1974)
- 7) FISCHER A.G. "White-Emitting A.C. Electroluminescent Powder Layer for Flat Panel Television "Electronics Letters 12, No.1, 30-2 (8 Jan 1976)
- 8) VECHT A. et al. "DC Electroluminescence in Alkaline Earth Sulphides" J. Lumin (Ne) 24-25, Pt2, 917-20 (Nov. 1981)

- 9) PENNEBAKER W. and O'HANLON J. "Low Energy Cathodoluminescence of ZnO: The Plasma Display" J.Appl. Phys. 45, No.3, 1315-22 (March 1974)
- 10) BRODY T.P. et al "A 6 x 6 inch, 20 Lines-per-inch Liquid Crystal Display Panel" IEEE Trans. Elec. Dev. 996-1001 (Nov. 1973)
- 11) LIPTON L.T. et al "A 2.5 Inch Diagonal, High Contrast, Dynamic Scattering Liquid Crystal Matrix Display with Video Drivers" SID 78 Digest 96-7 (1978)
- 12) FANG-CHEN LUO et al "Alphanumeric and Video Performance of a 6" x 6" 30 Lines-per-inch Thin Film Transistor Liquid Crystal Display Panel" SID 78 Digest, 94-5 (1978)
- 13) BENI G. "Recent Advances in Inorganic Electrochromics" Solid State Ionics (Ne) 3-4, 157-63 (Aug. 1981)
- 14) OLIVE G, LAKE R. and BEJAR J. "The Use of Photoconductive CdS:Cu,Cl Thin Films in a Laser-Addressed Electroluminescent Display Screen" Thin Solid Films 41, 151-60 (1977)
- 15) KOHASHI T. et al "A Solid-State Infrared Image Converter" IEEE Trans. Electron Dev. 19, No.1, 98-103 (Jan. 1972)
- 16) KOHASHI T. et al "DC-Controlled Solid-State X-ray Image Converter" IEEE Trans. Electron Dev. 19, No. 2, 234-8 (Feb.1972).

- 17) ZALM P. Philips Research Report 11, 353-417(1956)
- 18) WALSH J.W.T. "Photometry" 72-75 pub: Constable & Co.(1953).
- 19) WILSON J & HAWKES J.F.B. "Optoelectronics: An Introduction"  
30-32, 160-1, pub: Prentice-Hall (1983).

## CHAPTER 2 PRELIMINARY THEORY

2.1 INTRODUCTION

Many aspects of photoconductor performance are still not fully understood. Nonetheless several important characteristic relationships which quantify conductivity of a photoconductive material have been established. These will now be discussed.

Assuming that free holes are rapidly trapped, the conductivity ( $\sigma$ ) of a homogeneous, n-type semiconductor is given by:

$$\sigma = ne\mu_n \quad (2.1)$$

where  $n$  is the free majority carrier density,  $e$  is the electronic charge and  $\mu_n$  is the electron mobility. A change in conductivity produced by illumination of the material can be described by:

$$\Delta\sigma = \Delta ne\mu_n + ne\Delta\mu_n \quad (2.2)$$

The free majority carrier density is related to the photoexcitation rate  $f$  and the carrier lifetime  $\tau$  by:

$$n = f\tau \quad (2.3)$$

Rose (1) points out that this statement is a logical relationship rather than a physical law. It states that the population of a given category is proportional to the rate of influx into that category and the lifetime or residence time in that category. Application of this model cannot be continued once the electric field is high enough to allow free electrons to be multiplied by collision ionization. This, however, is not

a major problem since such behaviour only occurs near the critical field for breakdown and photoconductors are not normally operated under such conditions.

From 2.3 the change in the free majority carrier density can be written as:

$$n = \Delta f \tau + f \Delta \tau \quad (2.4)$$

Substitution of 2.3 and 2.4 in 2.2. gives the complete expression:

$$\Delta \sigma = e \mu_n \tau \Delta f + e \mu_n f \Delta \tau + e f \tau \Delta \mu_n \quad (2.5)$$

The significance of the three factors contributing to the photosensitive change in the conductivity has been concisely presented by Ray (2). The first term ( $e \mu_n \tau \Delta f$ ) relates the change in conductivity to the change in photoexcitation rate. The second term ( $e \mu_n f \Delta \tau$ ) suggests that carrier lifetime may change with excitation conditions. A positive value of  $\Delta \tau$  would account for the superlinear dependence of photocurrent on excitation intensity observed in some photoconductors, including CdS and CdSe (3). This will be discussed in more detail later. The third term ( $e f \tau \Delta \mu_n$ ) allows for mobility changes arising from an increase in the density of ionized impurity scattering centres (4), inhomogeneities in crystal potential or transitions from lower to higher mobility states.

The performance of a photoconductor is often quantified by the photoconductive gain factor  $G$  which is defined as:

$$G = \tau / T_R \quad (2.6)$$

where  $T_R$  is the majority carrier transit time between the

electrodes. This should not be confused with the sensitivity  $S$  of a photoconductor which is given by:

$$S = (\Delta i / V)L^2/P \quad (2.7)$$

where  $\Delta i$  is the photocurrent,  $V$  is the applied voltage,  $L$  is the electrode spacing and  $P$  is the absorbed radiant power.

Nonetheless, gain and sensitivity are related since

$$G = \tau / T_R = \tau / (L^2 / \mu_n V) = \tau \mu_n V / L^2 \quad (2.8)$$

$$\text{Therefore } G \propto S \cdot V / L^2 \quad (2.9)$$

The maximum value of  $G$  corresponds to the highest voltage that can be applied before carrier injection from the ohmic cathode dominates the conduction mechanism.

## 2.2 PHENOMENOLOGICAL PHOTOCONDUCTIVITY THEORY

The above characteristic relationships, useful though they are, give little indication of the actual mechanism by which photoconductivity occurs in an n-type semiconductor. The nature of carrier lifetimes and recombination processes will now be considered using a model first proposed by Rose in 1951 (5), and more fully described in his book "Concepts in Photoconductivity and Allied Problems" (6). The photoconductive properties of a material are treated in a collective and somewhat statistical way to obtain a semiquantitative description of various associated phenomena while retaining a direct concept of the physical nature of the processes involved.

Recombination of electrons and holes in a photoconductor

takes place predominantly at bound states within the forbidden gap which are associated with the presence of imperfections. Such imperfections could be caused by crystal defects or incorporated impurities. In CdS and CdSe it seems that the former play a major role in controlling the photoconductive properties (7) and in determining what effects are caused by impurity incorporation. High photosensitivities are not characteristic of intrinsic photoconductors. This is especially true of materials such as CdS and CdSe which have relatively large band gaps. Recombination in intrinsic photoconductors occurs very rapidly and carrier mobilities are low. Electron and hole lifetimes are comparable, each being typically about  $10^{-6}$ s for II-VI compounds (8). Robinson and Bube (9) have reported electron and hole lifetimes as low as  $10^{-9}$ s in single crystals of intrinsic CdSe.

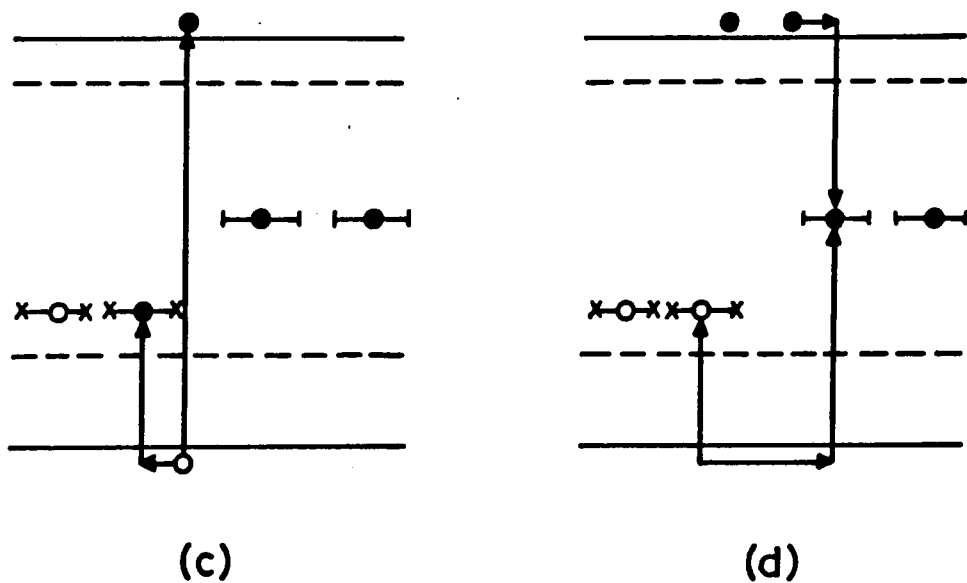
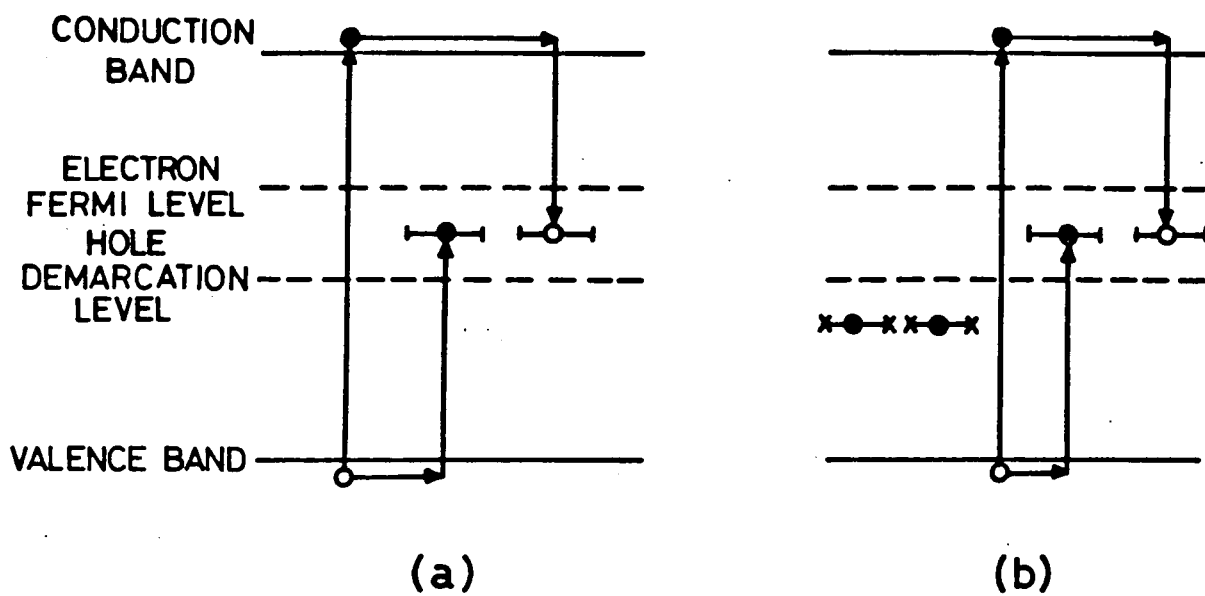
To prepare a sensitive photoconductor, therefore, a low density of those centres with a large majority carrier recombination cross section is required. The remaining centres should have as small a capture cross section as possible. In II-VI photoconductors the free hole formed by excitation of an electron across the band gap is quickly captured at an imperfection. Therefore the sensitizing centres must be of a type which, once they have captured a hole, have a small capture cross section for free electrons. Measurements of photoconductivity in ZnS and CdS by Bube (10) and others suggest that the values of the capture cross sections of such centres lie between  $10^{-20}$  and  $10^{-24}$  cm<sup>2</sup>. Such values are some five to nine orders of magnitude smaller than atomic dimensions,

indicating that the high photosensitivity of these materials is associated with the presence of these centres which are effectively surrounded by a potential barrier preventing electron capture.

Now that the importance of the nature, concentration and location of recombination centres has been emphasized, their mode of operation can be understood by referring to Fig.2.1 which shows an energy level representation of sensitizing centres in an n-type semiconductor.

In an insensitive intrinsic material (Fig.2.1(a)) recombination centres associated with crystal defects are present. These centres (henceforward referred to as Class I centres) are characterized by a large capture cross section for both electrons and holes, thereby causing a small majority carrier lifetime for electrons. Addition of sensitizing (Class II) centres as shown in (b) has no effect on the lifetime since, owing to their location relative to the hole demarcation level, their occupancy is determined by thermal equilibrium interchange with the valence band. However, when the situation is as shown in (c) the occupancy of the Class II centres is now determined by recombination kinetics. As a result a sensitizing effect arises in the following way.

Since the Class II centres have a very small capture cross section for electrons, holes captured by them have a longer lifetime there before recombination than have holes captured by



SYMBOLS :

- Electron
- Hole
- |— Class I centre
- x—x Class II centre

FIG.2.1 ENERGY LEVEL REPRESENTATION OF IMPERFECTION SENSITIZATION OF PHOTOCONDUCTIVITY

Class I centres. Consequently the majority of Class II centres become occupied by holes and, if the concentration of Class I and Class II centres is much larger than the density of free carriers, the electrons displaced from Class II centres will be effectively transferred to Class I centres. The lifetime of a free electron will now be increased as it cannot be captured by the majority of Class I centres which are already filled with electrons. It is also unlikely to be captured by any of the Class II centres which, as already mentioned, have an extremely small capture cross section for electrons. In the transition from the situation as in (b) to (c), which can be brought about by increasing photoexcitation intensity, the majority carrier lifetime and hence the photosensitivity of the material are also increased. This process has been represented by the second term ( $e \mu_n f \Delta T$ ) of (2.5) and, as stated there, results in superlinearity.

An increase in temperature can shift the Fermi level, causing the transition from (b) to (c) to be reversed, as a result of which the photosensitivity decreases. This phenomenon is known as thermal quenching of photoconductivity.

Optical quenching of photoconductivity can also occur. This is illustrated in Fig. 2.1(d). If a second source of photoexcitation is added, and is of a frequency such that electrons from the valence band are directly excited into the Class II centres, the resulting displaced holes may be captured by Class I centres and the sensitizing process is reversed. As

the Class II centres are relatively close to the valence band it can be deduced that the photo-excitation which causes optical quenching is of lower frequency than that which produces the sensitizing process. Optical quenching in II-VI photoconductors typically results from infra-red radiation, but in the case of intrinsic CdSe this has been found to occur only at temperatures below  $-50^{\circ}\text{C}$  (11). Quenching in the  $h\nu = 0.6$  to  $1.2\text{ eV}$  range in activated CdSe:Cu:Cl films has been reported (12), but again at low temperature only (90K).

### 2.3 SENSITIZATION BY IMPURITY INCORPORATION

The presence of foreign ions in a polar solid may greatly influence its electronic and optical properties. If the valency of the foreign ions is equal to that of the base lattice ions which they replace, the change of properties is a result of differences in the electronic configuration of the ions (13). If the valency of the foreign ions is different from that of the base lattice ions, incorporation is complicated by the necessity to maintain electro-neutrality. Such a general statement covers a wide range of cases and effects and an exhaustive review of the subject is beyond the scope of this report. Ryvkin, (14) however, has presented an extensive theoretical analysis of the kinetics of impurity photoconductivity which includes a discussion on charge exchange of impurity centres. The discussion will now be limited to the incorporation of copper and halogen ions into CdS and CdSe.

As explained in the previous section, intrinsic CdS and

CdSe exhibit low conductivity, low photosensitivity and a very rapid decay of photocurrent. Incorporation of halogen ions in increasing proportions results in increases of dark conductivity, photoconductivity and decay time (15). The presence of these ions may have two effects: crystal defects may be produced, or the halogen ions may simply replace a sulphur or selenium ion and act as a donor. Chlorine ions incorporated in CdSe, for example, could be represented by:



The resulting centre can be easily ionized at room temperature as the binding energy of the electron is low. Bube estimates the electron binding energy for chlorine ions in CdS to be about 0.04eV. The increase in the number of free electrons at room temperature resulting from halogen incorporation accounts for the increased dark conductivity of the material, and also causes a shift in the Fermi level. The latter effect, as discussed in conjunction with Fig. 2.1, results in the occupancy of Class II centres being determined by recombination kinetics, and the photosensitivity of the material is thereby increased. Incorporation of only a few parts per million of chlorine ions into CdS causes an increase of photosensitivity of between three and six orders of magnitude (16). If the concentration of incorporated halogen ions is further increased, a point is reached where the dark current at room temperature has increased to be equal to the current under illumination.

If copper ions are incorporated in CdS or CdSe which has been previously doped with halogen ions, a decrease in dark conductivity, photosensitivity and decay time will be observed.

The copper ions can be considered to be acting as low-lying acceptor centres in that they accept electrons from the halogen (donor) ions. In this way a stable neutral pair is formed:



When a hole is captured by such a copper centre, a positively charged centre with a relatively large capture cross section for free electrons will be formed. As the free electron concentration is reduced, the Fermi level is shifted back towards the valence band with a consequent decrease in photosensitivity as the number of active Class II centres is reduced.

Salehi Manshadi and Woods (17) have compared the effects of doping single crystal CdS with cuprous and cupric ions to produce either a  $\text{Cu}_2\text{S}$  (chalcocite) or  $\text{CuS}$  (covellite) surface layer. They found that the photosensitivity of the surface layer produced by doping with cuprous ions was more stable under illumination.

Fig. 2.2 (18) gives a general impression of the effect of halogen and copper ion incorporation on the conductivity of CdS or CdSe, both in the dark and under suitable illumination. It should be noted that there exists an optimum concentration of incorporated halogen and copper ions which give rise to the maximum ratio of illuminated conductivity to dark conductivity.

#### 2.4 SPEED OF RESPONSE

The importance of recombination centres having been established,

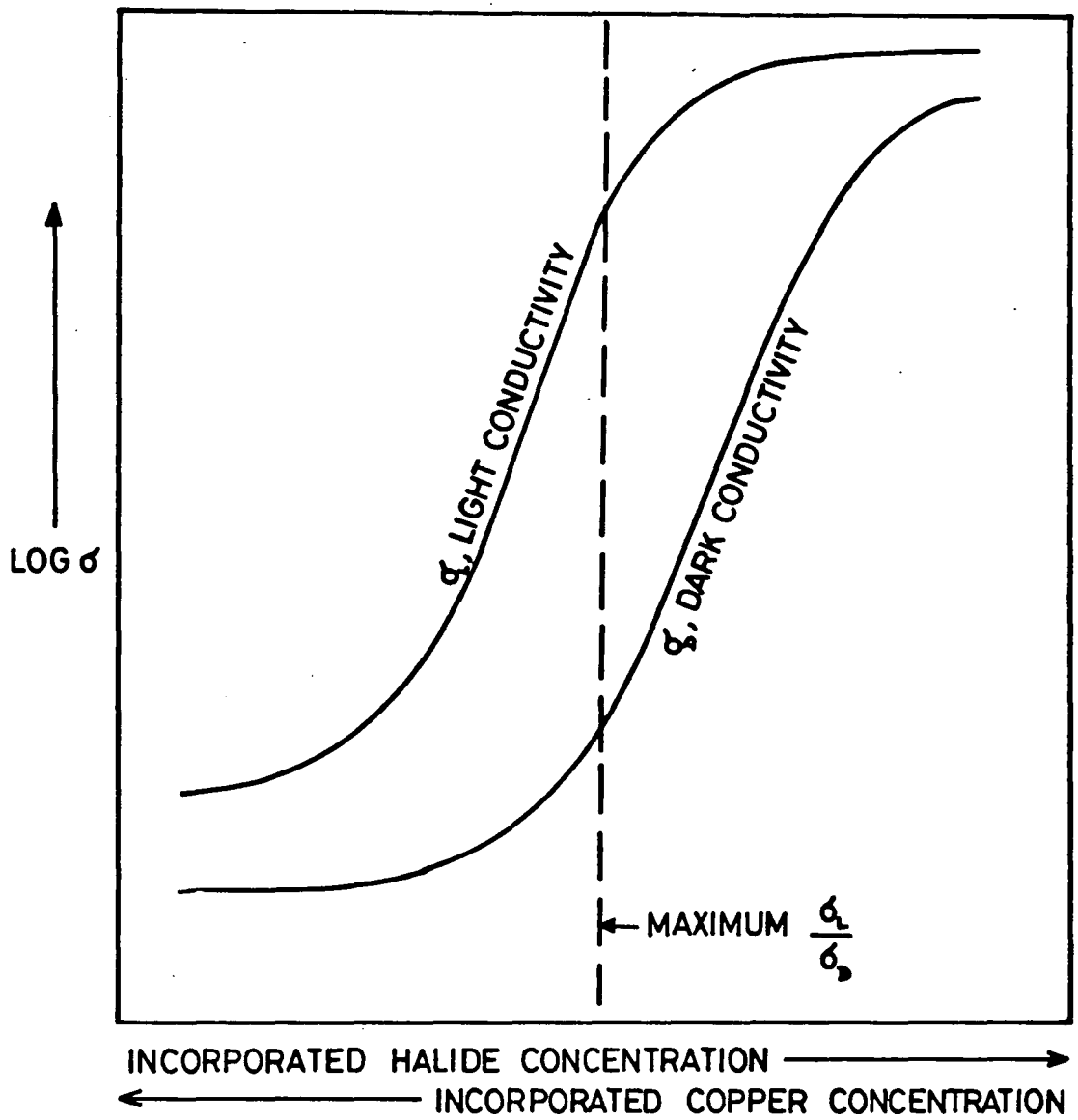


FIG.2-2 LIGHT AND DARK CONDUCTIVITY OF CdSe AS A FUNCTION OF INCORPORATED HALIDE OR COPPER CONCENTRATION (after Bube 1960)

it now becomes necessary to consider the role of traps to explain why the observed growth and decay times of photoconductivity almost invariably exceed the true majority carrier lifetime by several orders of magnitude (8). Occupancy of traps is determined by thermal equilibrium interchange with the adjacent band. In n-type photoconductors such as CdS and CdSe, the role of traps lying close to the conduction band is particularly important. Again, the model first proposed by Rose (5) will be used.

The true lifetime of a free electron can be defined as the average length of time that the electron spends in the conduction band. However, before a given electron eventually recombines, it may be trapped and later thermally excited back into the conduction band many times. Thus the decay of photoconductivity can be said to consist of two processes: an initial rapid decay caused by the direct recombination of free electrons from the conduction band, and a subsequent much slower decay process resulting from the recombination of electrons which have been thermally freed from traps via the conduction band. This model has been further discussed by Kiess and Binggeli (19) and Stöckmann (20)

The relative significance of these two decay processes is dependent on the photoexcitation conditions. If illumination of intensity sufficient to give a high free electron concentration is used, decay by direct recombination will predominate and the decay time will, in the limiting case, be equal to the true free electron lifetime. Under low intensity illumination, however,

indirect recombination will be the dominant mechanism resulting in a prolonged decay time. Measured decay times in CdS and CdSe typically range from a few microseconds to several seconds depending on the excitation intensity. Under the same intensity of illumination CdSe has generally been found to have a shorter decay time than has CdS. This is because the ionization energy  $E$  for holes from sensitizing centres is 0.6eV for CdSe and 1.1eV for CdS (2).

Decay time is also dependent on the physical structure of the material. Single crystal samples exposed to high intensity illumination exhibit decay times equal to the calculated majority carrier lifetime (using the measured values of applied field and gain). At lower excitation intensities the observed decay time is found to be between two and three orders of magnitude greater than the calculated lifetime. This ratio of measured decay time to calculated lifetimes is typically between 10 and  $10^3$  for sintered layers, and between  $10^3$  and  $10^5$  for powder layers under normal operating conditions (18). An additional characteristic of powder layers, arising from their non-ohmic behaviour, is a strong dependence of this ratio on the applied field.

## 2.5 SPECTRAL DISTRIBUTION OF PHOTONSENSITIVITY

Measurement of photoconductivity as a function of the wavelength of the photoexcitation usually reveals a maximum response at the wavelength for which the absorption constant is approximately

equal to the reciprocal of the crystal thickness. At shorter wavelengths the absorption constant is much higher and only the surface regions are excited. Since the majority carrier lifetime at the surface tends to be considerably shorter than the volume lifetime, this region of the material is typically less photosensitive. At longer wavelengths the incident illumination is only partially absorbed and hence the photosensitivity is again usually reduced.

If imperfections are present in appreciable concentrations, the spectral distribution of photosensitivity may be extended to longer wavelengths, since direct excitation of an electron to the conduction band from an imperfection centre lying in the forbidden gap requires less energy than similar excitation from the valence band. Thus incorporation of compensated copper acceptors into CdS (band gap = 2.4eV) can extend the range of high photosensitivity to around  $0.9\ \mu\text{m}$  ( $h\nu = 1.7\text{eV}$ ). A similar effect occurs in CdSe which can be made highly sensitive to visible and near infra-red radiation in this way.

Incorporation of halogen ions into CdS and CdSe does not affect the spectral response as the resulting compensated donor centres are, as previously mentioned, so close to the conduction band that they are in thermal equilibrium with it at room temperature.

A detailed discussion of the nature, distribution and concentration of traps and recombination centres in CdSe is beyond the scope of this report. These have, however, been

extensively investigated by other authors (21-24).

## 2.6 ELECTRODE REQUIREMENTS

The measured electrical behaviour of a photoconductor is influenced by the nature of the electrical contacts made to it. For most applications it is desirable that these contacts should be ohmic, i.e. capable of supplying an excess or reservoir of carriers ready to enter the photoconductor as needed. When ohmic contacts are successfully applied to a material known to have inherently linear I-V characteristics, such characteristics will indeed be experimentally observed. With CdS and CdSe powders which have highly non-linear I-V characteristics it is not so straightforward to estimate the degree with which the electrodes are acting as ohmic contacts. However, observed rectification by a supposedly homogeneous powder system would indicate the occurrence of additional contact processes.

An ohmic contact can be applied to an insulating n-type crystal by using a metal having a work function smaller than that of the crystal material. Thus for CdS and CdSe single crystals, diffused indium electrodes produce excellent ohmic contacts (25). If the crystals are homogeneous and photoconductive, the absence of any photovoltaic effect provides additional verification that the contacts are indeed ohmic. Manfredotti et al (23) used four types of contacts on CdSe single crystals. Of these, the indium melted contacts and the indium evaporated and diffused contacts were found to be ohmic

with good temperature and time stability. Rubbed on In-Ga eutectic contacts proved very ohmic but with poor time stability, while evaporated only indium contacts exhibited peculiar characteristics including I-V curves with a  $3/2$  slope or with a current saturation.

Most researchers who have investigated the photo-electronic properties of CdSe thin films used evaporated metal electrodes. Tanaka (26) applied evaporated indium electrodes to a sputtered CdSe film, while Mehta and Sharma (27) used evaporated gold contacts. This latter case is particularly interesting as Schottky barriers resulted at both contacts in the Au-CdSe-Au system. These contacts were found to be conducting under illumination but acted as blocking contacts in the dark. Despite previous claims that ohmic contacts were essential in order to obtain photoconductive gain greater than unity, comparable performance was obtained with this arrangement. Further investigations of metal: semiconductor interfaces on CdS and CdSe have been reported by Mead (28) and Brillson (29). Mead suggests that the surface barrier height on CdS is governed by the work function of the metal used, but on CdSe it is governed by the surface states. Brillson, however, produced evidence of a close correlation between metal: semiconductor barrier heights and heats of chemical reactivity for various electrode materials.

It is more difficult to make satisfactory electrical contacts to a loose powder and a standard method does not yet

seem to have been adopted. Sato and Yoshizawa (30) and Sato (31) compressed CdSe powder between etched copper electrodes. Nicastro and Offenbacher (32) placed particles of CdSe powder between copper wire and strips of tin-oxide coated glass, while Miyake (33) coated a conducting Nesa glass plate with a mixture of CdSe powder and resin binder and produced the second electrode by vacuum depositing aluminium to give a sandwich structure. Whether any of these arrangements resulted in truly ohmic contacts does not seem to have been established.

## 2.7 LIMITS TO PHOTOCONDUCTOR PERFORMANCE

If ohmic contacts can be applied to a homogeneous photoconductor, certain theoretical limitations to its performance can be represented mathematically.

For many practical applications, the most important quantity describing photoconductive performance is the product of the gain and the reciprocal of the response time. The maximum possible value of this product is directly related to the maximum voltage that can be applied to the photoconductor before the injection of carriers from the ohmic cathode dominates the conductivity of the crystal. Rose and Lampert (34) have shown that the maximum gain available under these conditions,  $G_{\max}$ , is given by:

$$G_{\max} = M. (\tau_o / \tau_{RC}) \quad (2.12)$$

where  $\tau_o$  is the observed response time,  $\tau_{RC}$  is the ohmic relaxation time of the photoconductor, and M is a multiplying

factor usually close to unity.  $M$  can be expressed as the ratio of the number of positive charges on the anode (corresponding to the number of traps filled by the field-injected carriers) to the number of traps filled by the photoexcitation process (including the free electrons). Traps play a dual role by giving rise to long response times and hence decreasing the  $G_{\max}/\tau_0$  value, and by permitting higher voltages to be applied before injected carriers dominate the conductivity and thus decrease the value of  $G_{\max}$ .

The value of  $M$ , and hence  $G_{\max}/\tau_0$ , may be increased by incorporation of suitable impurities, but as explained in section 2.3 there is a limitation to the improvement in performance that it is possible to achieve in this way. In any attempt to prepare a photoconductor for a particular application there must always be a compromise between high photosensitivity and maximum operating voltage, against fast speed of response. Nonetheless, homogeneous II-VI photoconductors, such as CdS and CdSe, with ohmic electrodes are capable of high gain and fast response (the limiting value of response time being the true free electron lifetime) under high intensity excitation. The penalty for achieving reasonable photosensitivity at low excitation intensities is a slow speed of response.

## 2.8 PHOTOCONDUCTIVITY IN POWDERS

Much of the general theory of photoconductivity outlined in the previous sections is applicable to powders. However, some

aspects of photoconductive performance are peculiar to powders, and will now be discussed.

A common characteristic of photoconductive powders is that the photocurrent increases faster than linearly with the applied voltage (1). In a sample of CdS powder mixed with a resin binder (35) the photocurrent was found to be approximately proportional to the fourth power of the applied voltage. Also the ratio of light to dark current was found to vary with applied voltage, passing through a maximum value at an intermediate voltage. Thomsen and Bube (36) attributed this type of non-linear I-V characteristic to the strong dependence of the apparent mobility on the applied voltage. To obtain the same photosensitivity as in single crystals or sintered layers, powder systems must be operated with applied fields in the region of  $10^4 \text{Vcm}^{-1}$  (8) Nicoll and Kazan were able to apply up to 1000 volts d.c. with an electrode spacing of 0.5 mm in the dark without causing breakdown, though illumination was found to reduce the maximum operating voltage due to photocurrent Joule heating within the material.

The performance of powder systems both with and without binding agents can be compared. Nicoll and Kazan claim that addition of a small amount of suitable binder may increase the observed photoconductivity of a powder by as much as one order of magnitude. However, photoconductivity lag following a change of the applied voltage has been observed in such systems (8) and is thought to be due to polarization of the powder-binder

system caused by application of an electric field.

Rose (1) also states that photoconductive powders are characterized by an almost linear dependence of photocurrent on illumination intensity. However, Nicoll and Kazan found that the photocurrent in their CdS powder-binder system was approximately proportional to the square root of the light intensity.

Since powders have such a large ratio of surface area to volume, surface conditions and inter-particle contacts are likely to have a major influence on conductivity. These have been extensively investigated by Miyake (33). Sato and Yoshizawa (30), Sato (31) and Beekmans (37) among others. Miyake concludes that the inter-particle contacts in a CdS powder-binder system behave as Schottky barriers, and that the barrier resistance is of similar magnitude to the photosensitive resistance. Sato and Yoshizawa, studying photoconductivity in compressed CdSe powder, conclude that the powder particles have a highly resistive surface region which has different electrical properties from the bulk. They suggest that the non-linear I-V characteristic of CdSe powder may be due to a high field effect as the current flow is constricted in this high resistance layer. The presence of adsorbed oxygen has been found to dramatically alter conductivity. This has been investigated on ZnO powder layers by Beekmans, while Bube (38) studied the effect on CdSe crystals, and suggests that adsorbed oxygen acts as an acceptor on the n-type surface thus reducing conductivity.

He also observed that the adsorption of oxygen may be photostimulated. A more detailed discussion of this phenomenon will be presented in Chapter 7 when the extent of the influence of oxygen adsorption and chemisorption upon electrical behaviour becomes apparent. A general review of investigations of the role of CdSe surface chemistry is given in the book "Surface Physics of Phosphors and Semiconductors" (39). Though the surface conductivity of powder particles may be very different from the bulk conductivity, it should be noted that at least there is no large anisotropy in the latter (40).

Many aspects of photoconductivity in powders are still not fully understood. These include the hysteresis effects reported by several authors, and the negative resistance, beyond a threshold voltage, of CdSe powder doped with copper and chlorine (32, 41).

A simplified model for a powdered photoconductor such as CdS and CdSe proposed by Bube (8) is shown in Fig. 2.3. The four processes represented in Fig.2.3 (2) can be described as follows: (A) depicts an electron moving over the inter-particle barrier and being photoexcited in the region of the barrier; (B) shows an electron flowing into the crystallite after tunnelling through the cathode barrier; (C) represents ionization of a deep filled level near the barrier, and (D) shows the capture of an excited hole at a sensitizing centre in the crystallite near the barrier. This last process results in an accumulation of positive charge near the barrier which decreases the barrier

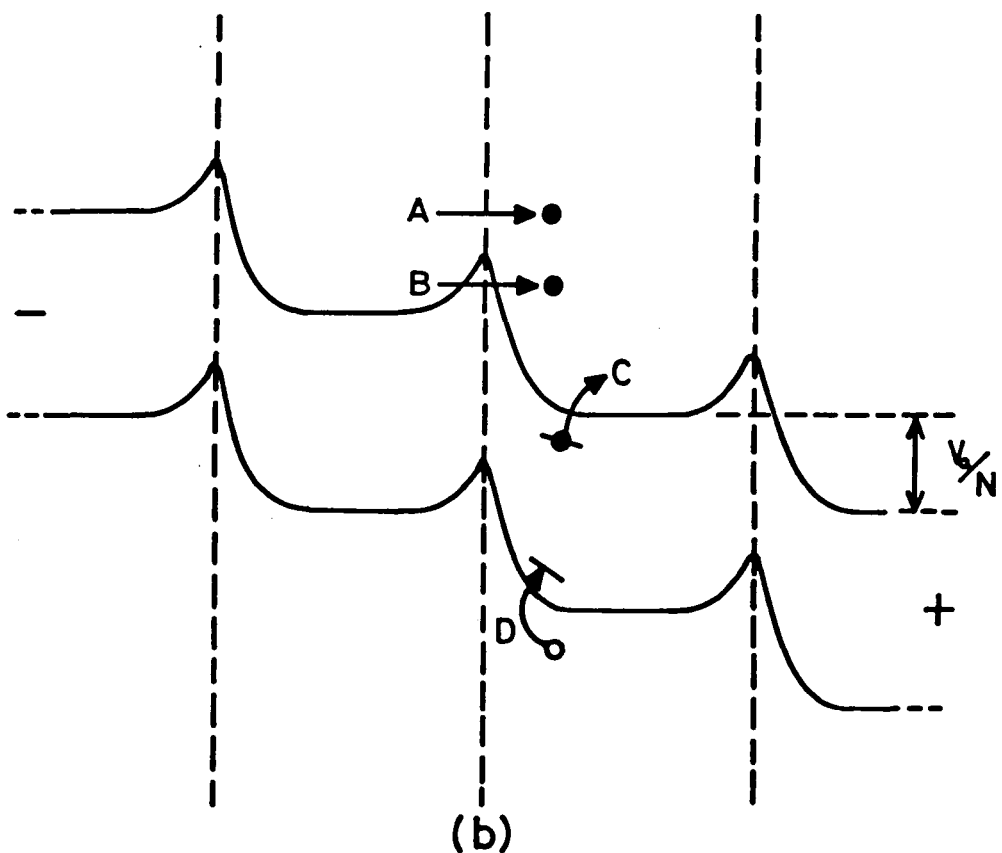
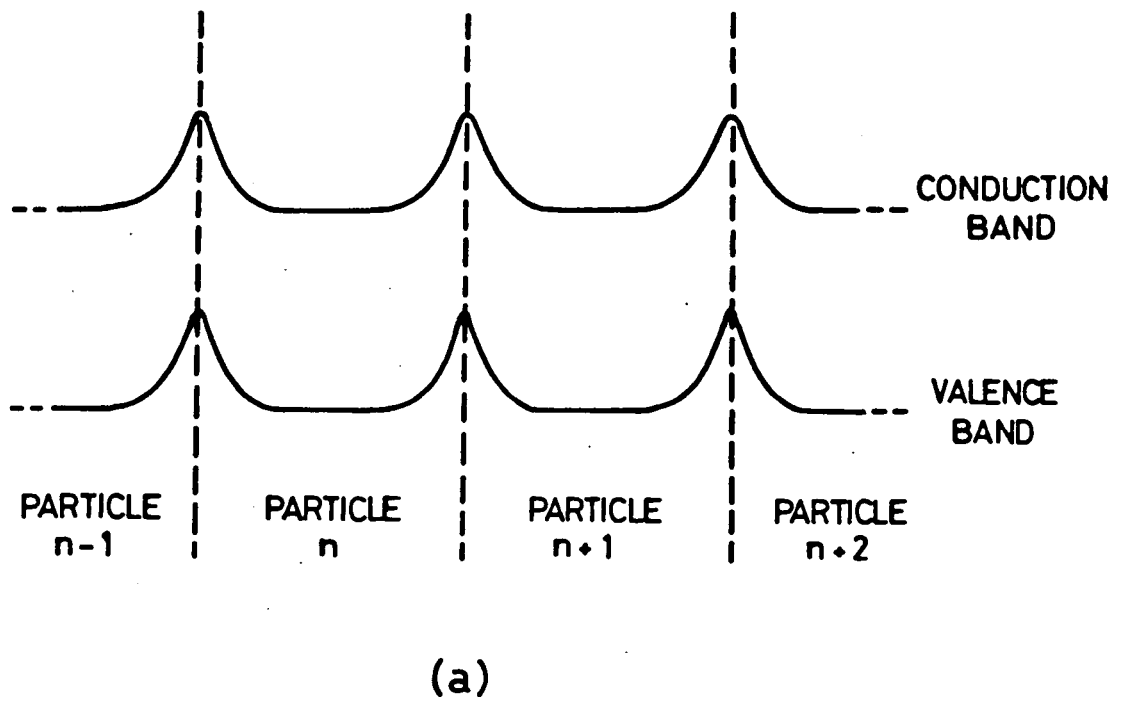


FIG.2·3 (a) SCHEMATIC ILLUSTRATION OF THE ENERGY BANDS OF CdS OR CdSe POWDER WITH BARRIERS BETWEEN PARTICLES.  
 (b) PROCESSES CONTRIBUTING TO CURRENT FLOW WHEN A VOLTAGE  $V_a$  IS APPLIED TO THE POWDER SHOWN IN (a) WITH  $N$  TOTAL PARTICLES ACROSS THE CELL GAP.

width. This charge accumulation process is time consuming and strongly dependent on the direction of the applied field, and may be associated with several characteristics of powders such as voltage dependent photosensitivity, polarization, voltage-associated lags and hysteresis effects.

## CHAPTER 2: REFERENCES

- 1) ROSE A. "Performance of Photoconductors" Proc. I.R.E. 1850-69 (Dec.1955)
- 2) RAY B. "II-VI Compounds" Chapter 5: "Photoconductivity and Associated Phenomena" 143-78. Pub: Pergamon Press (1969)
- 3) BUBE R.H. "Superlinear photoconductivity" Proc. Conf. on Photoconductivity, Atlantic City, 1954. 575-90. Pub: John Wiley & Son (1955)
- 4) See, for example: JAKIMAVICIUS I.A. et al. "The Effects of  $\text{CuCl}_2$  Concentration on Carrier Mobility in Sintered CdS Films" Sov. Phys-Collect (USA) 16, Pt 3, 64-5 (1976)
- 5) ROSE A. "An Outline of some Photoconductive Processes" R.C.A. Rev. 12, No.3, Pt 1, 362-415 (Sept. 1951)
- 6) ROSE A. "Concepts in Photoconductivity and Allied Problems" Pub: Interscience, New York (1963)
- 7) BUBE R.H., LIND E.L. and DREEBEN A.B. "Properties of Cadmium Sulfide Crystals with High Impurity Concentrations" Phys. Rev. 128, No.2, 532-9 (15 Oct.1962)
- 8) BUBE R.H. Chapter 13 "Photoconductivity" 657-705 in "Physics and Chemistry of II-IV Compounds" Ed: AVEN M. and PRENER J.S. Pub: North-Holland, Amsterdam (1967)

- 9) ROBINSON A.L. and BUBE R.H. "Photoelectronic Properties of Defects in CdSe Single Crystals" J. Appl. Phys. 42, No. 13, 5280-95 (Dec.1971)
- 10) BUBE R.H. "Photoconductivity of the Sulfide, Selenide and Telluride of Zinc or Cadmium" Proc. I.R.E. 1836-49 (Dec.1955)
- 11) BUBE R.H. "Infrared Quenching and a Unified Description of Photoconductivity Phenomena in Cadmium Sulfide and Selenide" Phys. Rev. 99, No. 4, 1105-16 (15 Aug. 1955)
- 12) RIZAKHANOV M.A., GASANBEKOV G.M. and KRONGAUZ V.T. "Spectrum of the Induced Impurity Photoconductivity in Activated CdSe:Cu:Cl Films in the 0.6 - 1.2 eV Range" Sov. Phys. - Semicond. (USA) 12, Pt 5, 589-90 (1978)
- 13) KROGER F.A., VINK H.J. and J. van den BOOMGAARD "Controlled Conductivity in CdS Single Crystals" Zeit. Phys. Chem. 203, 1-72 (May 1954)
- 14) RYVKIN S.M. "Kinetics of Impurity Photoconductivity" Phys. Chem. Sol. 22, 5-17 (1961)
- 15) BUBE R.H. "Photoconductivity and Crystal Imperfections in Cadmium Sulfide Crystals. Part II: Determination of Characteristic Photoconductivity Quantities" J. Chem. Phys. 23, No. 1, 18-25 (Jan.1955)

- 16) BUBE R.H. and THOMSEN S.M. "Photoconductivity and Crystal Imperfections in Cadmium Sulfide Crystals. Part I: Effect of Impurities." J. Chem. Phys. 23, No. 1, 15-17 (Jan.1955)
- 17) SALEHI MANSHADI M.A. and WOODS J. "Photoconductive Effects in Copper-doped Cadmium Sulphide" Phys. Stat. Sol. A. 40, K43-7 (1977)
- 18) BUBE R.H. "Photoconductivity of Solids" Pub: John Wiley & Sons, New York (1960)
- 19) KIESS H. and BINGGELI B. "Speed of Response of Photo-Currents in CdSe" R.C.A. Rev. 36, 485-98 (Sept.1975)
- 20) STÖCKMANN F. "On the Concept of Lifetimes in Photoconductors" R.C.A. Rev. 36, 499-507 (Sept.1975)
- 21) KINDLEYSIDES L. and WOODS J. "Electron Traps in Cadmium Selenide." J. Phys. D.: Appl. Phys. 3, 451-6 (1970)
- 22) TÜRE I.E.; RUSSELL G.J. and WOODS J. "Photoconductivity, Structure and Defect Levels in CdSe Crystals" J. Cryst. Growth 59, 223-228 (1982)
- 23) MANFREDOTTI C. et al. "Electron Trapping Levels in Cadmium Selenide Single Crystals" J. Appl. Phys. 44, No. 12, 5463-9 (Dec.1973)

- 24) TÜRE I.E., POULIN F., BRINKMAN A.W. and WOODS J. "Electron Traps and Deep Levels in Cadmium Selenide" Phys. Stat. Sol.A. 77, 583-44 (1983)
- 25) SMITH R.W. "Properties of Ohmic Contacts to Cadmium Sulphide Single Crystals" Phys. Rev. 97, No. 6, 1525-30 (15 March 1955)
- 26) TANAKA K. "Photoconductivity of CdSe Films Prepared by a Vapor Evaporating - Reactive Sputtering Method" Jap. J. Appl. Phys. 9, 1070-7 (Sept.1970)
- 27) MEHTA R.R. and SHARMA B.S. "Photoconductive Gain Greater Than Unity in CdSe Films with Schottky Barriers at the Contacts" J. Appl. Phys.44, No. 1, 325-8 (Jan.1973)
- 28) MEAD C.A. "Surface States on Semiconducting Crystals; Barriers on the Cd(Se:S) System" Appl. Phys. Lett. 6, No.6, 103-4 (15 March 1965)
- 29) BRILLSON L.J. "Transition in Schottky Barrier Formation with Chemical Reactivity" Phys. Rev. Lett. 40, No.4, 260-3 (23 Jan.1978)
- 30) SATO K. and YOSHIZAWA M. "Voltage-Current Characteristics of Compressed CdSe Powders" Jap. J. Appl. Phys. 13, No.4, 630-40 (April 1974)
- 31) SATO K. "Non-ohmic Current-voltage Characteristics of the Compressed CdSe Powder" Jap. J. Appl. Phys. 15, No.6, 1051-8 (June 1976)

- 32) NICASTRO L.J. and OFFENBACHER E.L. "Negative Resistance in Cadmium Selenide Powder - Comparison of Experiment with Theory" R.C.A. Rev. 33, 357-76 (June 1972)
- 33) MIYAKE T. "AC+DC Photoconductivities of Powdered Layers of CdS" Jap. J. Appl. Phys. 10, No. 4, 427-33 (April 1971)
- 34) ROSE A. and LAMPERT M. "Photoconductor Performance, Space-Charge Currents, and the Steady-State Fermi Level" Phys. Rev. 113, 1227-35 (1959)
- 35) NICOLL F.H. and KAZAN B. "Large Area High-Current Photoconductive Cells Using Cadmium Sulfide Powder" J. Opt. Soc. Am. 45, No.8, 647-50 (Aug.1955)
- 36) THOMSEN S.M. and BUBE R.H. "High Sensitivity Photoconductor Layers" Rev. Sci.Instr. 26, No.7, 664-5 (July 1955)
- 37) BEEKMANS N.M. "Effect of Oxygen Chemisorption and Photodesorption on the Conductivity of ZnO Powder Layers" J. Chem. Soc. Faraday Trans. I. 74, 31-45 (1978)
- 38) BUBE R.H. "Oxygen Sorption Phenomena on CdSe Crystals" J. Chem. Phys. 27, No.2, 496-500 (Aug.1957)
- 39) SCOTT C.G. and REED C.E. (Eds.) "Surface Physics of Phosphors and Semiconductors" 448-521 Pub: Academic Press (1975)

- 40) BURMEISTER R.A. and STEVENSON D.A. "Electrical Properties on n-type CdSe" Phys. Stat. Sol. 24, 683-94 (1967)
- 41) NICASTRO L.J. and OFFENBACHER E.L. "Negative Resistance in Cadmium Selenide Powder-Relative Absorption Coefficient" R.C.A. Rev. 34, 442-56 (Sept. 1973).

## CHAPTER 3 POWDER PREPARATION

### 3.1 INTRODUCTION

Photosensitive CdSe powder samples were prepared by incorporating copper and halogen ions into high purity CdSe powder. The preparation techniques used comprised numerous stages. The experimental condition at each stage could be varied over a wide range, and some processes were included, omitted or an alternative process substituted as required. To arrive at a reproducible method for producing suitable powder samples it was essential to establish a correlation between preparation conditions and measured performance. Such a wide range of behaviour, together with apparently inconsistent trends at times, was observed that over 170 powder samples were prepared in an attempt to establish this correlation. Thus a generalized description of powder preparation will be given, with specific details for each sample being given in abbreviated tabular notation in Fig. 3.4.

Untreated CdSe powder was obtained from four sources; three commercially prepared powders were used, and a quantity of powder was prepared in the laboratory by a chemical precipitation technique(1,2). The three commercial materials were all prepared to a claimed purity of 99.999%, and were supplied by Koch-Light Laboratories Ltd (England), E. Merck (West Germany) and Cerac Inc. (U.S.A.). The preparation of the

fourth source of CdSe powder in the laboratory merits further description.

### 3.2 LABORATORY MANUFACTURE OF CdSe POWDER

100g of 'Analar' grade anhydrous sodium carbonate ( $\text{Na}_2\text{CO}_3$ ) was dissolved in 400ml distilled water heated to between  $80^\circ$  and  $85^\circ\text{C}$ . When all the  $\text{Na}_2\text{CO}_3$  was seen to have dissolved the solution was found to be strongly alkaline with a pH of approximately 14. The pH was slowly reduced to 6 (neutral) by bubbling sulphur dioxide through the solution. The  $\text{SO}_2$  supply was removed and powdered selenium pellets (obtained from Koch-Light Laboratories Ltd, the claimed purity being again 99.999%) were gradually added to the solution until no more would dissolve. While this was being done, small white crystals appeared in the liquid. These and the excess selenium were removed by filtering the solution.

A solution of cadmium ions was prepared by dissolving 97.45g of 'Analar' grade cadmium sulphate ( $3\text{CdSO}_4 \cdot 8\text{H}_2\text{O}$ ) in 300ml distilled water. Each 10ml of this solution contained the gram equivalent of  $\text{Cd}^{++}$  ions to 1g of selenium.

The  $\text{CdSO}_4$  solution was added dropwise to the selenium solution and immediate precipitation was observed. Addition of the  $\text{CdSO}_4$  solution was continued while the flask was shaken frequently until the colour of the precipitate was seen to have

changed from the initial pale yellow to dark orange.

The mixture was then boiled vigorously for about 30 minutes which caused the suspension to become maroon in colour, after which it was left to cool and settle for several hours. After the remaining liquid had been removed by forced filtration, the precipitate was washed twice in about 400ml distilled water and then in a solution of 25ml glacial acetic acid ( $\text{CH}_3\text{COOH}$ ) in 50ml distilled water. Two more washes with distilled water followed, excess liquid at each stage again being removed by forced filtration. The moist solid residue was then placed in a drying oven for 40 hours at  $62^\circ\text{C}$ .

On removal from the drying oven the precipitate appeared to be an extremely fine, russet coloured powder. Approximately half of this powder was passed through a  $75\ \mu\text{m}$  mesh stainless steel sieve and then pre-fired for 60 minutes at  $700^\circ\text{C}$  in an argon atmosphere using the porous plug technique, details of which are given in the next section. When cooled this powder closely resembled the commercial CdSe powders in appearance, being a dull grey in colour and slightly cohesive.

### 3.3 POWDER SENSITIZATION

As predicted by the theory given in the previous chapter, untreated CdSe powder was found to have extremely high resistivity and low photosensitivity. The sensitization

procedure described here has been developed from a method used for ZnS phosphor preparation in an undergraduate experiment in this department(3,4). Many of the preparation stages used are similar to those mentioned by previous authors (5-12). Many authors, however, have omitted precise details of preparation conditions, small changes of which have been found to cause a major variation in the photoconductivity performance of the sensitized powder.

A generalized account of the sensitization process will now be given. Sequential stages will be numbered in order with lettered postscripts indicating alternative options. Process stages marked with an asterisk were omitted from the preparation of a significant proportion of samples.

- 1\* PRE-FIRING: A known weight of untreated CdSe powder chosen from the 4 available sources was transferred to a silica furnace tube. The tube was either flushed with high purity argon and sealed with a silica wool plug or left open to the atmosphere. A detailed description of the firing technique is given in section 3A. The tube and contents were fired for between 10 and 120 minutes, and the range of temperatures used was from 200° to 700°C. Such treatment was intended to remove any volatile contaminants and to stimulate the adsorption or desorption of oxygen depending on the ambient.

Some powder samples were found to have sintered into hard agglomerations, particularly those treated at higher temperatures. These were ground by hand using an agate mortar and pestle, and the resulting powder passed through a 75  $\mu\text{m}$  mesh stainless steel sieve.

- 2 DOPANT ADDITION: Copper and halogen ions were added to the powder samples in concentrations of the order of parts per million. To do this various solutions of suitable salts were prepared by successive dilution in distilled water or 'Analar' grade methanol. For convenience the concentration of a given solution (N) expressed in parts per million was defined as  $N = (N(D)/N(\text{CdSe})) \times 10^6$  where  $N(D)$  was the number of dopant ions present in 1ml of the solution, and  $N(\text{CdSe})$  was the number of molecules in 1g of CdSe (i.e. Avogadro's number divided by the gram-molecular weight of CdSe (=191.36)). Thus the volume of a given solution required for mixing with a known weight of CdSe powder to give a desired dopant concentration could be quickly calculated.

Halogen ions were introduced in the form of  $\text{CdCl}_2$  or  $\text{CdI}_2$ . Initially of 'Analar' grade, these were replaced by anhydrous salts (Cerac) of 99.999% claimed purity. 'Analar' grade NaCl and  $\text{NH}_4\text{Cl}$  were also tried but gave poor results - the latter dissociates into  $\text{NH}_3$  and HCl at about  $100^\circ\text{C}$ . A correspondingly dilute solution of HCL was also tried on one occasion but again proved to be unsatisfactory as it caused severe sintering on firing.

A variety of hydrated soluble cupric compounds were tried; these comprised  $\text{Cu(II)SO}_4 \cdot 5\text{H}_2\text{O}$  (initially 'Analar' grade, replaced by Koch-Light Puriss A.R. grade) and Puriss A.R.  $\text{Cu(II) (NO}_3)_2 \cdot 3\text{H}_2\text{O}$ ,  $\text{Cu(II) (CH}_3\text{COOH)}_2 \cdot \text{H}_2\text{O}$  and  $\text{Cu(II)Cl}_2 \cdot 2\text{H}_2\text{O}$ . The actions of cuprous and cupric ions were compared by also using Puriss A.R.  $\text{Cu(I)Cl}$ , though this was found to be much less readily soluble than the cupric compounds, and was incorporated in conjunction with the low concentration of HCL previously mentioned. Details of the complete range of dopants incorporated appear later in the sample preparation listings of Fig.3.4.

A calibrated 5ml pipette was used to add controlled volumes of dopant solutions with a precision of  $\pm 0.05\text{ml}$ . The powder and liquid mixture was stirred with a glass rod until it became a slurry of uniform consistency. The powder appeared to mix more readily with methanol based solutions than with aqueous ones. Excess solvent was removed by placing the slurry in a drying oven, sometimes preceded by rapid preliminary drying in a stream of hot air. This latter method was found to be particularly effective with methanol based dopant solutions and, combined with regular stirring of the slurry, reduced leaching effects. The temperature and duration of the oven drying was recorded for each sample.

On removal from the oven, as much of the dried slurry as possible was detached from the surface of the porcelain evaporating basin. The powder, unchanged in appearance, was again thoroughly mixed with a glass rod and ground and sieved as

previously described on the rare occasions when this was considered necessary. The resulting dry CdSe powder, hopefully uniformly coated with the desired dopants, was now ready for firing.

3A MAIN FIRING: POROUS PLUG METHOD. The treated CdSe powder was transferred into a transparent grade silica firing tube. This tube had an internal diameter of 1.5 cm, and was approximately 33 cm in length and sealed at one end, as shown in Fig. 3.1. Sometimes the powder was concentrated at the sealed end of the tube; the effect of distributing it in a thin layer along about 10 cm of the tube length was also investigated but did not yield conclusive results. The tube and contents were then either flushed with high purity argon or left exposed to the air, after which a porous plug some 3 to 5 cm long was inserted into the open end. This plug was made from compacted M-grade silica wool and thus allowed for thermal expansion of the ambient atmosphere during heating while limiting the diffusion of air into the firing tube.

A schematic illustration of the type of horizontal electric furnace used is given in Fig. 3.2. A platinum - platinum/13% rhodium thermocouple was used to monitor the temperature close to the powder sample being fired. The thermocouple was connected to a 'Eurotherm' potentiometric temperature controller in which the rate of change and the duration of the difference between the thermocouple e.m.f and a manually pre-set reference voltage governed the electrical power delivered to the copper

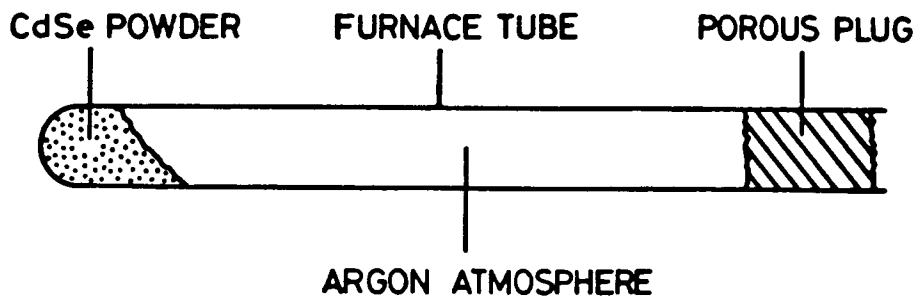


FIG.3.1 FURNACE TUBE USED IN POROUS PLUG METHOD

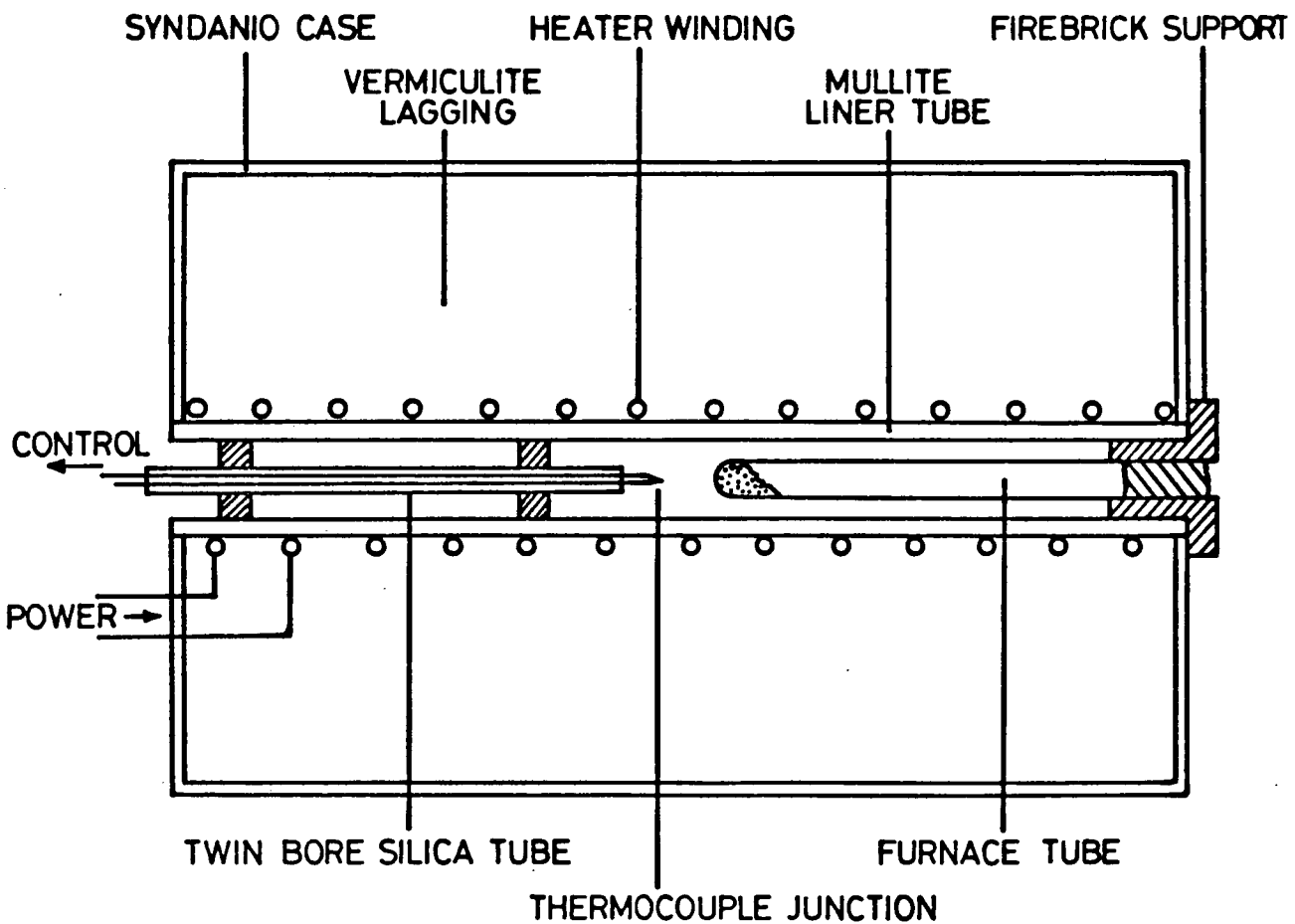


FIG. 3.2 HORIZONTAL ELECTRIC FURNACE CROSS-SECTION (not to scale)

heater coil. By matching the temperature controller characteristics with the thermal time constant of the furnace both a fast response time and the ability to override any spurious temperature fluctuations were achieved. The thermocouple to temperature controller reference setting was calibrated to British Standard 1826 (1952) giving guaranteed accuracy within  $\pm 1^{\circ}\text{C}$  for temperatures up to  $1100^{\circ}\text{C}$ .

The furnace was allowed to reach the chosen firing temperature of between  $400^{\circ}\text{C}$  and  $900^{\circ}\text{C}$  (a standard firing temperature of  $600^{\circ}\text{C}$  was eventually adopted) before the furnace tube was inserted. After a known period of time ranging from 10 to 150 minutes, but typically 90 minutes, the tube was withdrawn and left to cool at room temperature. Again the appearance of the powder was unchanged after firing. However, a variety of microcrystalline deposits was observed towards the open (cooler) ends of the firing tubes but the chemical nature of these was not investigated. When the tube and contents had returned to room temperature the porous plug was removed and the contents emptied into a suitable container.

### 3B MAIN FIRING: PARTIAL PRESSURE METHOD

This totally sealed firing technique was tried as an alternative to the porous plug method in an attempt to fire the powder samples in a more controlled atmosphere.

The dried and powdered slurry was transferred into a length of transparent grade silica tube of approximately 0.8 cm internal diameter which had been sealed at one end. The tube was then connected to a vacuum line and evacuated to a pressure of less than  $10^{-4}$  Torr by means of a rotary pump and a mercury diffusion pump. A schematic diagram of the apparatus used is given in Fig. 3.3. The vacuum system was isolated and high purity argon was slowly admitted into the firing tube, the pressure being monitored using a mercury manometer. When the pressure of argon in the firing tube reached approximately 260 Torr the argon supply was also isolated. This chosen pressure of argon was calculated to increase to about one atmosphere at the firing temperature of  $600^{\circ}\text{C}$ , assuming a room temperature of  $300^{\circ}\text{K}$ . The firing tube with contents was then sealed some 15 cm along from the closed end by heating the silica walls with a blowtorch beyond their softening point (i.e. around  $1200\text{-}1500^{\circ}\text{C}$ ) and then pinching them together.

The firing tube and contents were then placed in a pre-heated horizontal electric furnace, again typically at  $600^{\circ}\text{C}$ , for the required firing period before being withdrawn and allowed to cool at room temperature. Though physically smaller than the furnace used for the porous plug method, the furnace construction was similar and temperature control achieved by the same means. When cooled the firing tube was scored and snapped open and the contents were removed. Since the tubes were hermetically sealed, opening was often postponed until measurements were to be made on the contents.

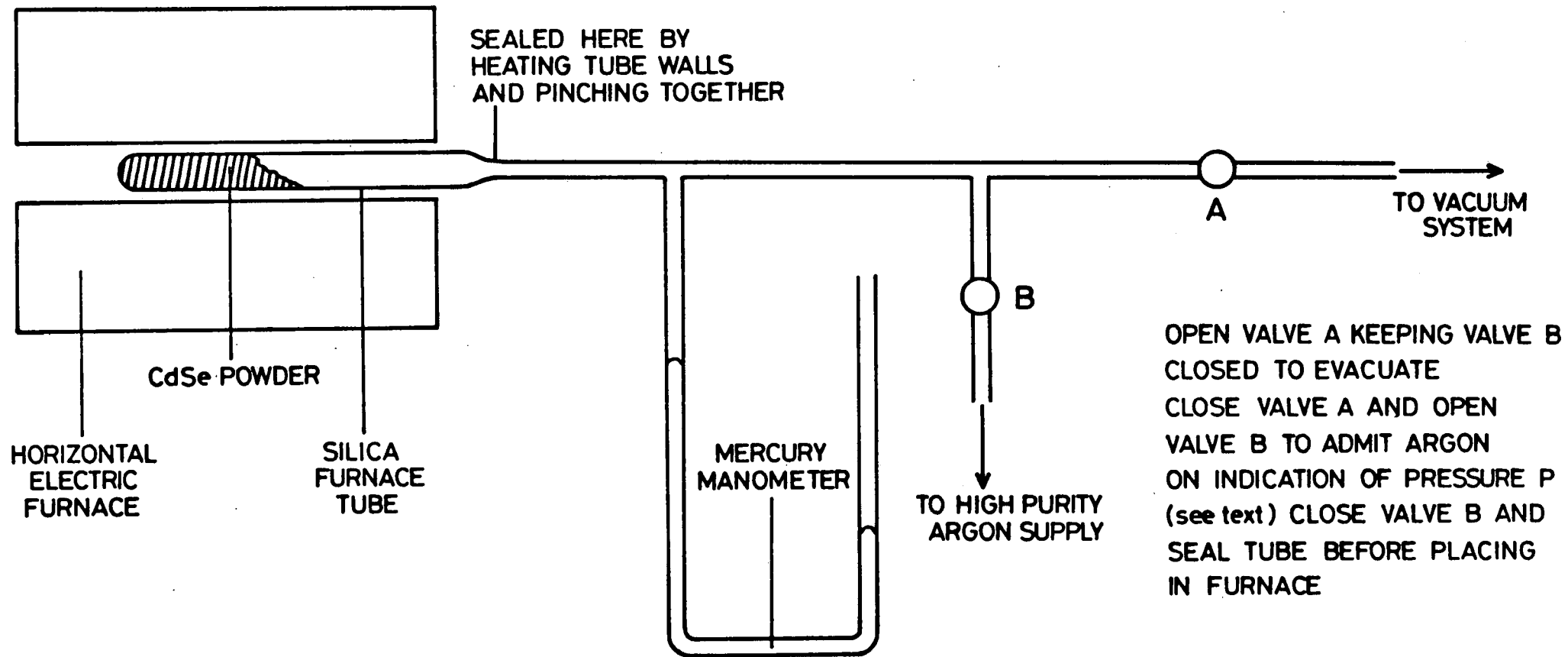


FIG. 3-3 APPARATUS USED IN PARTIAL PRESSURE FIRING METHOD (Not to scale)

4 FINAL TREATMENTS: After firing by either method some of the doped samples, particularly those treated with a high concentration of chlorine ions, were found to have sintered into hard agglomerates. These were crushed and ground using an agate mortar and pestle and then passed through a 75  $\mu$ m mesh stainless steel sieve.

By this stage some powder samples were ready for testing; others were washed to investigate the effect of soluble surface contaminants, if any were indeed present. Distilled water or 'Analar' grade methanol were used as washing agents, the powder being thoroughly stirred with approximately 75ml of liquid and left to settle in each case. After a final agitation excess liquid was removed from the resulting suspension by forced filtration through medium/fast filter paper using a Bernouilli pump. The washing process was repeated using the same agent in each case and then the powder was dried on the paper in the drying oven. When completely dry the powder could be easily detached from the paper by light tapping and was stored in a suitable container.

An alternative technique intended to combine the results of crushing and washing hardened agglomerates while reducing the detrimental effects caused by mechanical damage during grinding (cf. Chapter 6) was attempted. Approximately 75ml methanol was added to the sintered powder lump in a beaker which was then placed in an ultrasonic bath and agitated for about two minutes. Excess washing agent was again removed by forced filtration as

previously described.

### 3.4 INDIVIDUAL SAMPLE PREPARATION

An abbreviated listing of the preparation conditions for each individual powder sample is given in Fig.3.4. Brief notes will now be given in an attempt to outline the purpose behind the preparation of each series of powder samples.

The A series powders were an initial attempt to prepare photosensitive CdSe powder by establishing a suitable copper concentration in the presence of a high halogen concentration. These preparations were repeated with an additional pre-fire in argon to give the B series.

The C series of powder samples were prepared to compare the effect of three different sources of chlorine ions in the absence of copper. Also the effect of washing fired samples was investigated, and a less harsh sieving process introduced. These preparations were repeated using Merck instead of Koch-Light CdSe to give the D series.

The E series featured the initial appraisal of iodine instead of chlorine as the halogen ions used, and a reduction of firing temperature. These features were retained for the F series while experimentation with the copper concentration was reintroduced. The detrimental effect of grinding upon sample conductivity was strongly suspected by this stage and was

therefore omitted wherever possible. F6 and F6\* were prepared using chlorine ions for direct comparison with iodine.

In the G series of samples the effect of firing time was investigated, and 'Analar' Methanol was introduced as an alternative washing agent.

The partial pressure firing technique and Cerac CdSe powder were both tried for the first time in the H series. Powders H1 and H1\*, however, reverted to the use of Merck CdSe and the porous plug firing method. Methanol was tried instead of distilled water as a solvent for the dopant compounds.

High purity copper and halogen compounds were used for the first time in the J series of powder samples, and the relative merits of copper sulphate, nitrate and acetate evaluated. The same three copper compounds were used at lower concentrations in the K series. Copper sulphate was established as the most suitable cupric salt from these investigations, and was tried at three different concentrations in the L series.

Powder samples M1 and M1\* were prepared from CdSe powder produced in the laboratory as described previously. Sample M1 was fired in air for 15 minutes at 200°C before the preparation stages listed in Fig.3.4.

Cupric chloride was used as the source of both copper and halogen ions in the N series. The P series repeated these

preparations using cuprous chloride. However, forming a solution of cuprous chloride proved problematic so a small concentration of HCl was added. Use of cupric chloride was then repeated in the Q series but with a similar additional HCl concentration as a control.

An attempt was made to reproduce a method for CdSe powder sensitization described by Bube (11) in the R series. The very high CdCl<sub>2</sub> concentration caused sintering problems on firing, thus the preparations were repeated in the S series using a shorter firing duration. Investigation of the effect of firing conditions upon this method continued in the T series of samples in which a variety of firing times and temperatures were employed. Powder samples U1 and U2 were prepared in a similar way but iodine was again used as the halogen dopant.

The two powders of the V series provided a direct comparison between Koch-Light and Merck CdSe as starting materials. Sample X1 was fired in the mass spectrometer; a chemical analysis of this process is given in Chapter 6.

Reduced concentrations of both halogen and copper ions were tried in the Y series. Samples Y1\*, 2\* and 3\* were also fired in air for 2 hours at 200°C in darkness.

The entire sample series 1-16 constituted a systematic evaluation of the effect of powder sample preparation conditions on performance. The preparation details of these powders are displayed in a more comprehensive format in Fig.3.5. This

shows clearly how variation of preparation conditions was limited to four successive binary choices. Thus out of the total of 48 such samples prepared, 24 pairs were available to enable a statistical comparison between the effects of each choice to be made, all other preparation details being identical. The final powders were either unwashed or washed in methanol or distilled water; thus 16 groups of three samples were available for comparison of the effects of these processes. The powder samples in the 17 series were prepared in the same way as those of the 7 series except that the effects of three reduced incorporated Cu concentrations were investigated.

One completely different technique for producing CdSe powder doped with halogen ions was attempted. This iodine transport method will now be described with reference to Fig. 3.6. Ten grams of Koch-Light CdSe powder were purified by standard flow run refining and then placed in an 8cm long, 16mm I.D. silica tube together with 20mg. of iodine. This tube was evacuated for several minutes by a rotary pump and then sealed, the end wall angle being obtuse. It was placed in a vertical electric furnace, the temperature being 850°C in the region of the charge and some 30 deg.C lower at the sealed neck and end wall. The tube and contents were thus fired for two weeks resulting in the vapour phase transport of some of the material to the end wall where it formed a polycrystalline deposit. The residual charge and some of the transported material were ground separately to powder of  $<75\mu\text{m}$  particle size.

## FIG. 3.4: EXPLANATORY NOTES

Symbols used:

Source material: K = Koch-Light 99.999% CdSe Powder

M = Merck                   "       "       "

C = Cerac                   "       "       "

L = Laboratory-prepared CdSe powder (cf 3-2)

Solvent and/or washing agent: W = Distilled water

M = 'Analar' grade methanol

Grinding and sieving: Y = ground and passed through 75  $\mu\text{m}$   
mesh stainless steel sieve

Dash (-) indicates that process stage was omitted

Arrow ( $\longrightarrow$ ) indicates that details are as for preceding line.

Length of arrow gives quick indication of the extent of similarity between sample preparations.

Blank columns are also, by default, as for the preceding line.

Numbered exceptions:

- (1) 150  $\mu\text{m}$  mesh sieve used

- (2) Powder passed through 75  $\mu\text{m}$  mesh sieve without prior grinding
- (3) Distilled water + 0.01% (by volume) conc. HCl
- (4) " " + 0.1% " " " "
- (5) " " + 1.0% " " " "

HCl was used in (3), (4) and (5) to ensure that the CuCl was fully dissolved. The extra concentration of Cl ions due to the acid has not been included in the estimate of halogen ion concentration.

- (6) Powder passed through 150  $\mu\text{m}$  mesh sieve without prior grinding.
- (7) Powder ground but not sieved.
- (8) Highly concentrated dopant solutions used in small volumes to minimise drying time and possible reactions between solvent and powder. The  $\text{CuCl}_2$  was dissolved in 'Analar' grade methanol, the  $\text{CdCl}_2$  in distilled water. Hot air stream drying of the slurry was introduced.
- (9) Details of the main firing conditions are given in Chapter 5 (Section 5.4 ). A mass spectrometer was used to monitor changes in the ambient atmosphere.
- (10) The preceding sample was heated to 200°C in total darkness for 2 hours. This was performed in the drying oven.

			PRE-FIRE <sup>①</sup>			DOPANT INCORPORATION <sup>②</sup>						MAIN FIRING <sup>③</sup>			F.T. <sup>④</sup>	
SAMPLE SERIES	SUB-SERIES	SOURCE MATERIAL	TEMP. (°C)	TIME (mins)	GRIND & SIEVE	COPPER DOPANT: TYPE & GRADE	COPPER CONC'N (ppm)	HALIDE DOPANT: TYPE & GRADE	HALIDE CONC'N (ppm)	SOLVENT	GRIND & SIEVE	METHOD	TEMP. (°C)	TIME (mins)	GRIND & SIEVE	WASH. AGENT
															Y	W
A	1	K	-	-	-	CuSO <sub>4</sub> : 'Analar'	1K	CdCl <sub>2</sub> : 'Analar'	20K	W	Y	3A	700	60	Y	W
	2						100									
	3						10									
B	1	K	700	120	-	CuSO <sub>4</sub> : 'Analar'	1K	CdCl <sub>2</sub> : 'Analar'	20K	W	Y	3A	700	60	Y	W
	2															
	3															
C	1	K	-	-	-	-	-	CdCl <sub>2</sub> : 'Analar'	20K	W	-	3A	700	60	Y	W
	1*															-
	1**															①
	2							NH <sub>4</sub> Cl: 'Analar'							Y	W
	2*															-
	2**															①
	3							NaCl: 'Analar'							Y	W
	3*															-
	3**															①
D	1	M	-	-	-	-	-	CdCl <sub>2</sub> : 'Analar'	20K	W	-	3A	700	60	Y	W
	1*															-
	1**															①
	2							NH <sub>4</sub> Cl: 'Analar'				-	-	-	Y	W
	2*															-
	2**															①
	3							NaCl: 'Analar'							Y	W
3*															-	

FIG. 3-4 (i)

			PRE-FIRE <sup>①</sup>			DOPANT INCORPORATION <sup>②</sup>						MAIN FIRING <sup>③</sup>			F.T. <sup>④</sup>	
SAMPLE SERIES	SUB-SERIES	SOURCE MATERIAL	TEMP. (°C)	TIME (mins)	GRIND & SIEVE	COPPER DOPANT: TYPE & GRADE	COPPER CONC'N (ppm)	HALIDE DOPANT: TYPE & GRADE	HALIDE CONC'N (ppm)	SOLVENT	GRIND & SIEVE	METHOD	TEMP. (°C)	TIME (mins)	GRIND & SIEVE	WASH. AGENT
															Y	W
E	1	M	-	-	-	-	-	CdI <sub>2</sub> : 'Analar'	20K	W	-	3A	600	60	Y	W
	1*															-
	2															②
F	1	M	-	-	-	CuSO <sub>4</sub> : 'Analar'	100	CdI <sub>2</sub> : 'Analar'	20K	W	-	3A	600	60	②	W
	1*															-
	2						1K									W
	2*						10									W
	3						10K									W
	3*						1K									W
	4															W
	4*															-
	6							CdCl <sub>2</sub> : 'Analar'								W
G	1	M	-	-	-	CuSO <sub>4</sub> : 'Analar'	1K	CdI <sub>2</sub> : 'Analar'	20K	W	-	3A	600	30	②	W
	1*															-
	2												60			W
	2*												90			W
	3															-
	3*															M
	4															-
4*															-	

FIG. 3-4 (ii)

		① PRE-FIRE			② DOPANT INCORPORATION					③ MAIN FIRING			④ F.T.				
SAMPLE SERIES	SUB-SERIES	SOURCE MATERIAL	TEMP. (°C)	TIME (mins)	GRIND & SIEVE	COPPER DOPANT : TYPE & GRADE	COPPER CONC'N (ppm)	HALIDE DOPANT : TYPE & GRADE	HALIDE CONC'N (ppm)	GRIND & SIEVE	SOLVENT	METHOD	TEMP. (°C)	TIME (mins)	WASH. AGENT	GRIND & SIEVE	F.T.
G	5												120		M		
	5*																
	6												150		M		
	6*																
H	1	C	-	-	-	CuSO <sub>4</sub> : 'Analar'	1K	CdI <sub>2</sub> : 'Analar'	20K	W	②	3A	600	60	②	M	
	1*																
	2												90			M	
	2*																
	3											3B	75			M	
I	1	M	-	-	-	CuSO <sub>4</sub> : 'Analar'	1K	CdI <sub>2</sub> : 'Analar'	20K	M	②	3A	600	90	②	M	
	1*																
J	1	M	-	-	-	CuSO <sub>4</sub> : PurissAR	1K	CdI <sub>2</sub> : 5N	20K	W	-	3A	600	90		M	
	1*																
	2					Cu(NO <sub>3</sub> ) <sub>2</sub> : Pur. AR											
	2*																
K	1	M	-	-	-	CuSO <sub>4</sub> : PurissAR	100	CdI <sub>2</sub> : 5N	20K	W	-	3A	600	90		M	
	1*																
	2					Cu(NO <sub>3</sub> ) <sub>2</sub> : Pur. AR											
	2*																
	3					Cu(CH <sub>3</sub> COO) <sub>2</sub> : PAR											
	3*																

FIG. 3-4 (iii)

		① PRE-FIRE			② DOPANT INCORPORATION					③ MAIN FIRING			④ F.T.				
SAMPLE SERIES	SUB-SERIES	SOURCE MATERIAL	TEMP. (°C)	TIME (mins)	GRIND & SIEVE	COPPER DOPANT : TYPE & GRADE	COPPER CONC'N (ppm)	HALIDE DOPANT : TYPE & GRADE	HALIDE CONC'N (ppm)	GRIND & SIEVE	SOLVENT	METHOD	TEMP. (°C)	TIME (mins)	WASH. AGENT	GRIND & SIEVE	F.T.
L	1	M	-	-	-	CuSO <sub>4</sub> : PurissAR	100	CdI <sub>2</sub> : 5N	20K	W	-	3A	600	90		M	
	1*																
	2						1K										
	2*																
M	1	L	700	60	-	CuSO <sub>4</sub> : 'Analar'	1K	CdI <sub>2</sub> : 'Analar'	20K	W	-	3A	600	75		M	
	1*																
	2																
	2*																
N	1	C	-	-	-	Cu(II)Cl <sub>2</sub> : Pur. AR	1	Cu(II)Cl <sub>2</sub> : Pur. AR	2	W	-	3A	600	90		M	
	2						10		20								
	3						100		200								
P	1	C	-	-	-	Cu(I)Cl : Pur. AR	1	Cu(I)Cl : Pur. AR	1	③	-	3A	600	90	Y		
	2						10		10	④							
	3						100		100	⑤							
Q	1	C	-	-	-	Cu(II)Cl <sub>2</sub> : Pur. AR	1	Cu(II)Cl <sub>2</sub> : Pur. AR	2	③	⑥	3A	600	90	①		
	2						10		20	④							
	3						100		200	⑤							
R	1	C	-	-	-	Cu(II)Cl <sub>2</sub> : Pur. AR	1	CdCl <sub>2</sub> : 5N	200K	W	Y	3A	600	90	⑦		
	2						10										
	3						100										
S	1	K	-	-	-	Cu(II)Cl <sub>2</sub> : Pur. AR	1	CdCl <sub>2</sub> : 5N	200K	W	Y	3A	600	30	⑦		
	2						10										
	3						100										

FIG. 3-4 (iv)

SAMPLE SERIES	SUB - SERIES	SOURCE MATERIAL	PRE-FIRE <sup>①</sup>			DOPANT INCORPORATION <sup>②</sup>						MAIN FIRING <sup>③</sup>			F.T. <sup>④</sup>	
			TEMP.(°C)	TIME (mins)	GRIND & SIEVE	COPPER DOPANT : TYPE & GRADE	COPPER CONC'N (ppm)	HALIDE DOPANT : TYPE & GRADE	HALIDE CONC'N (ppm)	GRIND & SIEVE	SOLVENT	METHOD	TEMP.(°C)	TIME (mins)	WASH. AGENT	GRIND & SIEVE
3	M		-	-	-	CuSO <sub>4</sub> : PurissAR	500	CdI <sub>2</sub> : 5N	2K	M	②	3A	600	90	②	-
	W															W
	M															W
4	M											3B				-
	W															W
5	M							CdCl <sub>2</sub> : 5N	20K			3A			Y	-
	W															W
6	M											3B			②	-
	W															W
7	M											3A				-
	W								2K							W
8	M											3B				-
	W															W
9	M							CdI <sub>2</sub> : 5N	20K	W		3A			②	-
	W															W
10	M											3B				-
	W															W

FIG. 3-4 (vi)

SAMPLE SERIES	SUB - SERIES	SOURCE MATERIAL	PRE-FIRE <sup>①</sup>			DOPANT INCORPORATION <sup>②</sup>						MAIN FIRING <sup>③</sup>			F.T. <sup>④</sup>	
			TEMP.(°C)	TIME (mins)	GRIND & SIEVE	COPPER DOPANT : TYPE & GRADE	COPPER CONC'N (ppm)	HALIDE DOPANT : TYPE & GRADE	HALIDE CONC'N (ppm)	GRIND & SIEVE	SOLVENT	METHOD	TEMP.(°C)	TIME (mins)	WASH. AGENT	GRIND & SIEVE
T	1	K	-	-	-	Cu(II)Cl <sub>2</sub> : Pur. AR	10	CdI <sub>2</sub> : 5N	200K	⑧	-	3A	560	10	⑦	-
	2												400	120		
	3												900	30		
U	1	K	-	-	-	Cu(II)Cl <sub>2</sub> : Pur. AR	10	CdI <sub>2</sub> : 5N	200K	⑧	-	3A	600	10	①	-
	2															W
V	1	K	-	-	-	CuSO <sub>4</sub> : PurissAR	1K	CdI <sub>2</sub> : 5N	20K	M	⑦	3A	600	90	⑦	-
	2	M														W
W	1	M	-	-	-	CuSO <sub>4</sub> : PurissAR	10	CdI <sub>2</sub> : 5N	20K	M	-	3B	600	90		-
	2						100									
	3						1K									
X	1	M	-	-	-	CuSO <sub>4</sub> : PurissAR	1K	CdI <sub>2</sub> : 5N	20K	M	②	⑨	600	130		-
Y	1	M	-	-	-	CuSO <sub>4</sub> : PurissAR	25	CdI <sub>2</sub> : 5N	5K	M	②	3A	600	90		-
	1*															
	2						50									
	2*															
	3						100									
1	M		-	-	-	CuSO <sub>4</sub> : PurissAR	500	CdI <sub>2</sub> : 5N	20K	M	Y	3A	600	90	⑦	-
	W															W
	2											3B				-
	W															W

FIG. 3-4 (v)

SAMPLE SERIES	SUB - SERIES	SOURCE MATERIAL	PRE-FIRE <sup>①</sup>		DOPANT INCORPORATION <sup>②</sup>						MAIN FIRING <sup>③</sup>		F.T. <sup>④</sup>		
			TEMP.(°C)	TIME (mins)	GRIND & SIEVE	COPPER DOPANT : TYPE & GRADE	COPPER CONC'N (ppm)	HALIDE DOPANT : TYPE & GRADE	HALIDE CONC'N (ppm)	SOLVENT	GRIND & SIEVE	METHOD	TEMP.(°C)	TIME (mins)	GRIND & SIEVE
11	M							→ 2K			3A			-	-
	W													→	M
12	M												→	→	W
	W										3B			→	M
13	M							→ CdCl <sub>2</sub> : 5N	20K		3A			⑦	-
	W													→	M
14	M												→	⑧	-
	W										3B			→	M
15	M													→	W
	W										2K		3A	→	M
16	M													→	W
	W										3B			→	M
17	A							→ 5					3A	→	W
	B							→ 25						→	M
	C							→ 100						→	W

FIG. 3:4 (vii)

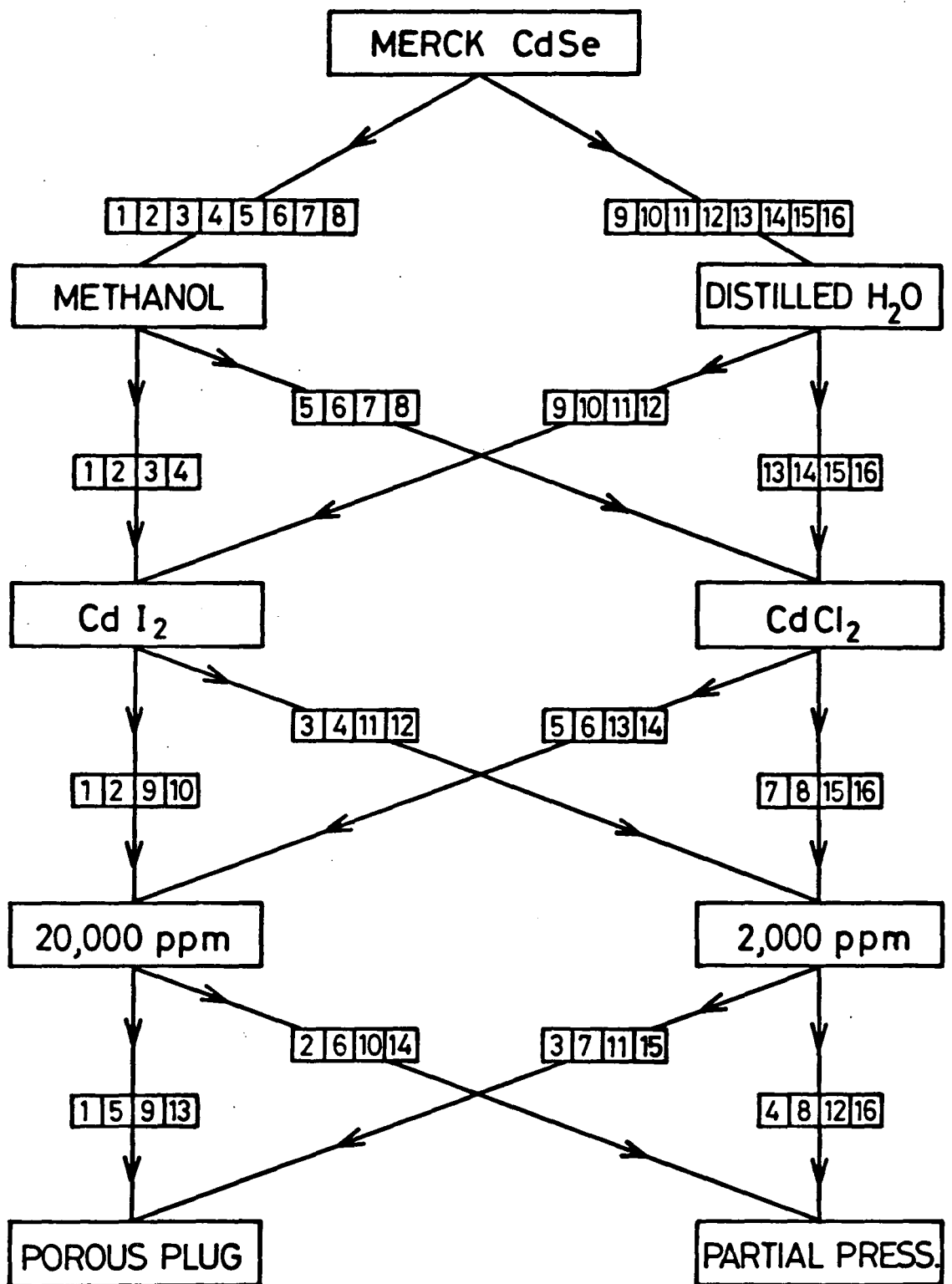


FIG. 3-5 FLOW DIAGRAM REPRESENTATION OF POWDER SAMPLE PREPARATION ROUTES FOR SYSTEMATIC ANALYSIS.

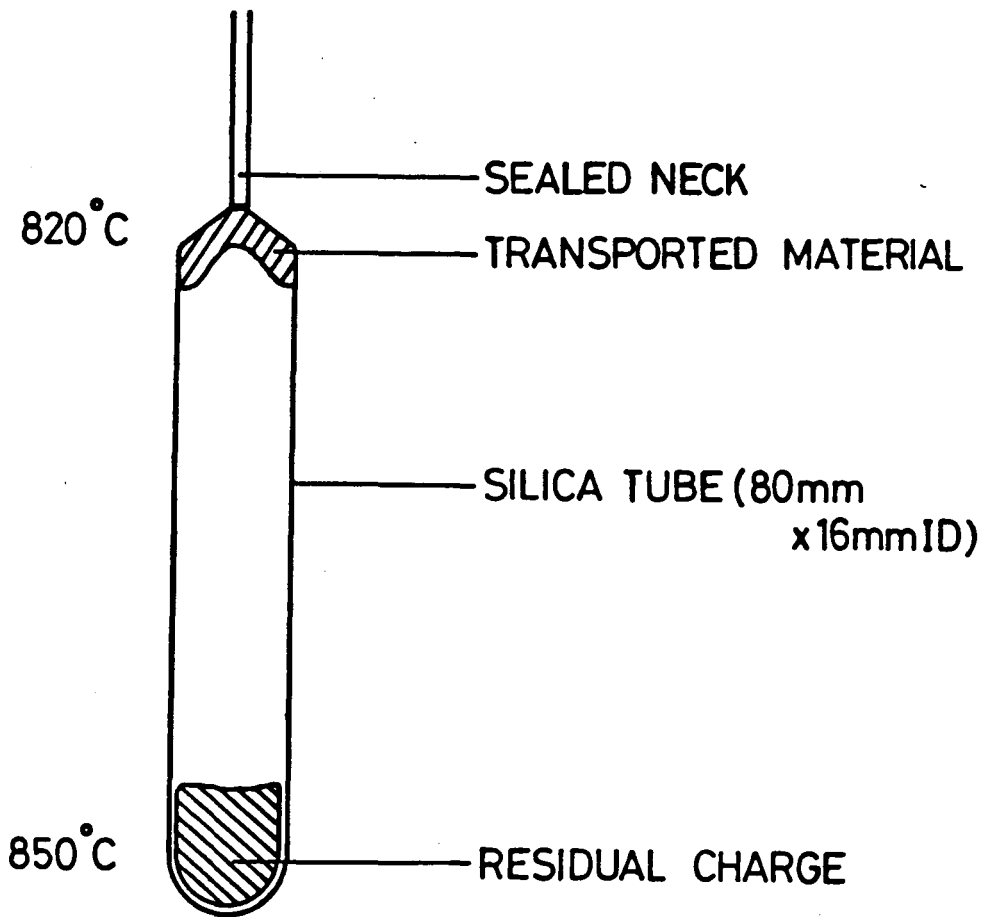


FIG.3·6 GROWTH TUBE USED FOR IODINE TRANSPORT METHOD

## CHAPTER 3: REFERENCES

- 1) LEVERENZ H.W. "Introduction to Luminescence of Solids" 475-6  
"Purification of ZnSe" Pub: Dover, New York (1968), Reprint of  
Wiley, New York (1950)
- 2) DUDDERIDGE J.L. Unpublished work performed at the G.E.C. Hirst  
Research Centre, Wembley, Middx. (1956)
- 3) ANON. Unpublished work performed at the G.E.C. Hirst Research  
Centre, Wembley, Middx (1957)
- 4) ANON. "To Prepare a Zinc Sulphide Phosphor and Measure its  
Spectral Emission Distribution" Department of Applied Physics and  
Electronics Undergraduate Teaching Experiment, University of  
Durham (1973)
- 5) THOMSEN S.M. and BUBE R.H. "High Sensitivity Photoconductor  
Layers" Rev.Sci. Instr. 26, No.7, 664-5 (July 1955)
- 6) NICOLL F.H. and KAZAN B. "Large Area High-Current Photoconductive  
Cells Using Cadmium Sulfide Powder" J. Opt. Soc. Am. 45, No.8,  
647-50 (Aug.1955)
- 7) ROTHSCHILD S. "Large-Screen, High Current Photoconductive Cells  
Using Zinc Sulfide Cadmium Sulfide, or Cadmium Sulfide, or  
Cadmium Selenide Phosphors" J.Opt. Soc. Am 46, No.8, 662-3 (1956)

- 8) MIYAKE T. "AC+DC Photoconductivities of Powdered Layers of CdS"  
Jap. J. Appl. Phys. 10, No.4, 427-33 (April 1971)
- 9) NICASTRO L.J. and OFFENBACHER E.L. "Negative Resistance in  
Cadmium Selenide Powder - Comparison of Experiment with Theory"  
R.C.A. Rev. 33, 357-76 (June 1972)
- 10) SATO K. and YOSHIKAWA M. "Voltage-current Characteristics of  
Compressed CdSe Powders" Jap. J. Appl. Phys. 13, No. 4, 630-40  
(April 1974)
- 11) BUBE R.H. "Photoconductivity of Solids" Chapter 4: Preparation of  
Photoconductors" 88-95 Pub: Robert E. Krieger, New York (1978)
- 12) MALIKOV V. Ya., KOSTENKO V.I. and SYSOEV L.A. "Improving the  
Electrical Characteristics of CdS Single Crystals Grown from the  
Melt" Inorg. Mat. (USA) 14, Pt 2, 166-8 (1978)

## CHAPTER 4: DEVICE FABRICATION

### 4.1 INTRODUCTION

Most experimental work was performed on sensitized but otherwise untreated CdSe powder samples. These samples were packed between two electrode surfaces and illuminated in a direction perpendicular to that of the applied electric field. This technique, a more detailed description of which may be found in the next chapter, was used repeatedly to obtain rapid and reliable comparisons between different sensitization techniques. For most practical applications, however, a more mechanically robust powder layer in which the directions of illumination and applied field coincide is needed. Such a layer would need to be relatively thin to achieve reasonable photosensitivity, and one of the electrodes should be transparent to the photoexcitation used.

Three general methods of improving particle to particle cohesion, and hence mechanical stability of powder samples, were tried. These may be briefly described as compaction under high pressure, sintering under high temperature or adhesion with a suitable binding agent.

Techniques similar to these used in conjunction with CdS and CdSe have been reported. Angelov and Milyashen (1) made conductivity measurements on pressed specimens of CdS, while

Thomsen and Bube (2) among others mention fabrication of sintered polycrystalline layers of activated CdS and CdSe. Sintering of CdSe powder under a pressure of 10,000 p.s.i. was used by Miller et al (3) as a stage in the preparation of CdSe liquid junction solar cells. The production of powder-binder layers in various configurations has been widely described (2,4,5). Alternative techniques for production of activated CdS layers include electrophoretic deposition from a CdS sol. (6,7) and chemical deposition from solution (8-11). Vacuum techniques include deposition by evaporation (12,13) and sputtering (14).

#### 4.2 FORMATION OF COMPRESSED PELLETS

From the published work of Sato and Yoshizawa (15) and others it is known that the observed electrical properties of CdSe powder exhibit a strong dependence on applied pressure. The extent of this dependence for extremely high applied pressure was studied by producing two compressed pellets, one from powder sample F2 and the other from a mixture of samples G4 and G4\*.

In each case 0.75g of the prepared CdSe powder was placed in a stainless steel die as shown in Fig. 4.1. The die was placed in a hydraulic press and connected to a rotary pump. A rough vacuum was produced above the powder by evacuating the cavity, from the top flat ring (bounded by neoprene 'O' ring seals) downwards, with a rotary pump. The powder was then compressed until a pressure of 3,000 p.s.i. (approximately

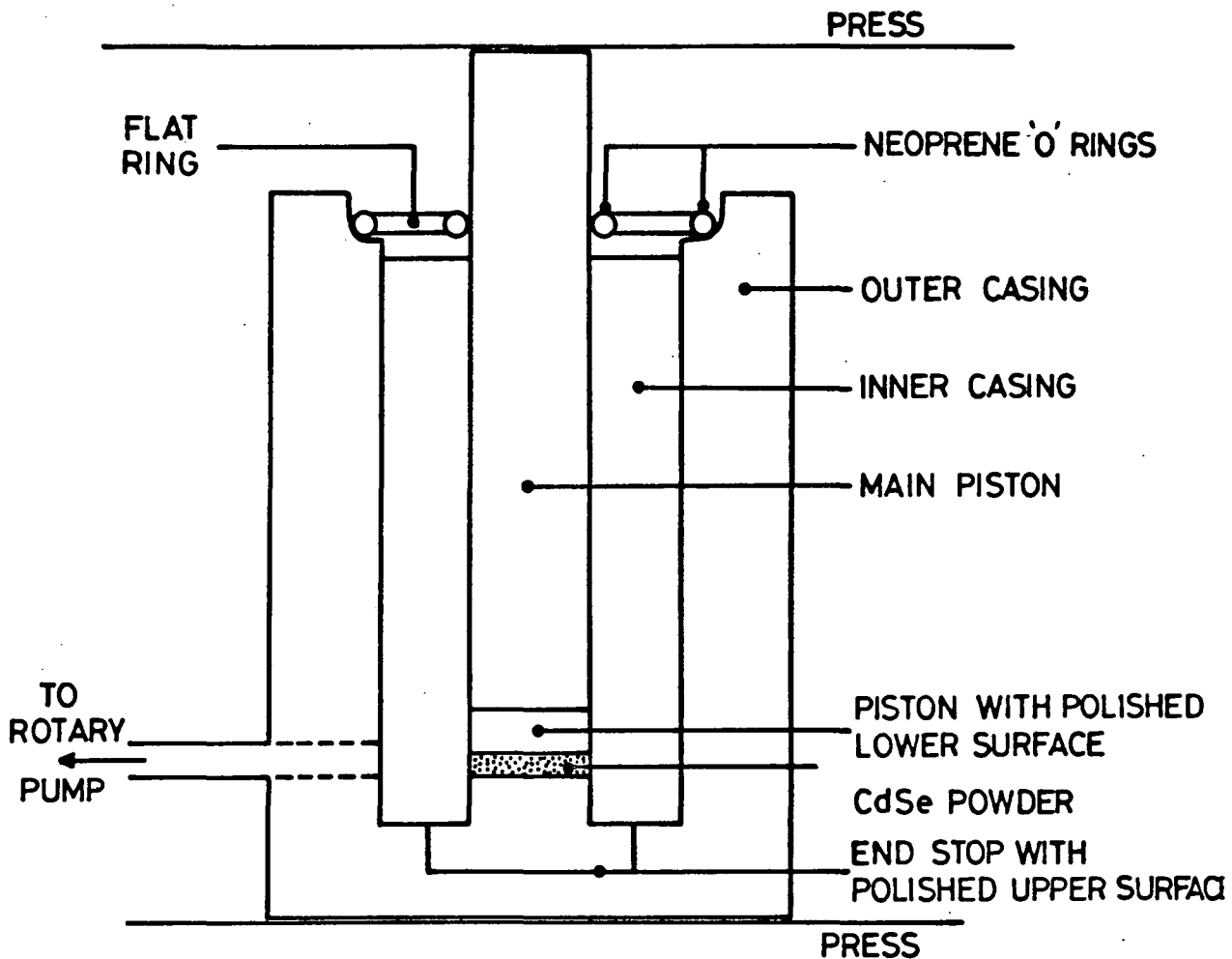


FIG. 4-1 CONSTRUCTION OF STAINLESS STEEL DIE USED TO PRODUCE COMPRESSED POWDER PELLETS (not to scale)

$2 \times 10^7$  Pa) was indicated. The die was then disconnected from the rotary pump, removed from the press and dismantled. The resulting pellet was in the form of a lustrous disc some 15 mm in diameter and between 1 and 2 mm in thickness. The flat surfaces were smooth and highly reflective, thus being almost metallic in appearance. These pellets were found to be reasonably robust but had a tendency to shed flakes if subjected to impact.

Three methods for providing electrical connections to these compressed pellets were investigated. These are shown schematically in Fig.4.2. In each case the direction of applied field was normal to the direction of illumination. In Fig. 4.2(a) two crocodile clips were simply attached to opposite sides of the pellet with a separation of approximately 2 mm between their tips.

In an attempt to improve this arrangement and provide parallel electrodes analogous to the powder test cell (c.f. Chapter 5), indium was evaporated under a pressure of some  $10^{-4}$  Torr and deposited on the pellet surface either side of a 2 mm wide masking strip. The crocodile clips were then attached to the two coated conducting regions of the pellet.

The third method used (Fig. 4.2(c)) was an attempt to produce ohmic contacts to the pellet bulk by a technique developed by Smith (16) which has been widely used since then in conjunction with II-VI single crystals.

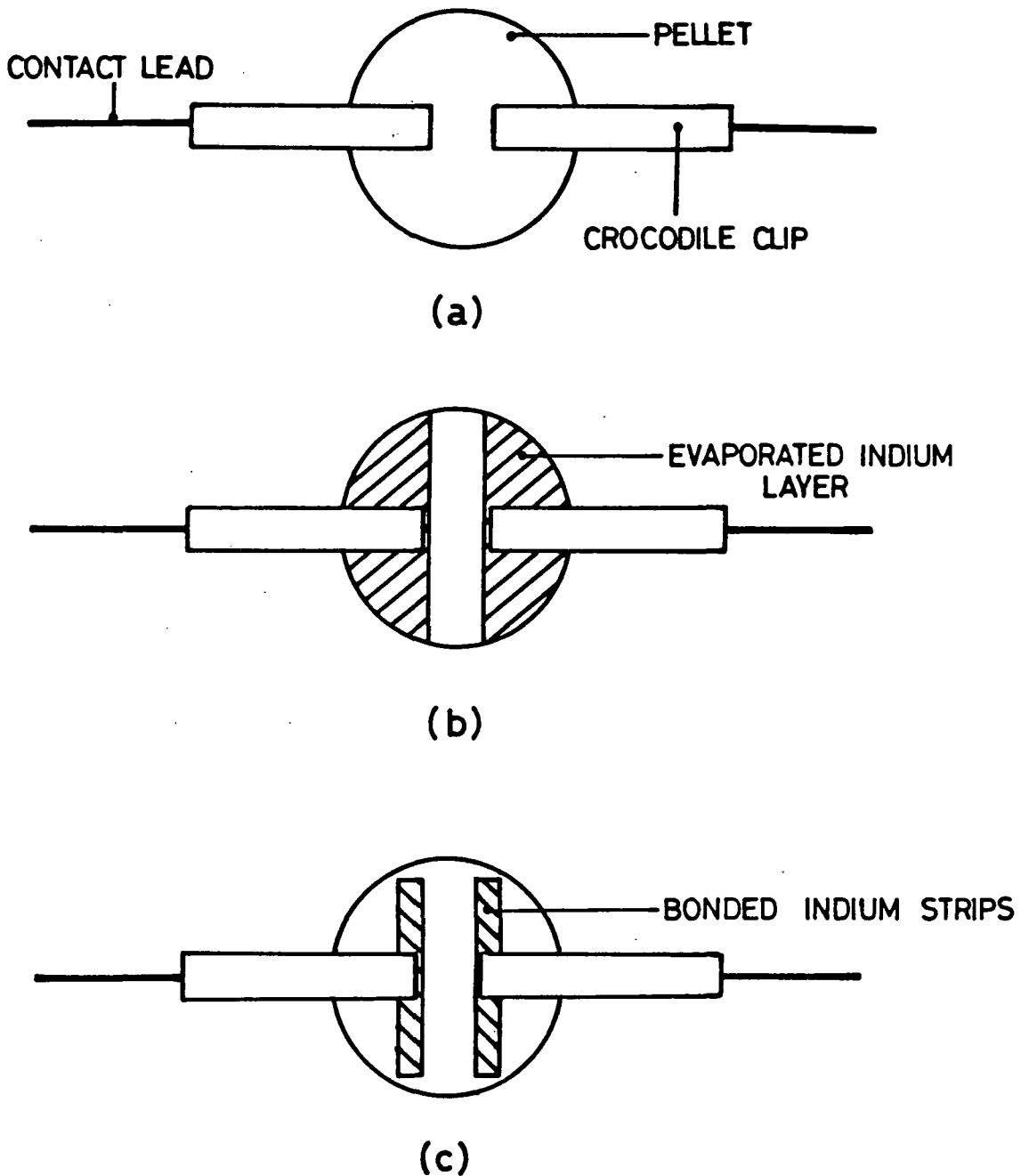


FIG.4·2 PELLET ELECTRODE ARRANGEMENTS (not to scale)  
 (a) CROCODILE CLIPS SIMPLY ATTACHED TO PELLET SURFACE  
 (b) VACUUM DEPOSITED INDIUM ELECTRODE PATTERN PRODUCED BY MASKING  
 (c) PARALLEL BARS OF INDIUM BONDED TO , AND PARTIALLY DIFFUSED INTO , THE PELLET BY HEAT TREATMENT

A length of 1.5 mm diameter indium wire was cleaned by etching it for approximately 30 seconds in concentrated nitric acid and then thoroughly rinsing in distilled water. A 15 mm section of this wire was then cut in half longitudinally to produce two semi-circular strips. These were placed parallel to each other, flat surface downwards, and separated by some 2 mm, on one of the flat faces of the pellet. The pellet and strips were then placed in an inert argon atmosphere and heated for 30 minutes by an electric filament maintained at 350°C. This treatment caused the indium to melt and bond to the surface of the pellet. Also it was hoped that some of the indium had diffused into the bulk material close to the pellet surface as has been shown to occur with single crystals of CdSe and CdS. Crocodile clips were then attached to the indium strips.

#### 4.3 FORMATION OF SINTERED LAYERS

The tendency of some doped powder samples to form hard, sintered agglomerates during the main firing was noticed on many occasions. Thus it was hoped to put this usually undesirable effect to advantageous use by forming powder layers before firing.

A quantity of 3 mm transparent-grade silica sheet was cut into rectangular slides measuring about 3 x 2 cm. A slurry was produced by mixing together CdSe powder with dopant solutions (details as for sample V2 in Fig. 3.4). Excess solvent was

removed from this slurry until it became like paste in consistency. It was then spread onto the silica slides and further dried in a stream of hot air. When all visible traces of moisture had disappeared the slides were inserted into a larger than usual (2.5 cm i.d.) transparent grade silica firing tube and fired for 90 minutes at 600°C using the porous plug technique. A cross section of this arrangement is represented in Fig. 4.3.

Indium electrode regions were produced by evaporation under vacuum through a suitable aluminium foil mask, the gap between the electrodes being approximately 1 mm in width and 10 mm in length. Each sample was then heated for 30 minutes at 250°C again using the porous plug method, to promote diffusion of some of the indium into the surface region of the sintered material. Contact leads were attached to the electrode areas, as shown in Fig. 4.4, by means of thermo-setting silver/epoxy paste. As in the case of the compressed powder pellets, the direction of applied electric field was normal to the direction of illumination.

#### 4.4 FORMATION OF PROTOTYPE POWDER-BINDER LAYERS

The photoconductive characteristics of sensitized CdSe powder mixed with a 5% nitrocellulose in butyl acetate solution binder (volume ratio approximately 4:1) were investigated using two different configurations. As can be seen from Fig. 4.5, the direction of the applied electric field is normal to the

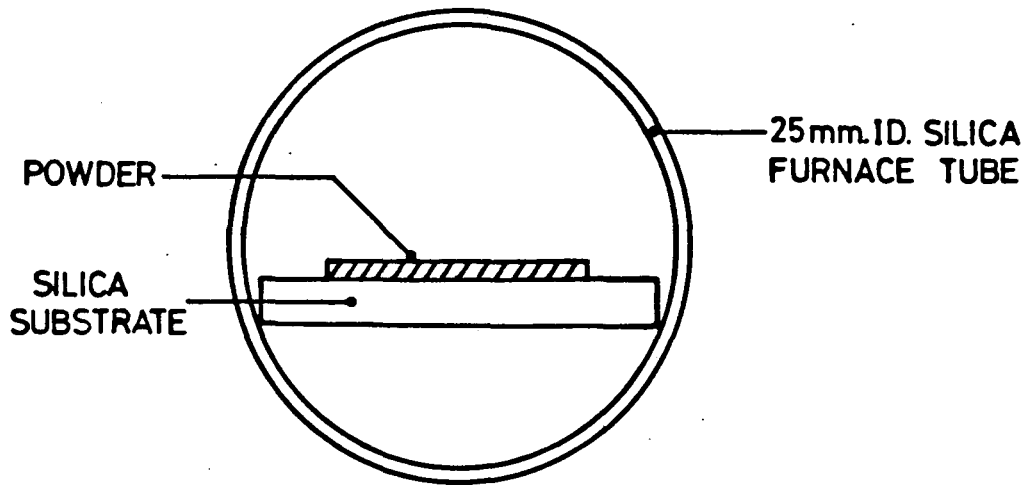


FIG.4.3 (not to scale) CROSS SECTION SHOWING ARRANGEMENT FOR FIRING SINTERED POWDER LAYERS USING POROUS PLUG METHOD

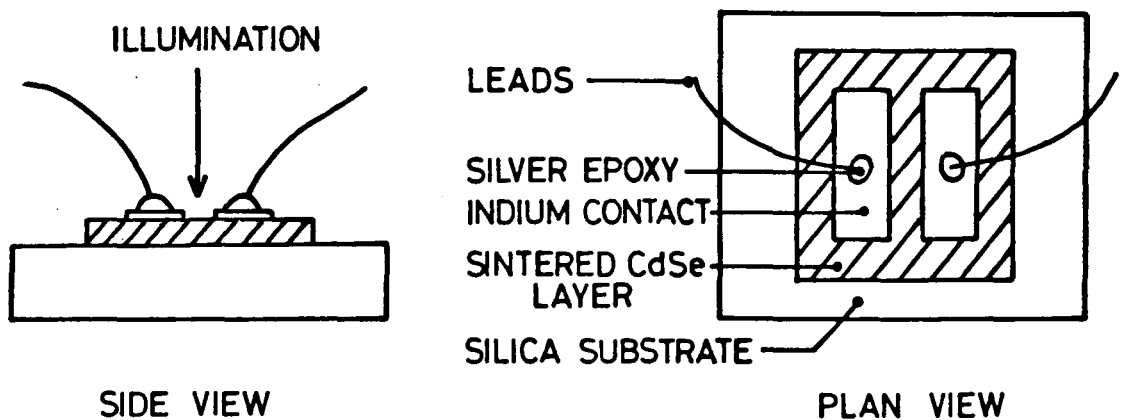
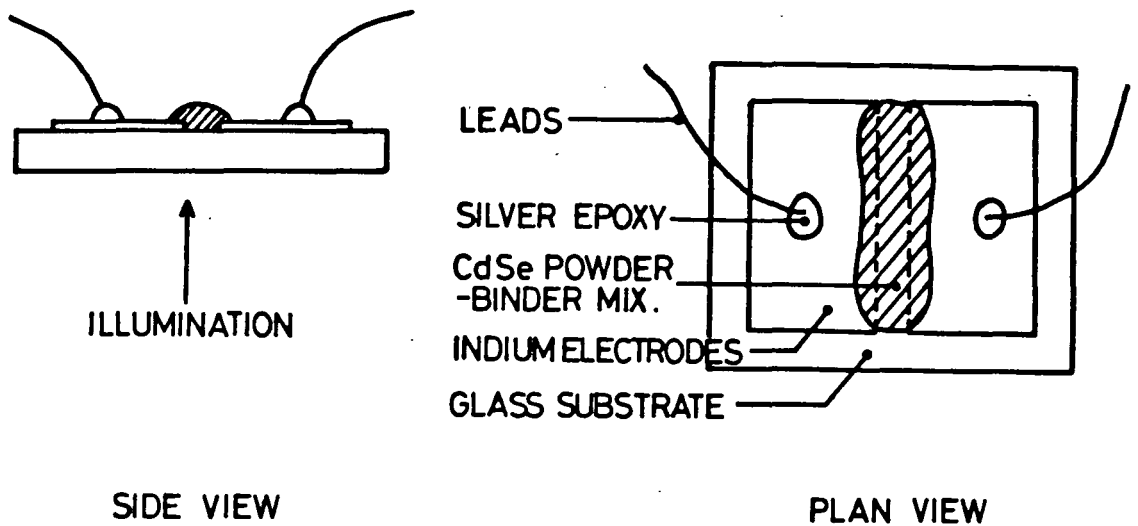
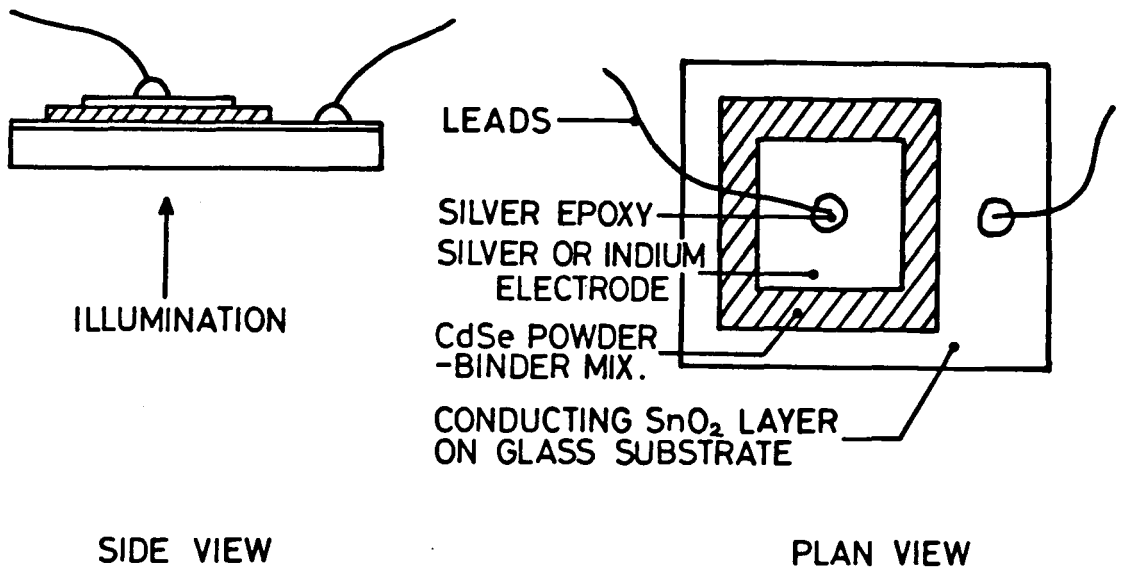


FIG.4.4 (not to scale) SINTERED POWDER LAYER ELECTRODE CONFIGURATION



(a)



(b)

FIG. 4·5 (not to scale) PROTOTYPE POWDER - BINDER LAYER ELECTRODE CONFIGURATIONS

(a) APPLIED FIELD NORMAL TO ILLUMINATION THROUGH SUBSTRATE

(b) APPLIED FIELD PARALLEL TO ILLUMINATION THROUGH SUBSTRATE

direction of illumination (a) in one arrangement and parallel in the other (b).

Fabrication of the first arrangement was commenced by preparing a clean microscope slide and depositing indium electrode areas by evaporation in vacuo through a suitable mask. The resultant conducting films were about 1 cm in width and 1 mm apart. A quantity of powder-binder mixture was prepared by thoroughly stirring together some sensitized CdSe powder and about one quarter of the volume of 5% nitrocellulose in butyl acetate solution with a glass rod. When the mixture reached a smooth, paste-like consistency it was pressed onto the microscope slide so that it formed a layer about 1 mm thick covering part of each electrode area and all of the gap between them. Excess butyl acetate was removed by gentle heating in a drying oven to produce a mechanically robust agglomeration. Contact leads were attached to the remaining exposed region of each indium electrode by means of thermo-setting silver/epoxy paste. The sample was illuminated through the thickness of the microscope slide onto the region in contact with the inter-electrode gap.

The second arrangement (Fig.4.5(b)) was fabricated on a conducting 'Nesa' glass substrate. The conducting layer (tin oxide deposited under vacuum) offers minimal attenuation to visible light. A thinner, more fluid powder-binder mixture was prepared by thoroughly mixing  $n$  grams of sensitized CdSe powder with  $2n$  ml of excess butyl acetate. Although this mixture

appeared to be relatively free-running it proved impossible to spray it using a simple compressed air gun owing to the CdSe powder particle size and density prohibiting the formation of an even suspension. Instead the mixture was poured onto the conducting surface of the substrate and allowed to flow freely before being dried in the oven. Two different techniques for producing the second electrode (approximately 1 cm x 1 cm square) to complete the sandwich structure were attempted; conducting silver paint was sprayed through a cardboard mask or, alternatively, indium was evaporated under vacuum through a similar aluminium foil mask. Connecting leads were attached to these electrodes and to the conducting substrate by means of silver/epoxy paste, and the completed devices were again illuminated through the substrate.

Powder sample V2 was used to make both types of device, thus enabling direct comparison with the sintered layer structure. In addition, several powder-binder devices of the former type were produced using powder sample 8 (see Fig.3.4 for details).

#### 4.5 FORMATION OF SCREEN PRINTED POWDER-BINDER LAYERS

Investigation of the electrical behaviour of the sandwich type devices described in the preceding section yielded disappointing results, each device tending to act either as an open circuit or a short circuit under all photoexcitation

conditions. These extremes of behaviour were due to excessive thickness resulting in a large dark series resistance or pinholes leading to localised conducting paths between electrodes. Clearly a more controlled means of determining the powder-binder layer thickness was required.

Amalnerkar et al (17) describe a screen printing technique for producing thick films of photoconducting CdS. This method was adapted for use with CdSe powder as follows.

Ten grams of Merck CdSe powder was placed in a ball mill together with a quantity of anhydrous, 99.999% pure CdCl<sub>2</sub> and CuCl<sub>2</sub> crystals. Typical proportions by weight were around 10% (CdCl<sub>2</sub>.2½H<sub>2</sub>O) and 0.05% (CuCl<sub>2</sub>.2H<sub>2</sub>O), adjusted for the lack of hydration. Two tungsten-carbide balls each about 1 cm in diameter were used to mill the dry mixture in air for 2 hours. After milling, the mixture was transferred to a transparent grade silica furnace tube, sealed using a porous plug without flushing, and fired in air for 2 hours at 500°C (cf. Chapter 3, Section 3, Part 3A for full details).

After it had cooled to room temperature the fired mixture was ball milled again, this time together with some 30ml of 'Analar' grade acetone, for 30 minutes and then allowed to dry in air for several hours. When all traces of acetone had vanished from the activated CdSe:Cu:Cl powder it was thoroughly mixed with 5% nitrocellulose in butyl acetate solution in a ratio of approximately 3:1 (powder:liquid). The resultant paste

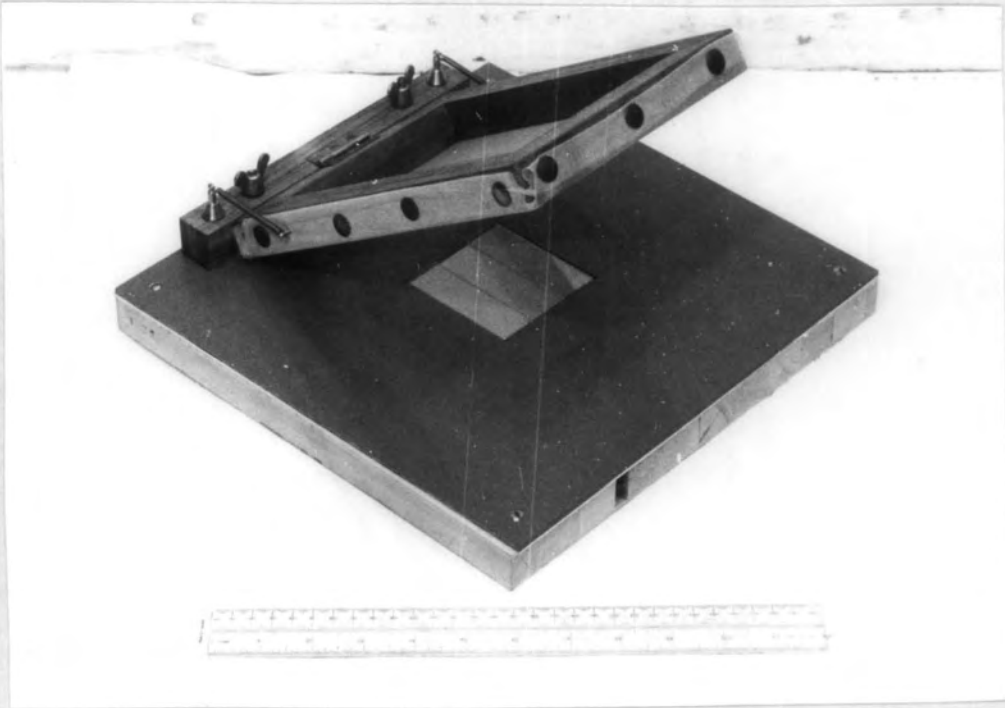
was of a consistency suitable for screen printing, and was deposited onto the pre-cut conducting glass substrates using the equipment shown in Fig. 4.6. The screen material used was a monofilament nylon fabric with a mesh size of c0.2 mm. The freshly coated substrates were placed in the drying oven at 85°C for about an hour to remove any excess butyl acetate. They were then fired, in batches of three, for 10 minutes at 600°C in a flowing inert (oxygen-free nitrogen) atmosphere in the firing tube shown in Fig. 4.7. The position of each slide in the tube was noted since the temperature at the extremes of their combined length was reduced to around 550°C. The nitrogen flow was maintained while the samples cooled to room temperature. The resistance between the exposed ends of the conducting substrate was found to be between 1 and  $2K\Omega$ , which is negligibly low in this context and confirms the suitability of this type of substrate for short duration heat treatment.

Ten circular electrodes were deposited on each screen-printed photoconducting layer, half of these were 2 mm and half were 4 mm in diameter. These were formed by evaporating gold or indium, in a vacuum of around  $2 \times 10^{-5}$  Torr, through a pre-formed brass contact mask with bevelled edges to prevent shadowing. A contact lead was stuck to the exposed substrate region, the second connection being made by pressing a gold ball against one of the circular electrodes using a micromanipulator.

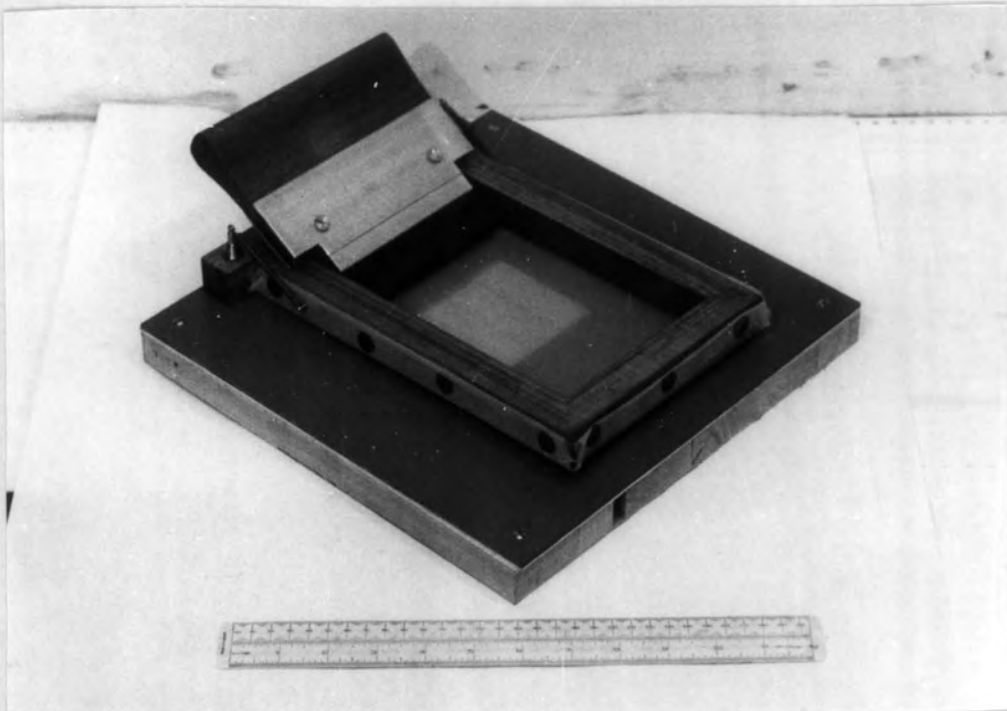
Several screen printed devices were fabricated under a

variety of conditions. A tabular listing of these samples is given in Fig. 4.8.

The photograph of Fig.4.9 shows several of the fabricated devices which have been described in this chapter.



a) Open, showing three substrate slides in position.



b) Closed, ready for addition of powder-binder mixture and printing.

Fig.4.6: Screen printing equipment.

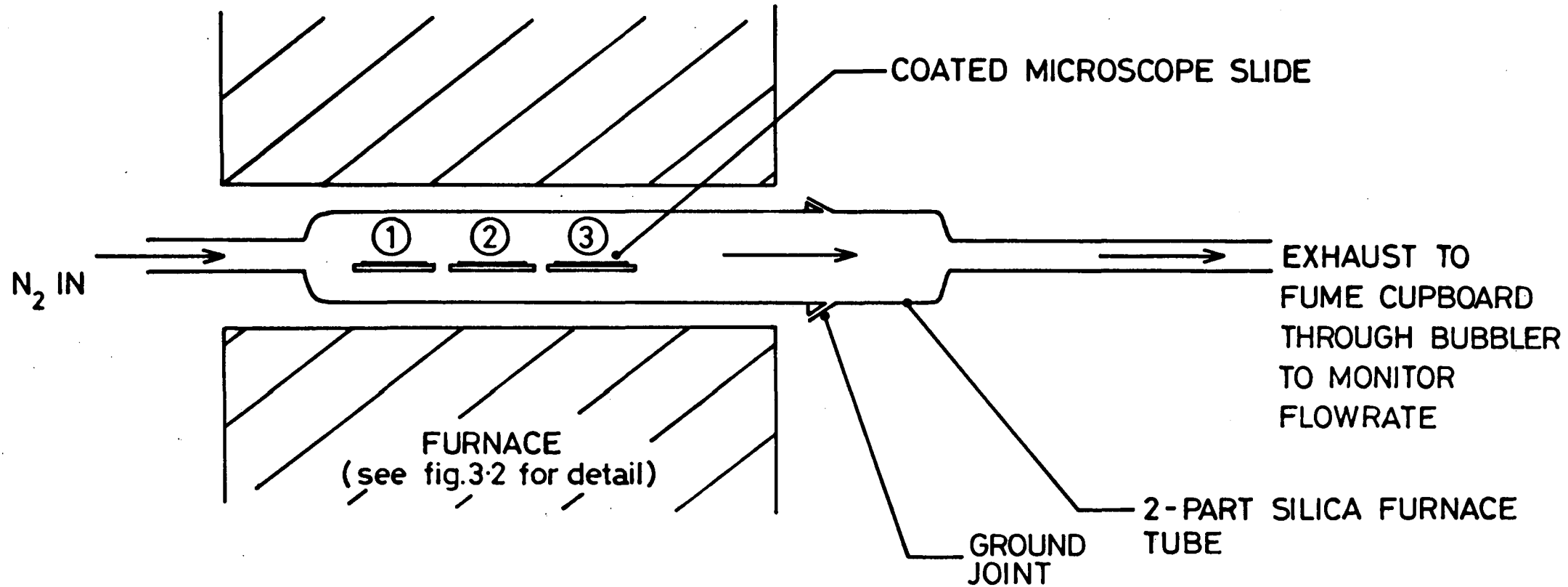


FIG. 4·7 (not to scale) APPARATUS FOR FIRING SCREEN PRINTED POWDER-BINDER LAYERS IN AN INERT ATMOSPHERE

POSITIONS ① ② ③ ARE REFERRED TO IN FIG.4·8

4-8 CHART SHOWING SCREEN PRINTED POWDER - BINDER LAYER PREPARATION CONDITIONS

SUB - SERIES	POWDER CONSTITUENTS					DRYING AFTER 30min BALL - MILLING WITH 30ml. ACETONE		DRYING AFTER SCREEN PRINTING		SUBSTRATE MAT'L. N = NESA GLASS M = MICRO SLIDE	FIRING POSITION (see FIG. 4-7)	ESTIMATED FIRING TEMPERATURE (°C)	ELECTRODE MATERIAL	STORAGE CONDITIONS			
	MERCCK CdSe (g)	ANHYDROUS 99.999% CuCl <sub>2</sub> (g)	ANHYDROUS 99.999% CdCl <sub>2</sub> (g)	PURISS. AR. CuSO <sub>4</sub> IN MEOH (ppm)	PURISS. AR. CdI <sub>2</sub> IN MEOH (ppm)	TEMP (°C)	TIME (HRS)	TEMP (°C)	TIME (HRS)					or AIR (A)	VACUUM (V)	DARK (D) or LIGHT (L)	TIME ELAPSED BEFORE TEST (DAYS)
A B C D E F	10	3x10 <sup>-4</sup>	6x10 <sup>-1</sup>	-	-	20	40	85	0.75	N	1	550-600		V	D	13	
										N	2	600	Au	A	D	10	
										N	3	600-550	Au	A	L	7	
										M	1-2	575-600	-	A	L	-	
										M	2-3	600-575	-	A	L	-	
										M	NOT FIRED	-	A	L	-		
A B C D E F	10	3x10 <sup>-3</sup>	1.2x10 <sup>-1</sup>	-	-	85	16	85	1	N	1	550-600	Au	V	L	6	
										N	2	600	Au	V	D	-	
										N	3	600-550	Au	A	L	6	
										N	1-2	575-600	Au	A	D	-	
										N	2-3	600-575	-	A	L	-	
										N	NOT FIRED	-	A	L	-		
A B C	10	-	-	50	20K	60	16	60	3	N	NOT FIRED	In	V	D	3		
										N	2	600	In	V	D	3	
										M	1	550-600	-	A	L	-	

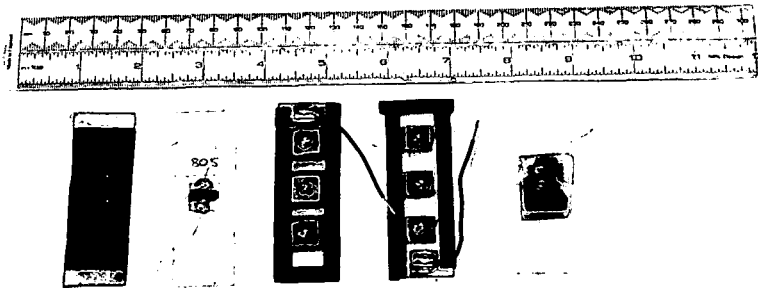


Fig. 4.9: General view of some fabricated devices showing (from left to right):

- a) Screen printed powder-binder layer on "Nesa" glass substrate.
- b) Prototype powder-binder device in which the applied field is normal to illumination through the substrate (Fig.4.5(a)).
- c) Prototype powder-binder device in which the applied field is parallel to illumination through the substrate (Fig.4.5(b)).  
The three square top electrodes are evaporated indium.
- d) As c), but electrodes are sprayed silver paint.
- e) Prototype sintered powder layer (Fig.4.4).

CHAPTER 4: REFERENCES

- 1) ANGELOV A. and MILYASHEN M. "Photoconductivity and Electrically Stimulated Currents in Pressed Specimens of CdS" Annual of University of Sofia Faculty of Physics 64, 219-228 (1970-72)
- 2) THOMSEN S.M. and BUBE R.H. "High Sensitivity Photoconductor Layers" Rev. Sci. Instr. 26, No. 7, 664-5 (July 1955)
- 3) MILLER B. et al. "Solar Conversion Efficiency of Pressure Sintered CdSe Liquid Junction Cells" J. Electrochem. Soc. 124, No.7, 1019-21 (July 1977)
- 4) ROTHSCHILD S. "Large-Screen High Current Photoconductive Cells Using Zinc Sulfide Cadmium Sulfide, or Cadmium Sulfide, or Cadmium Selenide Phosphors" J. Opt. Soc. Am. 46, No. 8, 662-3 (1956)
- 5) MIYAKE T. "AC + DC Photoconductivities of Powdered Layers of CdS" Jap. J. Appl. Phys. 10, No.4, 427-33 (April 1971)
- 6) WILLIAMS E.W. et al. "The Electrophoresis of Thin Film CdS/Cu<sub>2</sub>S Solar Cells" Solar Cells 1, 357-66 (1979/80)
- 7) UENO Y. et al. "Electrophoretically Deposited CdS and CdSe Anodes for Photoelectrochemical Cells" J. Electrochem. Soc. (USA) 130, No.1, 43-7 (Jan.1983)

- 8) CROITORU N. and JAKOBSEN S. "Properties of CdS Films and  $\text{Cu}_2\text{S}$ -CdS Junctions Prepared by Chemical Printing" Thin Solid Films 56, L5-7 (1979)
- 9) KAINTHLA R., PANDYA D. and CHOPRA K. "Photoelectronic Properties of Solution-Grown CdSe Films" Solid State Elec. 25, No.1, 73-6 (Jan.1982)
- 10) BOUDREAU R. and RAUH R. "Chemical Bath Deposition of Thin Film Cadmium Selenide for Photoelectrochemical Cells" J. Electrochem. Soc. (USA) 130, No.2, 513-6 (Feb.1983)
- 11) SOO-ILL LEE et al. "Optical Properties of Polycrystalline CdSe Films Prepared by a Bath Deposition Method" New Physics (Korean Phys.Soc.) 23, No.3, 294-9 (Sept.1983)
- 12) KARPOVICH I.A., OMAROV A.M. and ZVONKOV B.N. "Field Effect in Photosensitive CdSe Films" Sov. Phys. - Semicond. 2, No.3, 133-8 (Aug.1968)
- 13) KARPOVICH I.A., RIZHAKHANOV M.A. and KALININ A.N. "Surface Impurity Photoconductivity in CdSe Films" Sov. Phys. - Semicond. 4, No. 10, 1709-10 (April 1971)
- 14) ENIKEEVA K. and VERGUNAS F. "Role of Activation Powder in the Production of Thin-Film Photoresistors" Izv. Akad. Nauk. SSSR Neorg. Mater. 8, Pt 6, 1008-10 (1972)

- 15) SATO K. and YOSHIZAWA M. "Voltage-Current Characteristic of Compressed CdSe Powders" Jap. J. Appl. Phys. 13, No.4, 630-40 (April 1974)
  
- 16) SMITH R.W. "Properties of Ohmic Contacts to Cadmium Sulphide Single Crystals" Phys. Rev. 97, No.6, 1525-30 (15 March 1955)
  
- 17) AMALNERKAR D.P. et al. "Studies on Thick Films of Photoconducting CdS "Bull. Mater. Sci. 2, No.4, 251-64 (Nov 1980)

## CHAPTER 5: EXPERIMENTAL WORK

### 5.1 INTRODUCTION

The physical and electronic properties of powder samples were investigated before, during and after preparation using a variety of techniques. Some degree of correlation between observed physical nature and measured electronic performance was sought.

Physical analysis yielded information about the topography, structure and chemical nature of powder samples. A scanning electron microscope was used to investigate the topography of various powder samples and some fabricated devices. The crystallographic structure of samples following a variety of treatments was examined using standard X-ray powder photography and diffractometry, and on one occasion by operating a transmission electron microscope in the RHEED (Reflected high energy electron diffraction) mode. Chemical changes in the gaseous phase during powder sensitization were investigated by monitoring the firing of several samples with a mass spectrometer.

Measurements of electronic behaviour were made for all powder samples and devices which were produced. These measurements concentrated on the most pertinent aspects of photoconductive performance, namely magnitude and rate of response under a variety of conditions. The dependence of these

characteristics upon changes in photoexcitation, applied electric field and physical pressure were investigated.

## 5.2 INVESTIGATION OF TOPOGRAPHY

A Cambridge Instruments S600 scanning electron microscope (SEM), operated in the secondary emission mode, was used to examine particle topography and size distribution in various powder samples. The overall structure of some fabricated devices was also investigated. Use of this instrument enabled high magnifications to be achieved with specimen detail resolution better than 25nm under satisfactory operating conditions. Combined with this was a depth of field at least 300 times greater than that of a conventional optical microscope at the limit of resolution. A range of true image magnifications up to 10,000X was used.

The SEM was operated with an accelerating potential of around 7.5 kV. On striking the specimen material the incident electrons were either reflected from the surface or produced sufficient excitation in the bulk of the specimen material close to the surface to generate secondary electrons which were subsequently emitted. These were drawn to the collector by means of a negatively biased grid.

Loose powder samples were prepared for examination as shown in Fig. 5:1. A small quantity of powder was sprinkled onto the

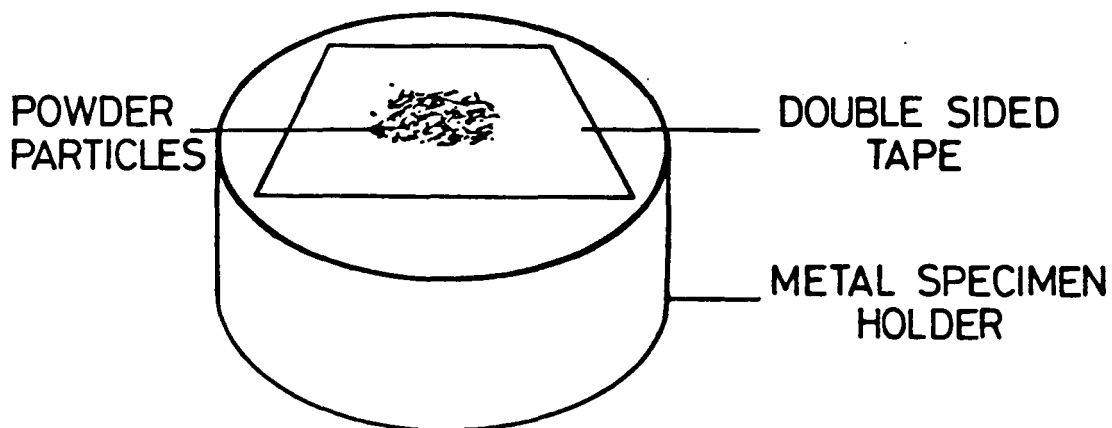


FIG.5.1 PREPARATION OF POWDER SAMPLES FOR EXAMINATION IN THE SCANNING ELECTRON MICROSCOPE

exposed surface of a portion of double sided adhesive tape which was stuck to the pallet. Excess powder was removed by gently tapping the pallet prior to insertion in the SEM. Charge storage with this arrangement was sometimes apparent but only on one occasion severe enough to seriously impair image formation. A variety of treated and untreated CdSe powder samples were examined in this way.

The overall structure of the screen printed powder-binder layers was investigated by breaking off a small portion of the coated substrate and attaching it to the pallet with suitable adhesive lacquer. Different sample orientations enabled both the exposed surface and the cross section of the deposited layer to be examined.

### 5.3 CRYSTALLOGRAPHIC ANALYSIS

Three techniques were used to investigate the changes in the crystallographic structure of various powder samples produced by different treatments.

Loose powder samples were prepared for X-ray analysis in a Debye-Scherrer powder camera by adhering a small quantity of each sample with collodium to a glass fibre. This was then rotated under exposure to a collimated beam of nickel-filtered copper  $K_{\alpha}$  radiation. The two components of this radiation have wavelengths of 1.54050 Å ( $K_{\alpha 1}$ ) and 1.54434 Å ( $K_{\alpha 2}$ ), and occur with intensities in a ratio of approximately 2:1. Thus when

doublets could not be resolved, a weighted mean wavelength of 1.54178 Å was used in calculations. Typically the X-ray generator was operated with a target potential of around 40 kV and a beam current of about 20mA. Exposure times ranged between 15 and 150 minutes.

An X-ray diffractometer provided an alternative and more convenient method of powder analysis, and was also useful for examining the structure of particles contained in fabricated layers. Loose powder samples were prepared for examination by sprinkling a small quantity of powder onto a clean glass slide, adding a few drops of acetone and spreading the resultant slurry around until an approximately uniform layer was produced. This quickly dried at room temperature. Copper  $K_{\alpha}$  radiation was again used with a similar target potential and beam current. The detector output was connected through a variable gain amplifier to an X-t chart recorder, and the diffracted radiation was scanned at a rate of one degree of arc per minute.

The structural nature of the immediate face of a screen printed powder-binder layer was examined using a transmission electron microscope operated in the RHEED mode. High energy electrons were directed towards the sample surface at a very low angle of incidence of up to a few degrees. The incoming beam may be diffracted in one of two possible ways depending on the smoothness of the surface, as shown in Fig. 5.2.

If the surface of the specimen is very smooth (Fig.5.2(b)), the electrons will penetrate the surface and be reflected by

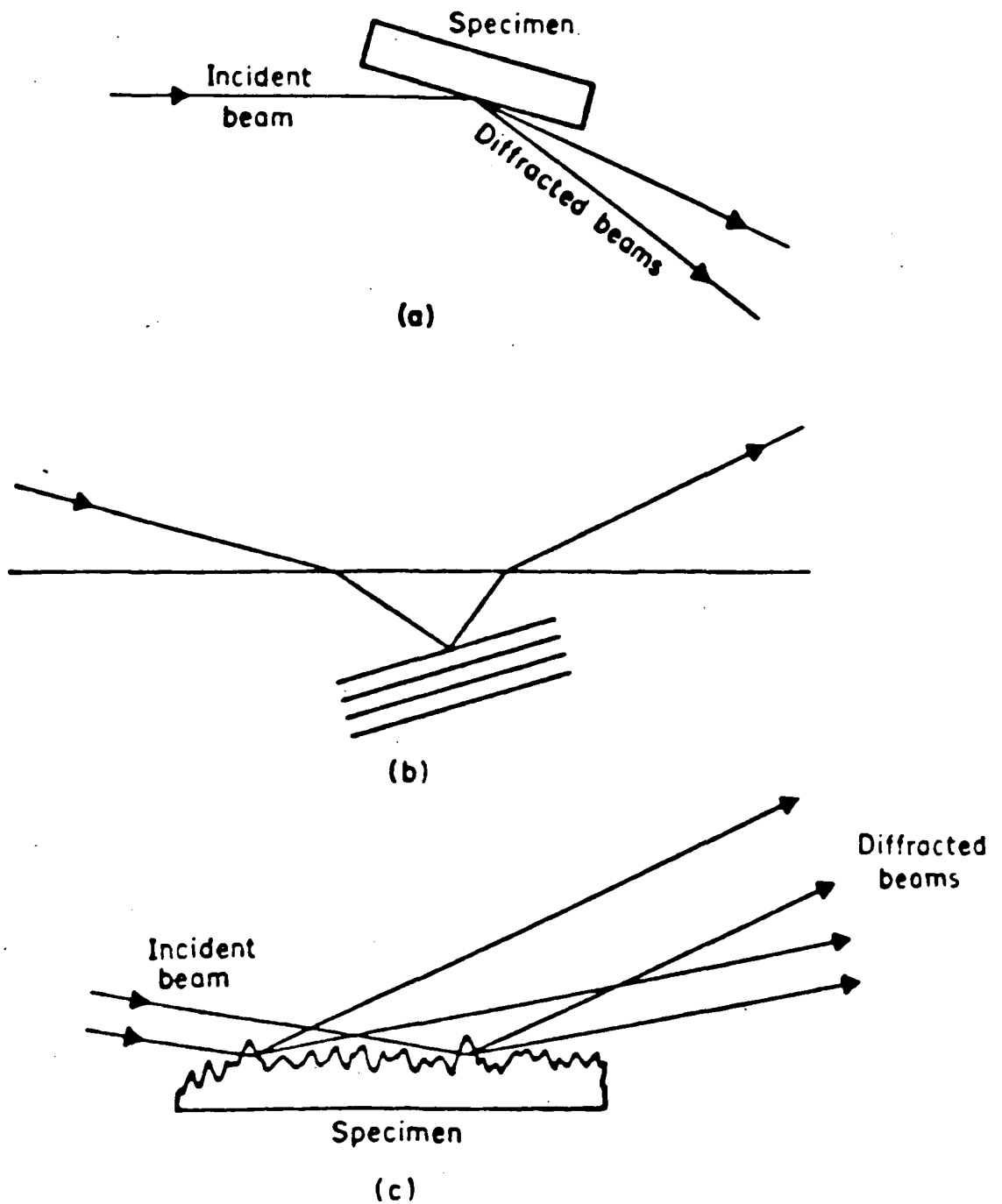


FIG. 5.2 TWO ALTERNATIVE MODES OF ELECTRON BEAM DIFFRACTION, DEPENDING ON SURFACE ROUGHNESS.  
 (from "ELECTRON DIFFRACTION" by T.B.Rymer, pub. Methuen 1970)

planes of atoms with suitable orientations. On entering and leaving the surface at a small grazing angle, the electrons are refracted through an appreciable angle because of the internal electrostatic potential of the solid. This refraction tends to distort the overall pattern produced by the emergent beams. However, electrons striking a rougher surface (Fig.5.2(c)) having irregularities of a few hundred angstroms or more do not enter or leave the solid at a small grazing angle, and thus refraction effects are negligible. It was hoped that the CdSe powder particle size would provide sufficient surface roughness for the latter circumstances to prevail.

#### 5.4 CHEMICAL ANALYSIS

The Chemical processes which occur in the gaseous phase during firing of both doped and untreated CdSe powder samples were investigated using an AEI MS10 mass spectrometer.

The untreated powder sample consisted of some 5g of Merck CdSe which was loaded into a 6mm internal diameter transparent grade silica tube close to the sealed end. The tube was then evacuated overnight through a bypass valve to a pressure of approximately  $10^{-6}$  Torr. A scan of background gases at room temperature having mass numbers ranging from 1 to 90 was then made. The bypass valve was closed and a controlled leak brought into operation. A horizontal electric furnace was used to heat the powder sample to 1000°C in 200 degC intervals, a scan from

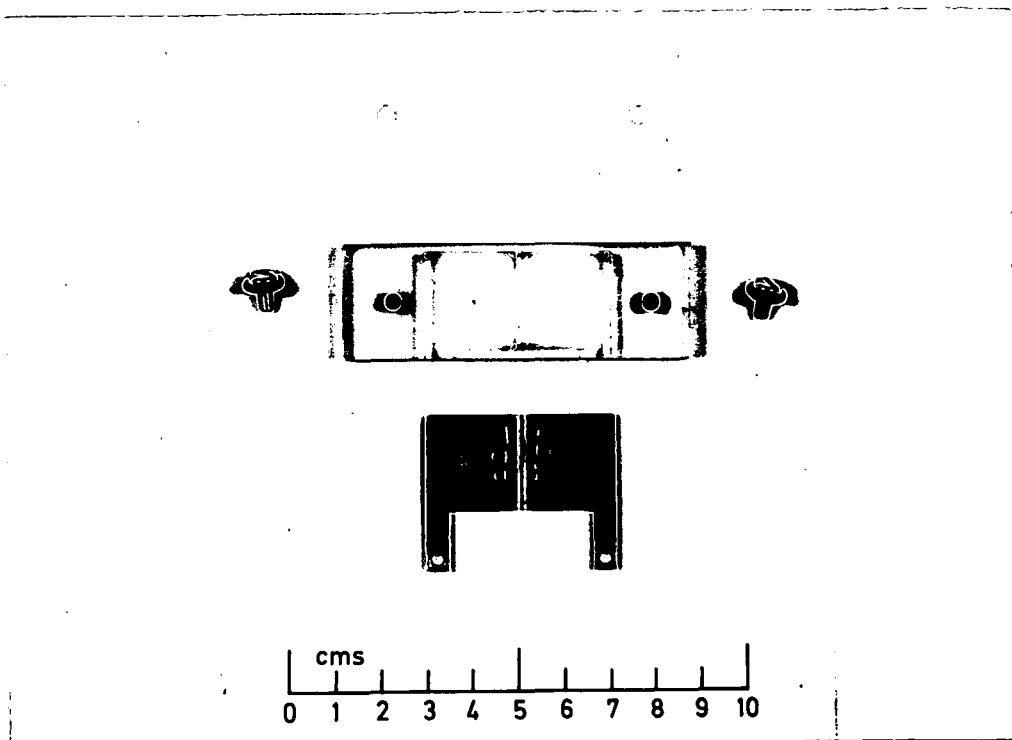
mass numbers 1 to 90 being made at each stage. A temperature-time curve representing this process is given with the results in Chapter 6.

The treated powder sample was prepared by doping 3g of Merck CdSe with 20,000 p.p.m. Cerac 99.999% CdI<sub>2</sub> and 1,000 p.p.m. Analar Puriss A.R. CuSO<sub>4</sub>, Analar methanol being used as the solvent in each instance. Further details are given in Fig.3.4 (Powder sample X1). Again a scan was made of the background gases at room temperature. The sample was heated to 600°C, further scans being made at 200°C and 400°C. The firing temperature was maintained at 600°C for 130 minutes during which another scan was made, and the final scan was made when the tube and contents had returned to room temperature following removal of the furnace.

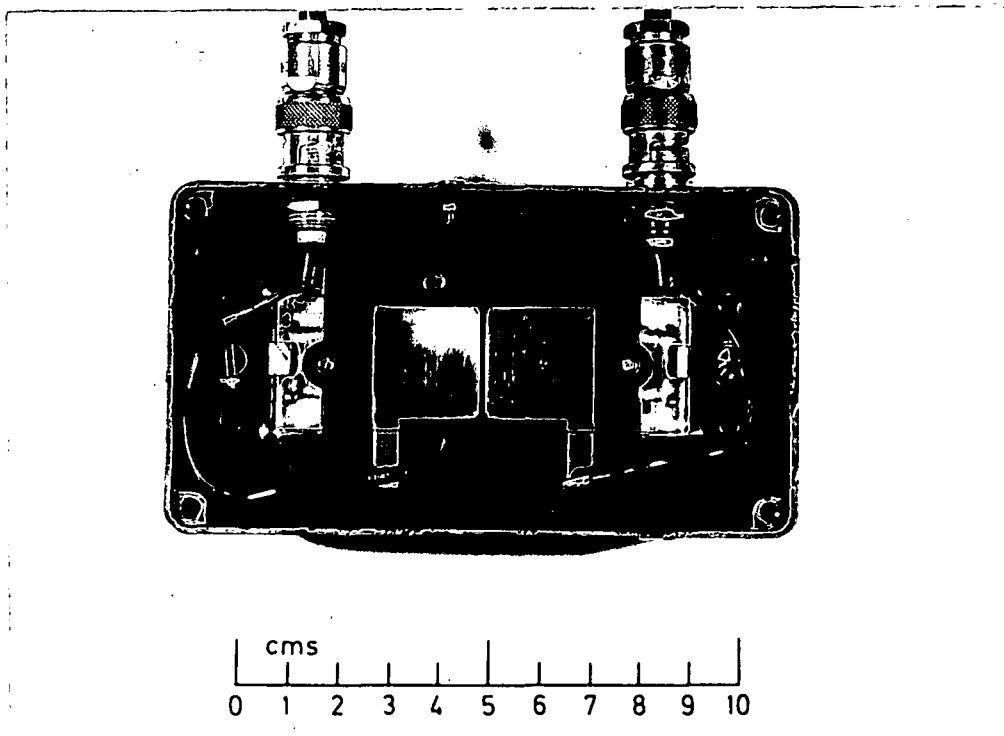
## 5.5 POWDER TEST CELL CONSTRUCTION

Two major physical problems are associated with electrical measurements made on loose powder samples: forming suitable electrical contacts and achieving reproducible packing densities. Both of these factors will affect measured electronic behaviour.

The initial powder test cell used is shown in Fig.5.3. The removable electrodes were prepared from 2mm copper sheet, the surfaces in contact with the powder samples being coated with an evaporated layer of indium. This layer, which required periodic



a) Fixed electrode powder test cell components: glass cover plate, perspex base with fixing screws, indium coated copper electrodes.



b) Rear view of powder test cell mounted in holder. Back cover plate has been removed.

Fig. 5.3: Fixed electrode powder test cell and holder.

renewal due to abrasion by the powder samples, was intended to reduce the work function between the CdSe powder and electrode surfaces to an acceptably low level. The electrodes were a flush fit into a recessed perspex block, separation being maintained by a raised dividing strip 1mm in height and width. Powder samples were packed into the resultant cavity with a spatula and a metal pressing tool of suitable dimensions. This arrangement produced opposed parallel electrode surfaces of 20 x 1mm separated by a 1mm powder-filled gap. A glass retaining cover made from a microscope slide was held in place by two bolts prior to mounting the test cell in the holder as shown. Contact leads were attached to the protruding tabs of the two electrode blocks, and external connections were provided by two BNC leads, the screening braid of each being electrically connected to the metal holder chassis. A metal backplate was bolted onto the chassis, and the powder samples were illuminated through the glass retaining cover via a central circular aperture 11mm in diameter. Scattering of reflected light within the test cell holder was minimised by painting all internal surfaces matt black.

This arrangement provided easy access to its components for cleaning and allowed rapid changeover of samples. It did not, however, guarantee reproducible packing densities and was therefore replaced by a more sophisticated and versatile system. The second powder test cell, which was used for measurements on all powder samples from W1 onwards (c.f. Fig.3.4), will now be described.

Construction of the second powder test cell had many features in common with that of the first, the main innovation being that one of the electrodes was free to slide under the action of an external pneumatic ram. The overall layout of the new system is depicted schematically in Fig. 5.4, and shown as a photograph in Fig. 5.5.

The powder samples were placed between a pair of parallel electrode surfaces having cross sectional areas of  $0.382 \text{ cm}^2$ , again constructed from indium coated 2mm copper sheet. The dividing ridge in the perspex block was omitted from this design. The polished perspex retaining cover was again held in position by two bolts. The powder test cell was mounted in a recessed Tufnol block within the metal holder, and electrical connections were provided as before.

A rigidly mounted pneumatic ram of 2.5 cm stroke x 32 mm bore was operated from a cylinder of oxygen free nitrogen at pressures up to 60 p.s.i. This action compressed the powder samples by reducing the intervening space between the fixed and sliding electrodes. Since changing the inter-electrode separation altered the applied field for a constant d.c. bias, this was monitored by means of an incorporated vernier scale to an accuracy of  $1/35 \text{ mm}$ . Simple computer programs were written in BASIC to give resistance to resistivity transforms with error estimates for all possible inter-electrode distances, and sample pressures for ram pressure up to 60 p.s.i. in 0.5 p.s.i. intervals. A Bourdon gauge was used to monitor ram supply

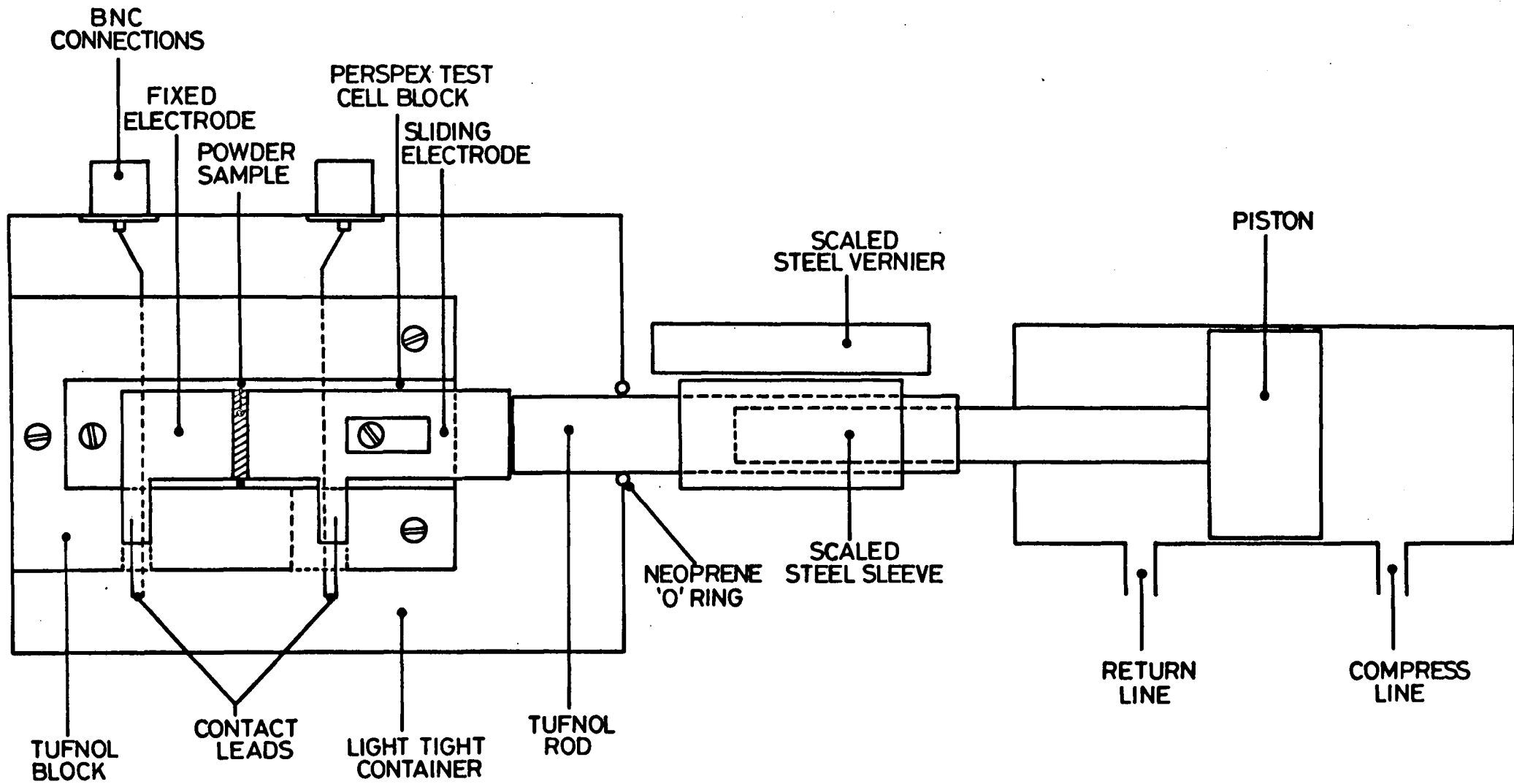
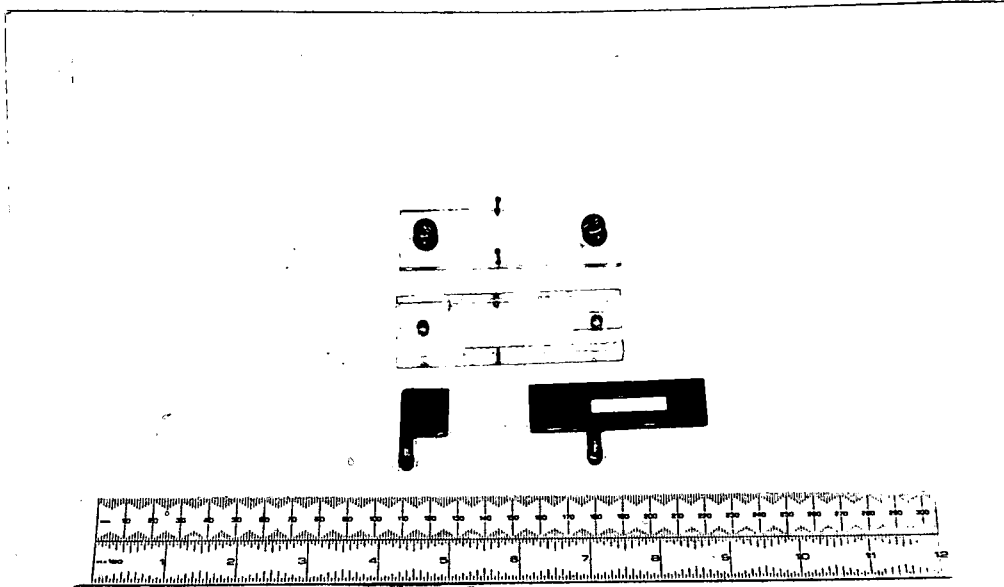
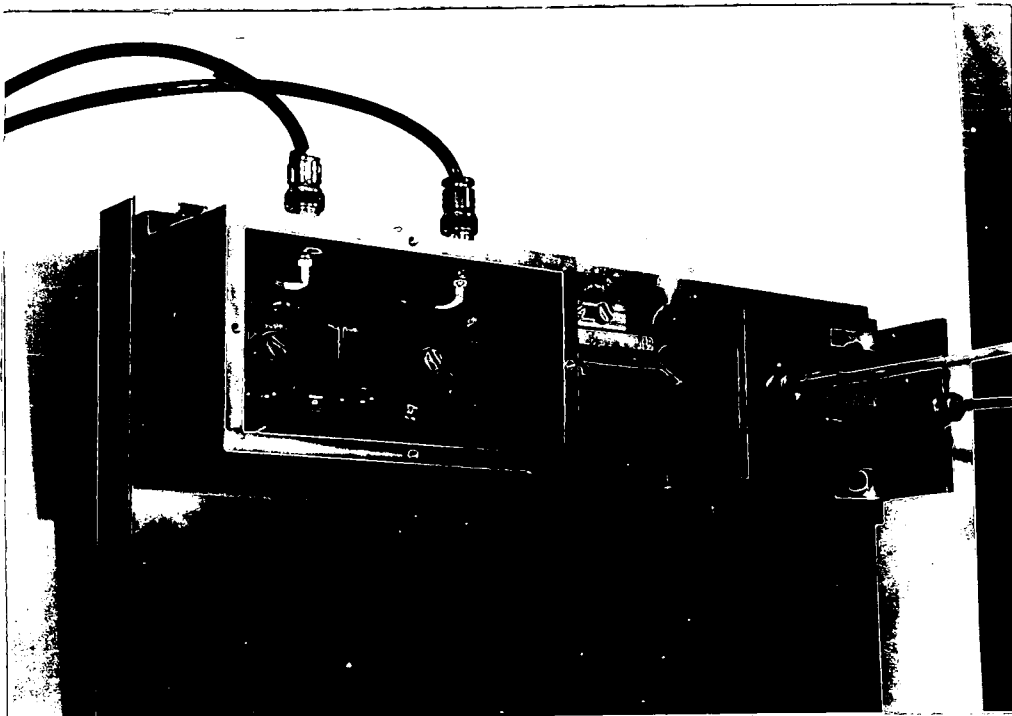


FIG. 5-4 SCHEMATIC REPRESENTATION OF MOVING ELECTRODE POWDER TEST CELL IN HOLDER WITH ASSOCIATED COMPRESSION APPARATUS



a) Sliding electrode powder test cell components: perspex cover plate with mounting screws, perspex base and indium coated copper electrodes.



b) Powder test cell mounted in compression apparatus.

Cover plate of light-tight box has been removed.

Fig.5.5 Sliding electrode powder test cell and compression apparatus.

pressure to better than  $\pm 0.5\%$  accuracy. Alternative arrangements for measuring the electrical characteristics of powdered semiconductors under compression have been described by Povkhan (1) and Sato and Yoshizawa (2).

It is appropriate at this point to discuss the discrepancy between calculated and true resistivity for powder samples investigated using this apparatus. Fig.5.6 shows a simplified representation of a powder sample in the dark and under illumination. In the absence of photoexcitation the calculated and true resistivities of the powder sample are, within the scope of this discussion, identical. It is not, however, valid to assume that the entire bulk of the powder sample will be subjected to the same intensity of photoexcitation. A simple theoretical relationship links the intensity of photoexcitation ( $I_d$ ) with the depth below the exposed sample surface ( $d$ ):

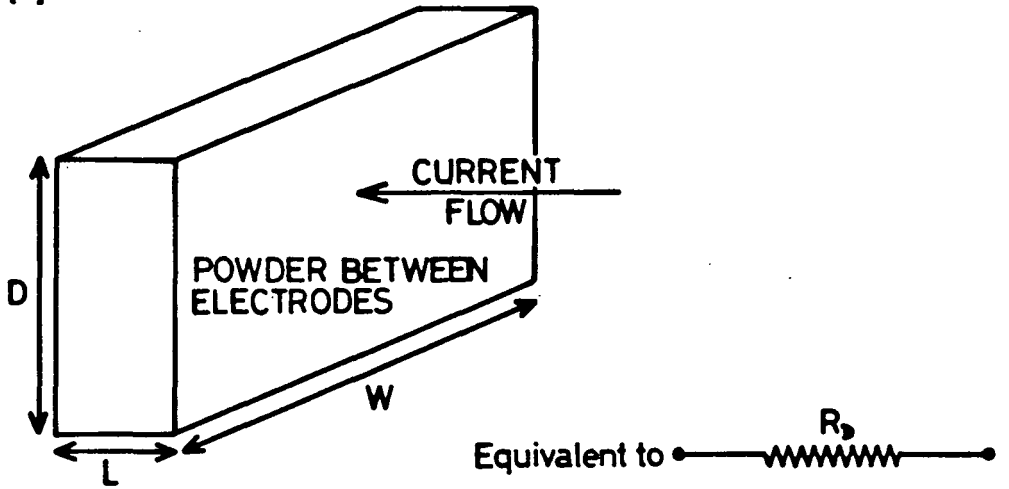
$$I_d = I_0 \exp (-\alpha d) \quad (5.1)$$

$I_0$  = photoexcitation intensity at the exposed sample surface

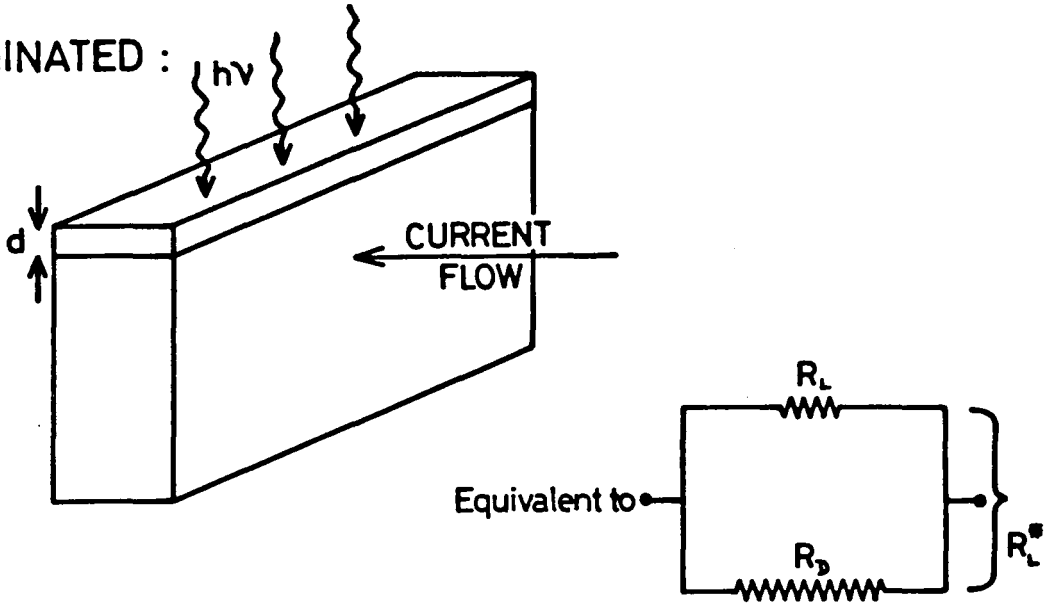
$\alpha$  = linear absorption coefficient.

The situation is further complicated by the fact that  $\alpha$  is wavelength dependent. Values of the relative absorption coefficient  $\alpha$  in CdSe powder of approximately  $(1.5 \text{ to } 4) \times 10^{-5} \text{ cm}^{-1}$  for wavelengths of between  $0.6$  and  $1 \mu\text{m}$  have been reported by Nicastro and Offenbacher (3). Their value of approximately  $4 \times 10^{-5} \text{ cm}^{-1}$  at  $\lambda = 0.6 \mu\text{m}$  may be compared with an

DARK :



ILLUMINATED :



SYMBOLS USED :

- D - ELECTRODE DEPTH
  - W - ELECTRODE WIDTH
  - d - PENETRATION DEPTH OF ILLUMINATION
  - L - ELECTRODE SEPARATION
  - $R_D$  - DARK RESISTANCE
  - $R_L$  - LIGHT RESISTANCE
  - $R_L^*$  - APPARENT LIGHT RESISTANCE (MEASURED)
  - $\sigma_D$  - DARK CONDUCTIVITY
  - $\sigma_L$  - TRUE LIGHT CONDUCTIVITY
  - $\sigma_L^*$  - APPARENT LIGHT CONDUCTIVITY (CALCULATED)
- } ELECTRODE AREA  $A = D \times W$
- } ILLUMINATED POWDER CROSS-SECTION  $a = d \times W$

FIG. 5-6 DISCREPANCY BETWEEN CALCULATED AND TRUE CONDUCTIVITY UNDER ILLUMINATION

$\alpha$  value of approximately  $7.5 \times 10^{-6} \text{cm}^{-1}$  obtained by Parsons et al (4) for CdSe single crystals. More important in this context, however, is the effect of light scattering in powder samples. As a result of this a loose powder sample approximately  $150 \mu\text{m}$  in thickness was found to transmit less than 0.1% of incident radiation over the wavelength range  $0.3 - 1.0 \mu\text{m}$ .

The model of Fig. 5.6 assumes that a small but finite depth of the powder sample is subjected to the full incident photoexcitation intensity while the remainder is in the dark. Since the direction of current flow is normal to the direction of illumination, the measured resistance  $R_L^*$  may be considered as a parallel combination of the resistances of the two powder sample regions, namely  $R_L$  and  $R_D$ . Thus:

$$\frac{1}{R_L^*} = \frac{1}{R_L} + \frac{1}{R_D} \quad (5.2)$$

Using the symbols defined in Fig. 5.6 we may consider this relationship in terms of conductivity:

$$\begin{aligned} \sigma_{L^*} \cdot \frac{(A-a)}{L} &= \sigma_L \cdot \frac{a}{L} + \sigma_D \cdot \frac{(A-a)}{L} \\ \therefore \sigma_L &= \frac{(\sigma_{L^*} - \sigma_D) \cdot (A-a)}{a} \end{aligned} \quad (5.3)$$

Thus, for small values of  $a$  and  $\sigma_D$ , the calculated and true illuminated resistivities of the powder sample may be related by the ratio of the depth of the total sample to the depth of the photoexcitation penetration:

$$L = \frac{L^* \cdot D}{d} \quad (5.4)$$

While this model does not yield a precise numerical relationship, it serves to illustrate that the true response of the illuminated region of the powder samples is several orders of magnitude greater than that indicated by the recorded results.

## 5.6 ELECTRICAL AND OPTICAL APPARATUS

A circuit diagram of the electrical measurement apparatus used is given in Fig.5.7. This arrangement enabled direct recordings of I-V characteristics to be made using a reproducible rate of change of applied voltage, and was preceded by several less sophisticated systems with manually operated power supplies (not illustrated) which, nonetheless, functioned in a similar way.

The power supply used was a 0 to  $\pm 100$ v d.c. linear voltage ramp generator with ramp rates ranged from 5 to 500mV sec<sup>-1</sup>. The output of this unit was connected to the powder sample under test and also, via a high impedance potential divider network, to the X channel input of a Bryans BS312 X/Y/t chart recorder. Voltage limits could be preset to any desired value within the operational range. Powder sample performance under higher applied fields was investigated by substituting a 0-300v d.c. manually operated power supply. A Gould Instruments DMM7A digital multimeter, having an impedance of  $10M\Omega$ , was used to give a direct reading of the applied field for all types of power supply.

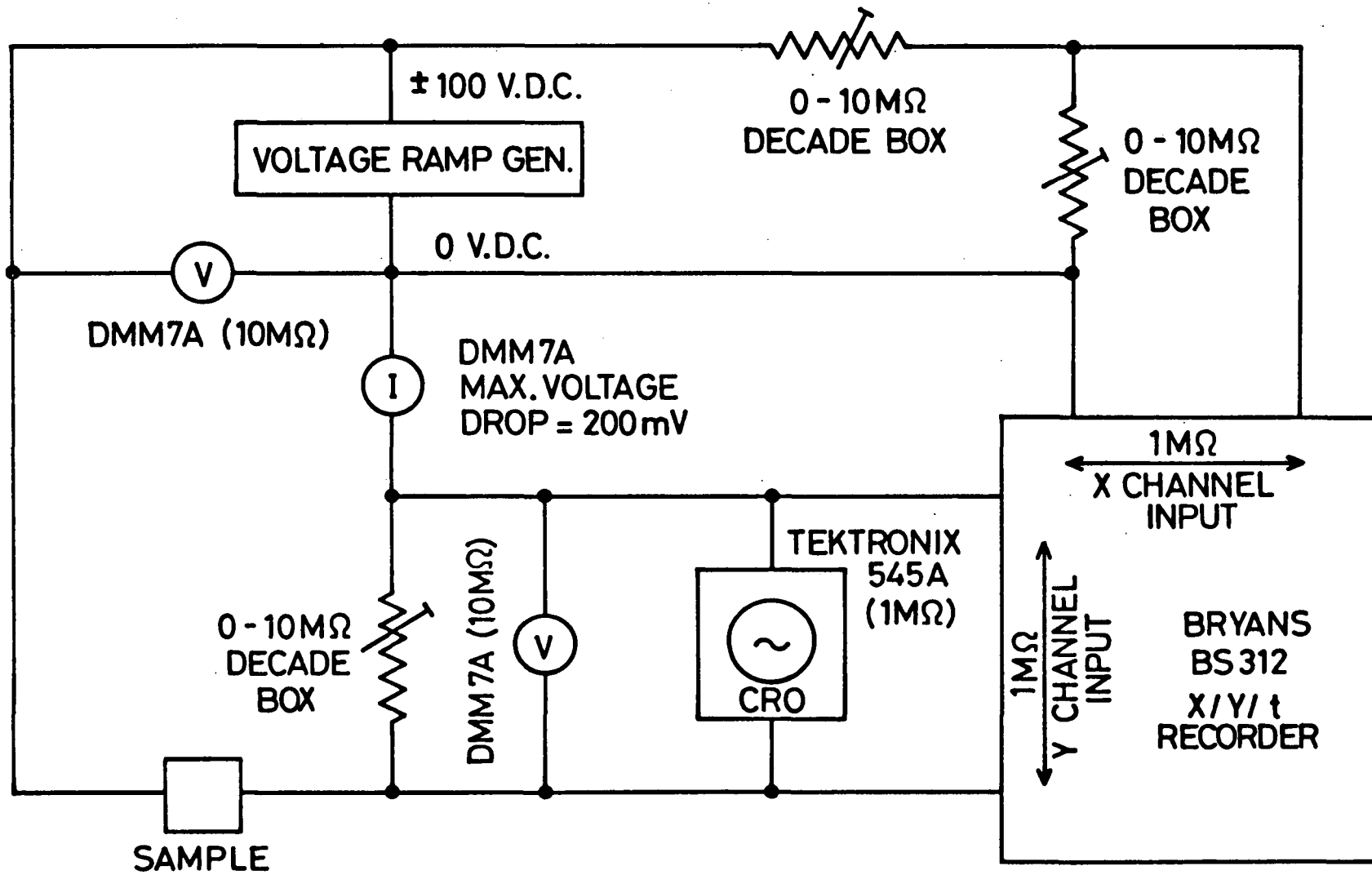


FIG.5-7 CIRCUIT DIAGRAM OF ELECTRICAL MEASUREMENT APPARATUS

Current flow through each powder sample was monitored by two methods. Current levels greater than  $10^{-7}$ A were indicated by another DMM7A multimeter operated as a series connected ammeter. Another voltmeter used in conjunction with a current sensing decade box measured lower current levels. The voltage drop produced across the decade box was also used to drive the Y-channel input of the chart recorder. By selecting appropriate decade box settings this voltage drop was limited to 200mV and, when necessary, loading due to the voltmeter and chart recorder was allowed for in estimates of the true current magnitude.

A cathode ray oscilloscope was included in this sub-network for measurement of speeds of response to changes in photoexcitation intensity or applied field. The resultant traces, in which a zero signal reference line was always included, were recorded using a camera attachment.

Screened coaxial leads were used for all parts of the test circuit which carried the sample current. Also included in this screening network, which was connected to a common earth, were the metal sample holder box and the chart recorder inputs. These precautions resulted in a signal to noise ratio of better than 20dB.

The light source used for the majority of measurements was a 250w, 24v d.c. quartz-iodine lamp. The sensing attachment of a direct reading E.E.L. light-meter was placed in the plane of the powder samples and the positions of the lamp and condensing lens

adjusted to give a roughly collimated beam with a flux density of approximately  $600 \mu\text{W cm}^{-2}$  at the sample surface. This value was chosen as being equivalent to the radiant emittance of a typical uniform flat electroluminescent panel (Tannas and Goede (5)), and within an order of magnitude of that recorded for the d.c.e.l. panels tested (Chapter 1).

The spectral distribution of the output energy from the lamp operated at rated power was investigated by passing the light through a Hilger and Watts diffraction grating monochromator onto a PIN-10-DF photodiode operated in the photovoltaic mode. The output voltage from this detector, which has approximately level response over the wavelength range  $0.45 - 0.95 \mu\text{m}$ , was plotted on a Honeywell X-t chart recorder while the incident wavelength was changed at a constant rate by the monochromator motor drive. The resultant plot, which is shown in Fig.5.8, confirms the suitability of this light source as a substantial proportion of the output energy occurs in the  $0.6 - 0.9 \mu\text{m}$  wavelength range which is the high photosensitivity region for CdSe.

Fig.5.9 shows the overall optical arrangement used. The inside surface of the metal tube was painted matt black to reduce the amount of stray ambient light reaching the sample. The dependence of sample conductivity on photoexcitation intensity was investigated by inserting neutral density filters at the tube entrance. Attenuations of 50,70,90 and 99% were achieved in this way, the resultant flux densities being 300, 180, 30 and  $3 \mu\text{W cm}^{-2}$  respectively.

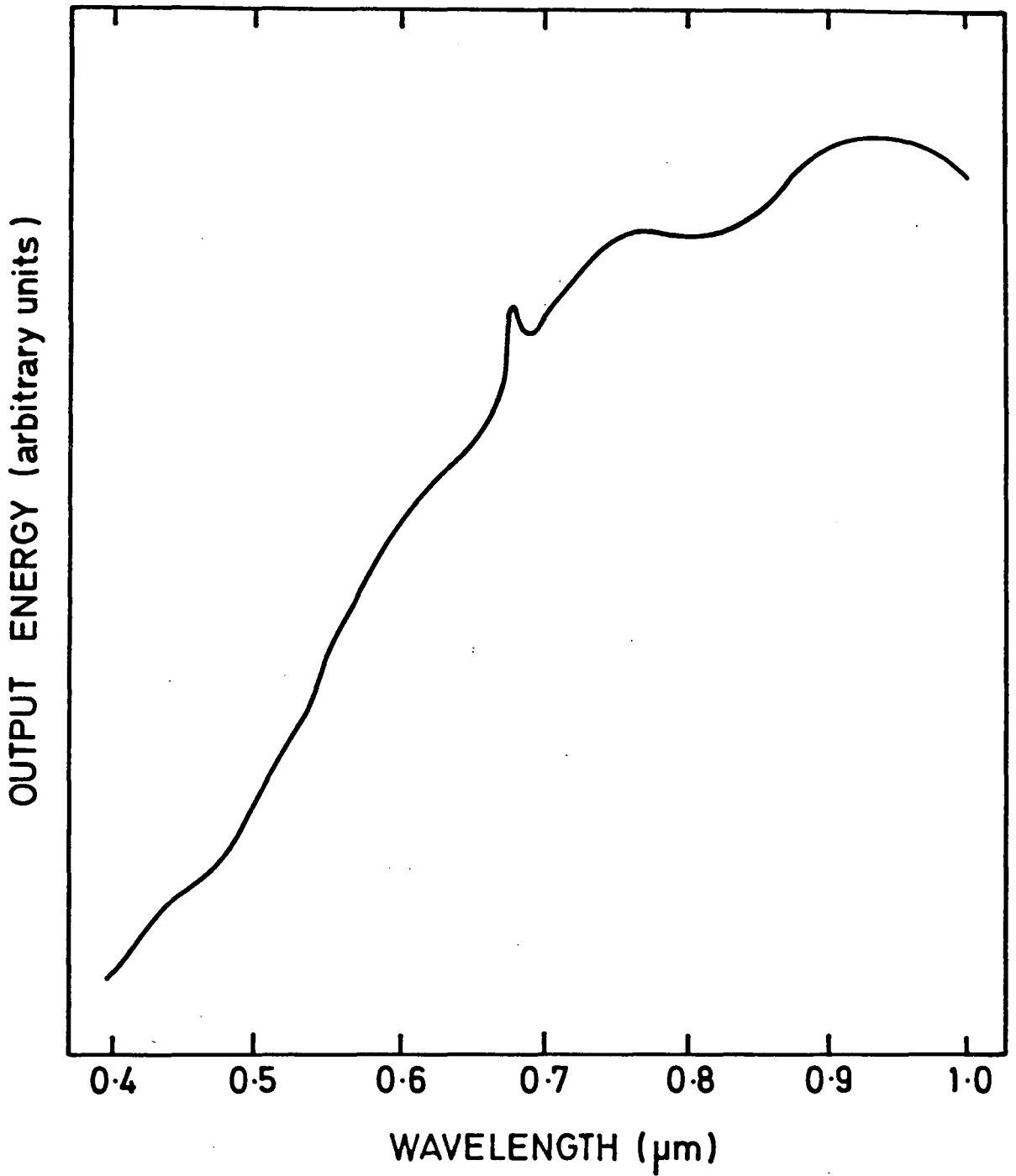


FIG.5.8 SPECTRAL DISTRIBUTION OF THE OUTPUT ENERGY OF THE 200W, 24 V.D.C. QUARTZ- IODINE LIGHT SOURCE.

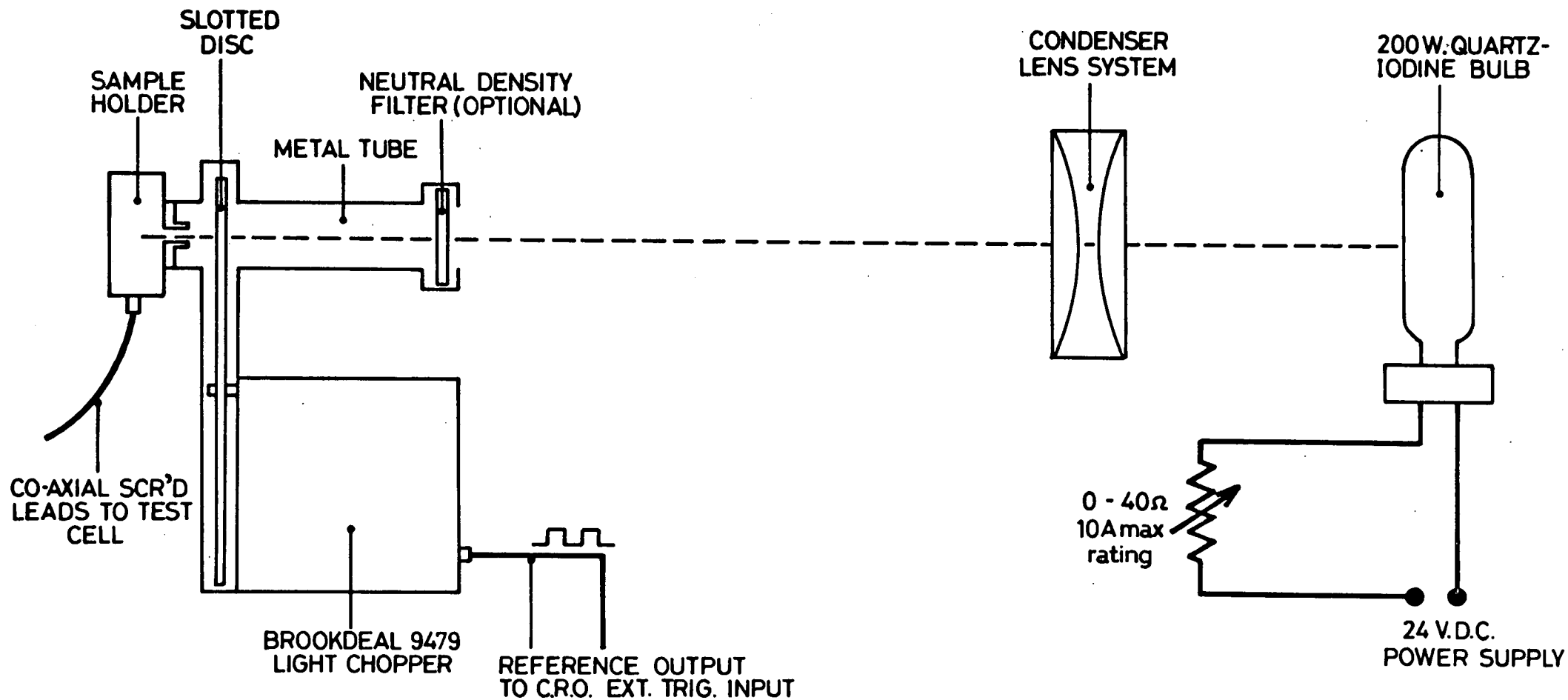


FIG. 5-9 (not to scale) SCHEMATIC DIAGRAM OF OPTICAL APPARATUS USED

An Ortec-Brookdeal 9479 programmable light chopper was used to investigate speed of response to alternating periods of illumination and darkness. Chopping rates ranged from 10 to 1000Hz. A reference square wave output from the unit was connected to the external trigger input of the oscilloscope mentioned in the previous section. The finite transition time from light to darkness and vice versa as the image of the chopper blade traverses the powder sample has been calculated to be approximately  $7/F$  milliseconds for chopping frequency  $F$ . The contribution of this to observed response characteristics, particularly at higher chopping rates, is negligible.

A variety of miscellaneous phenomena were observed using the electrical and optical equipment described in this section. Such results discussed in Chapter 7 will be accompanied by a brief explanation of their derivation.

## CHAPTER 5: REFERENCES

- 1) POVKHAN T.I., DEMIDOV K.B. and AKIMOV I.A. "Cells for the Investigation of the Electrophysical Properties of Powdered Semiconductors" Instrum. and Exp. Tech. (USA) 17, No.3, Pt 2, 881-3 (1974)
- 2) SATO K. and YOSHIZAWA M. "Voltage-Current Characteristics of Compressed CdSe Powders" Jap. J. Appl. Phys. 13, No. 4, 630-40 (April 1974)
- 3) NICASTRO L.J. and OFFENBACHER E.L. "Negative Resistance in Cadmium Selenide Power - Relative Absorption Coefficient" R.C.A. Rev. 34, 443-56 (Sept.1973)
- 4) PARSONS R.B., WARDZYNSKI W. and YOFFE A.D. "The Optical Properties of Single Crystals of Cadmium Selenide" Proc. Roy. Soc. London, 262A, 120-31 (1961)
- 5) TANNAS L. and GOEDE W.F. "Flat Panel Displays: A Critique" IEEE Spectrum 26-32 (July 1978)

## CHAPTER 6

### RESULTS OF PHYSICAL ANALYSIS

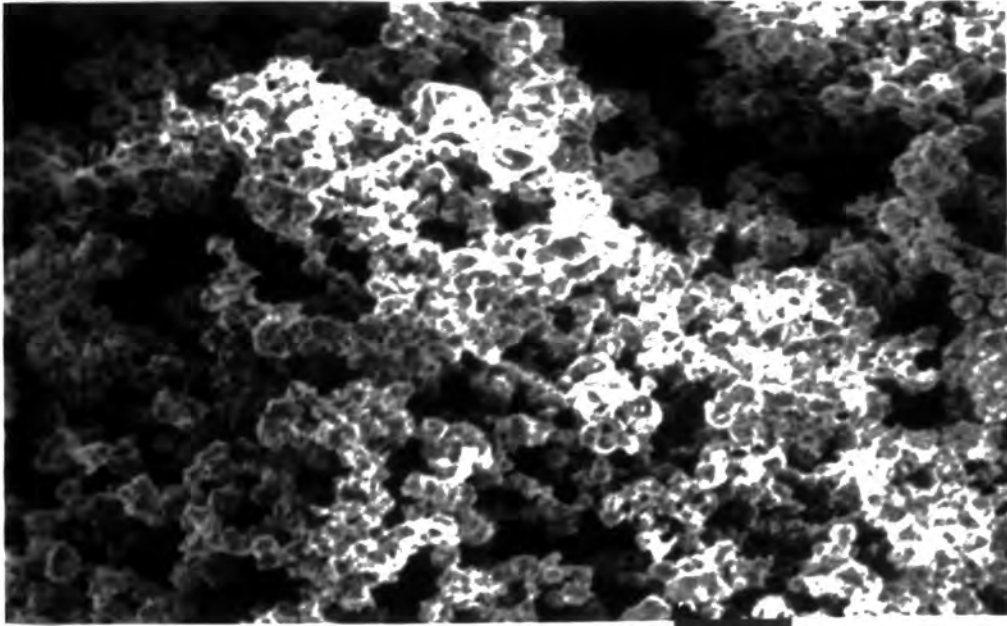
#### 6.1 INTRODUCTION

The results presented in this chapter were obtained from a relatively small proportion of the many powder samples and devices prepared. The information gained, however, is more generally applicable, and is an essential precursor to the interpretation of the results obtained from the electronic measurements discussed in Chapter 7.

The complex nature of the CdSe powder system is highlighted by analytical techniques such as X-ray diffractometry and mass spectroscopy. These reveal that CdSe powder is both structurally unstable and chemically reactive, and both of these properties will affect the performance of a sensitized powder as a photoconductor.

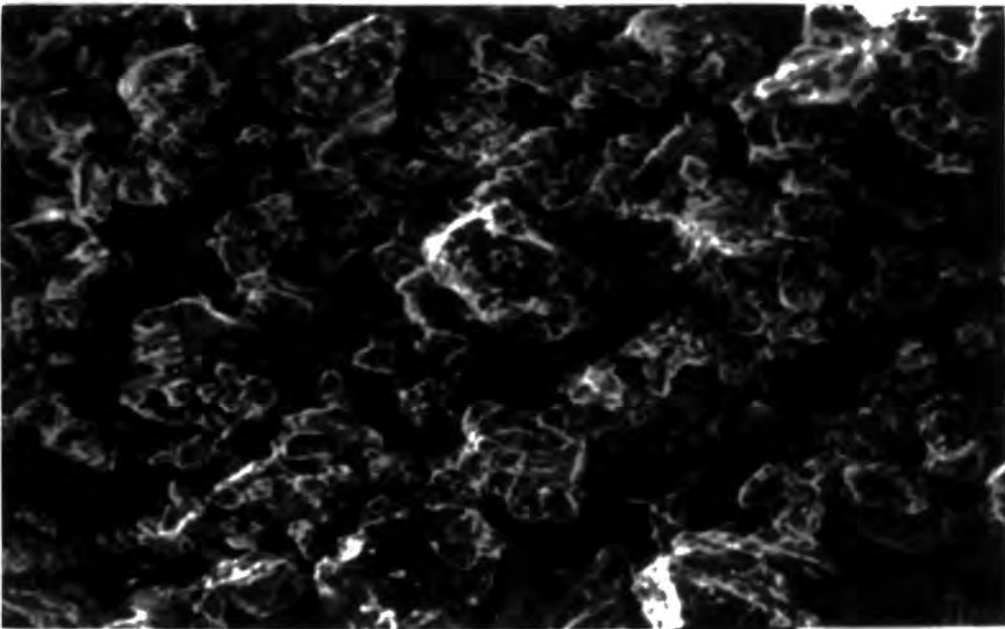
#### 6.2 RESULTS OF TOPOGRAPHIC ANALYSIS

S.E.M. photographs of typical regions of untreated Cerac, Koch-Light, Merck and pre-fired, laboratory produced CdSe powder samples are given in Figs 6.1-4. Though these materials appear identical to the naked eye, marked differences in the topography and size distribution of the constituent particles are revealed



10 $\mu$

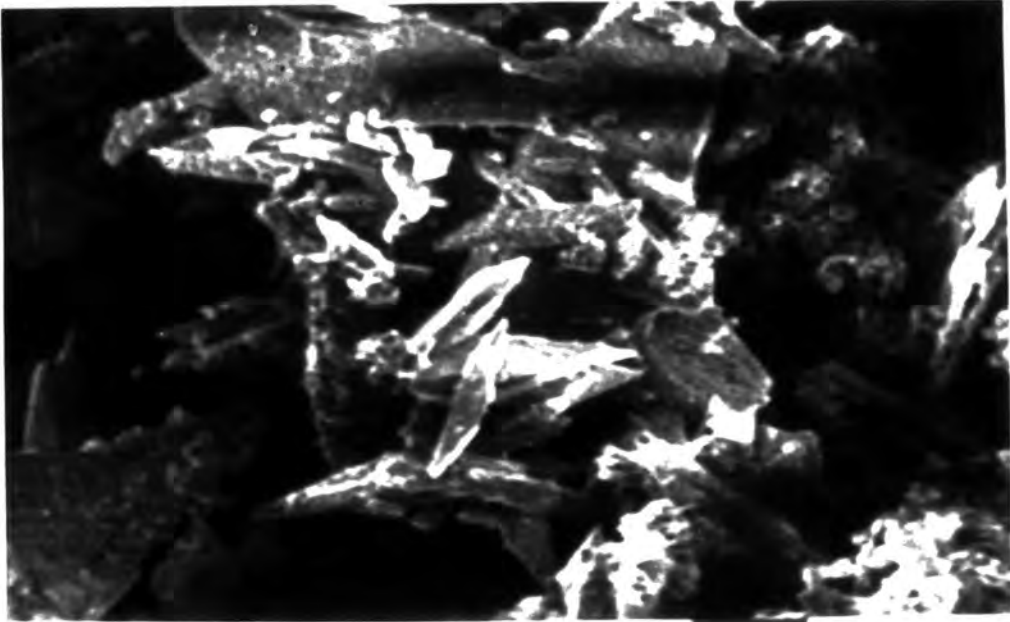
Fig.6.1: Untreated Cerac CdSe powder particles.



10 $\mu$

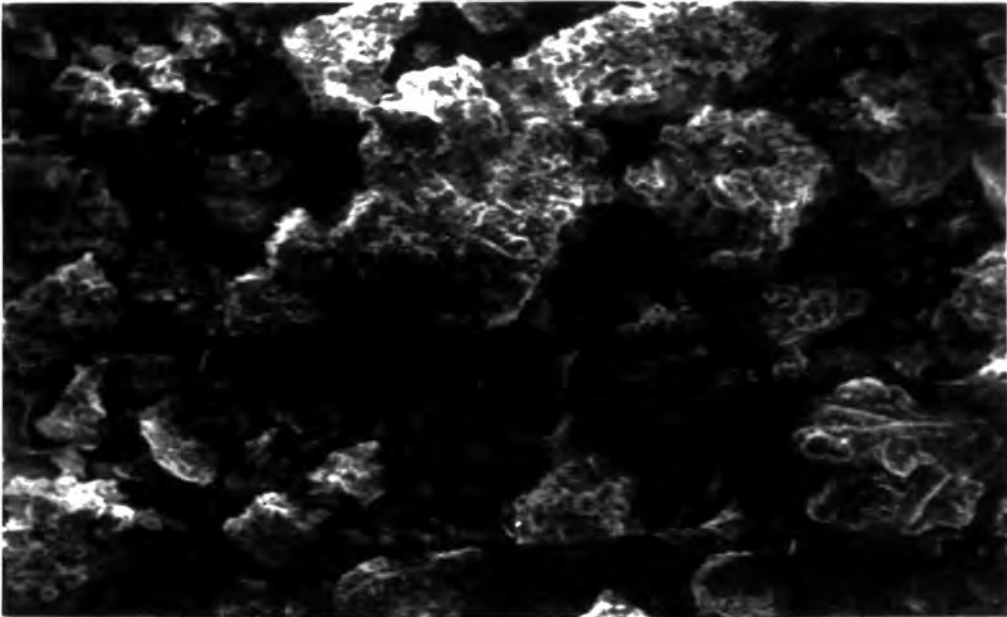
Fig.6.2: Untreated Koch-Light CdSe powder particles.

S.E.M. photographs (secondary emission mode).



10 $\mu$

Fig.6.3: Untreated Merck CdSe powder particles.



20 $\mu$

Fig.6.4: Pre-fired laboratory manufactured powder particles.

N.B. Lower magnification than Figs. 6.1-3.

under magnification.

The particles of Cerac CdSe powder appear to be irregularly shaped but approximately isodiametric. Particle size seems to be highly uniform and is estimated from Fig.6.1 to be around 2-3  $\mu\text{m}$  on average. The Koch-Light CdSe powder particles are similar in shape to those of the Cerac powder, but appear to be, on average, an order of magnitude larger with a broader particle size distribution. In contrast the particles of Merck CdSe powder resemble angular single crystal platelets. There is a large range of observed particle sizes from around 5 to 50  $\mu\text{m}$  in length.

The particles of pre-fired, laboratory produced CdSe powder, shown in Fig. 6.4 under half the linear magnification of the preceding 3 photographs, are similar in shape to the Cerac and Koch-Light powder particles. The large, light coloured lumps appear to be agglomerates of smaller particles similar to those visible in the background areas. The average size of the latter is estimated to be around 5-10  $\mu\text{m}$ . Since this powder has been sieved through a 75  $\mu\text{m}$  mesh the agglomerates, which are apparently up to about 50  $\mu\text{m}$  in diameter, would have been able to pass through unbroken.

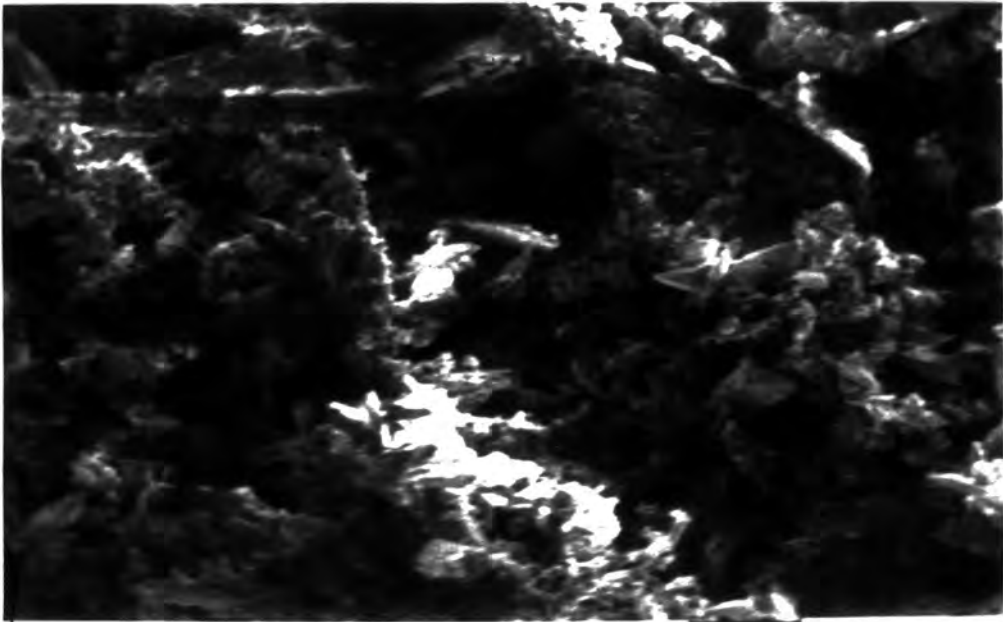
Though the methods of production of the three commercial CdSe powders is not known, it is suggested that the Cerac and Koch-Light powders may have been produced using a precipitation technique similar to the preparation of CdSe powder in this

laboratory. The Merck powder, however, appears to have been produced by an entirely different process.

The shape, size distribution and ratio of surface area to volume of the source material powder particles determine the total surface area available for interaction with doping agents, oxygen, water vapour etc. As an illustration, 1g of CdSe powder, assuming that each particle was spherical with a radius of  $2\mu\text{m}$ , would have a surface area of approximately  $0.26\text{m}^2$ .

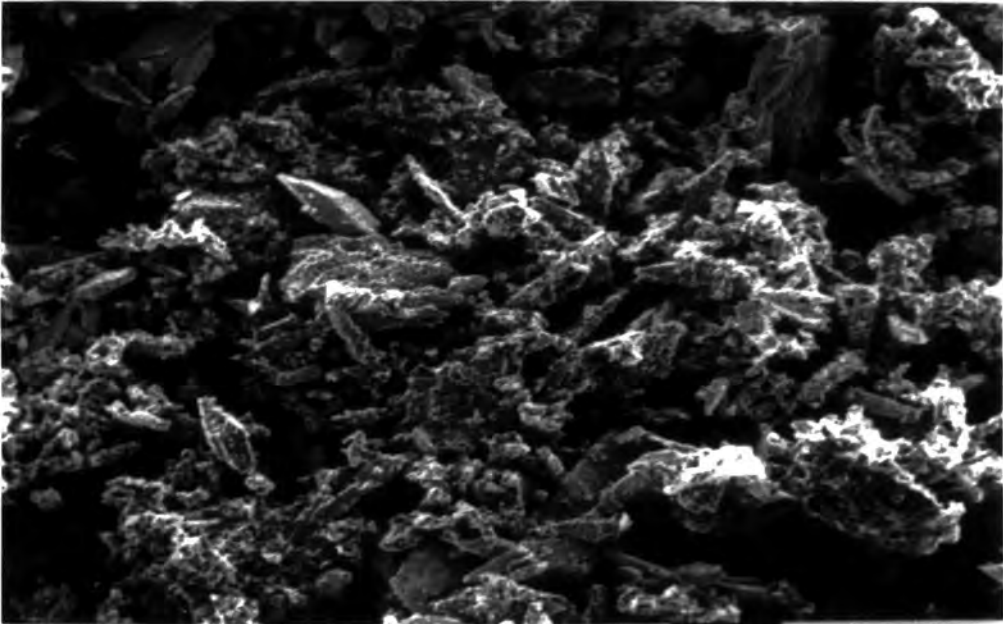
The photographs in Figs.6.5-8 show typical regions of samples taken from four stages in the preparation of a photosensitive powder. Fig.6.5 again shows particles of the untreated source material, in this case Merck CdSe powder, Particles which have been mixed with aqueous dopant solution and dried but not yet fired are shown in Fig.6.6. The overall appearance of the particles is unchanged, though the clarity of the image is noticeably enhanced, probably due to the formation of a highly conducting surface layer.

However, a radical change occurs during the firing process as shown by Fig.6.7. The angular particles have become much smoother and more rounded, and somewhat smaller and more even in size. The photograph also suggests that considerable agglomeration of the particles has occurred. Fig. 6.8 shows the powder particles after being washed in methanol and allowed to dry. This process has had no visible effect on the size or shape of the particles, and even after vigorous stirring has



20 $\mu$

Fig.6.5: Untreated Merck CdSe powder particles.



20 $\mu$

Fig.6.6: Merck powder particles after addition of dopant solutions.

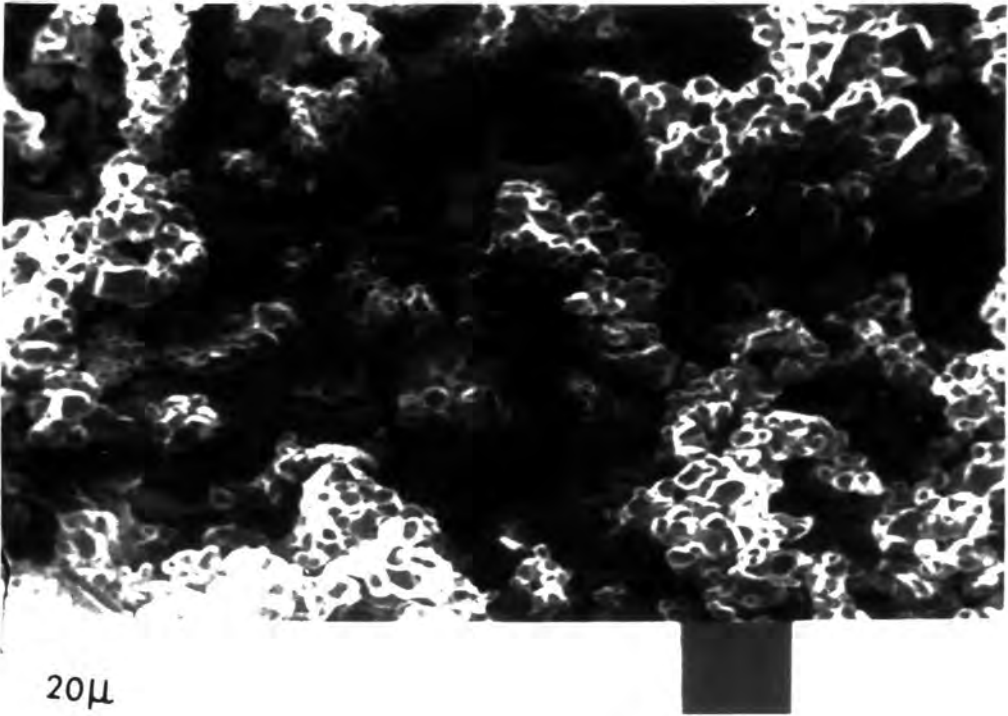


Fig.6.7: Doped Merck powder particles after firing.

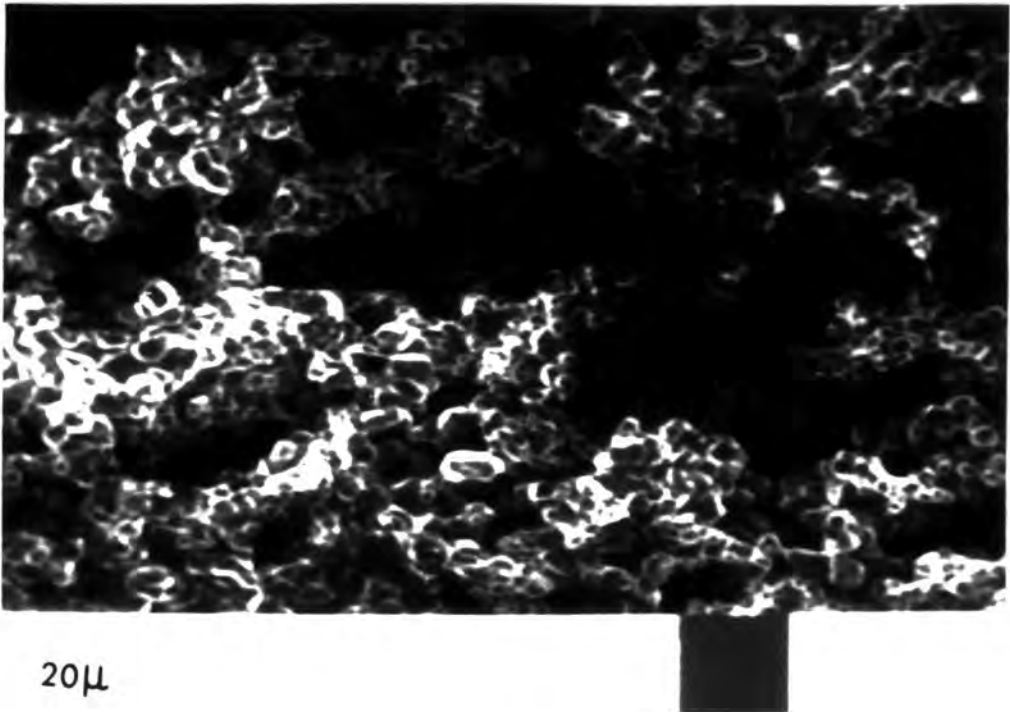


Fig.6.8: Doped fired Merck powder particles after washing in 'Analar' methanol.

apparently failed to break up the agglomerates.

This series of observations is comparable with the findings of Sato et al (1) in which the angular edges of CdSe powder particles were observed to have become rounded following annealing for 30 minutes at 400°C. Mellikov et al (2) have reported that both CdS and CdSe powder particles become rounded with a mosaic surface structure after annealing at 700°C with a variety of halides.

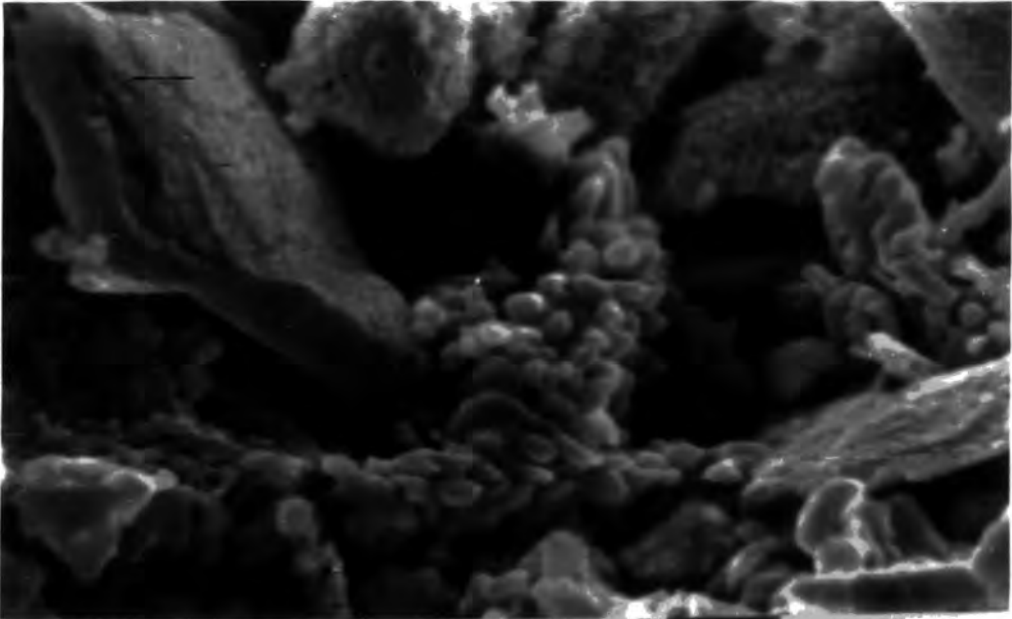
The effect of ball milling on particle shape and size is shown in Figs.6.9-11. Again the angular nature and broad size distribution of Merck CdSe powder particles are shown in Fig.6.9. After ball-milling the powder for 2 minutes (Fig.6.10) we see that the particles have become more rounded with an average diameter of around  $1\mu\text{m}$ . Ball milling for a further 30 minutes (Fig.6.11) has reduced the mean particle size to below  $1\mu\text{m}$ . However, the most significant effect of prolonged ball milling is the structural transition discussed in section 6.3.

The two S.E.M. photographs of Fig.6.12 show a typical region of a screen printed powder-binder layer in cross section. The glass substrate is toward the bottom of each picture. The thickness of the deposited layer is observed to range from about 40 to  $70\mu\text{m}$ . Furthermore the thickness fluctuates periodically at approximately  $200\mu\text{m}$  intervals. This correlates with the mesh size of the screen printing fabric used, and suggests that the



40 $\mu$

a) Untreated Merck CdSe powder particles.



4 $\mu$

b) As above, but under approximately 10 x higher magnification.

Fig.6.9 Initial size distribution of Merck CdSe powder particles.

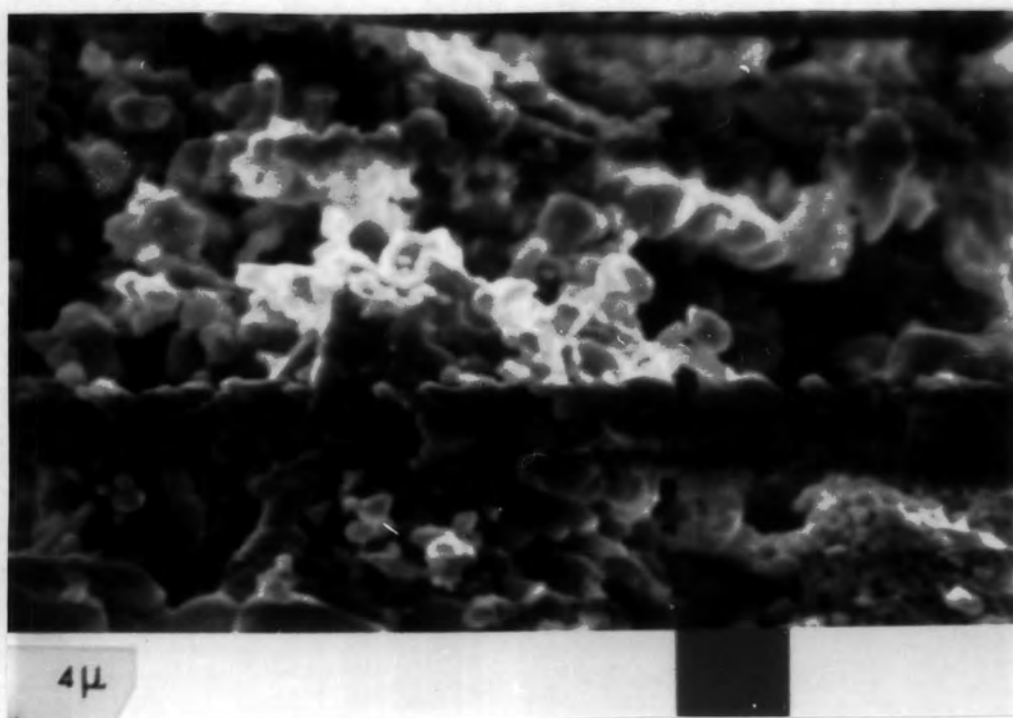


Fig.6.10: Merck CdSe powder particles after 2 minutes dry ball milling.



Fig.6.11: Merck CdSe powder particles after 32 minutes dry ball milling.

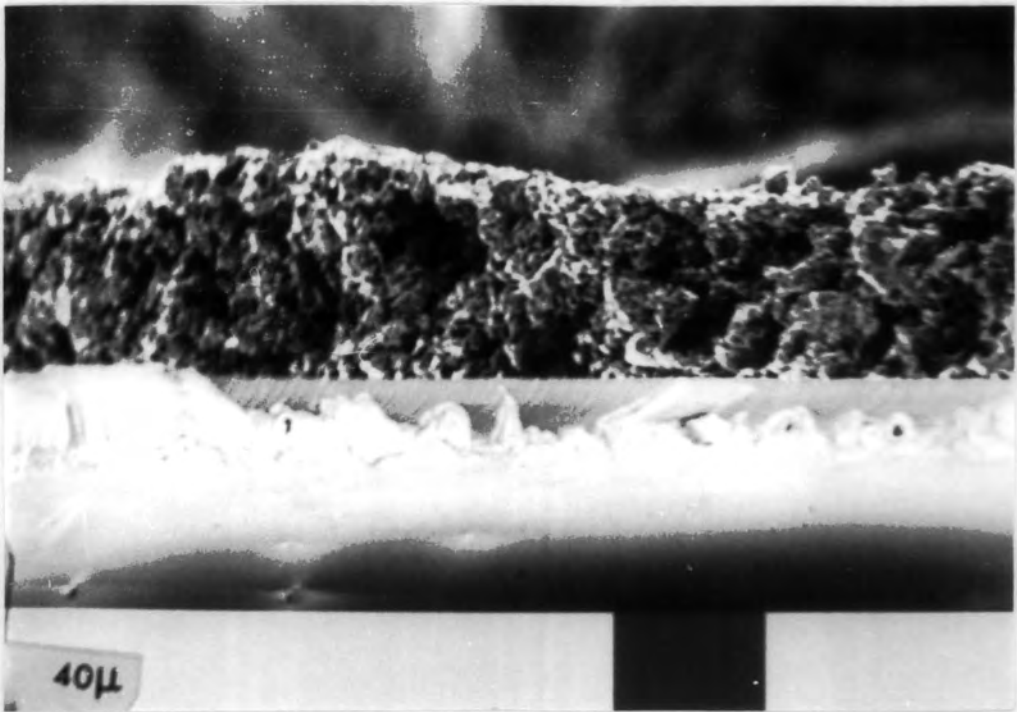
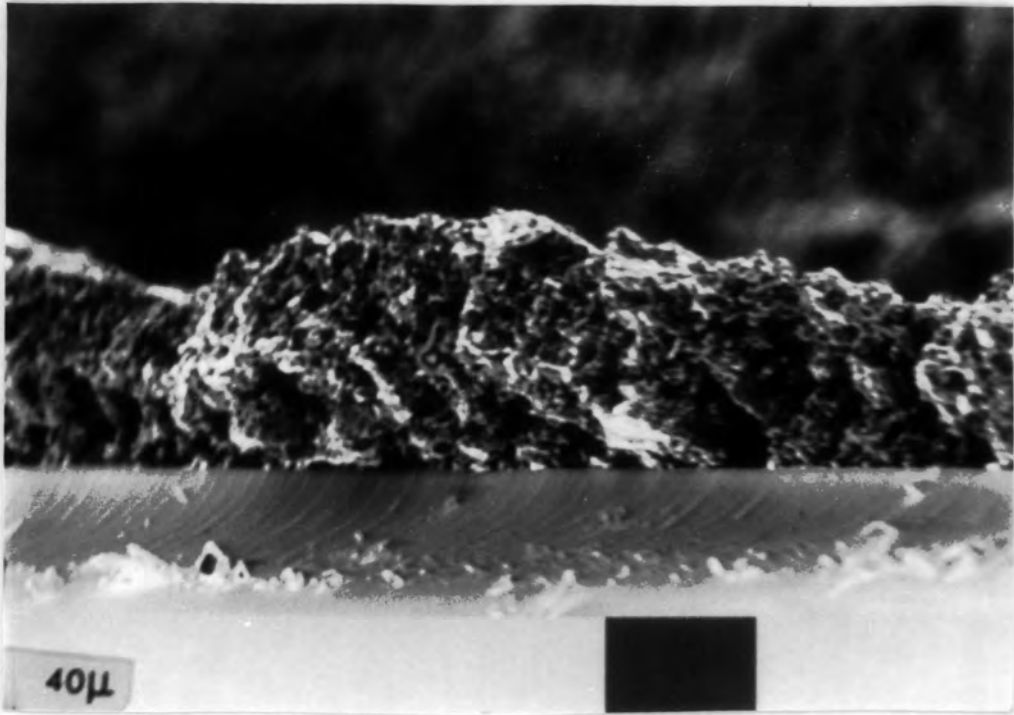


Fig. 6.12: Two cross sections of a screen printed powder-binder layer on a glass substrate.

imprint of the grid pattern is not entirely lost by the mixture flowing after deposition on the substrate. Though addition of an increased proportion of binder would be expected to improve uniformity of layer thickness, it might also be expected to impair the desired electronic properties of these devices.

### 6.3 RESULTS OF CRYSTALLOGRAPHIC ANALYSIS

It has been known for many years that CdSe usually crystallizes in either the wurtzite hexagonal or sphalerite cubic modification (3) the wurtzite structure being more common. The form may be dictated by heat treatment (4,5), stoichiometry (6), or the presence of certain bulk impurities (7) or ambient oxygen (8). During the preparation of various powder samples, in particular those used for screen printing of powder-binder layers, it became apparent that a phase transition was associated with mechanical treatment of CdSe powder. Concurrent research work on single crystals of CdSe and other II-VI compounds revealed that a similar structural change occurred in the surface regions of mechanically polished crystals (Russell, Fellows, Oktik, Ture and Woods (9))

Initial crystallographic analysis by X-ray powder photography of untreated samples of Koch-Light, Merck, Cerac and laboratory-manufactured CdSe powder invariably indicated a wurtzite structure. A typical pattern, with its characteristic two groupings of three strong rings towards the low  $\theta$  end, may

be seen in Fig.6.13(a). Additional photographs taken following incorporation of various dopants routinely used in sample preparation, and/or firing by either the porous plug or partial pressure techniques were all indistinguishable from Fig.6.13(a), and thus it was concluded that these treatments did not cause any significant structural change. It is worth recalling that the external appearance of powder particles in the S.E.M. following such treatments was radically changed.

In comparison, ball-milling of CdSe powder produced little change in the appearance of powder particles except the expected reduction in average size. However, the remaining X-ray photographs of Fig. 6.13 indicate that a progressive change in the structural nature of the particles was taking place. The largest incremental change indicated by the photographs occurred between 8 and 16 minutes ball milling time. Particularly noticeable is the degeneration of the characteristic triplets of strong lines mentioned previously. A wurtzite to sphalerite transition was suspected at this stage, and was confirmed by a more precise quantitative analysis using the X-ray diffractometer.

Fig.6.14 shows six X-ray diffractometer traces. The reduced background noise of traces (e) and (f) resulted from an increased time constant in the signal amplifier. Again the two triplets of strong lines associated with the wurtzite structure are immediately noticeable on trace (a). A listing of estimated line positions and intensities is given in Fig.6.15 together

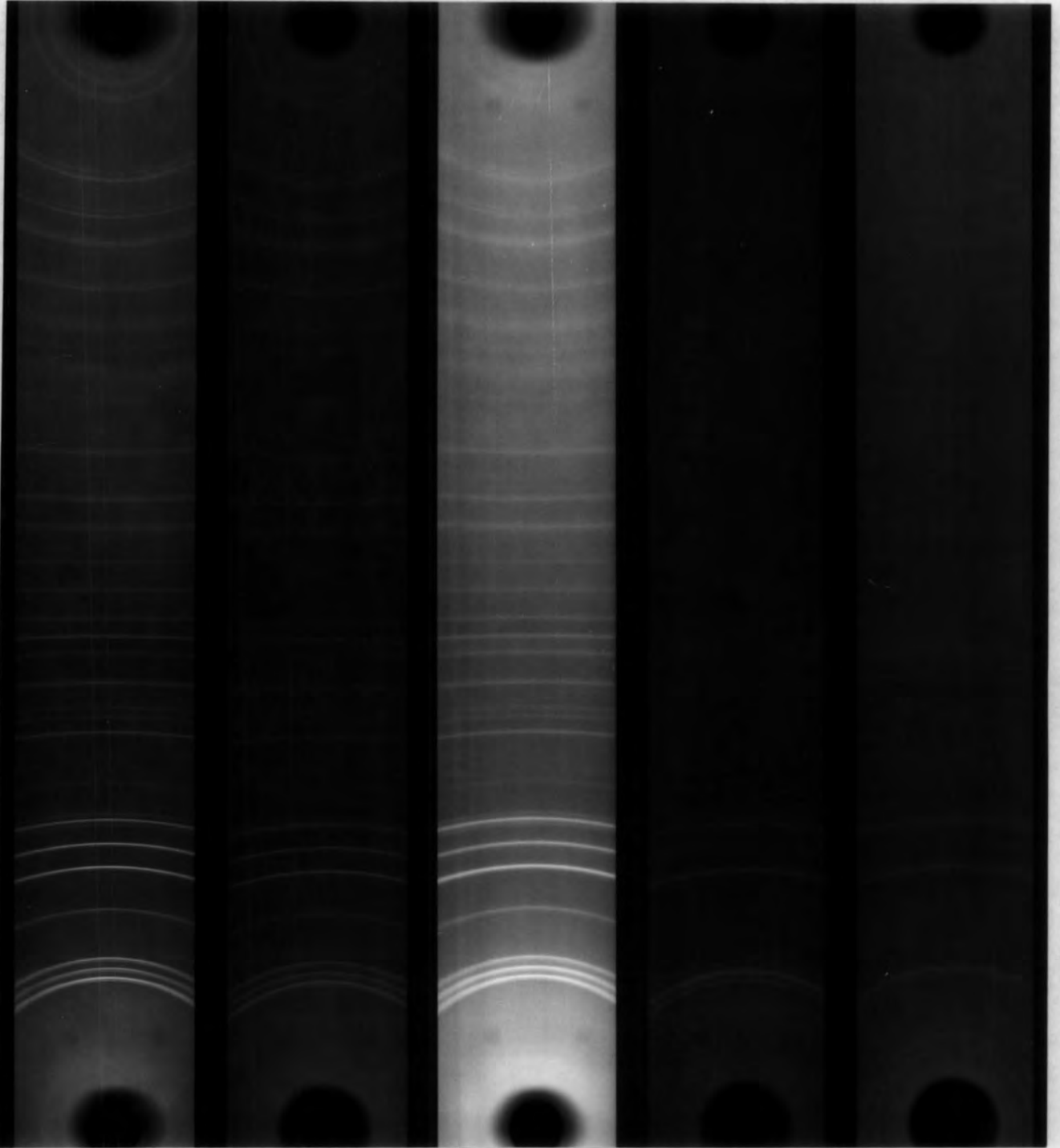
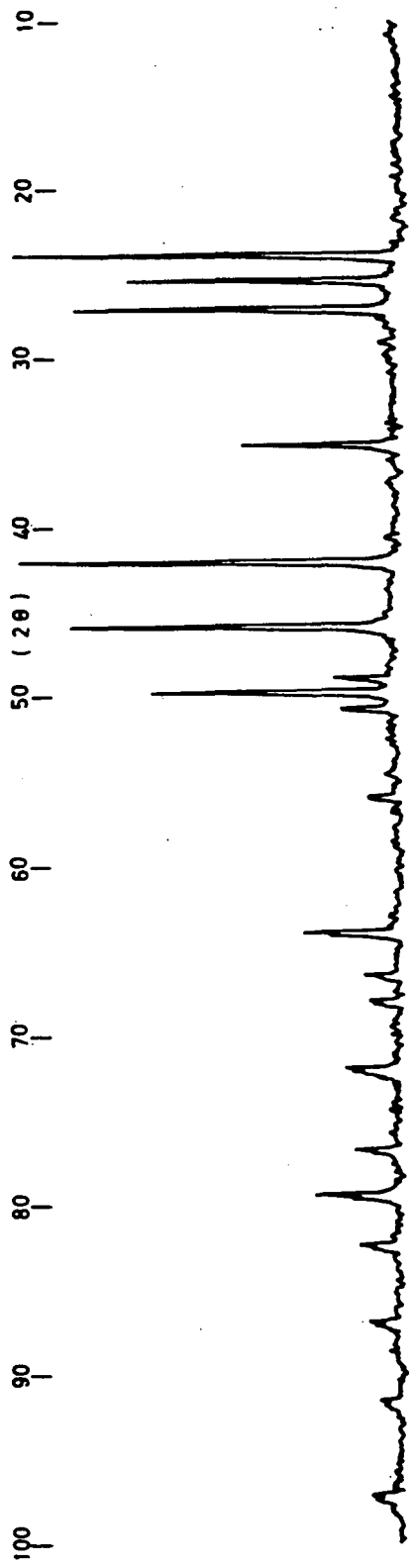


Fig.6.13: X-ray powder photographs of CdSe powder. From left to right:  
a) Untreated Merck CdSe. Remaining photographs show Merck CdSe after ball milling in air for b) 4,c) 8, d) 16 and e) 64

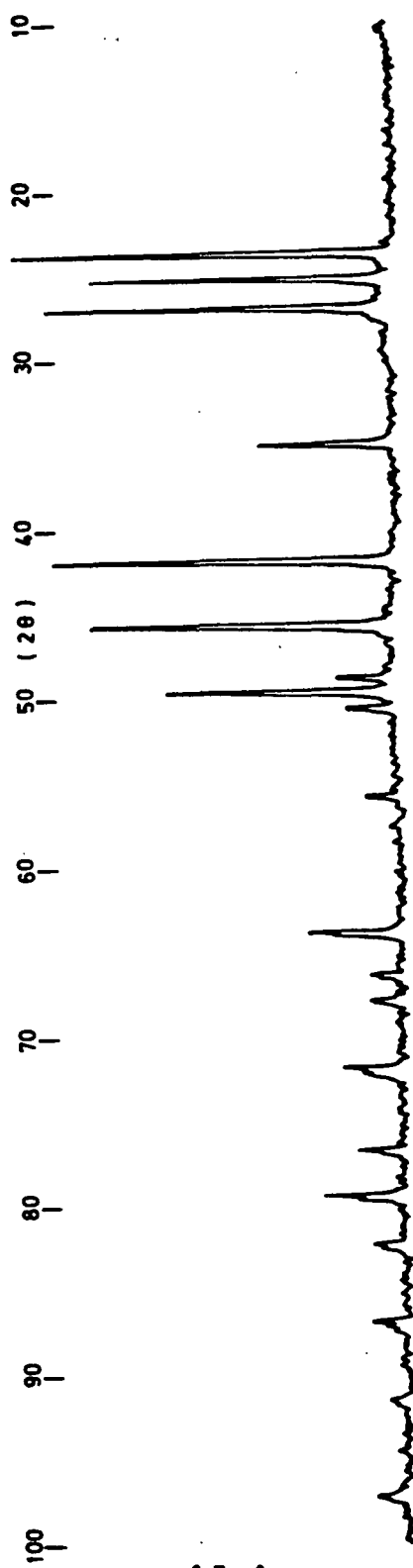
Fig. 6.14 (continued over next 2 pages):

X-ray diffractometer traces derived from 6 samples.

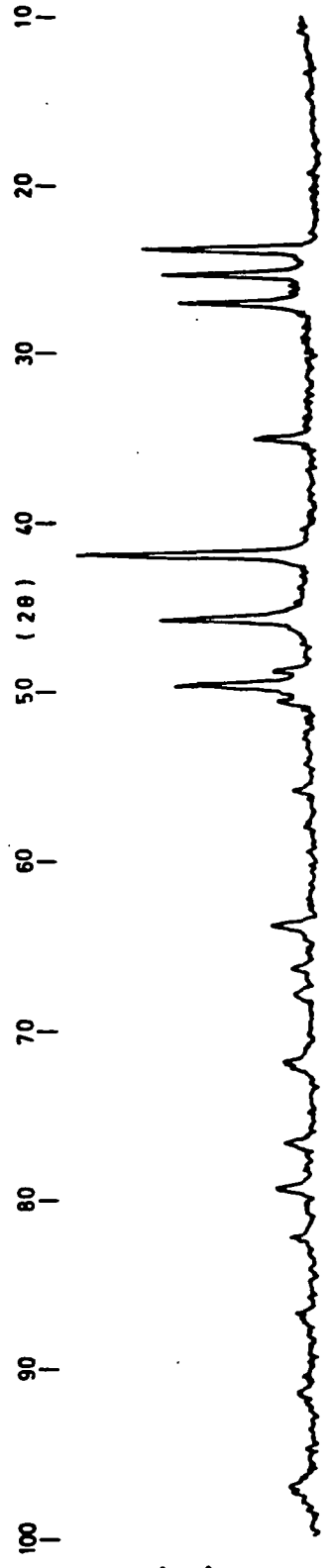
- (a) Untreated Merck CdSe powder.
- (b) Merck CdSe powder after 2 minutes dry ball milling.
- (c) Merck CdSe powder after 16 minutes dry ball milling.
- (d) Merck CdSe powder after 64 minutes dry ball milling.
- (e) Screen printed powder-binder layer prior to final firing (device 2F in Fig. 4.8).
- (f) Screen printed powder-binder layer after final firing (device 2E in Fig. 4.8)



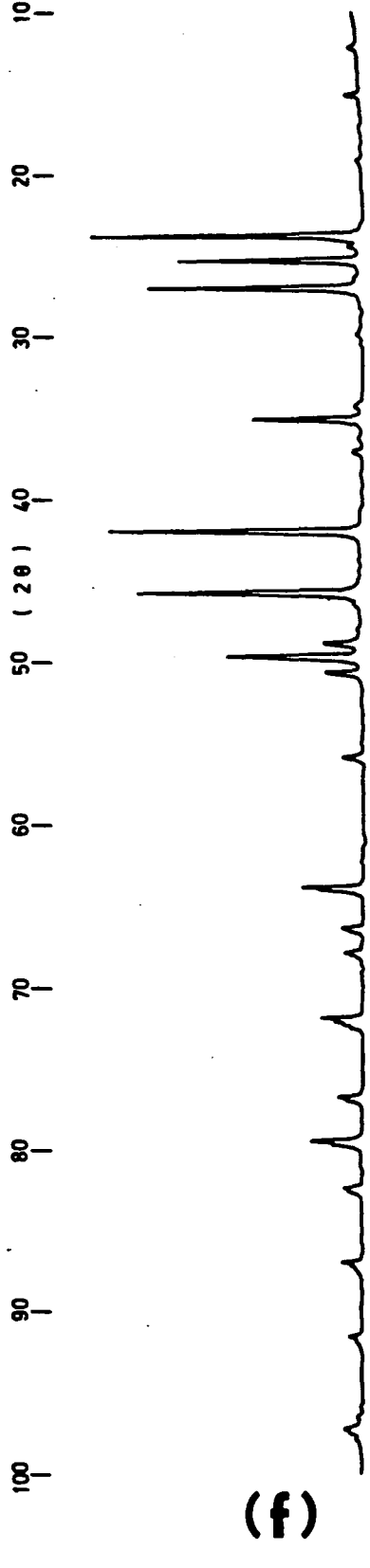
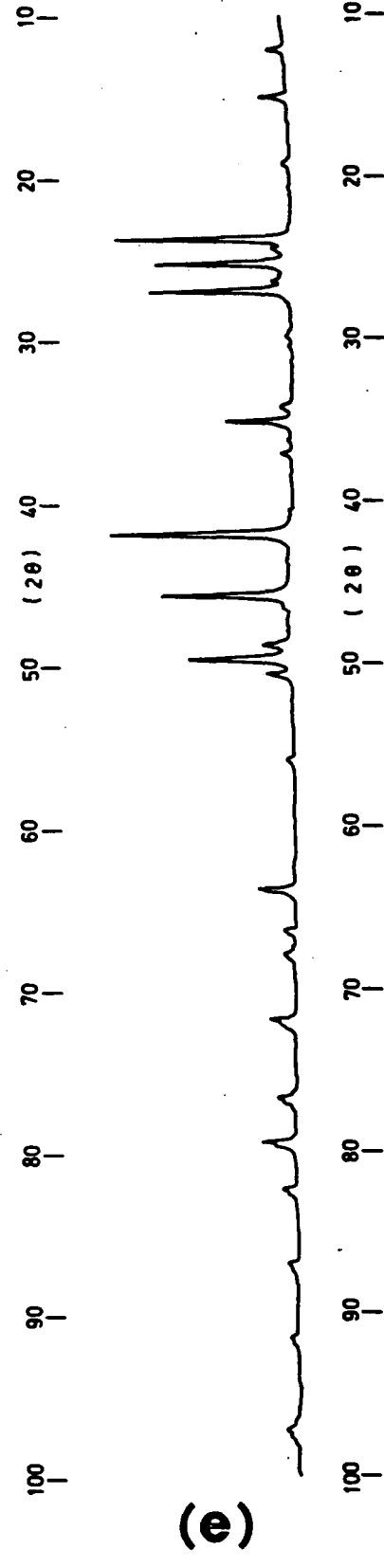
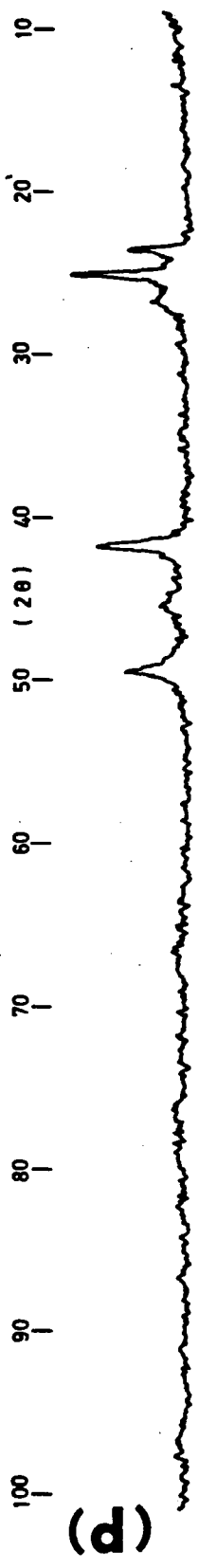
**(a)**



**(b)**



**(c)**



2θ							d <sub>hkl</sub>			hkl	Intensity						
a	b	c	d	e	f	$\bar{x}$	$\bar{x}$	a	Wzite ASTM	Wurtzite ASTM	A S T M	a	b	c	d	e	f
23.95	23.85	23.83	23.66	23.79	23.88	23.83	3.734	3.716	3.720	1 0 0	100	100	>100	49	22	46	71
25.46	25.36	25.36	25.12	25.28	25.40	25.33	3.516	3.498	3.510	0 0 2 ①	70	73	81	44	36	36	49
27.18	27.05	27.06	26.82	27.00	27.09	27.03	3.299	3.281	3.290	1 0 1	75	86	92	40	16	37	56
35.22	35.10	35.13	—	35.04	35.15	35.13	2.554	2.548	2.554	1 0 2	36	46	42	22	—	18	30
42.08	41.96	42.00	41.82	41.92	41.99	41.96	2.153	2.147	2.151	1 1 0 ②	85	98	91	66	29	48	66
45.87	45.78	45.83	—	45.73	45.80	45.80	1.981	1.978	1.980	1 0 3	70	85	82	45	—	35	59
48.98	48.87	48.89	—	48.77	48.89	48.88	1.863	1.860	1.863	2 0 0	12	23	23	18	—	10	12
49.79	49.70	49.70	—	49.62	49.73	49.71	1.834	1.833	1.834	1 1 2	51	67	64	42	—	28	36
50.80	50.70	50.65	60.58	50.60	50.72	50.68	1.801	1.797	1.800	2 0 1 ③	11	22	21	17	22	9	11
56.00	55.90	—	—	55.90	55.89	55.92	1.644	1.642	1.645	2 0 2	8	15	16	—	—	3	7
63.97	63.85	63.85	—	63.80	63.90	63.87	1.458	1.455	1.456	2 0 3	20	31	30	19	—	11	18
66.46	66.40	—	—	66.35	66.40	66.40	1.408	1.407	1.407	2 1 0	8	16	16	—	—	5	7
67.95	67.88	—	—	67.80	67.89	67.88	1.381	1.380	1.380	2 1 1	8	15	15	—	—	5	7
71.99	71.87	71.90	—	71.80	71.88	71.89	1.313	1.312	1.312	1 0 5	13	21	22	16	—	8	12
76.80	76.72	76.67	—	76.65	76.78	76.72	1.242	1.241	1.2411	3 0 0	10	18	19	16	—	6	8
79.48	79.43	79.20	—	79.36	79.44	79.38	1.207	1.206	1.2055	2 1 3	18	28	27	18	—	10	15
82.41	82.33	—	—	82.29	82.39	82.36	1.171	1.170	1.170	3 0 2	8	17	15	—	—	6	6
86.97	86.92	—	—	86.90	86.93	86.93	1.121	1.120	1.1201	2 0 5	7	15	16	—	—	4	7
—	97.20	—	—	97.20	97.20	97.20	1.028	—	1.0273	2 2 2	6	—	15	—	—	5	6
101.75	101.70	—	—	101.65	101.71	101.70	0.994	0.994	0.9932	2 1 5	9	17	16	—	—	5	9

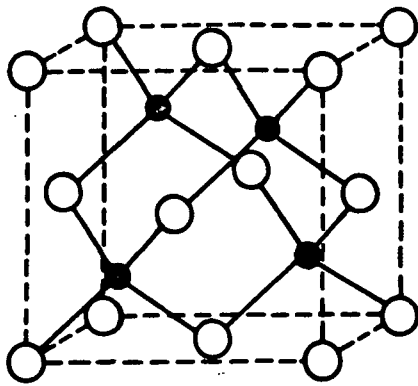
FIG. 6-15 ESTIMATED LINE POSITIONS AND INTENSITIES DERIVED FROM THE X-RAY DIFFRACTOMETER TRACES OF FIG. 6-14 , TOGETHER WITH CALCULATED AND REFERENCE INTERPLANAR SPACINGS AND INDEXING.

① } CORRESPONDING PLANES IN { 111  
 ② } THE SPHALERITE STRUCTURE { 220  
 ③ } MAY BE INDEXED AS :- { 311

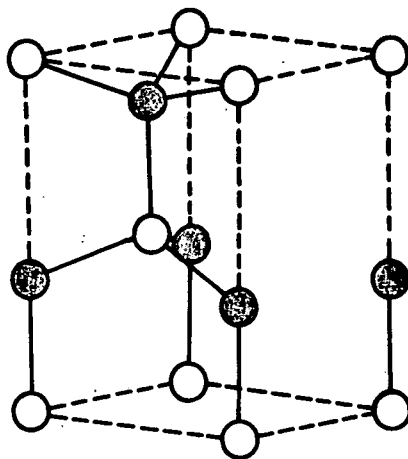
with reference values obtained from the ASTM index card for wurtzite CdSe (cadmoselite). Though no change in the X-ray diffraction is apparent from traces (a) (e) and (f), the remaining three traces obtained from ball milled powder samples again indicate a progressive change of structure.

At this point the indexing of the three lines confirming a sphalerite structure should be explained. These have been labelled, (1), (2) and (3) on Fig. 6.15, and have mean estimated values of  $2\theta$  of  $25.33^\circ$ ,  $41.96^\circ$  and  $50.68^\circ$  respectively. Within 4% error these means increase in the sequence 3, 8 and 11, indicating a corresponding integer sequence of  $(h^2+k^2+l^2)$  of 3, 8 and 11. Thus these lines represent planes which may be indexed by selecting values of h, k, and l to satisfy the above relationships i.e. 111, 220 and 311. These planes suggest a structure having face centred cubic translational symmetry since it is a characteristic of f.c.c. structures that reflections occur only when h,k,l are all even or all odd (10). Fig.6.16(a) (11) illustrates how the sphalerite structure has f.c.c. translational symmetry with a basis of two atoms, one at 000 and the other at  $1/4\ 1/4\ 1/4$ . Each thus has four nearest neighbours, all of the opposite chemical species and placed at tetrahedral angles.

The structure factor for the sphalerite form will differ slightly from that for a simple face centred cubic lattice. Thus it is possible that slight reflections do occur from sets of



(a)



(b)

FIG. 6-16 SPHALERITE AND WURTZITE STRUCTURES  
 (from "Solid State Physics" by  
 J.S.Blakemore , pub. Saunders 1974 )  
 (a) SPHALERITE ( ZINC BLENDE ) STRUCTURE  
 SHOWING F.C.C. TRANSLATIONAL SYMMETRY  
 (b) WURTZITE STRUCTURE SHOWING  
 HEXAGONAL UNIT CELL

planes for which  $h, k$  and  $l$  are a mixture of odd and even integers. If this is so, however, these lie below the background noise level of the diffractometer system and hence are undetectable. Similarly, the absence of detectable 200 ( $d_{hkl}=3.05\text{\AA}$ ) and 222 ( $d_{hkl}=1.76\text{\AA}$ ) lines suggests that this is a sphalerite structure.

In comparison Fig. 6.16(b) shows the wurtzite structure. The arrangement of nearest neighbours is the same as for sphalerite; it is the disposition of second nearest neighbours which produces a hexagonal crystal whose cohesive energy is only slightly different from that of the corresponding cubic modification. Indeed, the only structural difference between wurtzite and sphalerite lattices is in the stacking sequence of atomic planes perpendicular to the  $c$ -axis.

Estimates of the lattice parameter ( $a$ ) of the sphalerite CdSe structure may be derived from the 111, 220 and 311 lines previously mentioned using the relationship  $a=d_{hkl} \cdot (h^2+k^2+l^2)^{\frac{1}{2}}$ . These give values of  $a$  of  $6.090\text{\AA}$ ,  $6.090\text{\AA}$  and  $5.973\text{\AA}$  respectively, from which a mean estimated lattice parameter of  $6.051\text{\AA}$ . This is in excellent agreement with Stuckes and Farrell's estimate of  $6.052\text{\AA}$ . (7)

An attempt to illustrate this structural change quantitatively has been made by considering the intensities of six major lines on each of traces (a), (b), (c) and (d). Of these lines, three are uniquely associated with the wurtzite structures. If these intensities are now normalised with

respect to one of the wurtzite-only lines, as in Fig.6.17, a relative increase in the intensities of the shared lines would confirm that the powder particles were at least partially adopting the sphalerite structure. Such a trend does indeed occur, and is perhaps best illustrated visually by the graph of Fig.6.18. It should be noted that, as with the X-ray powder photographs of Fig.6.13, there is no significant evidence of this structural transition occurring as a result of ball milling times less than around 8 minutes. These observations, however, should be compared with the work of Takeuchi et al (12) who ball milled CdS powder for up to 30 hours yet failed to detect any evidence of a hexagonal to cubic phase transition.

Referring back to Fig.6.14 we see that neither sample (e) nor (f) shows comparably significant evidence of the sphalerite structure. This is perhaps surprising on first appraisal when we recall that the constituent powder of both of these devices was ball milled for a total time of 150 minutes during preparation, and from the results obtained from samples (b), (c) and (d), an overwhelming predominance of the sphalerite structure might be expected. The wurtzite structure of layers (e) and (f) was re-confirmed by RHEED analysis (13,14) which produced the characteristic rings shown in Fig.6.19.

The first stage in the preparation of layers (e) and (f) (c.f. Section 4.5) was the dry ball milling of 10g Merck CdSe with 3mg  $\text{CuCl}_2$  and 120mg  $\text{CdCl}_2$  for 120 minutes. It is almost certain that the CdSe powder had a predominantly sphalerite

I	hkl		Normalised Intensity						
	ASTM (W)	W	S	a	b	c	d	e	f
100	1 0 0	—		100	108	105	115	107	109
70	0 0 2	1 1 1		73	76	95	189	84	75
75	1 0 1	—		86	86	86	86	86	86
85	1 1 0	2 2 0		98	85	140	155	112	101
70	1 0 3	—		85	76	97	73	81	91
11	2 0 1	3 1 1		22	19	37	119	21	17

**I = INTENSITY**  
**W = WURTZITE**  
**S = SPHALERITE**

**FIG. 6-17 ESTIMATED LINE INTENSITIES DERIVED FROM THE X-RAY DIFFRACTOMETER TRACES OF FIG. 6-14 NORMALISED WITH RESPECT TO THE 101 (WURTZITE) LINE OF TRACE (a).**

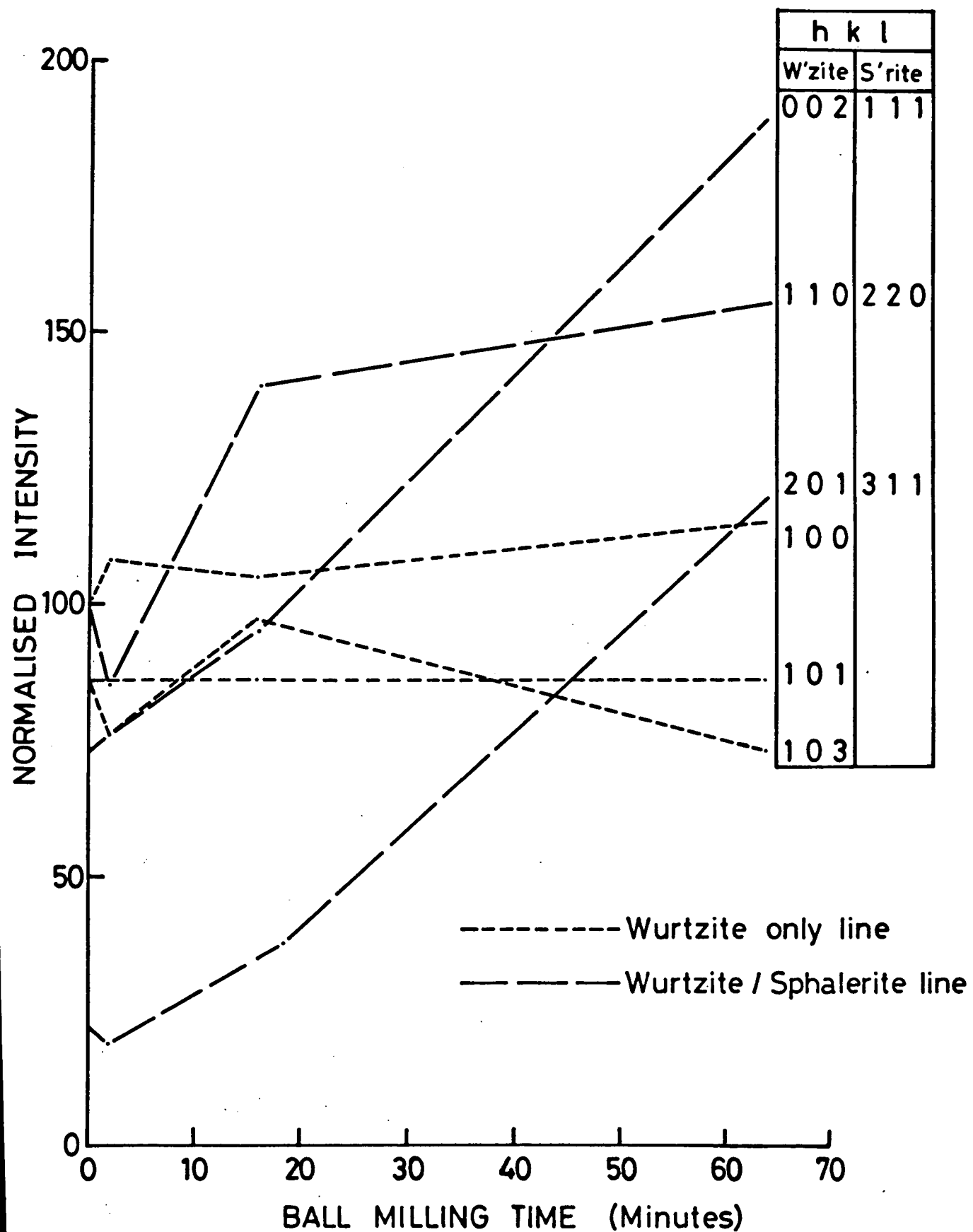


FIG. 6-18 NORMALISED LINE INTENSITIES (c.f. FIG. 6-16) AS A FUNCTION OF BALL MILLING TIME.

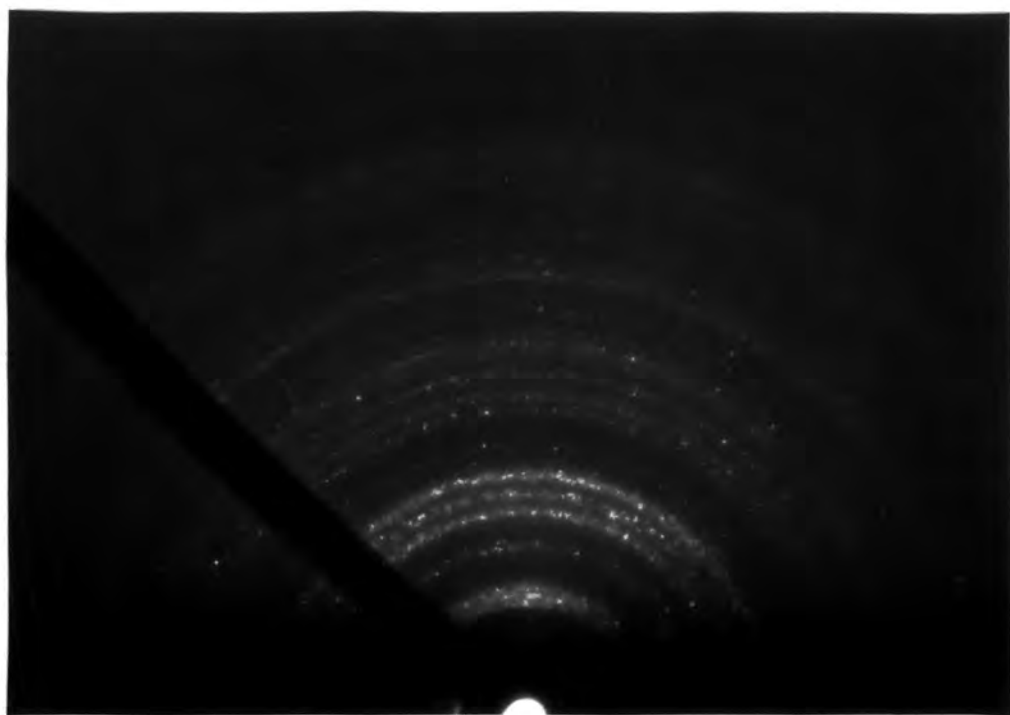


Fig. 6.19: RHEED pattern showing hexagonal (wurtzite) structure of silk screen printed powder-binder layer.

structure following this treatment. Even if chemical interaction between the CdSe and dopants can ensure a wurtzite structure, such interaction between dry crystals at room temperature could only have been minimal. The milled powder mixture was then fired in air for 2 hours at 500°C. It is considered most likely that the powder underwent a phase change during this firing (and reverted to a predominantly wurtzite structure) for two reasons. Firstly, it has been noted (5) that the cubic phase of CdSe is metastable and partial conversion to the hexagonal phase commenced on heating to 130°C. Complete conversion followed heating at 700°C for 10 hours. Secondly, mass spectrometer analysis (discussed in more detail in the following section) has indicated that large quantities of water vapour and oxygen (the latter combined with CO to give CO<sub>2</sub>) are evolved from CdSe powder heated to temperatures above around 200 to 400°C. Though it has yet to be conclusively established whether these radicals prompt the formation of, or are more readily absorbed by, the sphalerite structure, their presence has been associated with this form of CdSe.(8,15)

#### 6.4 RESULTS OF CHEMICAL ANALYSIS

The results of the six mass spectrometer scans made using an untreated Merck CdSe powder sample are presented as a graph in Fig.6.20. The inset shows how the sample temperature was varied as a function of time during the measurement period, assuming linear temperature rises between successively increased

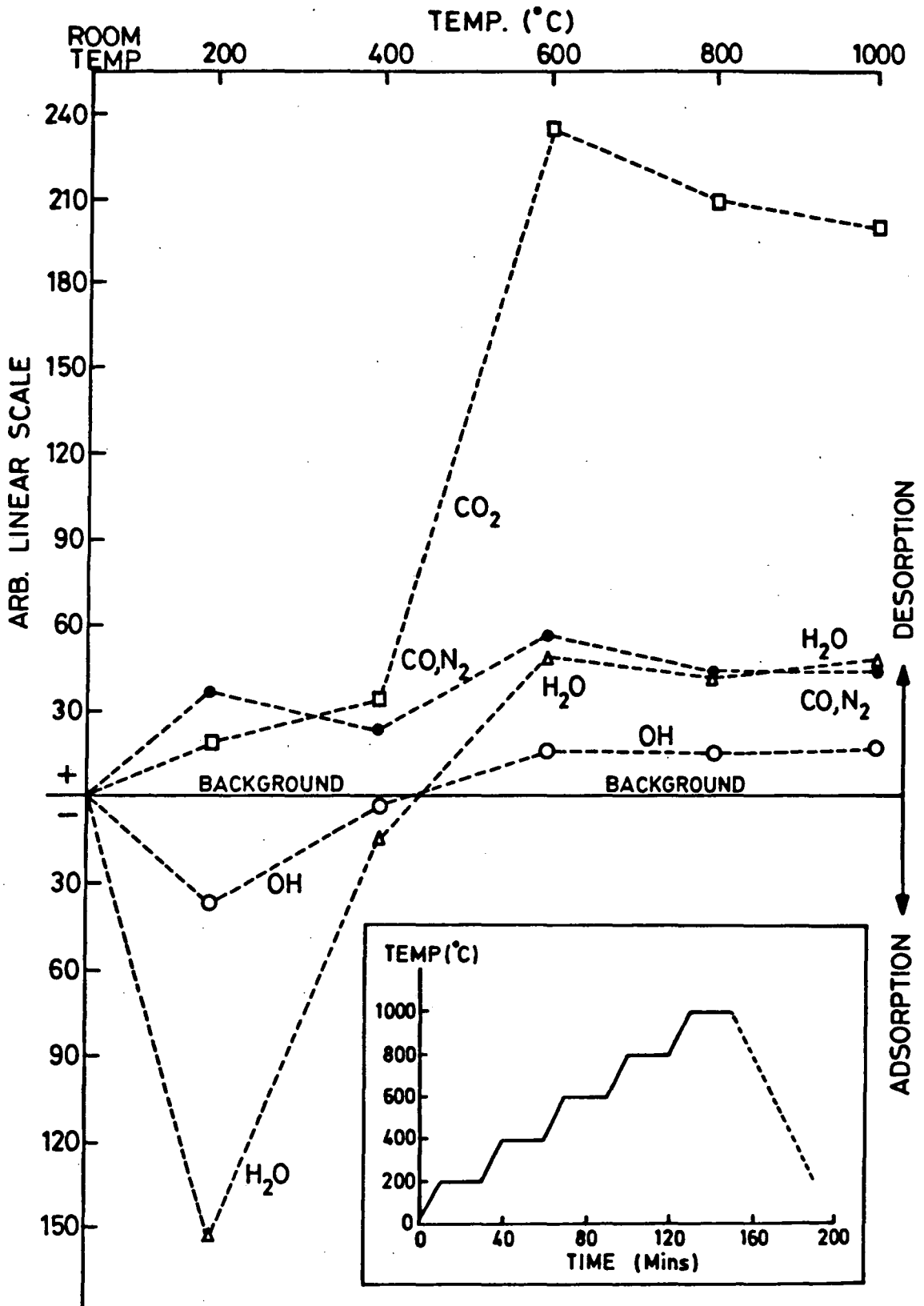


FIG.6-20 MAIN GASES ADSORBED AND DESORBED DURING FIRING OF UNTREATED MERCK CdSe POWDER.

INSET - TEMPERATURE - TIME PROFILE

Eurotherm settings. The main graph shows the recorded levels of the principal mass numbers as a function of sample temperature. Positions on the arbitrary linear scale were obtained by subtracting the recorded level for a given mass number at room temperature from the corresponding level at each elevated temperature. Thus a negative position indicates absorption by, and a positive position desorption from, the powder sample.

The most prominent features of this graph are the adsorption of water vapour up to some temperature between 200 and 400°C after which it is given off, and the enormous quantity of carbon dioxide evolved beyond this temperature. Previous study has shown that carbon monoxide is evolved when an empty, evacuated silica tube is heated. This would then be free to react with any oxygen or water vapour evolved from the CdSe powder, or may even act as a reducing agent removing adsorbed oxygen from the surface region of powder particles. As will be described in Chapter 7, the electronic behaviour of various powder samples strongly suggests that this does indeed happen. Studies of the thermal desorption spectra of pure CdS single crystal platelets (16) indicate that monatomic oxygen desorption predominates from 400-700K. In that experiment only the CdS material was heated, thereby avoiding the additional CO generation described here. The experimentally observed connection between the sphalerite structure and adsorbed oxygen in the presence of water vapour has been mentioned in the preceding section. Thus the apparent adsorption of water vapour at temperatures between room temperature and around 200°C may be



linked with the observation by Türe, Russell and Woods (15) that ageing in air to cause the surface structure of CdSe crystals to change from wurtzite to sphalerite may be accelerated by heating to temperatures within this range. They report that CdSe crystals heated in air for 16 hours at 100°C gave similar RHEED pattern indications of sphalerite structure as similar crystals exposed to air for more than 2 months at room temperature.

Fig. 6.21 shows mass spectrometer readings obtained from the doped CdSe sample, again presented in the form of a graph. To recap, this sample comprised 3g of Merck CdSe powder doped with 20,000 p.p.m. Cerac 99.999% CdI<sub>2</sub> and 1,000 p.p.m. Analar Puriss. A.R. CuSO<sub>4</sub>. Both types of dopant were introduced as solutions in Analar methanol. Many more mass numbers than from the untreated CdSe sample were detected, again only the principal ions detected have been included in Fig. 6.21. The overall vapour pressure in the firing tube (which was continually monitored during both mass spectrometer experiments) was observed to increase suddenly by an order of magnitude to approximately 10<sup>-5</sup> Torr at an indicated temperature of 380°C. Again the detected levels of mass numbers corresponding to carbon dioxide and water vapour rose sharply between 200 and 400°C, and these may have been largely responsible for the pressure increase. It is also worth noting that CdI<sub>2</sub> melts at 387°C, though free iodine molecules are too massive to have been detected by the limited range of mass numbers detectable. Similarly the peaks at mass numbers 112(Cd) and 192(CdSe) reported by Chung and Farnsworth (17) for CdSe crystals heated

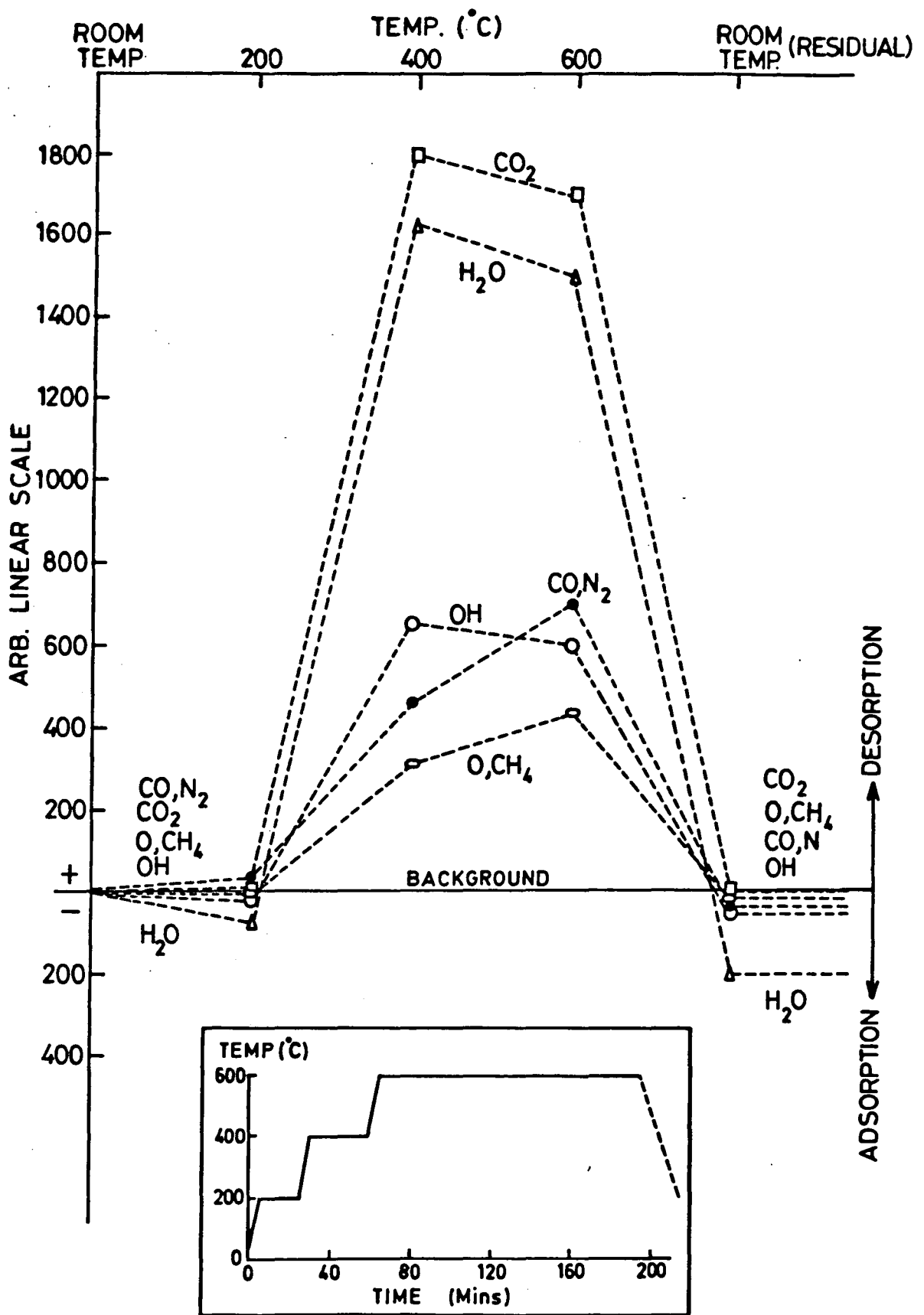


FIG.6-21 MAIN GASES ADSORBED AND DESORBED DURING FIRING OF DOPED MERCK CdSe POWDER.

INSET - TEMPERATURE - TIME PROFILE

above 400-500°C were outside the detection range. However, doubly ionized Cd (mass number 56) was not detected in appreciable quantities. Methanol vapour with associated cracking patterns was given off throughout the firing process, and sulphur dioxide (not shown) was detected in large quantities at around 600°C.

Caution must be exercised in drawing detailed conclusions from these mass spectrometer results. The inherent ambiguity in interpretation of these results may be illustrated by considering the recorded levels obtained for mass number 28. These indicate the partial pressure of nitrogen and/or carbon monoxide, and have been presumed to be due to CO because of their correlation with the carbon dioxide (mass number 44) levels. Furthermore these results cannot confirm whether the high carbon dioxide levels were produced by oxidation of carbon monoxide as already suggested, or whether the carbon monoxide presence is due to cracking of the carbon dioxide.

The most general conclusion which can be made from these investigations is that both doped and undoped samples, being in powder form, and therefore having a large surface area to volume ratio, were extremely reactive and contained large quantities of adsorbed gasses at, and slightly above, room temperature.

## 6.5 MISCELLANEOUS PHYSICAL OBSERVATIONS

The most generally observed physical variable during the preparation of sensitized powder samples was the degree of sintering which occurred during firing. This was found to vary from being negligible to being severe enough to necessitate grinding and/or sieving of the fired powders. Since it has been discovered that mechanical treatment of CdSe can promote a phase change (Section 6.4), ground powders might be expected to exhibit characteristic properties. In general such samples were found to have low conductivities and poor photosensitivity, and thus sintering during firing came to be regarded as a problem. Koch-Light CdSe suffered more from sintering than identically treated Merck powder, as did samples doped with CdCl<sub>2</sub> compared with those doped with the same concentration of CdI<sub>2</sub>. It is worth noting that Bube, while describing the preparation of sensitized CdS and CdSe powders in "Photoconductivity of Solids"(18), refers to CdCl<sub>2</sub> as a "solvent flux". The most severe sintering of all was encountered during the preparation of the P and Q series of powder samples, and was attributed to the presence of HCl required to assist solution of the Cu(I)Cl and Cu(II)Cl<sub>2</sub> dopants.

It is possible that grinding of sensitized powders may have altered their electrical properties without causing a phasechange. The chemical homogeneity of powder particles was not established, and they are unlikely to have been uniformly doped throughout their bulk. Thus fired powder particles may be

considered as consisting of a relatively intrinsic, highly resistive core surrounded by a conducting, photosensitive surface layer of unknown depth. Mechanical treatment of such powders could partially remove these surface regions, or greatly increase the concentration of strains and dislocations, both of which may act as Class I recombination centres.

In contrast, if we turn our attention to the mechanical stability of fabricated devices, the so-called "sintered layers" were found to be unacceptably brittle. Bonding between powder particles, and especially between the powder and the substrate glass, was weak. The devices prepared using a mixture of sensitized powder and nitro cellulose binder, especially those printed using the silk screen technique, proved much more satisfactory. Adhesion to the substrate material was strong irrespective of whether this was plain or 'Nesa' coated glass. The compressed powder pellets were smooth and lustrous in appearance. They suffered, however, from a tendency to flake in planes perpendicular to the direction of compression if roughly handled.

To the naked eye all powder samples appeared uniformly grey no matter what treatments they had undergone. The one exception was the CdSe powder prepared in laboratory. This was russett coloured after precipitation and drying, but changed to the usual grey colour following the prefire in argon at 700°C. This change may have been due to the loss of volatile impurities or to a change in powder particle size. The firing process was found to have caused sufficient sintering to make grinding necessary, despite the lack of added dopants.

## CHAPTER 6: REFERENCES

- 1) SATO. K., NISHIMURA M. and YOSHIZAWA M. "DC Conductivity of Compressed CdSe Powders" Jap.J.Appl. Phys. 12, No. 8, 1274-7 (1973).
- 2) MELLIKOV E. Ya. et al "Effect of the Nature of the Fusing Agent on the Mechanism of Crystallization and Morphology of Phosphor Crystals Based on CdS and CdSe" Bull. Acad. Sci.(USSR) Physical Series (USA) 40, Pt.11, 63-4 (1976).
- 3) GOLDSCHMIDT V.M. "Laws of Crystal Chemistry" Naturwissenschaften 14, 477-85 (1926)
- 4) NAGATA S. and AGATA K. "On the Crystal Structure of Cadmium Selenide of Selenium Rectifier" J. Phys. Soc. Jap. 6, 523-4 (1951)
- 5) PASHINKIN A. and SAPOZHNIKOV R. "A Cubic Modification of Cadmium Selenide" Sov. Phys. - Cryst. 7, No.1, 501-2 (1962)
- 6) DÄWERITZ L. "Stoichiometry and Phase Composition of Vacuum Deposited Films of A(II) B(VI) Compounds" J. Cryst. Growth 23, 307-12 (1974)
- 7) STUCKES A.D. and FARRELL G. "Electrical and Thermal Properties of Alloys of CdTe and CdSe" J. Phys. Chem. Solids. 25, No.5, 477-82 (May 1964)

- 8) TANAKA K. "Photoconductivity of CdSe Films Prepared by a Vapor Evaporating-Reactive Spattering Method" Jap. J. Appl.Phys. 9, No.9, 1070-7 (1970)
- 9) RUSSELL G.J., FELLOWS A.T., OKTIK S., TÜRE E. and WOODS J. "Mechanically Induced Phase Transformations in CdS, CdSe and ZnS" J. Mat. Sci. Lett. 1, 176-8 (1982)
- 10) CULLITY B.D. "Elements of X-Ray Diffraction" pub: Addison-Wesley Inc., London (1967)
- 11) BLAKEMORE J.S. "Solid State Physics" Second Edition. Pub: W.B. Saunders Co., Philadelphia, London, Toronto (1974)
- 12) TAKEUCHI M.,KANETO F. and NAGASAKA H. "Effects of Grinding on the Photoconductive Properties of CdS Powder J. Soc. Mater. Sci. (Japan), 23, Pt 250, 536-40 (1974)
- 13) HIRSCH P.B. et al "Electron Microscopy of Crystals" Pub: Butterworth (1965)
- 14) ANDREWS K., DYSON D. and KEARN S. "Interpretation of Electron Diffraction Patterns" Pub: Hilger and Watts, London (1967)
- 15) TÜRE I, RUSSELL G. and WOODS J. "Photoconductivity, Structure and Defect Levels in CdSe Crystals "J. Cryst. Growth 59, 223-228 (1982)

- 16) SCHUBERT R. and BÖER K. "Description of Oxygen and its Influence on the Electrical Properties of CdS Single Crystal Platelets "J. Phys. Chem. Solids 32, 77-92 (1971)
  
- 17) CHUNG M.F. and FARNSWORTH H.E. "Effect of Bulk Resistivity, Annealing Temperature and Illumination on Oxygen Sorption and CdSe Surfaces" Surface Sci. 25, 321-31 (1972)
  
- 18) BUBE R.H. "Photoconductivity of Solids" Pub: Robert E.Krieger, New York (1978).

## CHAPTER 7: RESULTS OF ELECTRONIC MEASUREMENTS

### 7.1 INTRODUCTION

At least one aspect of electrical behaviour was investigated for almost every one of the 171 powder samples prepared as well as for most of the fabricated devices. Thus a large number of electronic measurements were made, and these were frequently found to require collective analysis before correlations between electrical behaviour and preparation conditions became apparent. The latter will not be described again in this chapter; instead details of the preparation of specific samples should be obtained when required by reference back to the comprehensive listings of Fig. 3.4.

Most information about the role of preparation conditions in determining electronic characteristics is gained by comparison of results obtained for different samples. To reliably attribute an observed variation in electrical behaviour to a single preparation stage, it is necessary for all other stages to be invariant. This was the basis for preparation of the final 48 powder samples (i.e. those commencing with numerals) listed in Fig.3.4. Analysis of the previous powder samples by comparison was more complex, and led to assessment of 6 additional preparation stages. These were frequently not simple binary alternatives, but a spectrum of possibilities, sometimes with an insufficient number of results for a conclusive trend to be established.

Having linked observed electrical behaviour to preparation conditions by these statistical treatments of results, interesting features in the performance of individual samples will be discussed later in the chapter.

The principal parameters of electronic behaviour derived from results recorded for the early series of powder samples were conductivity in darkness ( $\sigma_D$ ), and under constant illumination ( $\sigma_L$ ), and the rise and fall time constants  $\tau_R$  and  $\tau_F$  for the transitions between these states. The derivation of these parameters will now be explained.

Values of  $\sigma_D$  and  $\sigma_L$  were derived from the current-voltage characteristics experimentally recorded for each sample. In common with previous observations of conduction in CdSe powders (1,2), these typically exhibited a superlinear dependence of current on applied field. Thus  $\sigma_D$  and  $\sigma_L$  were also both typically dependent on the applied field. When comparing values of  $\sigma_D$  and  $\sigma_L$  between samples, therefore, care was taken to ensure that they had been calculated from current levels at the same applied field in each case. When calculating  $\sigma_L$ , allowance was not made for the limited photoexcitation penetration depth, and the entire powder test cell cross sectional area was considered as for  $\sigma_D$ . Hence values of  $\sigma_L$  presented in this chapter correspond to  $\sigma_L^*$  of Fig.5.6 and the associated discussion. It is certain that the true increases in conductivity due to photoexcitation were underestimated by several orders of magnitude. However, since the results for all powder samples were derived on this basis, comparisons remain valid.

Values of  $\tau_R$  and  $\tau_F$  were derived from measurements of current-time characteristics generated by abrupt transitions from darkness to full illumination ( $\tau_R$ ) or vice versa ( $\tau_F$ ). These characteristics were in the form of photographed C.R.O. traces or X-t plotter graphs depending on the speed of response. In most cases the steady state dark current  $I_D$  was assumed to be negligibly small in comparison with steady state photocurrent  $I_L$ . Furthermore it was assumed that both types of transition were approximately exponential in form. This was found to be reasonably true of photocurrent rise curves, but a characteristic 'tail' was observed at the end of many decay curves. A cause of these 'tails' was discussed in Section 2.4. More importantly, however, extensively prolonged decay curves provided evidence of photochemical changes taking place in some samples.

## 7.2 POWDER SAMPLES: STATISTICAL OBSERVATIONS

An important preliminary statistical comparison was made between the measured electrical behaviour of pairs of identically prepared powder samples. The degree of reproducibility observed has a direct bearing on the significance which may be attached to comparisons of such results obtained from dissimilar powder samples. Fig. 7.1 graphically illustrates the reproducibility of measured values of  $\sigma_D$  and  $\sigma_L$  for 6 pairs of identically prepared samples. These histograms were generated by dividing the higher measured value by the lower for each pair of results. The

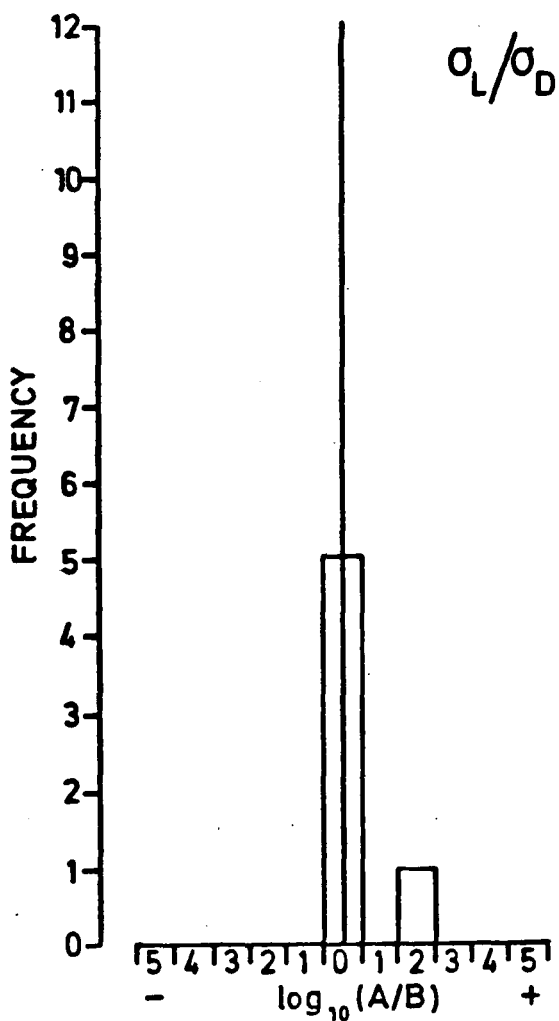
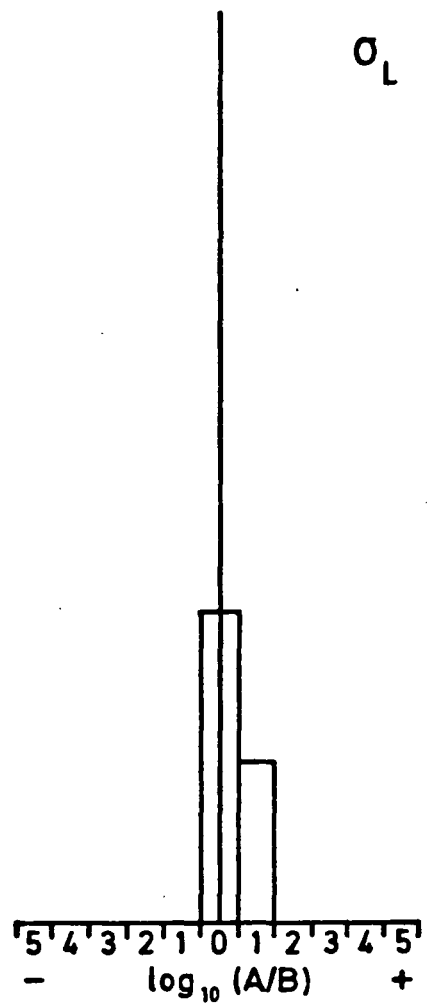
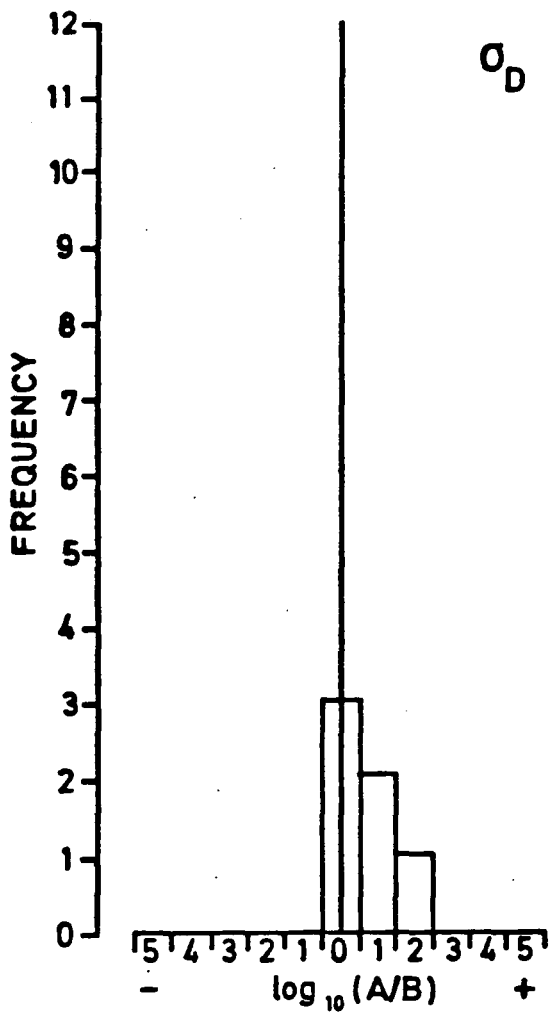


FIG. 7.1 RELATIVE CONDUCTIVITIES FOR 6 PAIRS OF IDENTICALLY PREPARED POWDER SAMPLES.

A = HIGHER MEASURED  $\sigma_D$  OR  $\sigma_L$  VALUE  
 B = LOWER MEASURED  $\sigma_D$  OR  $\sigma_L$  VALUE  
 FOR EACH PAIR.

dimensionless value  $|\log_{10}(A/B)|$  may be considered as the exponent of each ratio when written in scientific notation. Thus it is apparent that  $\sigma_D$ ,  $\sigma_L$  and  $\sigma_L/\sigma_D$  were typically within one order of magnitude (o.m.) of each other. Only on 2 occasions were they two o.m. apart, and one of these ratios was only  $1.07 \times 10^2$ . Therefore differences in relative measured conductivities between dissimilar powder samples consistently exceeding 1 o.m. may be considered significant and hence associated with the varied preparation stages. Photocurrent rise and fall time constants  $\tau_R$  and  $\tau_F$  were between 1 and 10ms for all 12 powders tested, the highest ratio between results for identically prepared samples being around 3. Typical ratios of measured values were between 1 and 1.5, indicating a high degree of reproducibility. However, little variation in measured values of  $\tau_R$  and  $\tau_F$  was observed for the whole range of powder samples tested, especially when compared with the ratios of measured conductivities which spanned up to 5 orders of magnitude.

If we now consider the effect of the preparation stages of the earlier (A to Y) series of powders, the logical starting point is the influence of source material i.e. untreated CdSe powder. Of the three commercially produced powders, Merck and Cerac yielded similar conductivities and response times after sensitization. The one measurable comparison between Merck and Koch-Light powders, however, revealed that although measured dark conductivities were identical within experimental error, the light conductivity  $\sigma_L$  of the Merck Powder was some 2 o.m. higher. In general, powders prepared from Koch-Light CdSe exhibited the lowest photosensitivities, hence its use as a source material was

discontinued in the later samples. These findings are, perhaps, initially surprising since all three commercial powders were prepared to the same (99.999%) claimed purity. Also it will be recalled from the previous chapter that Koch-Light and Cerac CdSe were similar in appearance while the Merck powder particles were more angular in shape, suggesting a different preparation technique. However, the lower photosensitivity of Koch-Light powder samples may be associated with long-term exposure to the atmosphere. Both the Cerac and Merck powders were supplied in small bottles sealed under vacuum. In contrast the Koch-Light CdSe was in a large bottle which had been opened months before use in sensitized powder sample preparation. It was also noted that the Merck powder was more readily "wetted" by dopant solutions, perhaps owing to the more angular particle shapes.

The effect of pre-firing was only investigated in a small number of samples and was therefore not conclusively established. Pre-firing Koch-Light CdSe powder was found to reduce conductivity levels below the threshold of measurement apparatus sensitivity. Similar treatment of the laboratory produced powder for 60 minutes caused the colour change and sintering described earlier. Photosensitivity was found to have been reduced by 2 orders of magnitude. It is suspected that impurity levels in this powder were substantially higher than in the commercially produced powders.

The effect of copper compound was initially investigated by comparing the performance of samples doped with similar concentrations of copper sulphate, nitrate and acetate. Though

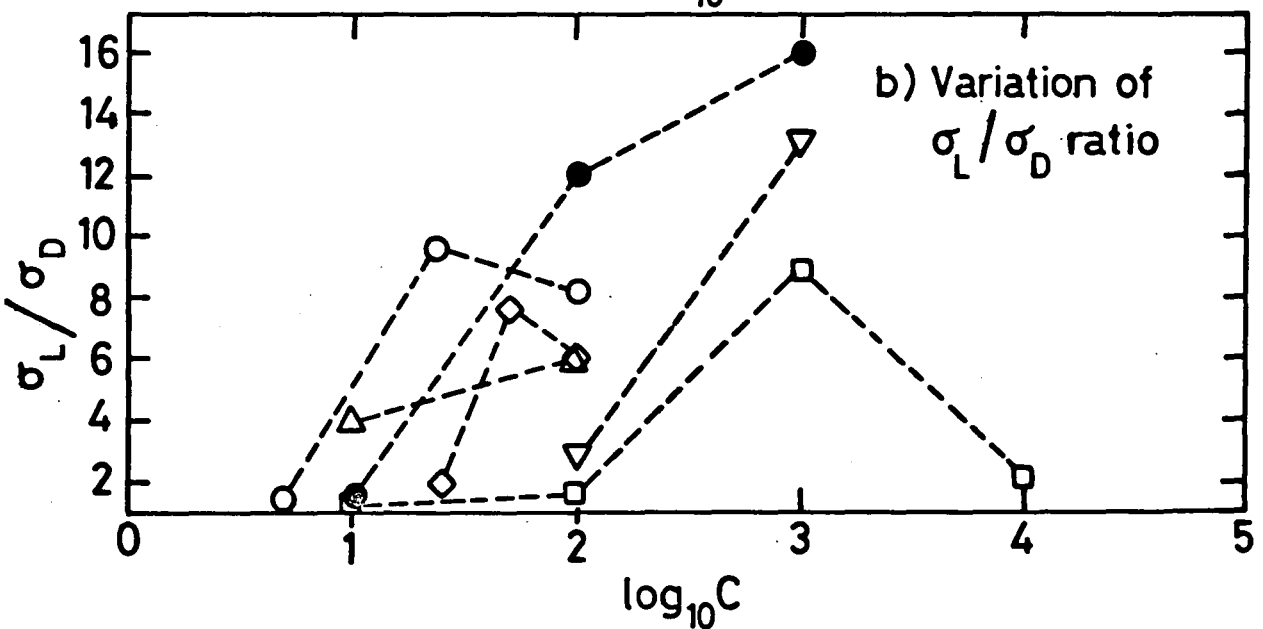
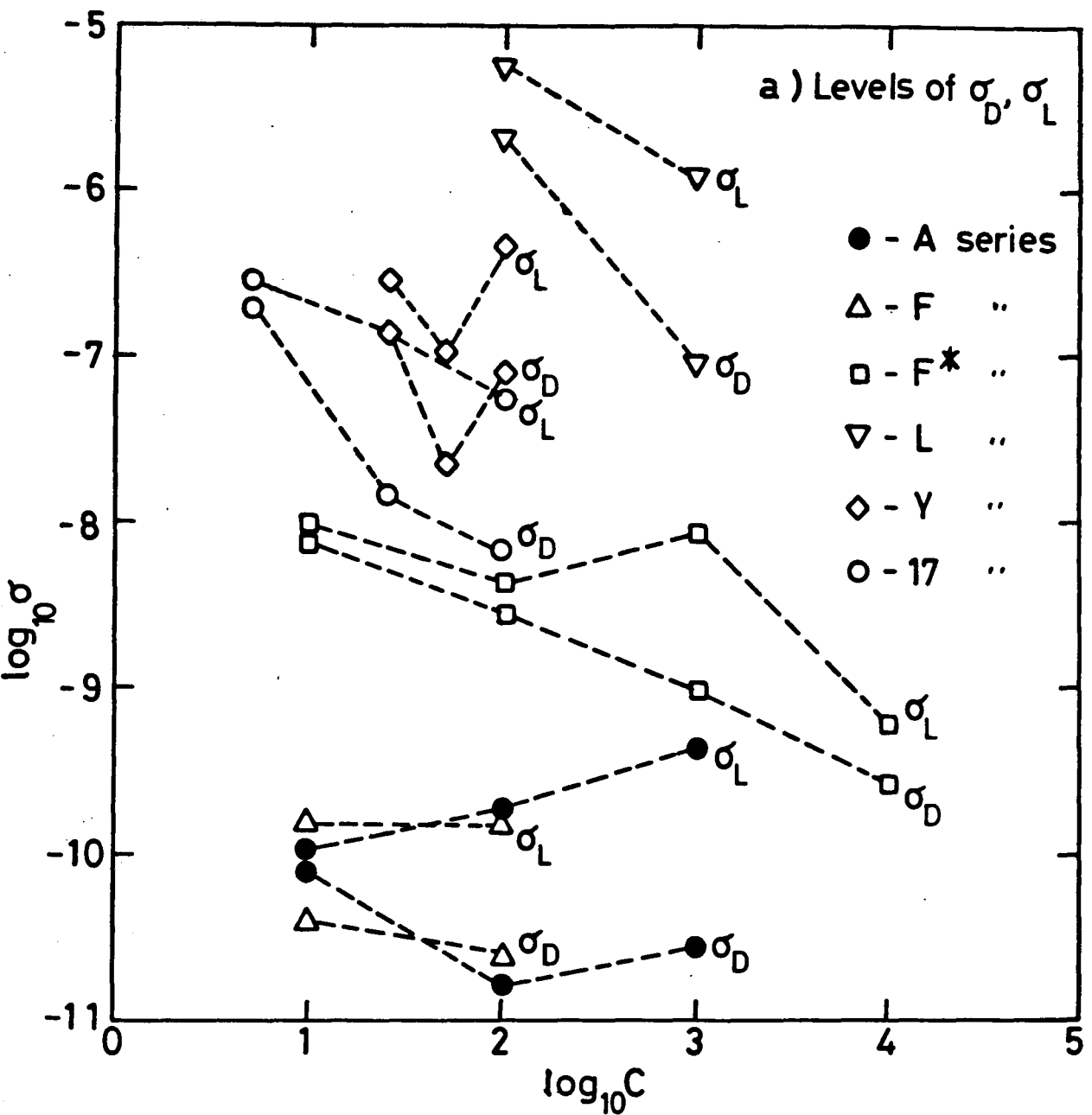
numerous results were obtained no clear pattern emerged. Copper sulphate produced the best results for unwashed samples with  $\sigma_L/\sigma_D$  ratios of up to  $5.3 \times 10^4$  (sample J1\*). However, sample K2 doped with copper nitrate yielded the highest  $\sigma_L/\sigma_D$  ratio (34) of all samples which were washed in distilled water. Powders prepared with copper acetate exhibited higher dark and photocurrent levels, but lower photosensitivity.

Comparison between the effects of doping with Cu(I)Cl and Cu(II)Cl<sub>2</sub> were overshadowed by the problems of solubility associated with cuprous compounds. The HCl which was added with the cuprous chloride to assist solution is thought to have been responsible for the extremely severe sintering of powder samples doped with the resulting mixture. Nonetheless Cu(I)Cl appeared to promote high sample conductivity, though again poor photosensitivity. Neither type of chloride produced such successfully sensitized powders as those prepared with copper sulphate, and thus the latter was used as the copper dopant in the majority of samples.

The optimum copper concentration (for the range of commonly used halide concentrations) was found to be around 1000 p.p.m. (CuSO<sub>4</sub>). Maximum  $\sigma_L/\sigma_D$  ratios were recorded at this concentration, though not the highest absolute levels of dark current and photocurrent. These increased at lower concentrations, as did the response time constants  $\tau_R$  and  $\tau_F$ . Increasing the copper concentration above 1000 p.p.m. produced the opposite effect, as would be expected from the discussion of Chapter 2.

The general characteristic shown in Fig.2.2 should be compared with the data presented in Fig.7.2. These sets of conductivity versus incorporated copper concentration curves were derived from measurements on 6 series of powder samples, the incorporated halogen concentration being constant throughout each series. In the 17 series this was 2,000 p.p.m., in the Y series it was 5,000 p.p.m. and in the other four series it was 20,000 p.p.m. The type of halogen incorporated was chlorine in the A and 17 series and iodine in the remainder. Though these results are broadly scattered, a general increase in photosensitivity for Cu concentrations around 1,000 p.p.m. when in conjunction with 20,000 p.p.m. halogen doping is apparent. The Y and 17 series pass through peak  $\sigma/\sigma_0$  ratios for lower Cu concentrations of around 50 and 25 p.p.m. respectively, and it should be noted that these are in conjunction with corresponding halogen doping levels of 5,000 and 2,000 p.p.m. Thus a degree of interdependence between the effect of copper and halogen concentrations upon photosensitivity is exhibited and is in agreement with the activator and co-activator model outlined in Chapter 2. The F\* series of samples in particular exhibit the expected reduction of dark conductivity resulting from increased copper doping levels.

Comparable information about the role of halogen source and concentration in powder sensitization was repeatedly investigated in the numbered samples which are discussed later in this section. Other comparisons which were made using the early powders but more systematically investigated in the later series are the effects of dopant solvent, firing method and



7.2 DEPENDENCE OF  $\sigma_D$  AND  $\sigma_L$  FOR SIX SERIES OF POWDER SAMPLES UPON INCORPORATED Cu CONC.(ppm) C.

washing of samples.

In an attempt to improve powder photosensitivity, the 'Analar' grade dopants initially used were replaced by high purity chemicals of Puriss A.R. (99.999%) quality. Comparison of results obtained for samples G4 and J1\* indicates that this substitution is associated with increased  $\sigma_L$  levels, reduced  $\sigma_D$  levels and a 3 o.m. increase in the  $\sigma_L/\sigma_D$  ratio. Measurement and all other preparation conditions were identical for this pair of samples. Furthermore the time stability of  $\sigma_D$  and especially  $\sigma_L$  was improved by the use of high purity dopants, perhaps owing to a reduction of photochemical reactions involving trace impurities.

Although a variety of firing durations and temperatures were tried, correlations between these and measured electrical performance were not consistent, and appeared to be dependent on other factors such as the nature and concentration of dopants present. For example, samples G1\*, G2\* and G3\* which were fired for 30, 60 and 90 minutes respectively, exhibited conductivity, photosensitivity and response time constants all increasing with firing time. Similar samples fired for 90, 120 and 150 minutes respectively showed a less definite trend in behaviour, though conductivity levels did decrease for firing times in excess of 90 minutes. Generally the problem of powder firing conditions appears to be a compromise between several effects. While increasing firing time at elevated temperature may be expected to increase sensitization by improved dopant diffusion into the powder particles, it may also cause reaction with uncontrolled

impurities present and the loss of any volatile chemical agents. Sintering during firing was found to be a serious problem with some dopants as mentioned previously, and the subsequent grinding required had a generally de-sensitizing effect. These problems were aggravated by elevated firing temperatures. The most dramatic and consistent trend related to firing conditions was determined by the choice of firing method as will be described shortly.

The statistical observations described in the remainder of this section are based on results obtained from the later series of powder samples. They were sporadically investigated during the course of earlier powder preparation, but the large sample population available using the later powders was felt to provide more reliable correlations. A theoretical maximum of 24 comparisons could be made for each preparation choice investigated; in practice this figure was invariably somewhat lower since full data sets were not obtainable (using the instrumentation described) for all powder samples.

The effect of dopant solvent on sample conductivity levels is shown by the histograms of Fig. 7.3. It may be seen that powders prepared using dopants dissolved in methanol produced marginally better results in terms of photosensitivity, though the majority of compared conductivity levels were within 1 order of magnitude of each other. A further breakdown of these results reveals that there is no correlation between dopant solvent and washing agent e.g. powders prepared with dopants dissolved in methanol do not necessarily exhibit higher conductivity levels

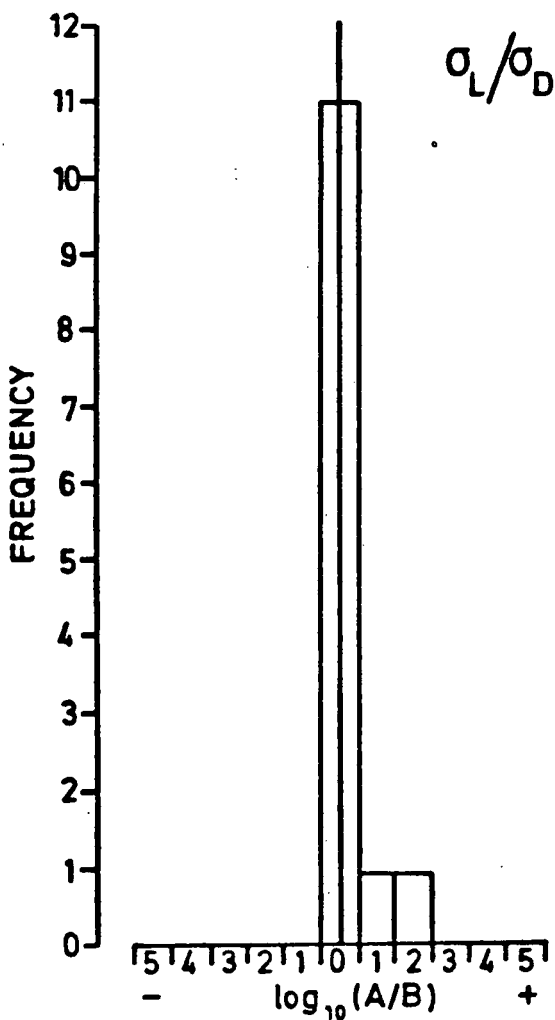
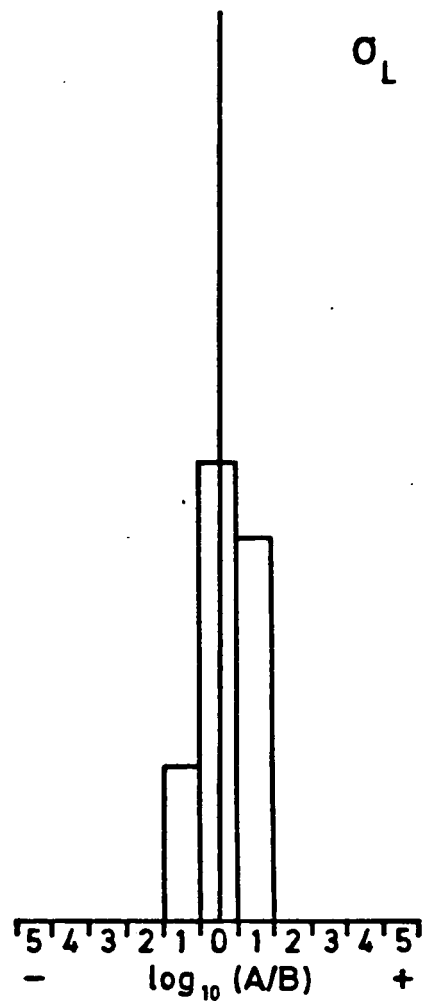
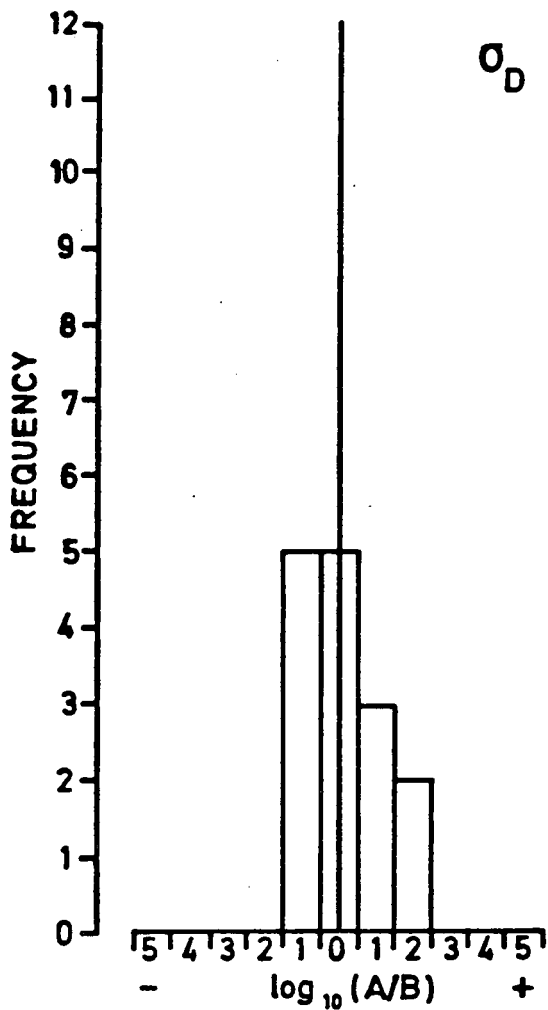


FIG. 7-3 RELATIVE CONDUCTIVITIES FOR POWDER SAMPLES PREPARED WITH DOPANTS DISSOLVED IN,  
 A : METHANOL  
 B : DISTILLED WATER

after washing in methanol than after washing in distilled water.

The histograms of Fig. 7.4 illustrate the dependence of conductivity levels on the type of halogen compound used. These results strongly suggest that higher concentrations of halogen ions diffuse into the CdSe powder during firing if the source is CdI<sub>2</sub> rather than CdCl<sub>2</sub>. This difference may be related to the lower melting and boiling points for CdI<sub>2</sub> of 387°C and 796° respectively, compared with corresponding values for CdCl<sub>2</sub> of 568°C and 960°C. Thus the vapour pressures of these two compounds at a firing temperature of 600°C would be considerably different. Indeed, a purple vapour was clearly visible within firing tubes containing samples doped with CdI<sub>2</sub> indicating an appreciable partial pressure of free iodine.

Increasing the proportion of CdI<sub>2</sub> or CdCl<sub>2</sub> added to the CdSe powder from 2,000 to 20,000 p.p.m. was found to cause only a slight increase in conductivity levels as shown by Fig.7.5. The ratio of dark to light current remained unchanged within an order of magnitude for all samples. It should be recalled that the same concentration of CuSO<sub>4</sub>(500 p.p.m.) was present in each case, and that incorporation of the two dopants into each powder sample is likely to be strongly interdependent. Cross referencing these with the previous set of results reveals that this behaviour was equally typical of CdI<sub>2</sub> and CdCl<sub>2</sub> doped samples. Of the 9 conductivity increases of an order of magnitude or more, 5 were recorded for samples doped with CdI<sub>2</sub> and 4 for samples doped with CdCl<sub>2</sub>. The unchanged ratios of light to dark conductivities imply that the halogen ions are not present in the fired powder

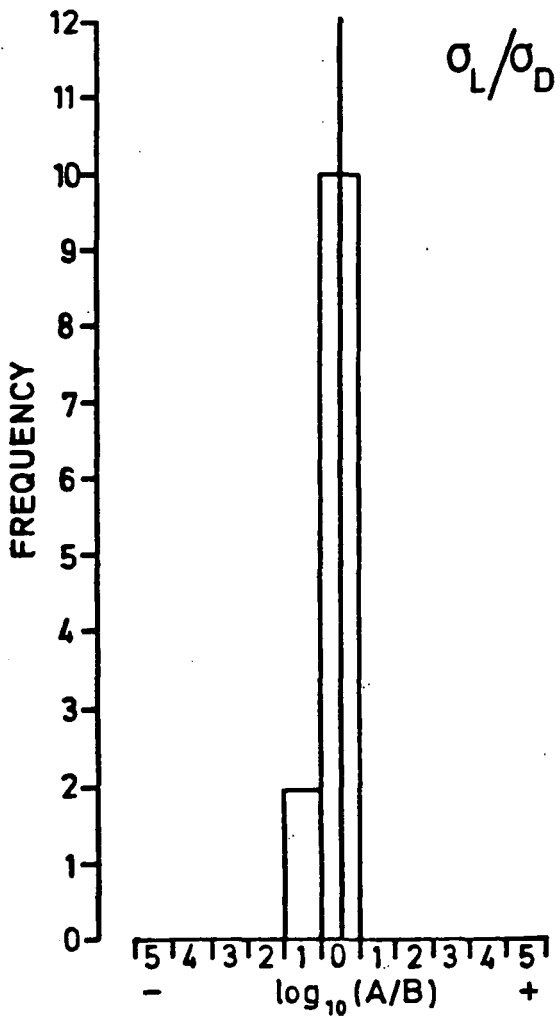
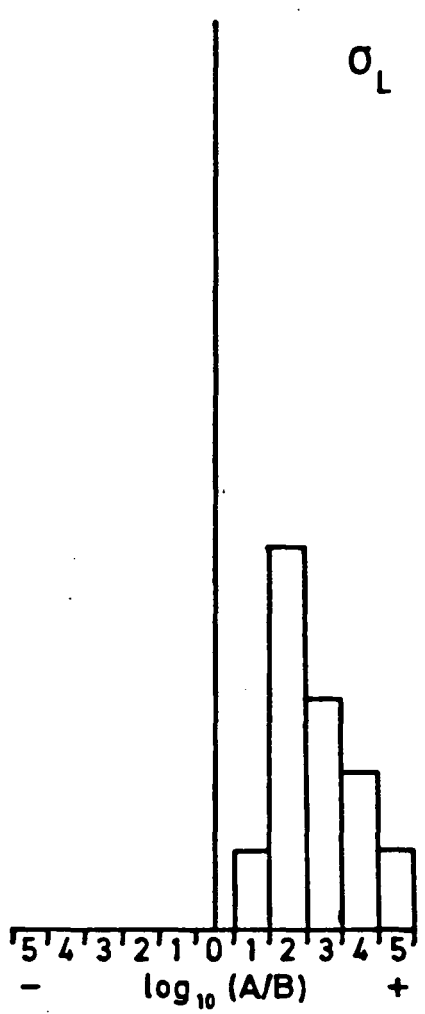
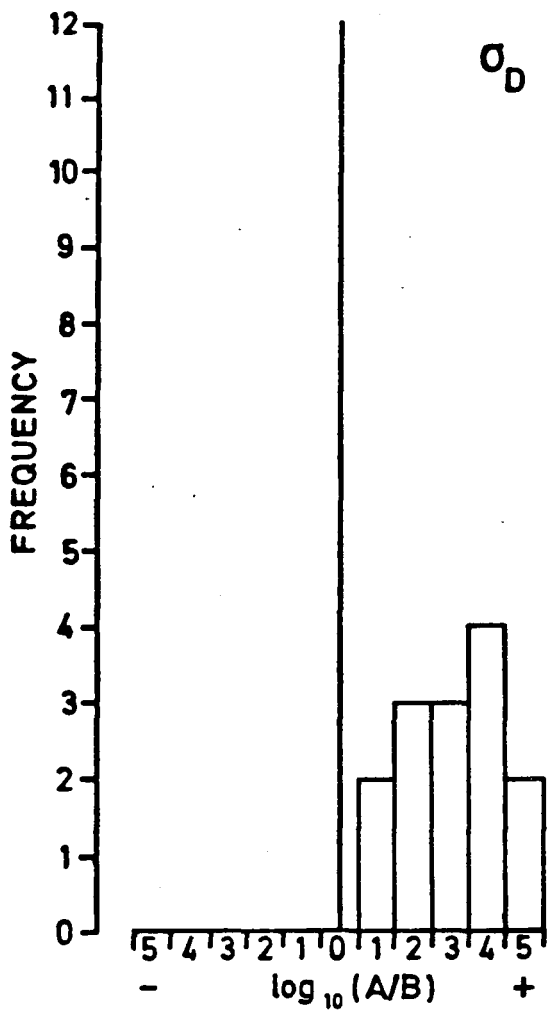


FIG. 7.4 RELATIVE CONDUCTIVITIES FOR POWDER SAMPLES PREPARED USING ,  
 A : 99.999% Cd I<sub>2</sub>  
 B : 99.999% Cd Cl<sub>2</sub>

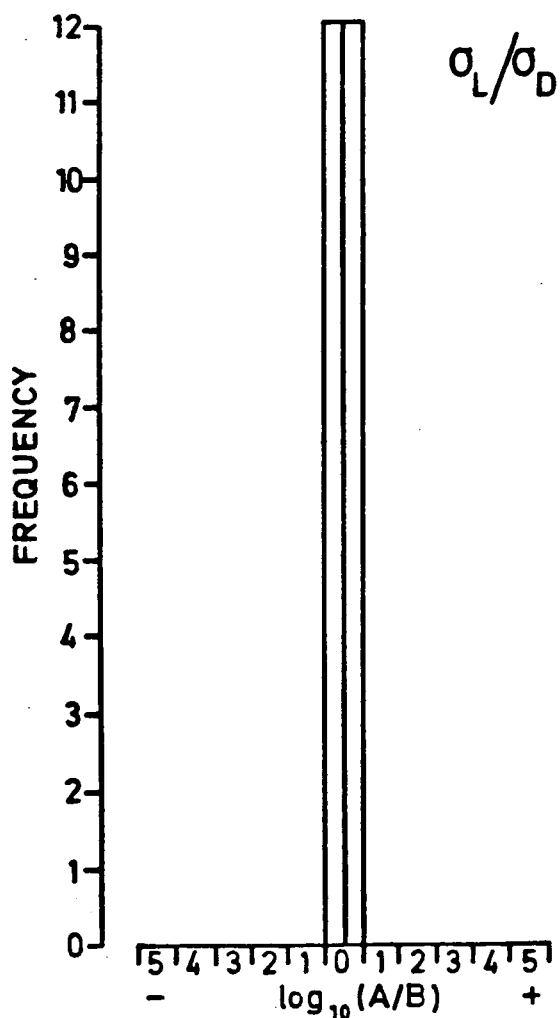
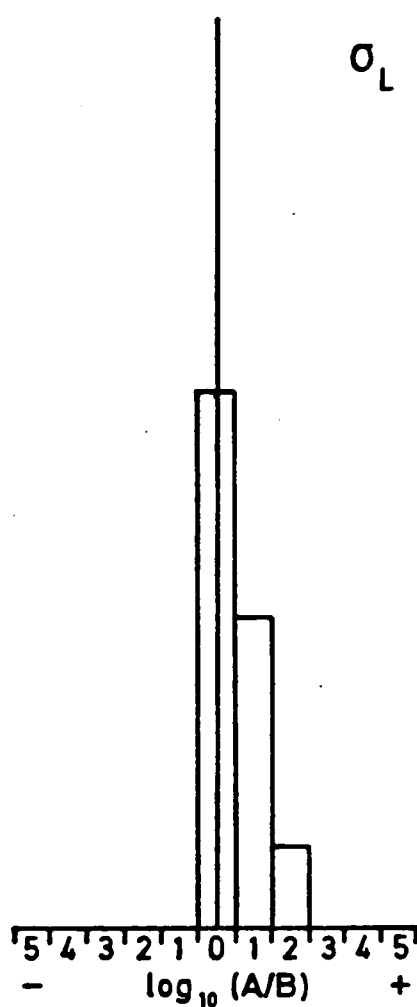
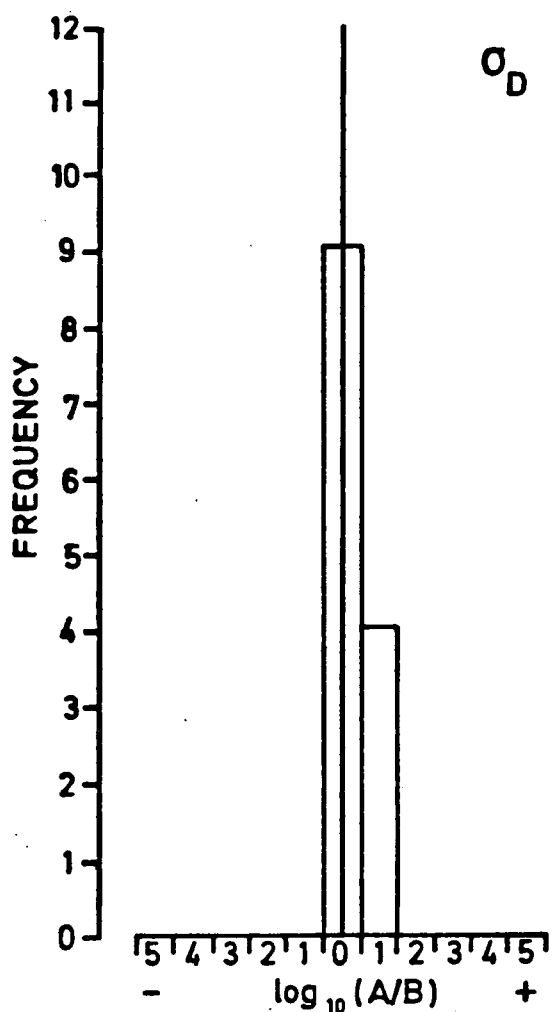


FIG. 7-5 RELATIVE CONDUCTIVITIES FOR POWDER SAMPLES PREPARED USING ,  
 A : 20,000 ppm Cd I<sub>2</sub> OR CdCl<sub>2</sub>  
 B : 2,000 ppm Cd I<sub>2</sub> OR CdCl<sub>2</sub>

samples at saturation levels, but rather that similar proportions have been incorporated in each case.

The most differentiated results obtained from this series of experiments become apparent when the two firing methods are compared. Fig. 7.6 illustrates the consistent increase of conductivity levels by several orders of magnitude characteristic of powders fired using the partial pressure technique. An explanation of this effect in terms of CdSe surface chemistry may be given as follows.

It will be recalled from the preceding chapter that large quantities of CO<sub>2</sub> were detected when a CdSe powder sample was heated in a fused silica tube. It was suggested that this was due to desorbed oxygen from the CdSe powder combining with CO liberated from the silica tube itself, or even a direct reducing action by the CO on the CdSe powder particle surfaces. Many authors have observed comparable changes in the measured conductivity levels and photosensitivity of both CdSe and CdS in various forms attributed to the effects of atmospheric water (3) and oxygen (4-16). A review of these findings will be incorporated in the discussion at the end of this chapter. Generally it is concluded that adsorbed oxygen acts predominantly as an acceptor on the CdSe surface and may therefore decrease the surface conductivity by many orders of magnitude.

Any oxygen lost from the surface of CdSe powder particles as a result of thermal desorption or chemical action of CO or other

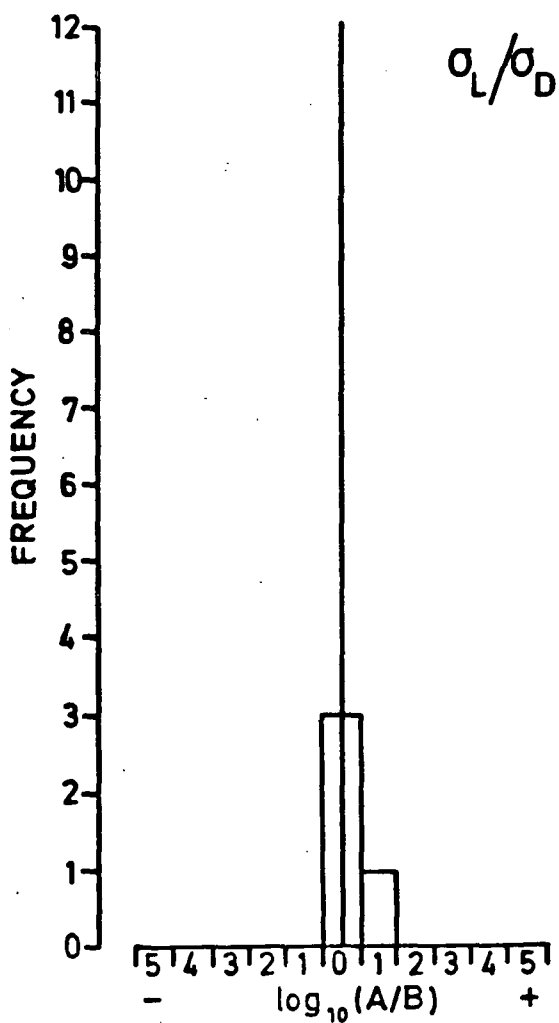
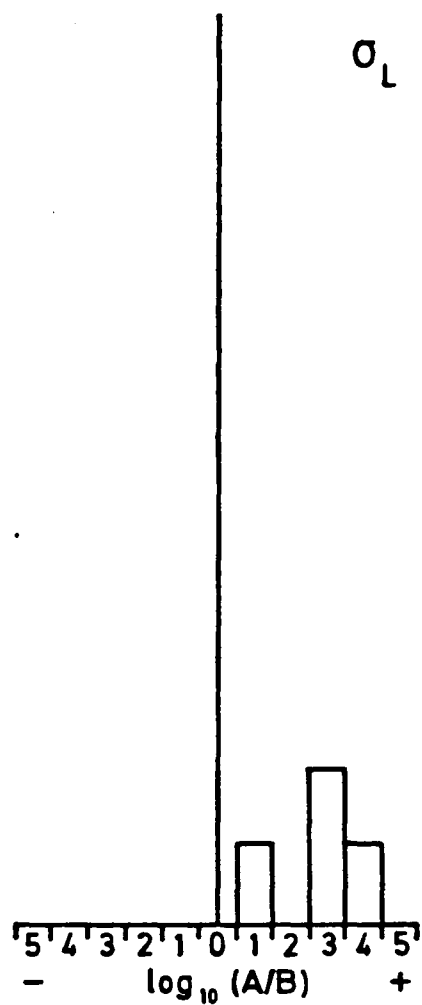
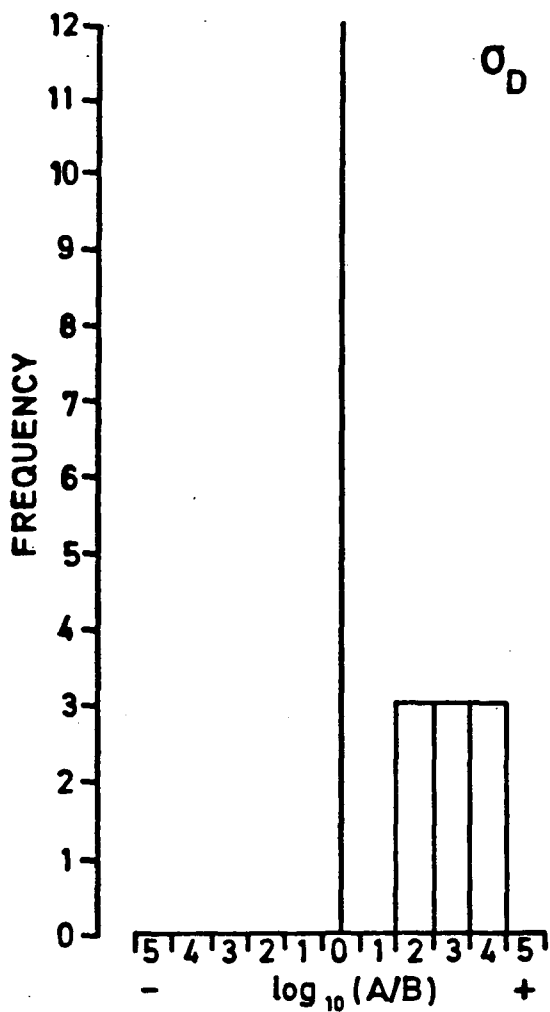


FIG. 7-6 RELATIVE CONDUCTIVITIES FOR POWDER SAMPLES PREPARED USING,  
 A : PARTIAL PRESSURE FIRING METHOD  
 B : POROUS PLUG FIRING METHOD

reducing agents present during the porous plug firing method could be replaced upon cooling as atmospheric oxygen was drawn back into the firing tube. This could not, however, occur in the partial pressure firing tubes which remained sealed and evacuated until their contents were loaded into a powder test cell for measurement. Furthermore these tubes were sealed prior to firing by heating the silica necks to a temperature between 1200 and 1500°C and pinching as described in Chapter 3. Such treatment would liberate relatively large quantities of CO from the silica, some of which would inevitably remain in the sealed portion of the tube.

Supporting evidence for this explanation is provided by the repeated observations that when samples prepared by the partial pressure method were re-tested after prolonged exposure to the atmosphere at room temperature their conductivity levels were found to have fallen by several o.m. Indeed, in several cases measured electrical performance subsequently approached that of the equivalent samples produced by the porous plug firing method.

The final set of statistical comparisons made using the later series of powders was between unwashed, fired powder samples, and portions of the same samples which had been washed in either 'Analar' grade methanol or distilled water. These results are shown in the histograms of Figs. 7.7 and 7.8, and consistently indicate that neither washing agent has either a large or a desirable effect on conductivity levels. Distilled water was found, on average, to cause greater reduction of conductivity levels.

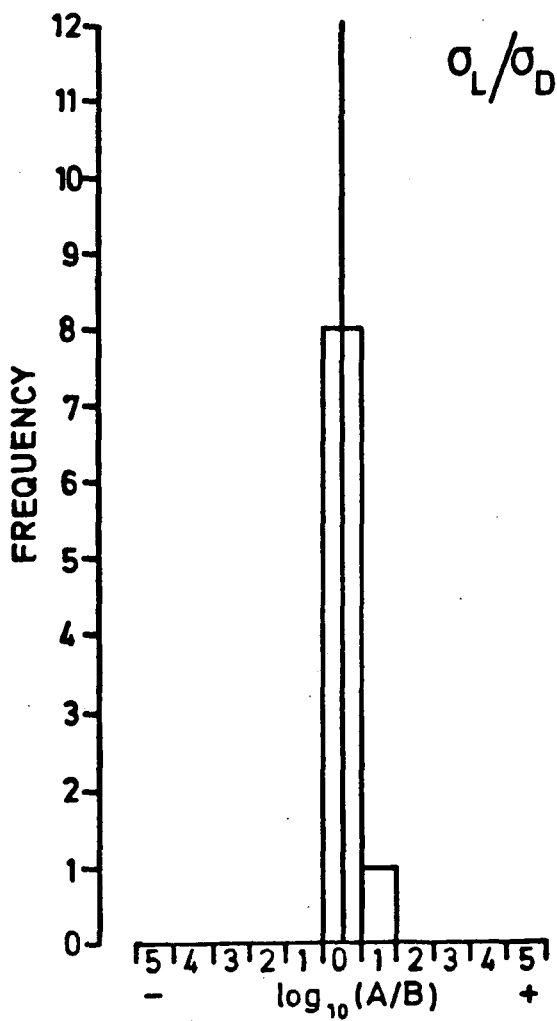
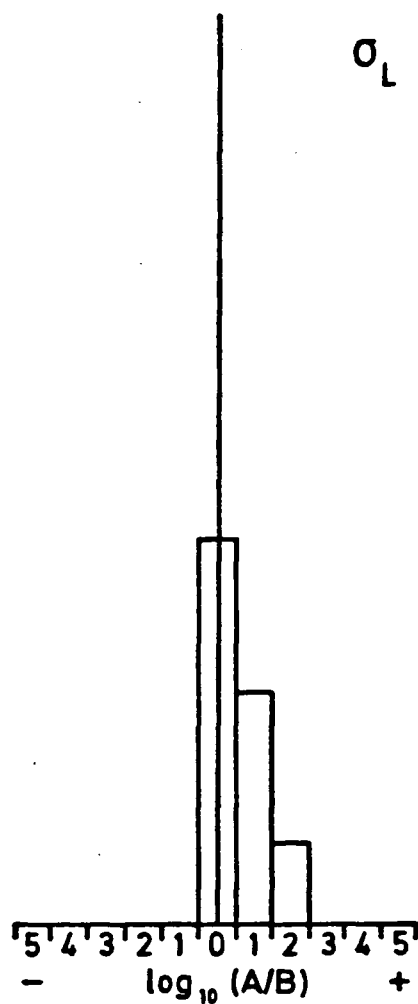
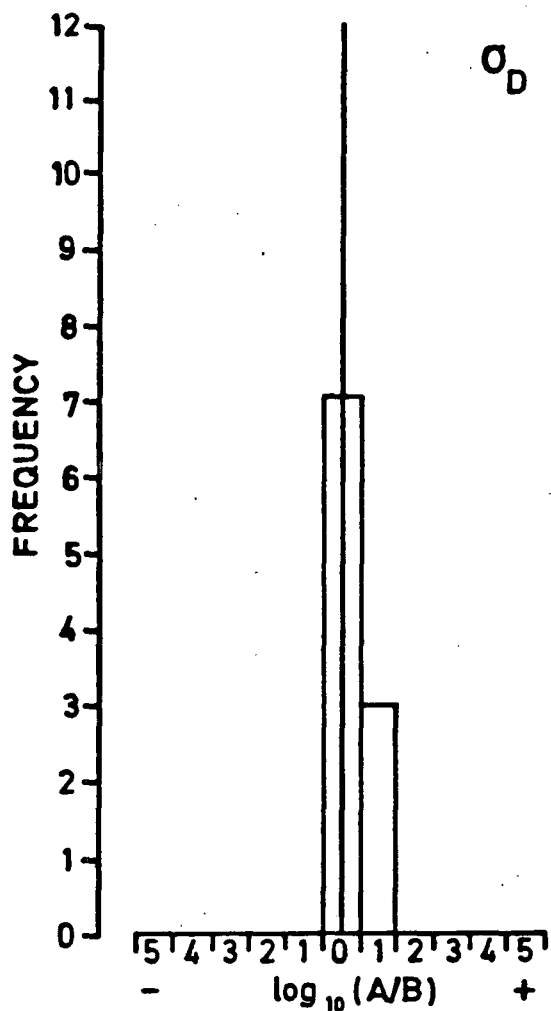


FIG. 7.7 RELATIVE CONDUCTIVITIES FOR POWDER SAMPLES, A: UNWASHED B: WASHED IN 'ANALAR' METHANOL

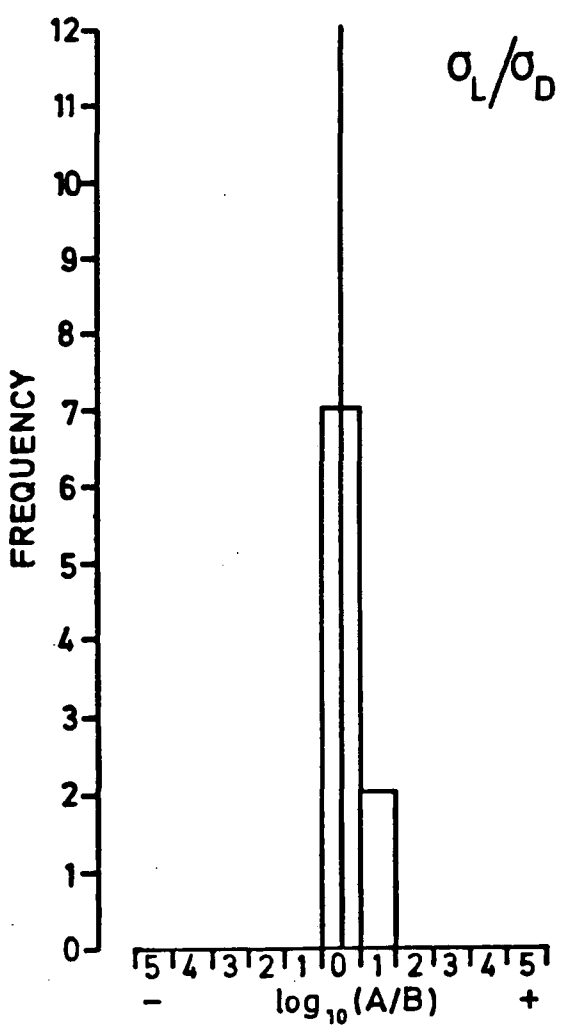
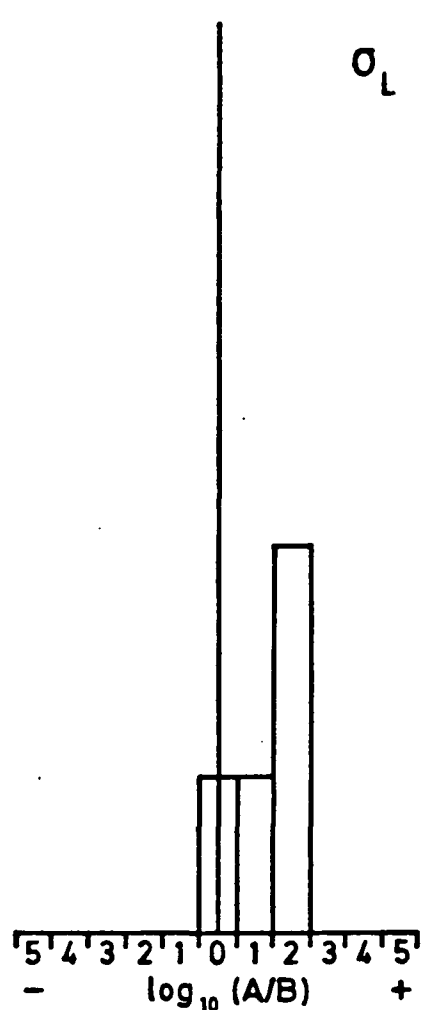
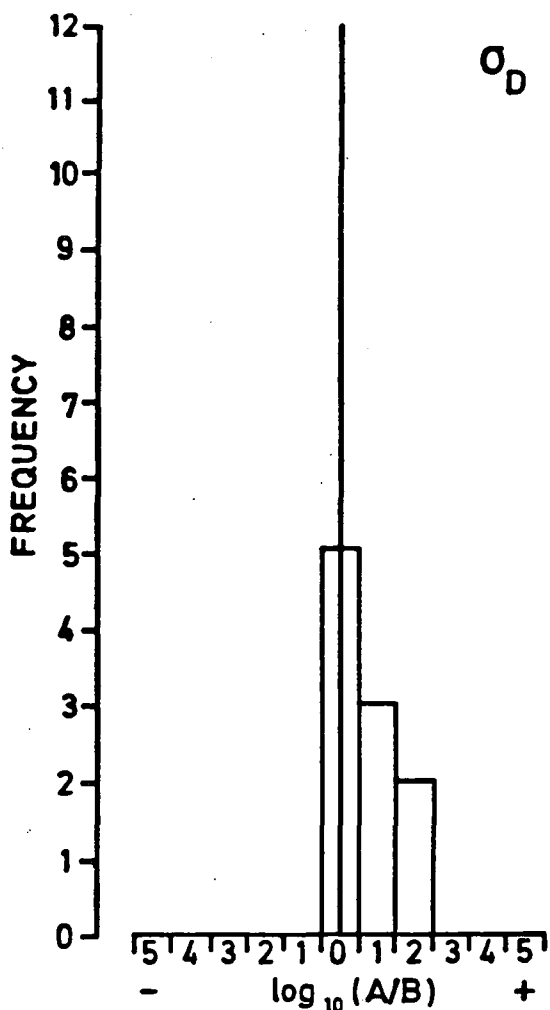


FIG. 7-8 RELATIVE CONDUCTIVITIES FOR POWDER SAMPLES,  
 A : UNWASHED  
 B : WASHED IN DISTILLED WATER

### 7.3 POWDER SAMPLES: INDIVIDUAL RESULTS

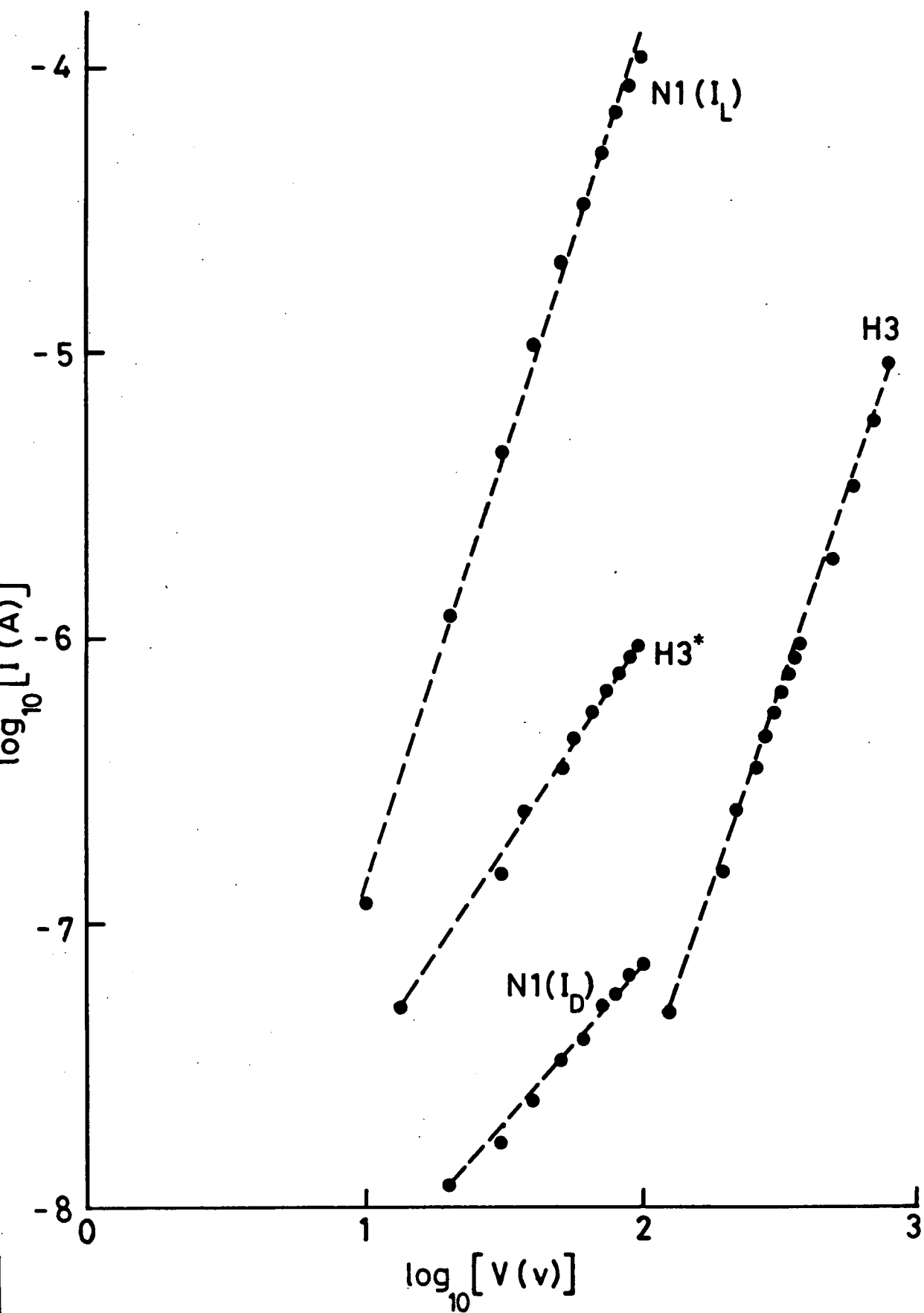
A broad range of I-V characteristics under steady state conditions of darkness or photoexcitation were observed. Both dark and light currents were found to have a superlinear dependence on the applied voltage over all regions measured until breakdown occurred. Fig. 7.9 shows the I-V characteristics recorded for 3 different powder samples. Both H3 and H3\* exhibited no measurable photoresponse while N1 was typical of a successfully sensitized powder. The experimental points shown here may be fitted well to the simple relationship

$$I \propto V^m$$

where  $m$  is the gradient of each linear plot. Values of  $m$  may be estimated from Fig. 7.9 to be around 2.7 and 1.5 for H3 and H3\* respectively. For sample N1 (and this was typical of the I-V characteristics of photosensitive samples) the value of  $m$  for the photocurrent was higher than that for the dark current (1.1 for  $I_D$  and 3.0 for  $I_L$ ). These values for  $m$  lie within the range (1 to 5) characteristic of powder systems (23). Breakdown in sample H3 occurred at a D.C. bias of between 800 and 900 volts; in this region the applied field was approximately  $10^4 \text{Vcm}^{-1}$ . Most powder samples, however, were tested over a bias range of 0-100v. In their study of I-V characteristics of compressed CdSe powders (1) Sato and Yoshizawa found that behaviour was ohmic at low applied voltages and then obeyed the relation

$$\log_{10}(I-I_0) \propto V^{\frac{1}{2}}$$

in which  $I_0$  is described as the "ohmic current". This behaviour was exhibited by both doped and undoped powder samples in darkness, in vacuo and at room temperature. Fig.7.10 shows an



G. 7 · 9 I - V CHARACTERISTICS FOR POWDER SAMPLES H3, H3\* AND N1

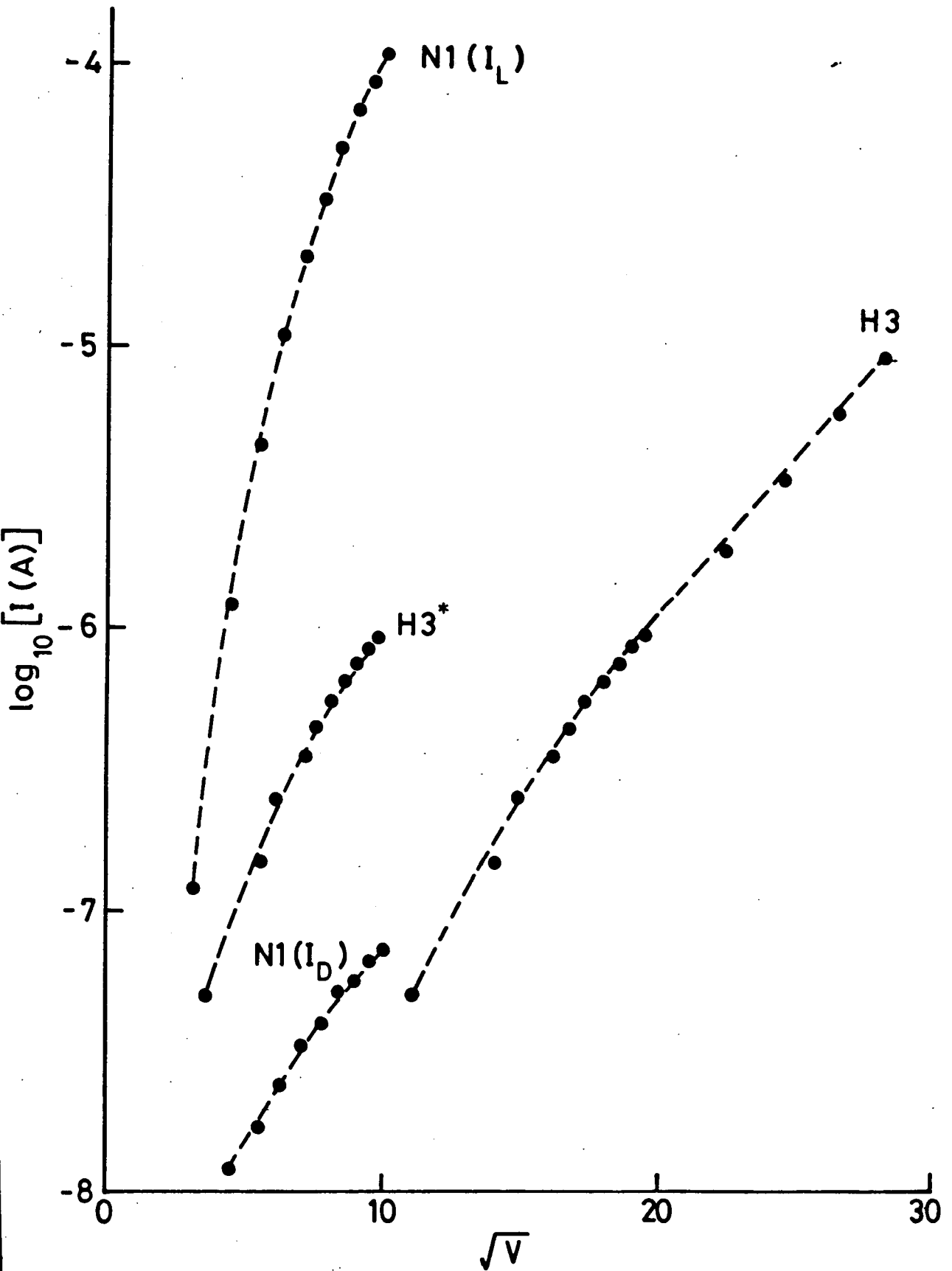


FIG. 7-10 EXPERIMENTAL POINTS OF FIG.7-9 REPLOTTED TO TEST I - V RELATIONSHIP PROPOSED BY SATO & YOSHIKAWA

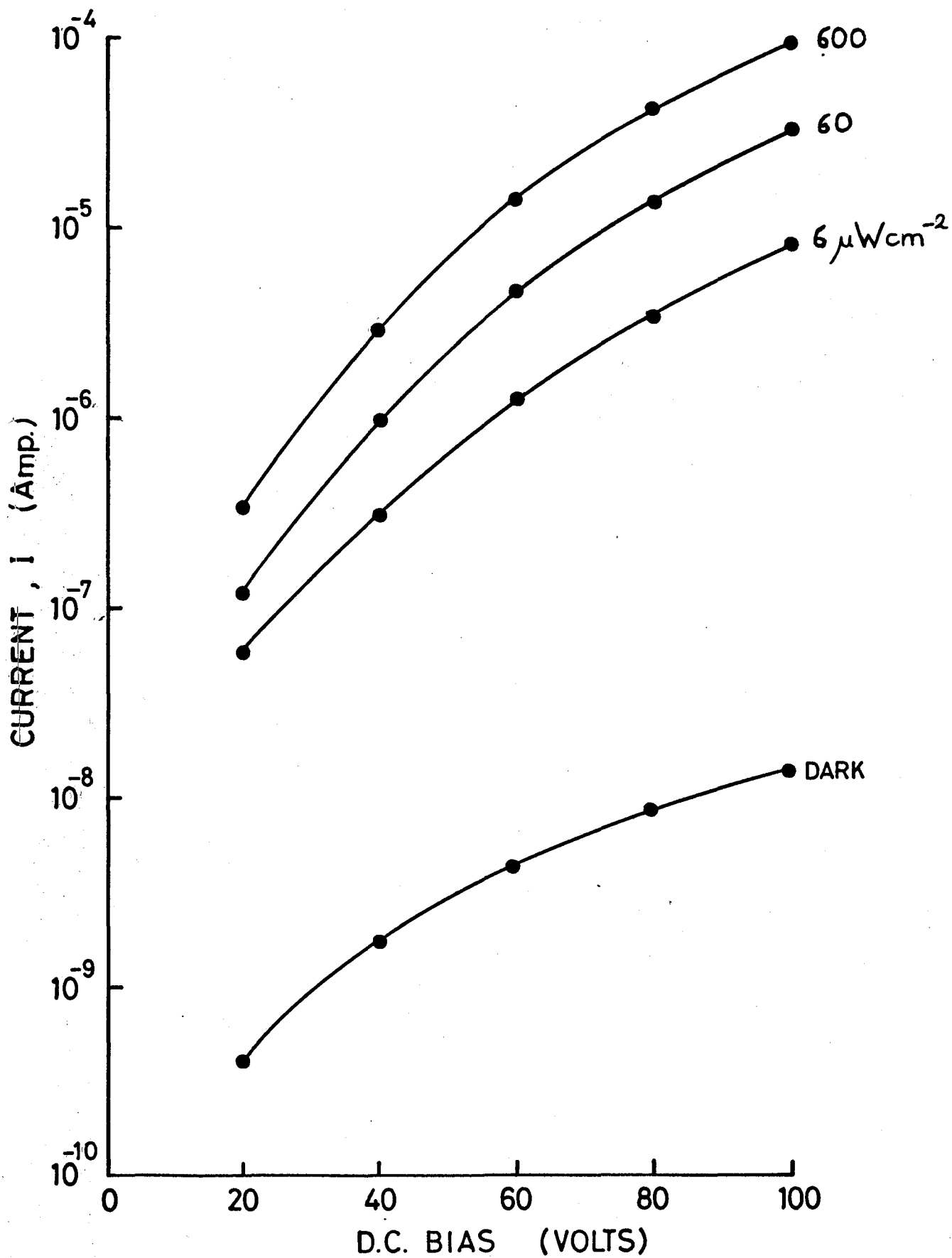


FIG. 7-11 DEPENDENCE OF CURRENT-VOLTAGE CHARACTERISTICS OF SAMPLE L1\* UPON PHOTOEXCITATION INTENSITY

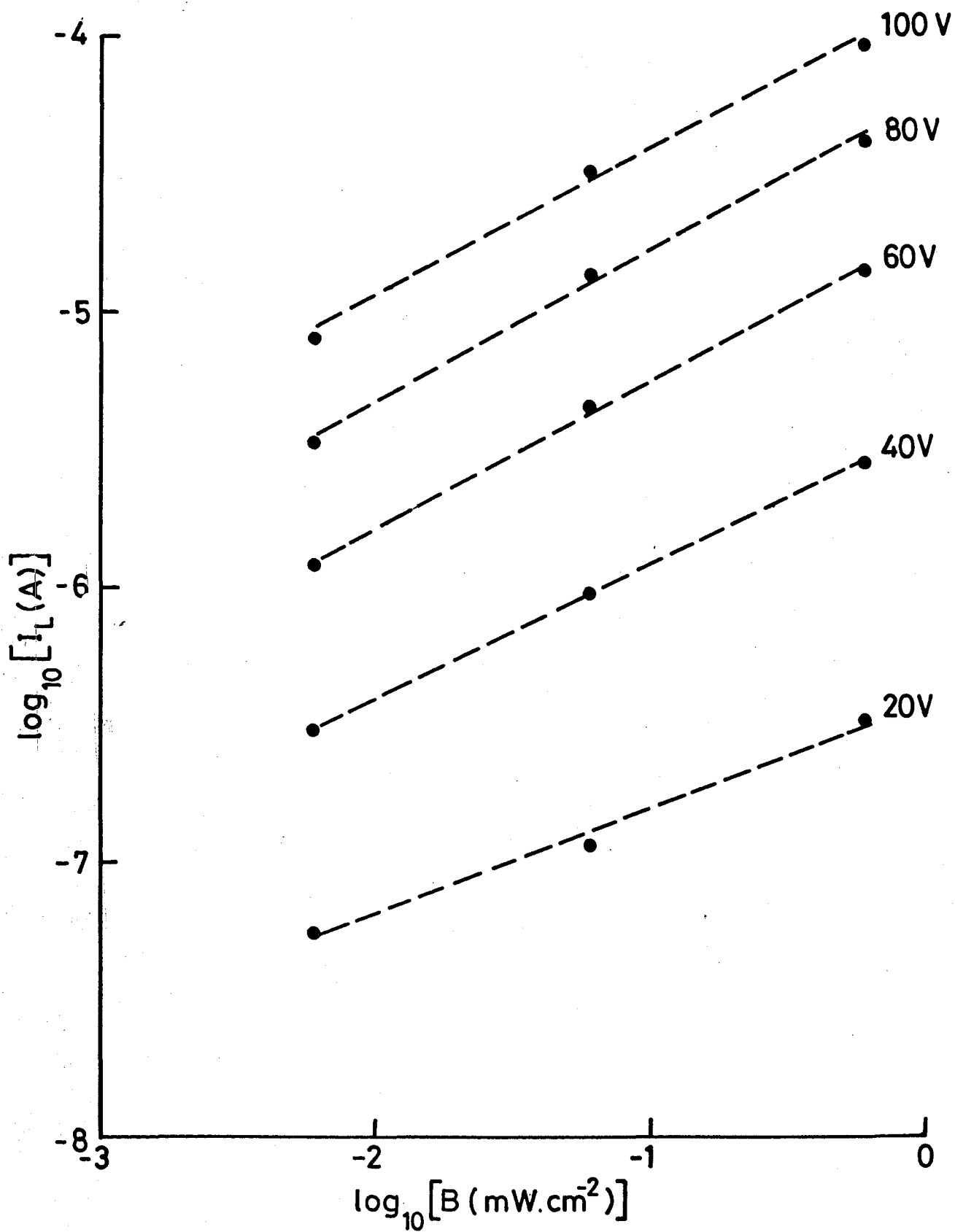


FIG. 7-12 DEPENDENCE OF PHOTOCURRENT OF SAMPLE L1\* UPON PHOTOEXCITATION INTENSITY B

attempt to fit the experimental points of Fig.7.9 to this relationship on the assumption that  $I_0$  is small enough to be discounted. As can be seen from the repeated downward curves of Fig.7.10 this assumption does not appear to be valid despite the fact that no ohmic regions of the I-V characteristics of these samples were experimentally observed. However, detailed measurements in the 0-10v range were not undertaken.

The early powder samples, which were all tested in the fixed electrode powder test cell, exhibited a broad range of current levels at 100v. The minimum dark current recorded under these conditions was  $9 \times 10^{-10}$ A (powder sample J1\*) and the maximum was  $1.52 \times 10^{-5}$ A (L2). Observed photocurrent for 4,000 Lux photoexcitation ranged from less than  $5 \times 10^{-8}$ A (E2) to  $3.24 \times 10^{-4}$ A (L2). An initial photocurrent of  $1.2 \times 10^{-3}$ A was recorded for powder sample G4, but this decayed irreversibly to about  $2.5 \times 10^{-5}$ A after several hours. Variation of current with time was observed in many samples and will be discussed later. The maximum ratio of light to dark current was  $5.3 \times 10^4$  (J1\*) while several samples such as H3 mentioned previously exhibited no measurable photosensitivity.

Figs 7.11 and 7.12 show the dependence of I-V characteristics and photocurrent upon photoexcitation intensity B for powder sample L1\*. Since neutral density filters were used to achieve the different flux densities, the spectral distribution of the illumination remained unchanged. The gradients of Fig.7.12 confirm a sub-linear dependence of photocurrent upon photoexcitation intensity (B), in this case

$I_L \propto B^{0.4}$  approximately. Note that this relationship is virtually unaffected by operating voltage over the range investigated. These results are in close agreement with the findings of Nicoll and Kazan (24) and Amalnerkar et al (25). The former reported that the photocurrent in a sensitized CdS powder-binder system was approximately proportional to  $B^{0.5}$  while Amalnerkar et al's studies of doped CdS thick films revealed a range of behaviour:  $I_L \propto B^{0.5-1}$  for 0.05-0.1% by weight Cu incorporation.

The dependence of conductivity-voltage characteristics upon applied pressure was investigated and recorded for all of the later (numbered) series of powder samples. Compression was not intended to be a technique for device fabrication as the powder-binder systems were found to have superior mechanical stability and electronic characteristics. However, by applying a known, constant pressure to each sample, and allowing for the resultant variation of electrode spacing, it was hoped that the importance of interparticle contacts would be experimentally demonstrated, and that reproducible packing densities would allow more reliable comparison between samples. Pseudo - three dimensional graphs were produced using a suitable plotting routine acting upon an extended data file. Data storage and processing routines were written in FORTRAN H (Extended) and run on the NUMAC computing service. Two plots were produced for each powder sample: the first showed dark and light conductivities as a function of applied voltage (V) and ram supply pressure (P), the second showed pressure and voltage dependence of the conductivity ratio. Fig. 7.13 shows an example of this type of

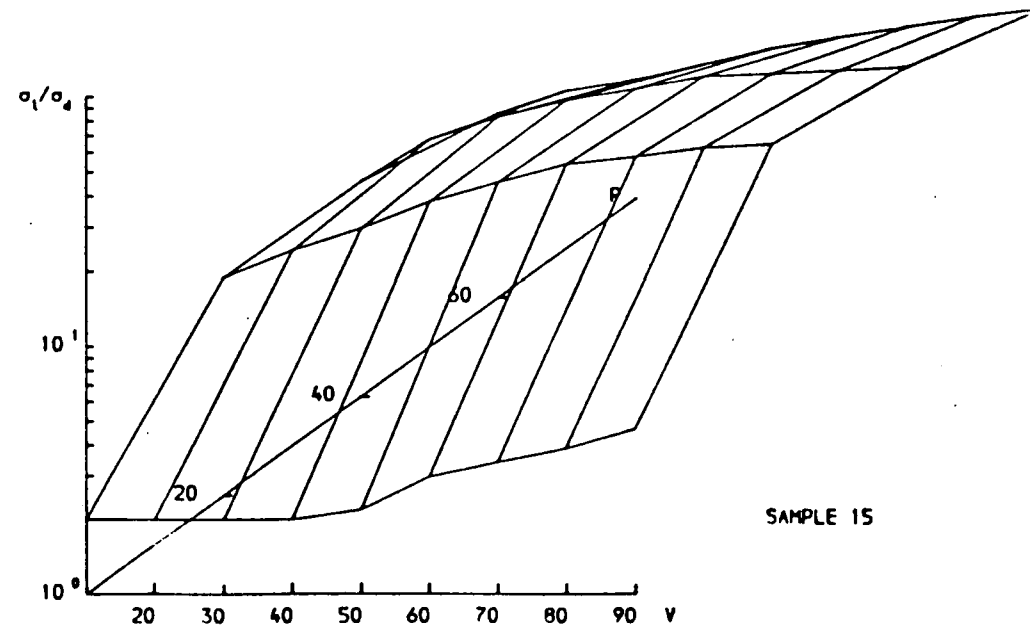
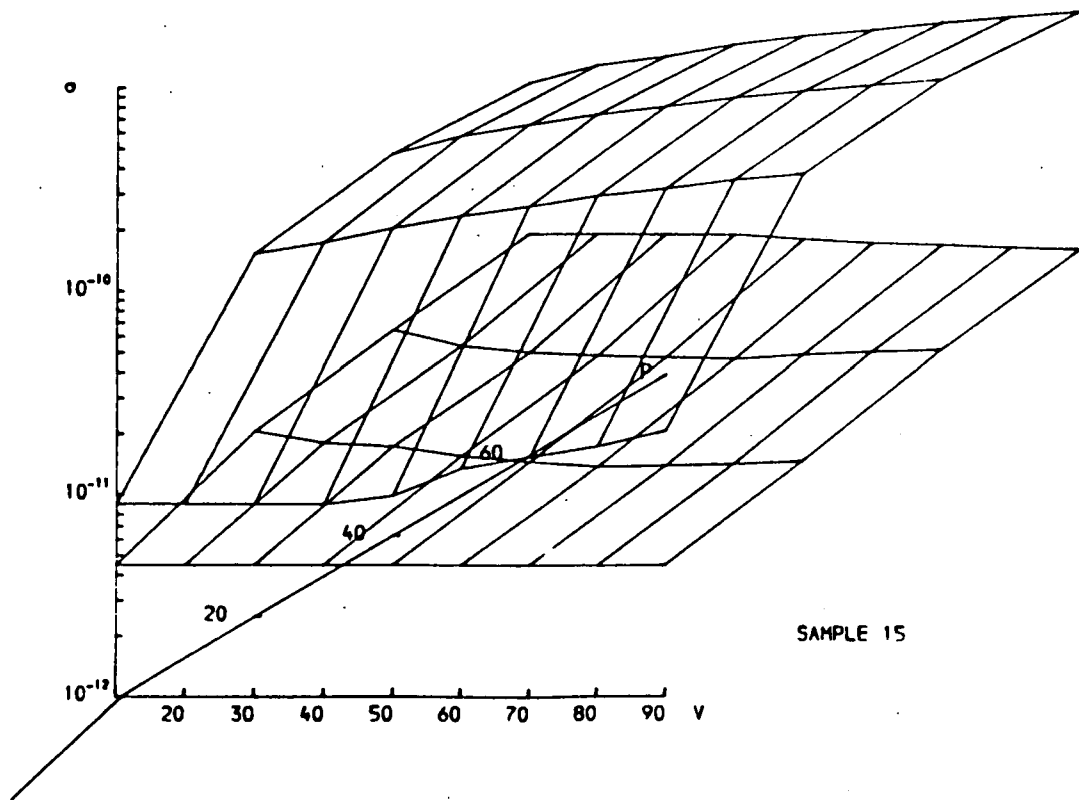


FIG. 7-13 CONDUCTIVITY OF POWDER SAMPLE 15 AS A FUNCTION OF APPLIED VOLTAGE AND PRESSURE

plot for which a full dataset was recorded. A relatively large increase in conductivity due to compression compared with that due to photoexcitation is shown, as is a reduction of light to dark conductivity ratio with increased pressure. Unfortunately this form of presentation is difficult to interpret visually. The dependence of conductivity upon applied pressure is perhaps more clearly shown in the conventional plots of Figs. 7.14 and 7.15. It should be noted that the units of pressure  $P$  used in Figs. 7.13 and 7.14 are a measure of the piston air supply pressure (p.s.i.) while those of Fig. 7.15 are units of pressure directly applied to the powder sample (Pa). The extent to which inter-particle contact determines overall sample conductivity is clearly emphasised by Fig. 7.14. Initial compression of the sample using a piston supply pressure of 20 p.s.i. applied approximately  $3 \times 10^6$  Pa pressure to the powder sample. This was sufficient to increase the dark conductivity by some 3 orders of magnitude, a larger increase than that caused by photoexcitation in this case. A general feature of these results, shown clearly in Fig. 7.15, is that dark conductivity is increased more rapidly than light conductivity by compression and hence the ratio decreases. This is thought to result from mechanical disruption during compression of the shallow sample surface region which is penetrated by the photoexcitation; thus inter-particle contact is enhanced less than throughout the bulk of the sample.

Sato and Yoshizawa (1) investigated dependence of dark current  $I$  upon applied pressure  $P$  over the voltage range for which ohmic behaviour was observed (typically  $\leq 10$  v). They proposed the relation  $I \propto P^n$  but did not discuss changing

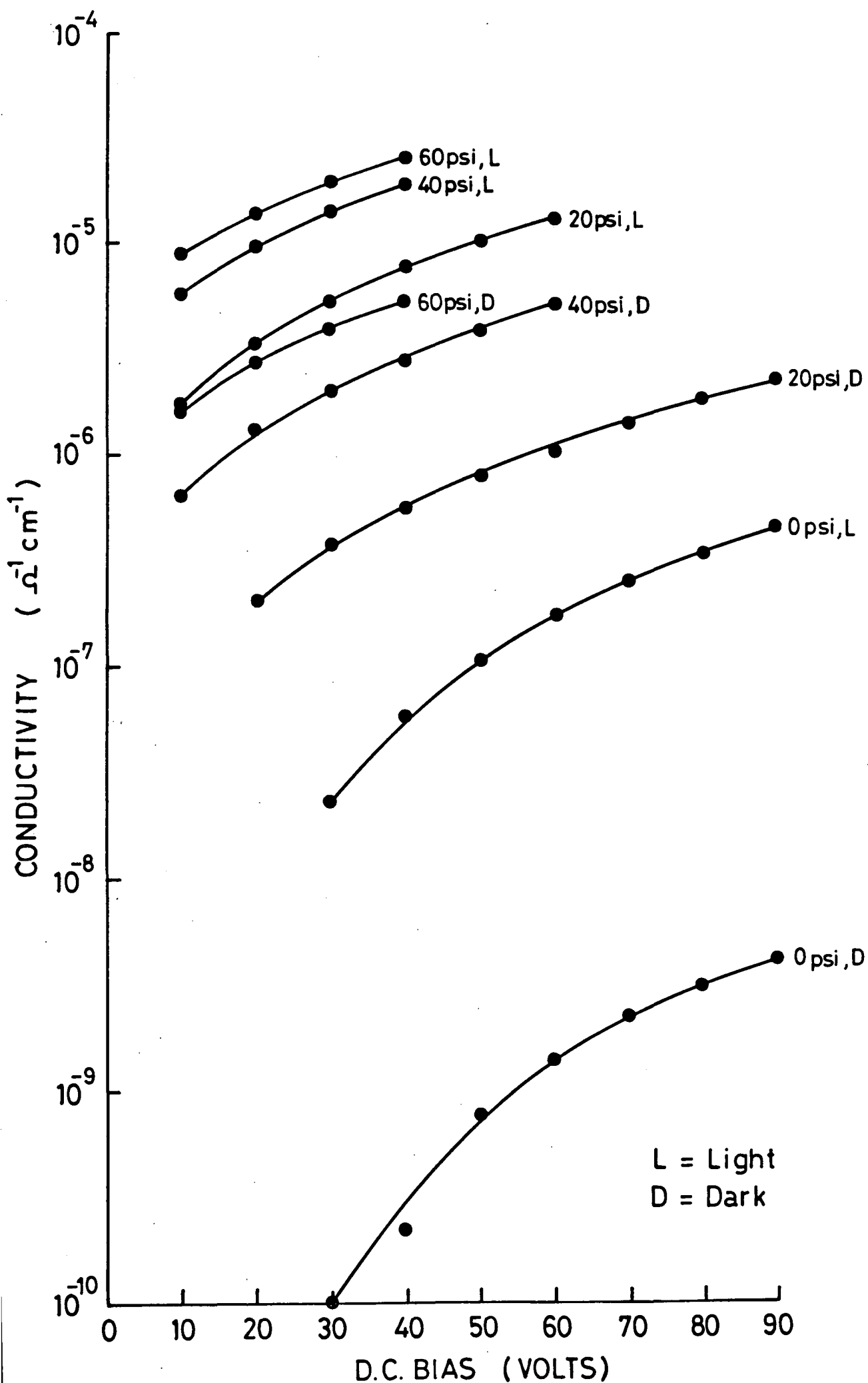


FIG. 7-14 CONDUCTIVITY - VOLTAGE CHARACTERISTICS FOR POWDER SAMPLE 1 COMPRESSED BY PISTON PRESSURES OF 0, 20, 40 AND 60 psi.

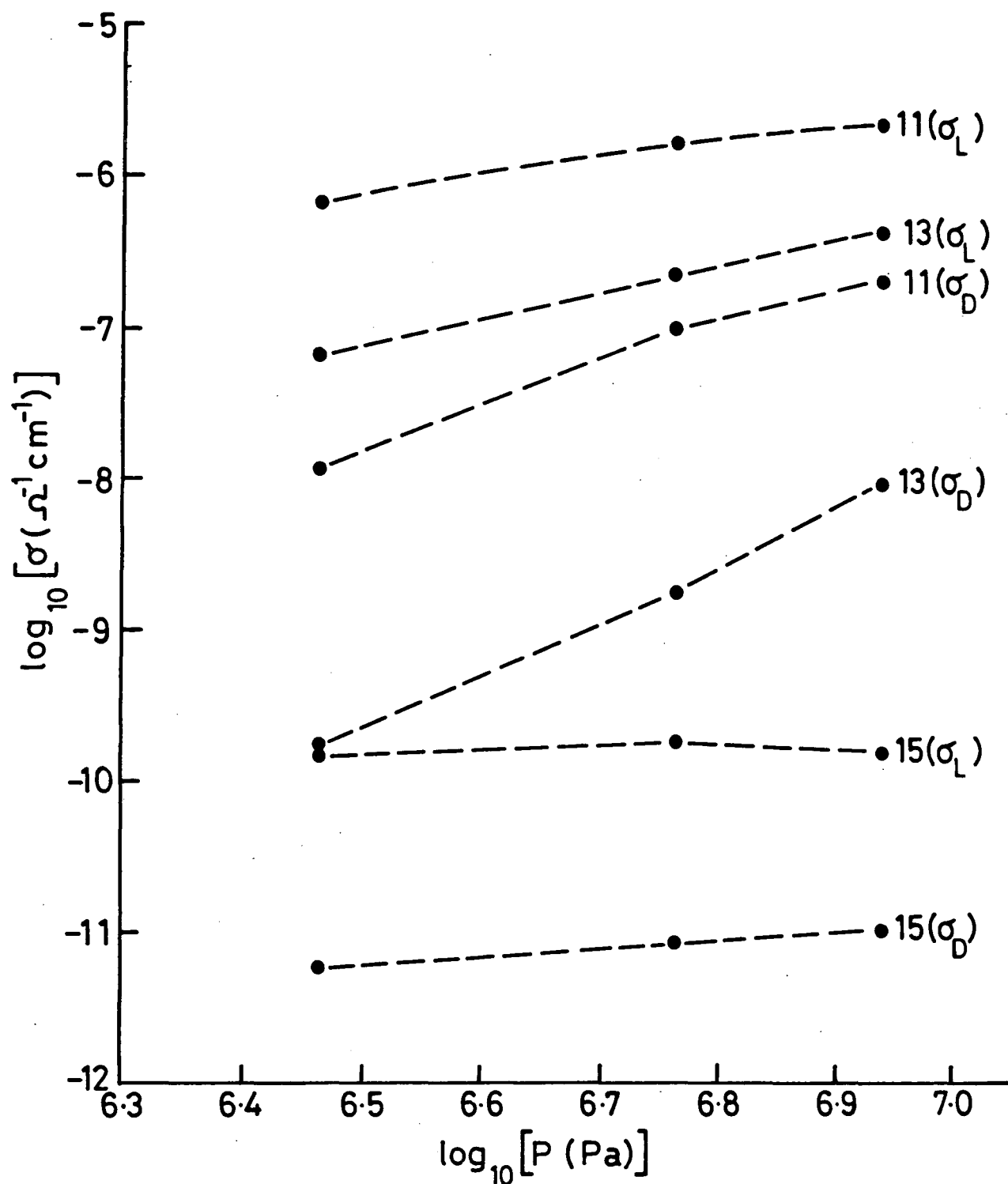


FIG. 7.15 DEPENDENCE OF  $\sigma_D$  AND  $\sigma_L$  AT 90V UPON APPLIED PRESSURE FOR SAMPLES 11, 13 & 15

electrode separation (and hence changing electric field for constant voltage) as a result of compression. Furthermore, as stated previously, a region of ohmic behaviour was not experimentally observed in the course of this work as higher operating voltages were used. Nonetheless, from the limited data points of Fig.7.15 a relation  $\sigma_D \propto P^n$  appears to hold approximately true, with values of n between around 0.5 and 3.5.

The powder samples represented in Figs 7.13-15 were all prepared by the porous plug technique. Samples produced using the partial pressure method were typically so highly conducting that only partial datasets could be recorded. Whether in darkness or under illumination current levels rose so rapidly with increased voltage or pressure that electrical breakdown was repeatedly observed. This, together with poor time stability of dark and photocurrents severely limited the range of plots which were produced. Following electrical breakdown during dark conductivity measurement, recorded levels under illumination were actually lower than those at the same voltage and pressure in darkness. Therefore ratios of dark and light conductivities were usually not determined, and assumed to be unity.

The I-V characteristics of powder produced by the iodine transport method were investigated. Ground samples of both the transported material and the residue were tested in the fixed electrode powder test cell. As shown in Fig.7.16(a) the transported material was found to be approximately an order of magnitude more conductive than the residue, though neither powder was appreciably photosensitive. It is interesting to compare

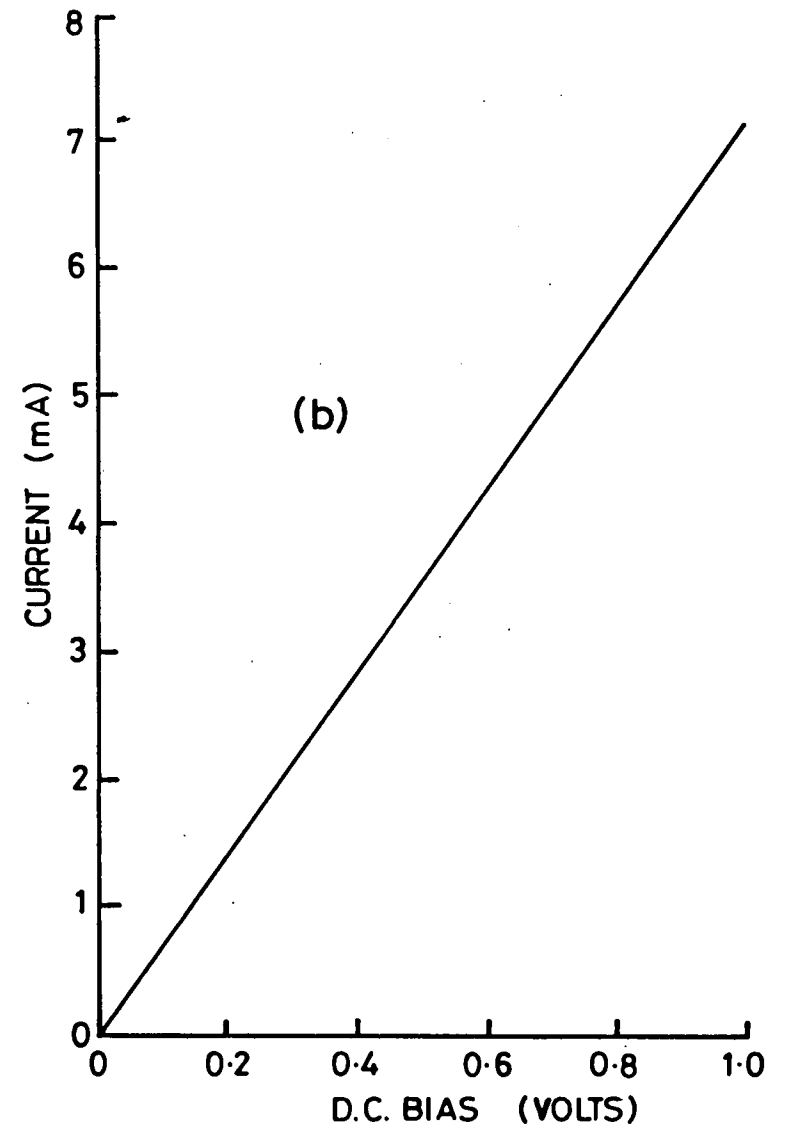
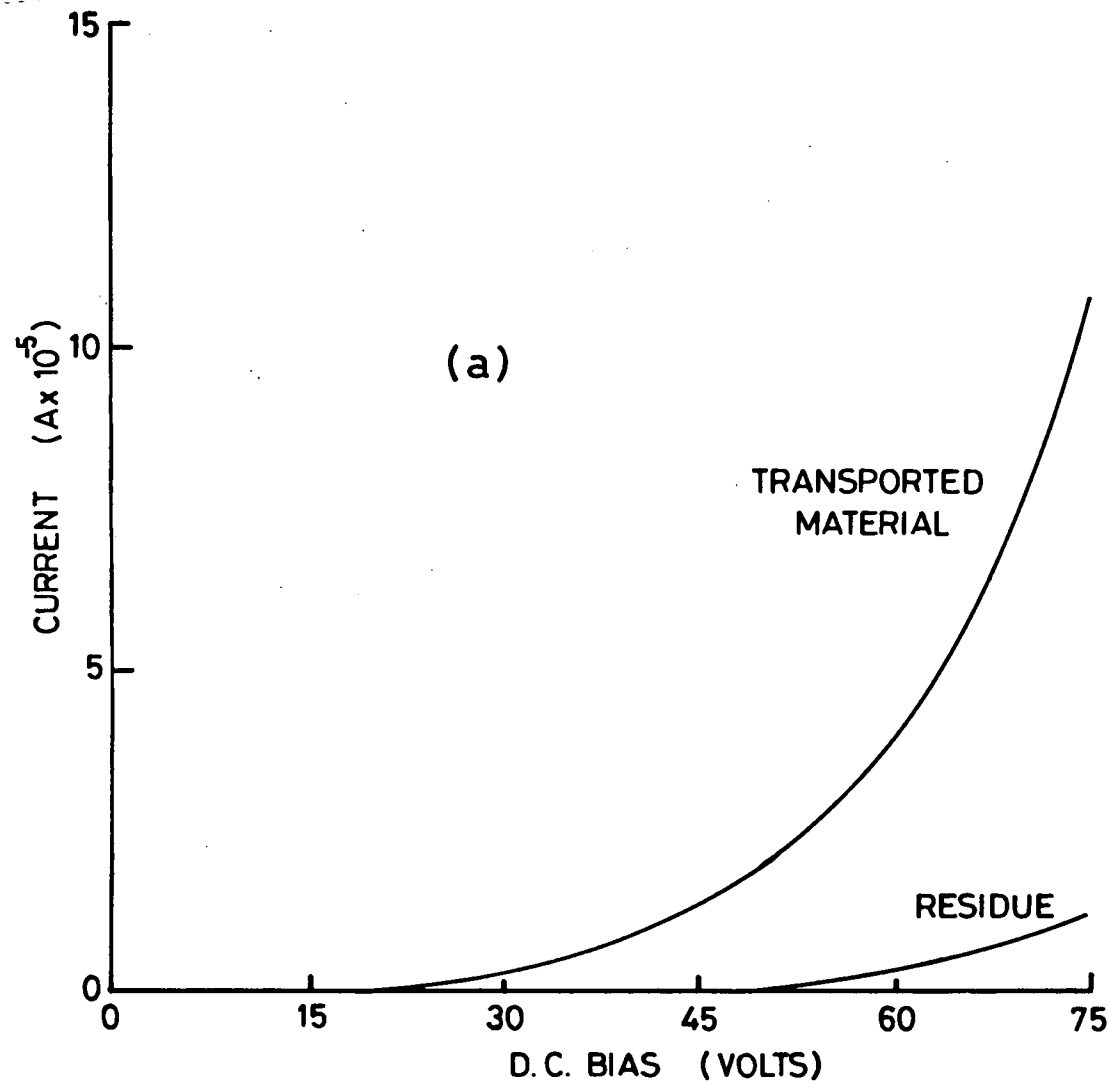


FIG. 7-16 I-V CHARACTERISTICS FOR (a) POWDERS GROUND FROM THE TRANSPORTED MATERIAL AND FROM THE RESIDUE IN THE IODINE TRANSPORT TUBE AND (b) TWO POLYCRYSTALLINE CUBES CLAMPED TOGETHER

these results with similar measurements made on 2mm cubes of the same transported material. These cubes were polycrystalline, and ohmic contacts were affixed by melting and partial diffusion of indium as previously described. The resistivity between such contacts on opposite faces of a single cube was found to be approximately  $2.5 \Omega \text{ cm}$ . However, when two cubes, each with a single contact, were clamped together, the resistivity was found to be around  $27 \Omega \text{ cm}$ . The I-V characteristic was linear over the low range of applied bias (Fig. 7.16(b)). Though the linearity of the powder I-V characteristic was not recorded in detail over the same range, it is clear from the graph that the powder resistivity was many orders of magnitude higher, certainly in excess of  $10^6 \Omega \text{ cm}$ .

Gathering of data to generate I-V characteristic curves was frequently complicated by fluctuations in the measured current under steady state conditions. A commonly recorded phenomenon was decay of conductivity, either in darkness or under illumination. Often this was found to have reversible and irreversible components. An example of how this appeared as hysteresis when I-V characteristics were plotted automatically using the voltage ramp generator is shown in Fig. 7.17. Initially the voltage was ramped from zero to around 90v at a steady rate of  $0.5 \text{ v s}^{-1}$ . This upper limit voltage was then maintained for a few minutes and the current slowly decreased. On returning at the same rate to zero applied bias a second current voltage curve was thus generated. Upon repeating this procedure a second hysteresis loop was produced indicating an initial slight increase in the conductivity compared with the previous curve, though falling

short of a return to the original measured performance.

A different time dependence of recorded dark current exhibited by one of the partial pressure fired powder samples is shown in Fig. 7.18. In this case the apparent conductivity was found to increase with time upon reaching the upper applied voltage limit; however, upon repeating the cycle the levels were found to have been reduced. These plots emphasize the importance of considering timing of measurement and previous treatment of each powder sample when recording I-V characteristics. Thus when obtaining the set of conductivity - voltage - pressure data for the 48 numbered powder samples care was taken to perform measurements in the same sequence for each sample. In cases of substantial recorded current fluctuation such as shown in Figs. 7.17 and 7.18, data points were taken from the initial curve obtained by ramping the applied voltage from zero to the upper limit.

Three examples of photocurrent recorded as a function of time at constant applied voltage are given in Figs 7.19-21. The first two curves were generated by plotting the points shown; the third was produced directly on an X-t recorder. These were not the largest decreases of photocurrent recorded. The measured photocurrent of sample G6, for example, fell from  $11.2 \mu\text{A}$  to  $0.1 \mu\text{A}$  over a period of 3-4 hours under steady state conditions, i.e. a decay covering 2 orders of magnitude. The deviation from a single component exponential process for the decay curve exhibited by sample H2 is shown in Fig. 7.22. If the decay were a true exponential with a single time constant  $\tau_f$  the equation

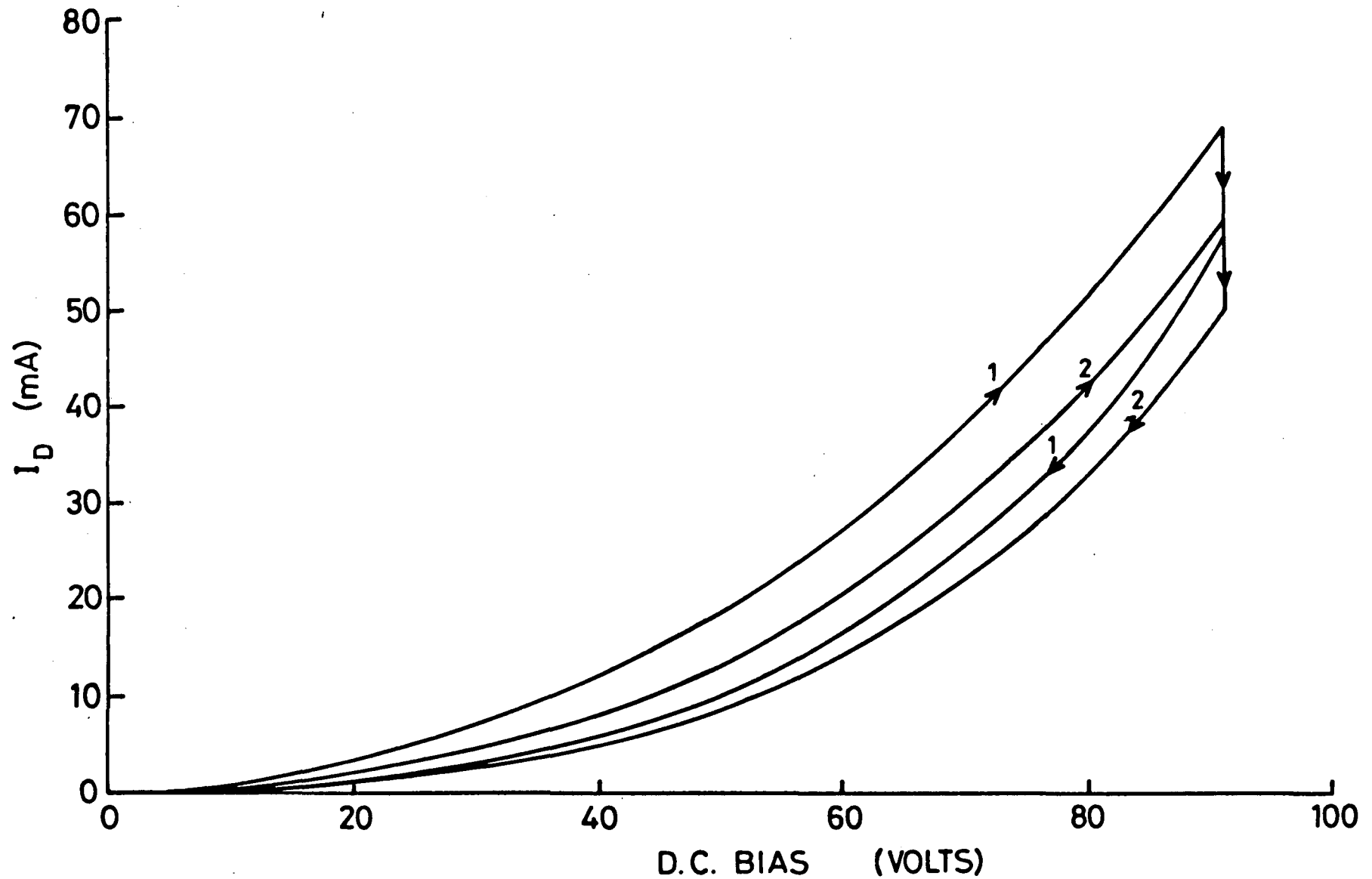


FIG. 7-17 PARTIALLY REVERSIBLE DECAY OF DARK CURRENT FOR POWDER SAMPLE 1 COMPRESSED AT 40 p.s.i.

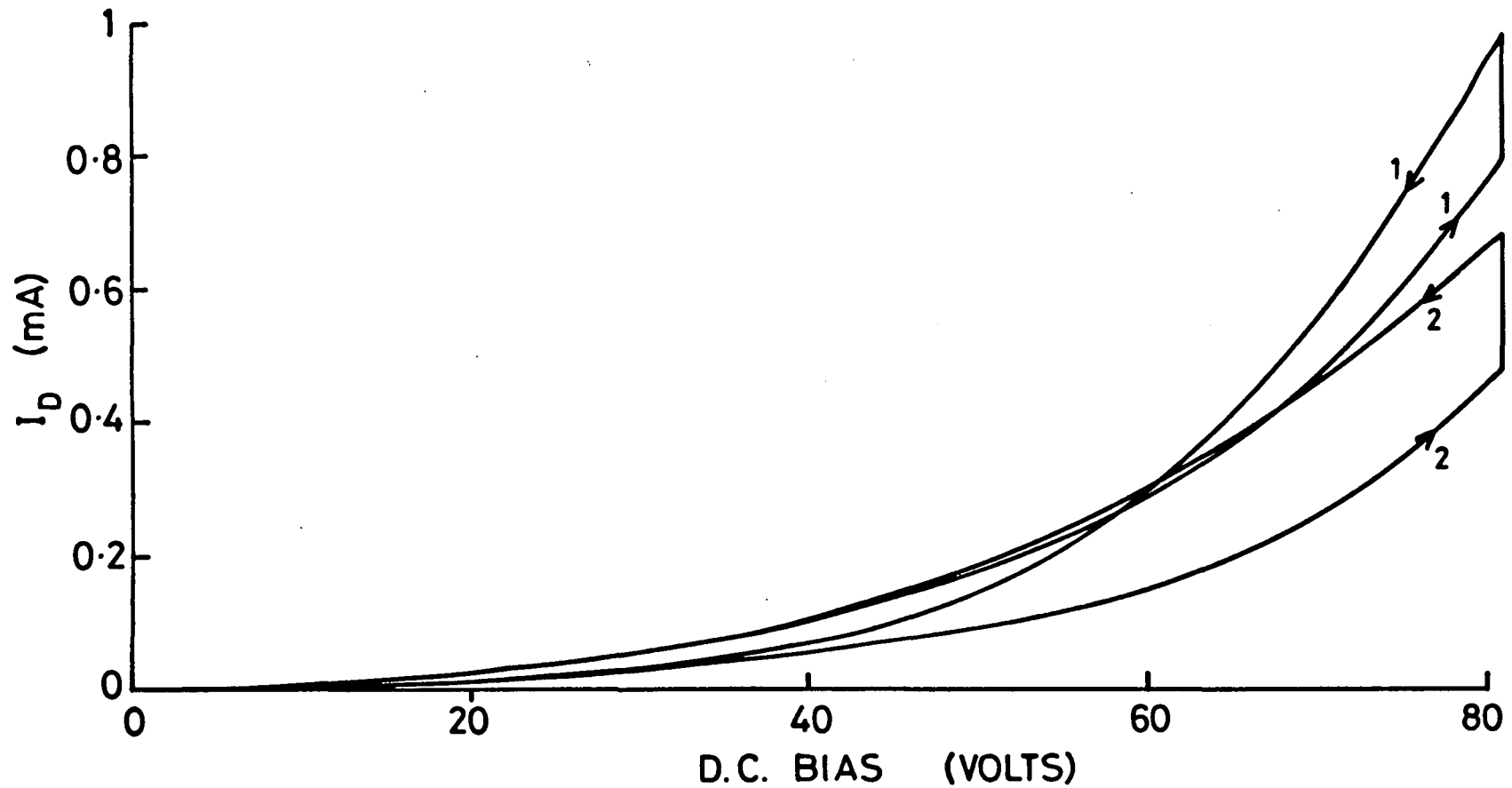


FIG. 7-18 TIME VARIATION OF DARK CURRENT FOR POWDER SAMPLE 2 COMPRESSED AT 20 p.s.i.

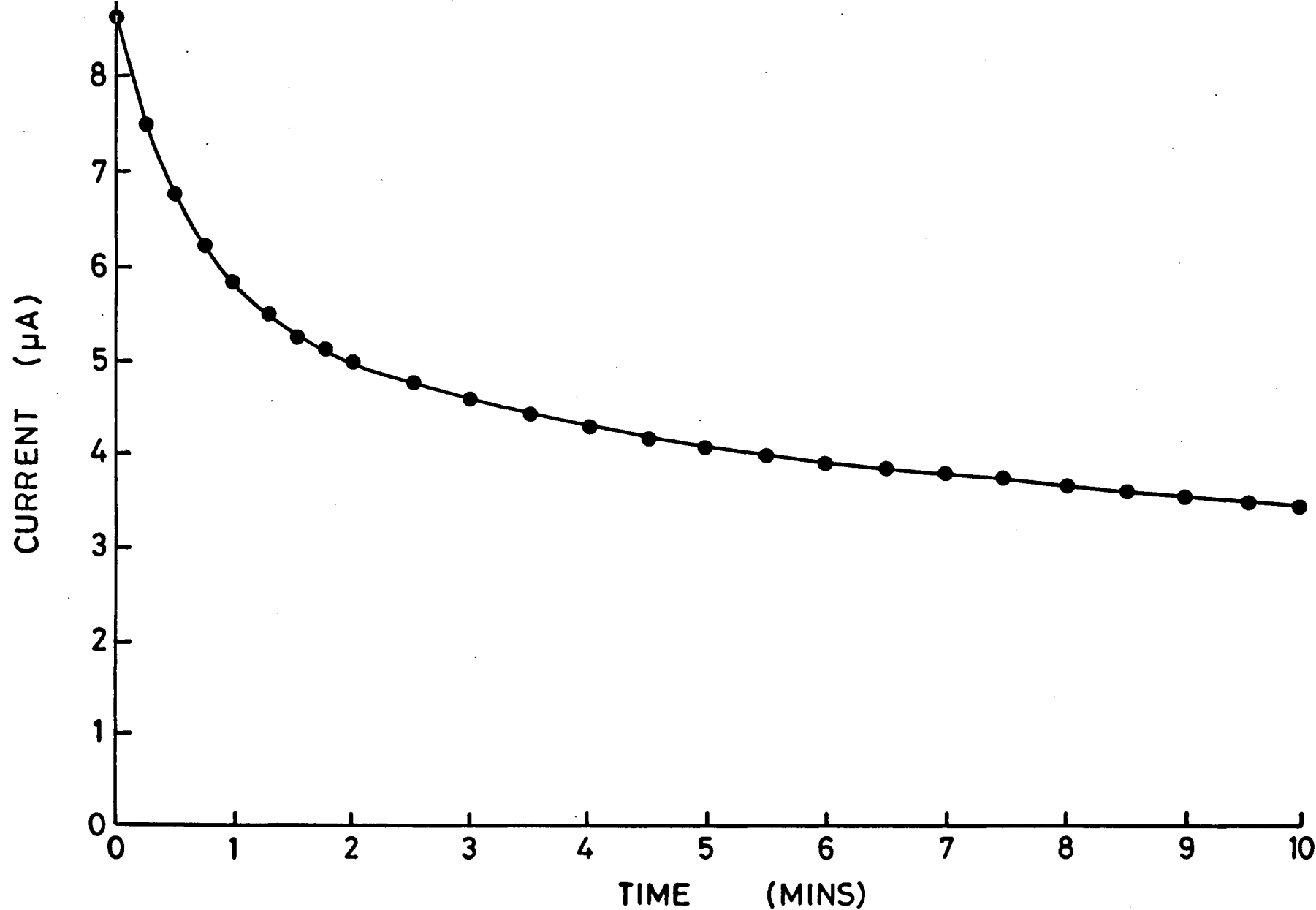


FIG. 7-19 DECAY OF PHOTOCURRENT WITH TIME FOR POWDER SAMPLE H2.  
CONSTANT D.C. BIAS = 100 V.

given in 7.1 could be written as:

$$\ln(I(t)) = -t/\tau_F + \ln(I_L)$$

This is an equation of the form  $y = mx+c$ ; therefore plotting  $\ln(I(t))$  against  $t$  as in Fig. 7.22 might be expected to produce a linear slope with gradient  $-1/\tau_F$  and intercept  $\ln(I_L)$ . This is not the case. Furthermore, saturation of such decay was not observed even though the rate slowed down in all cases.

The X-t recorder was also used to produce the plots of Figs. 7.23-25 which show the response of three different powder samples to transitions from darkness to illumination and vice versa. Noteworthy features of these plots are the variation in photocurrent with time and the prolonged decay of the dark current back toward its original level (especially noticeable in Fig.7.24). Fluctuations of photocurrent with time were evident in each case, but the general trend was an increase with time for samples J1\* and J3\* yet a decrease for sample L2.

An exponential increase of photocurrent over a time interval of several minutes was observed for powder sample K2, however, as shown in Fig. 7.26. This is confirmed by the plot of Fig. 7.27, from which a time constant  $\tau_R = 52s$  has been derived. The decay characteristic, on the other hand, is again not an exponential with a single time constant, as shown by Fig. 7.28. The fact that these conductivity changes occur over timespans of minutes suggests that they are due to photochemical effects rather than direct changes of carrier population and mobility due to

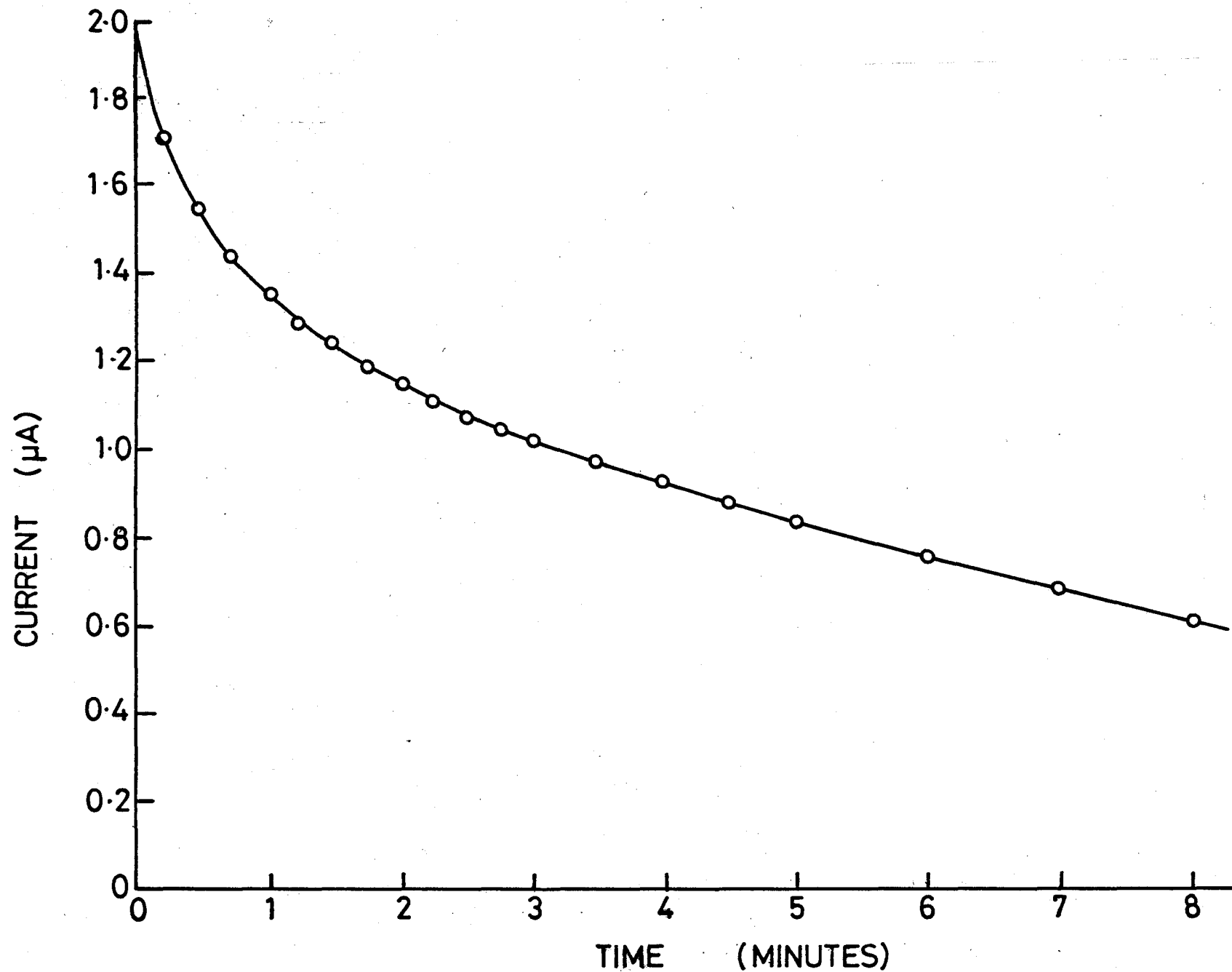


FIG. 7-20 DECAY OF PHOTOCURRENT WITH TIME FOR POWDER SAMPLE 11.  
CONSTANT D.C. BIAS = 100V

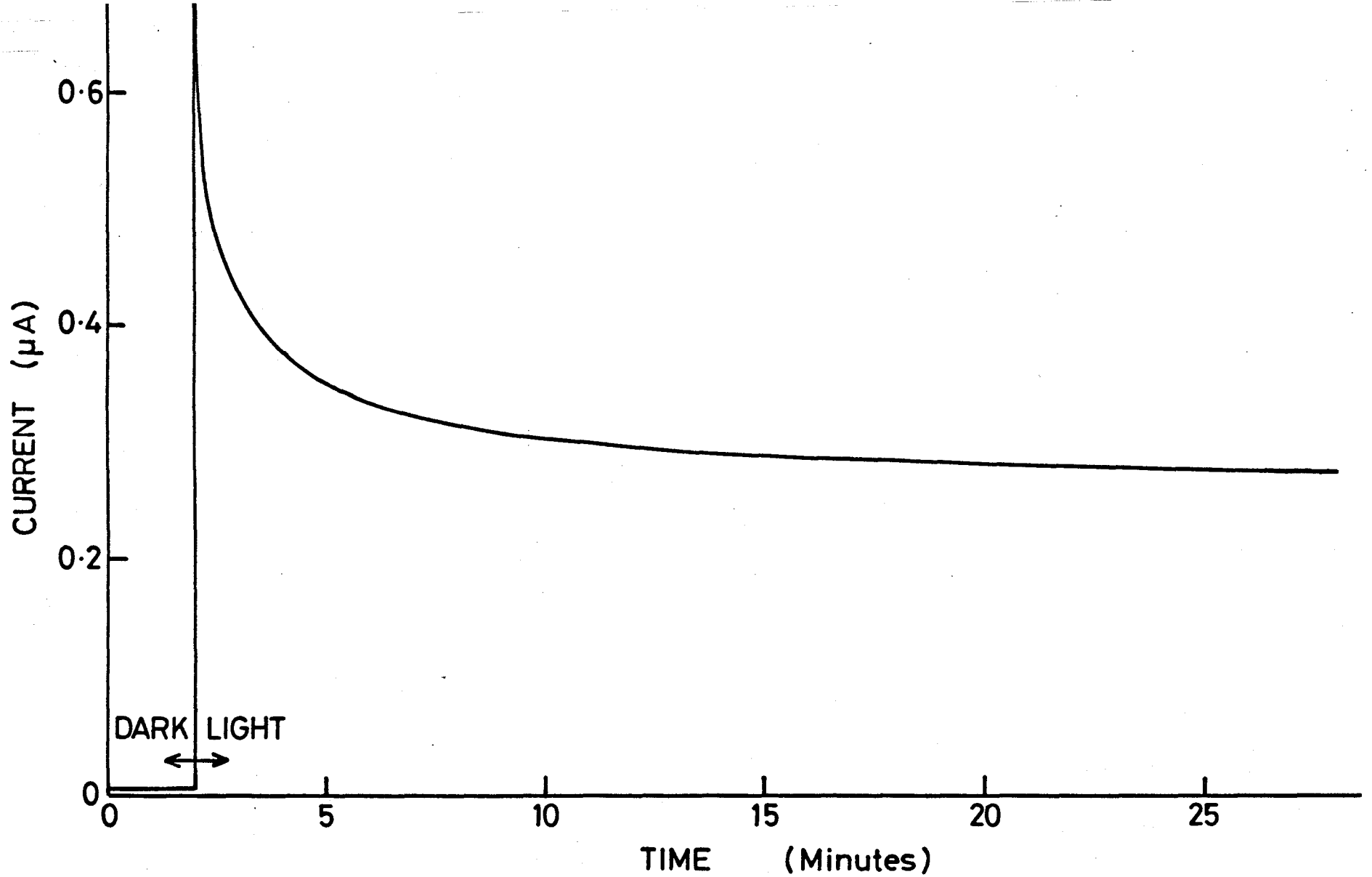


FIG. 7-21 DECAY OF PHOTOCURRENT WITH TIME FOR POWDER SAMPLE M1.  
CONSTANT D.C. BIAS = 100 V.

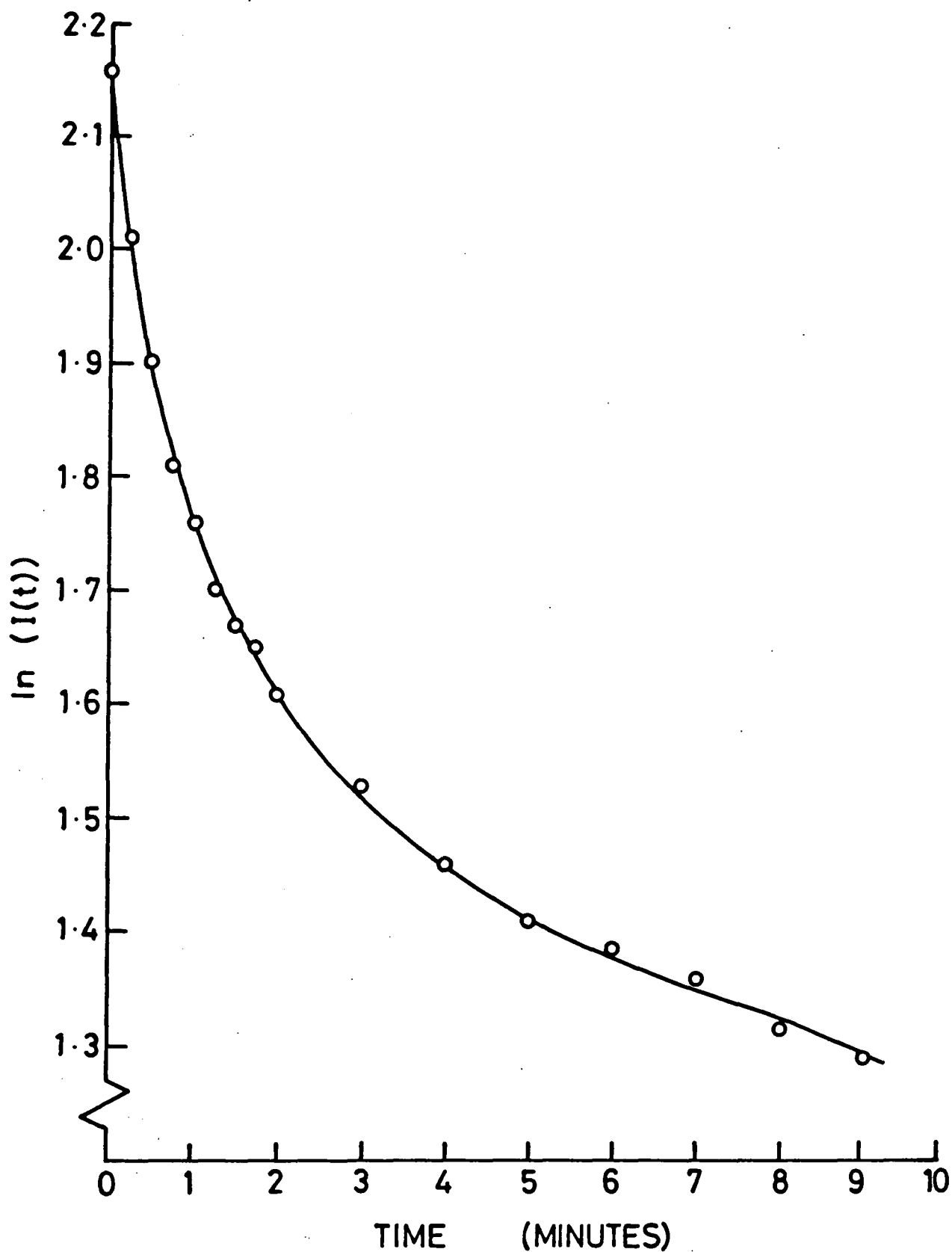


FIG. 7-22 PLOT SHOWING THE NON-EXPONENTIAL NATURE OF THE PHOTOCURRENT DECAY CURVE OF SAMPLE H2 (FIG. 7. )

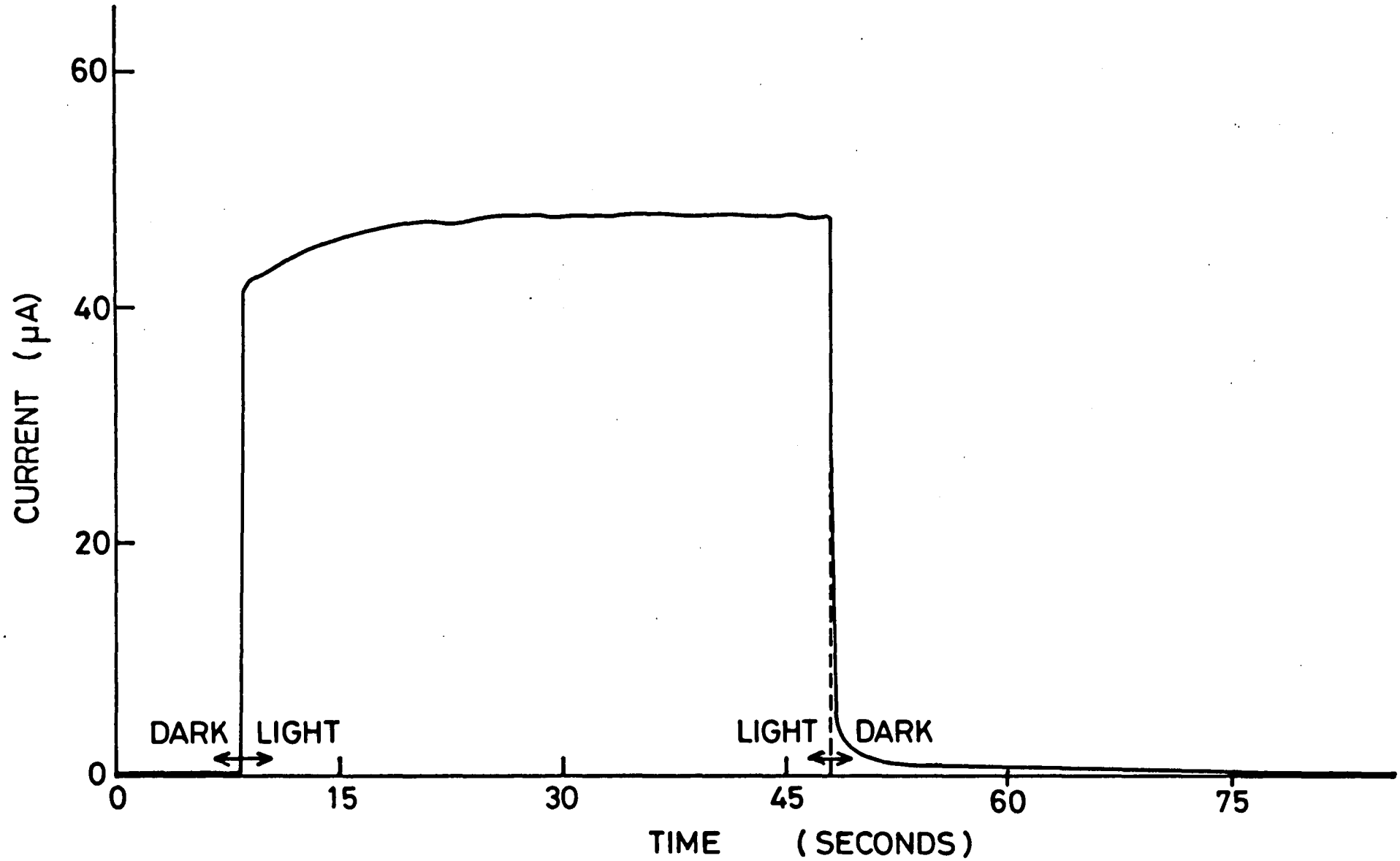


FIG. 7-23 TIME DEPENDENCE OF DARK AND LIGHT CURRENTS FOR POWDER SAMPLE J1\*.  
CONSTANT D.C. BIAS = 100 V.

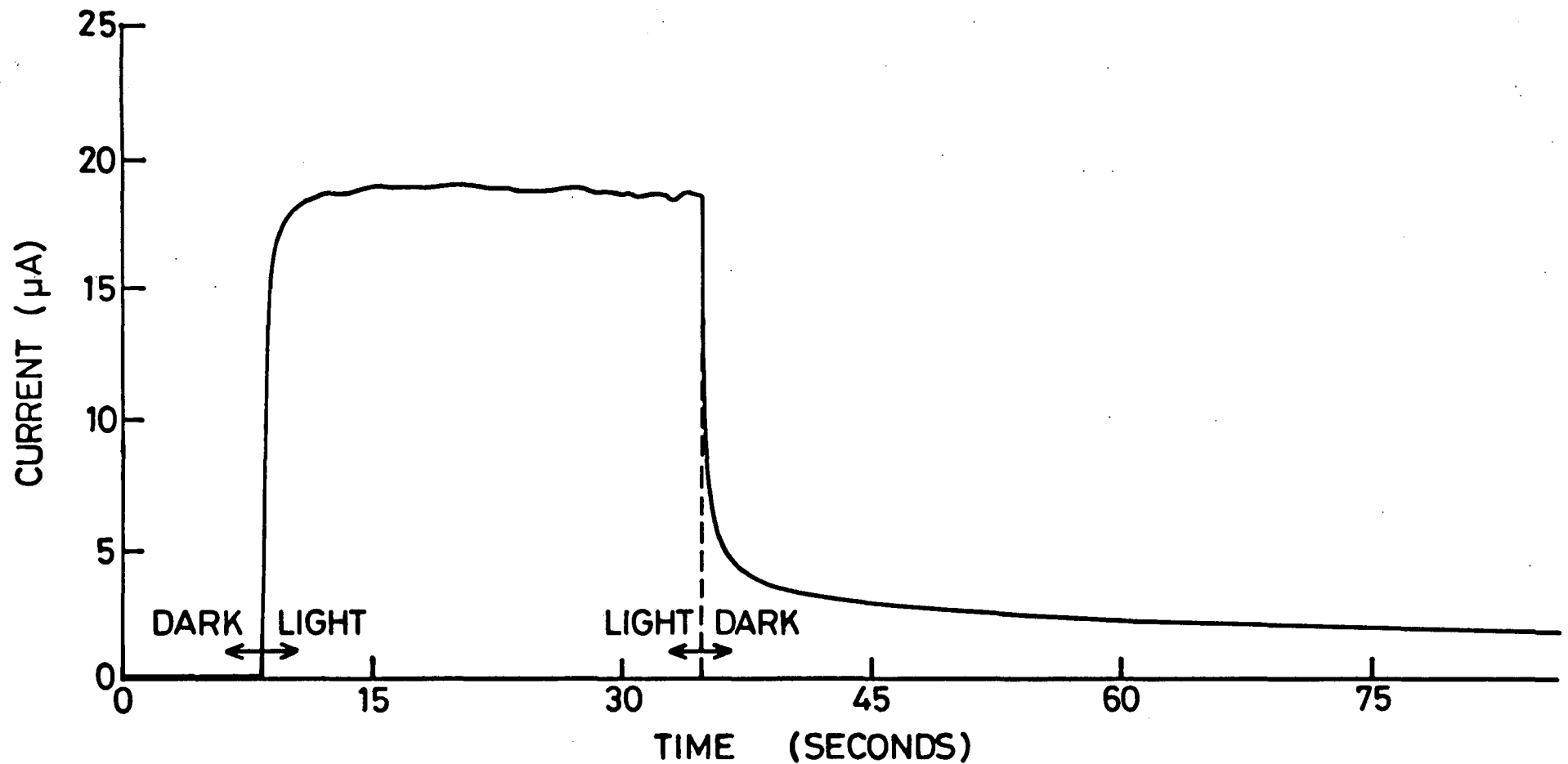


FIG. 7-24 TIME DEPENDENCE OF DARK AND LIGHT CURRENTS FOR POWDER SAMPLE J3\*.  
CONSTANT D.C. BIAS = 100 V

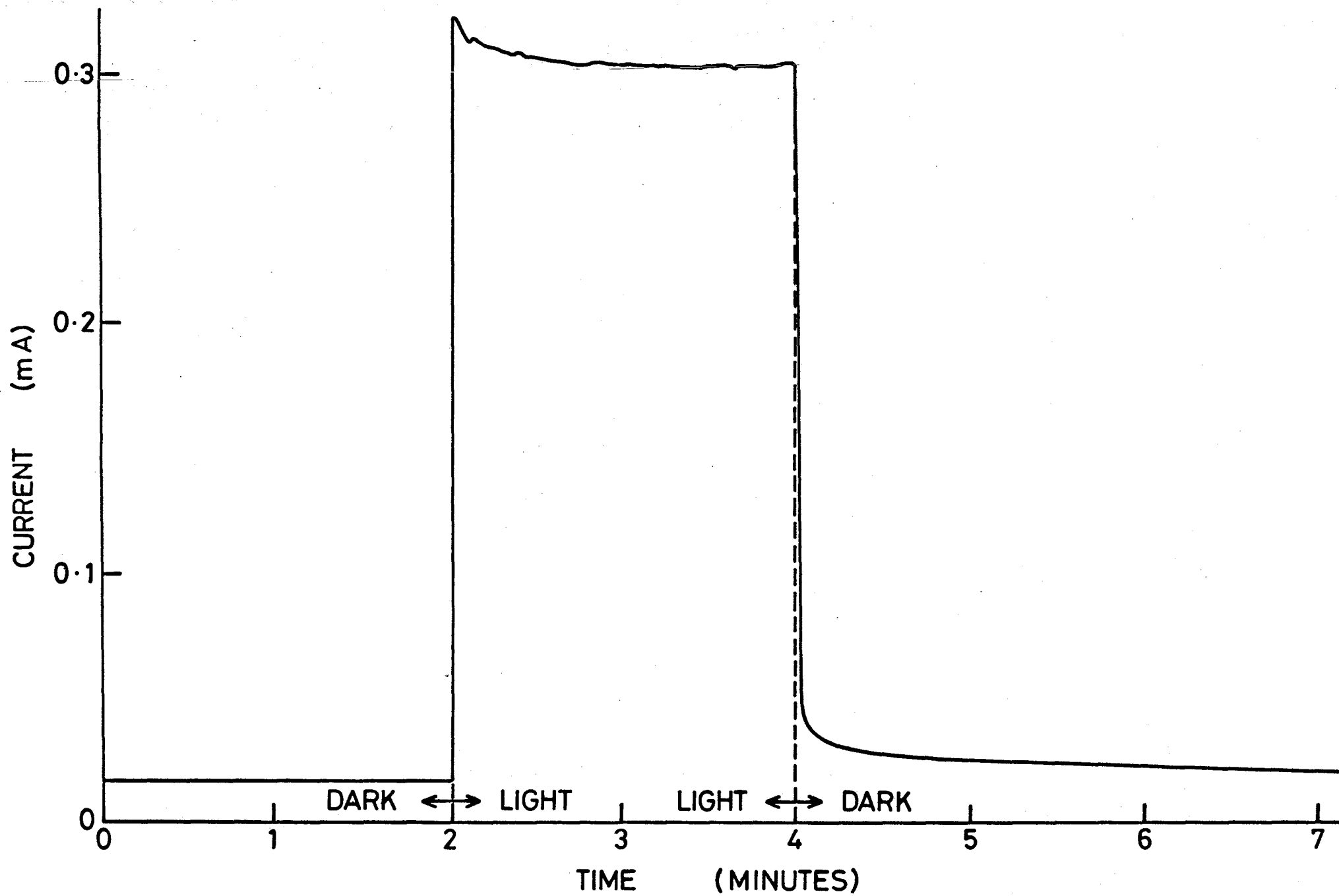


FIG. 7-25 TIME DEPENDENCE OF DARK AND LIGHT CURRENTS FOR POWDER SAMPLE L2. CONSTANT D.C. BIAS = 100V

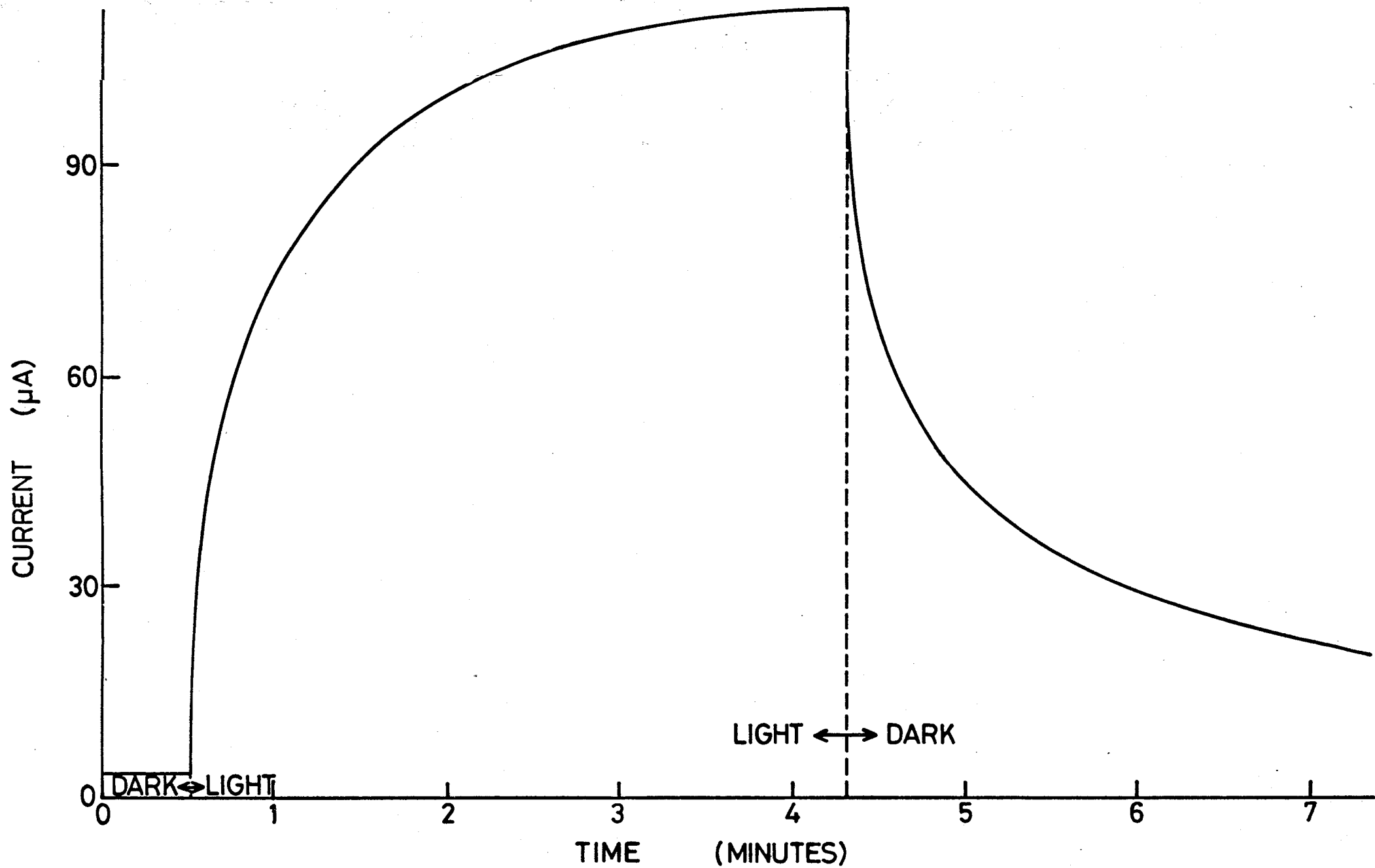


FIG. 7-26 TIME DEPENDENCE OF DARK AND LIGHT CURRENTS FOR POWDER SAMPLE K2.  
 CONSTANT D.C. BIAS = 100 V

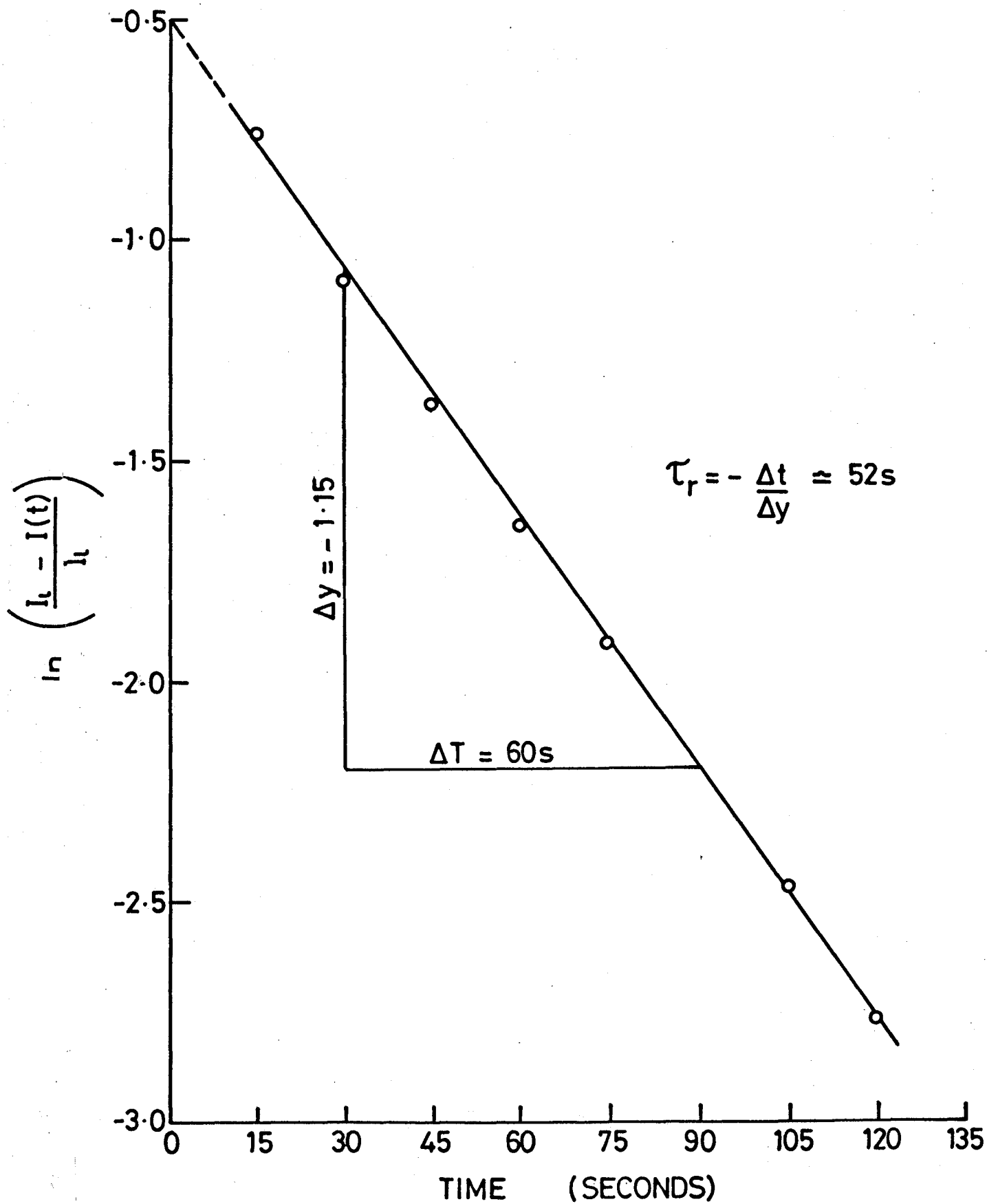


FIG. 7-27 PLOT SHOWING DERIVATION OF  $\tau_r$  FROM RISE CURVE OF FIG. 7-26

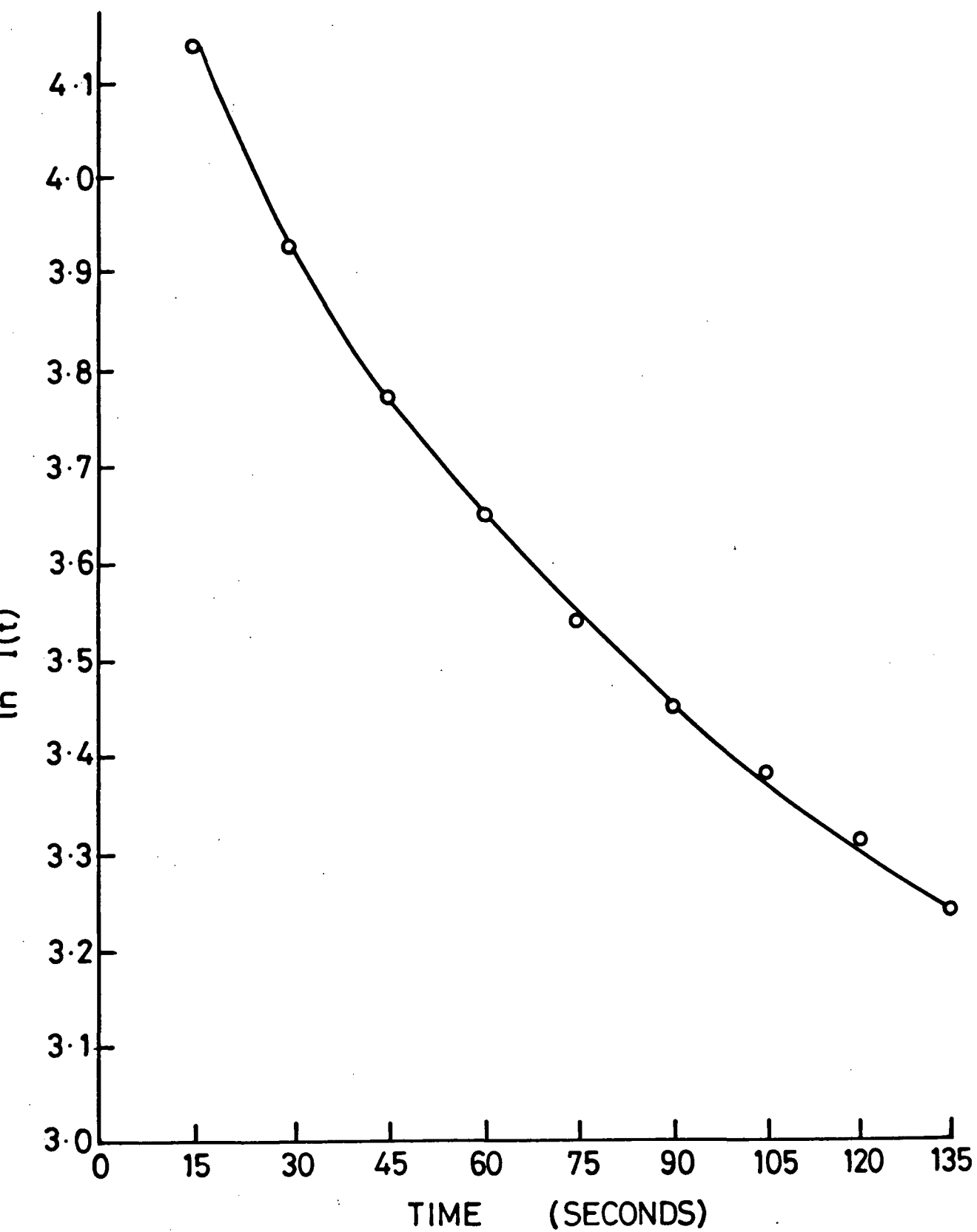


FIG.7-28 PLOT SHOWING THE NON-EXPONENTIAL NATURE OF DECAY CURVE OF FIG.7-26.

photoexcitation. Comparable characteristics in ZnO have been reported by Beekmans (17) and Miller (18) and will be discussed in the final section of this chapter.

Investigation of current transients due to changes in photoexcitation conditions were investigated using the C.R.O. and chopped light source as described in Chapter 5. The timescale of these observations was comparable with the true time constants for carrier generation and recombination. Many C.R.O. traces were photographed; as with the I-V characteristics, however, a limited selection will be shown to indicate the range of observed behaviour. Six such traces are shown in Figs. 7.29 and 7.30. The lower, linear trace on each photograph, when discernible from the base of the grid, is a reference marker representing zero signal level. Fig. 7.29(a) shows a trace that is typical of many observations in terms of speed of response. It will be recalled that the long term decay of photocurrent for this powder sample under steady state conditions was shown in Fig. 7.20. The speed of response appears to be slightly too slow for steady values of dark and light current to be attained during the chopping cycle. Using the approximations outlined in the introduction to this chapter, photocurrent rise and decay time constants of approximately 8 and 10ms respectively were estimated. Most of the powder samples investigated in this way exhibited longer decay than rise times.

Fig. 7.29(b) shows the absence of even a transient response from an insensitive powder sample, the I-V characteristics of which were shown in Fig.7.8. In this instance, however, washing

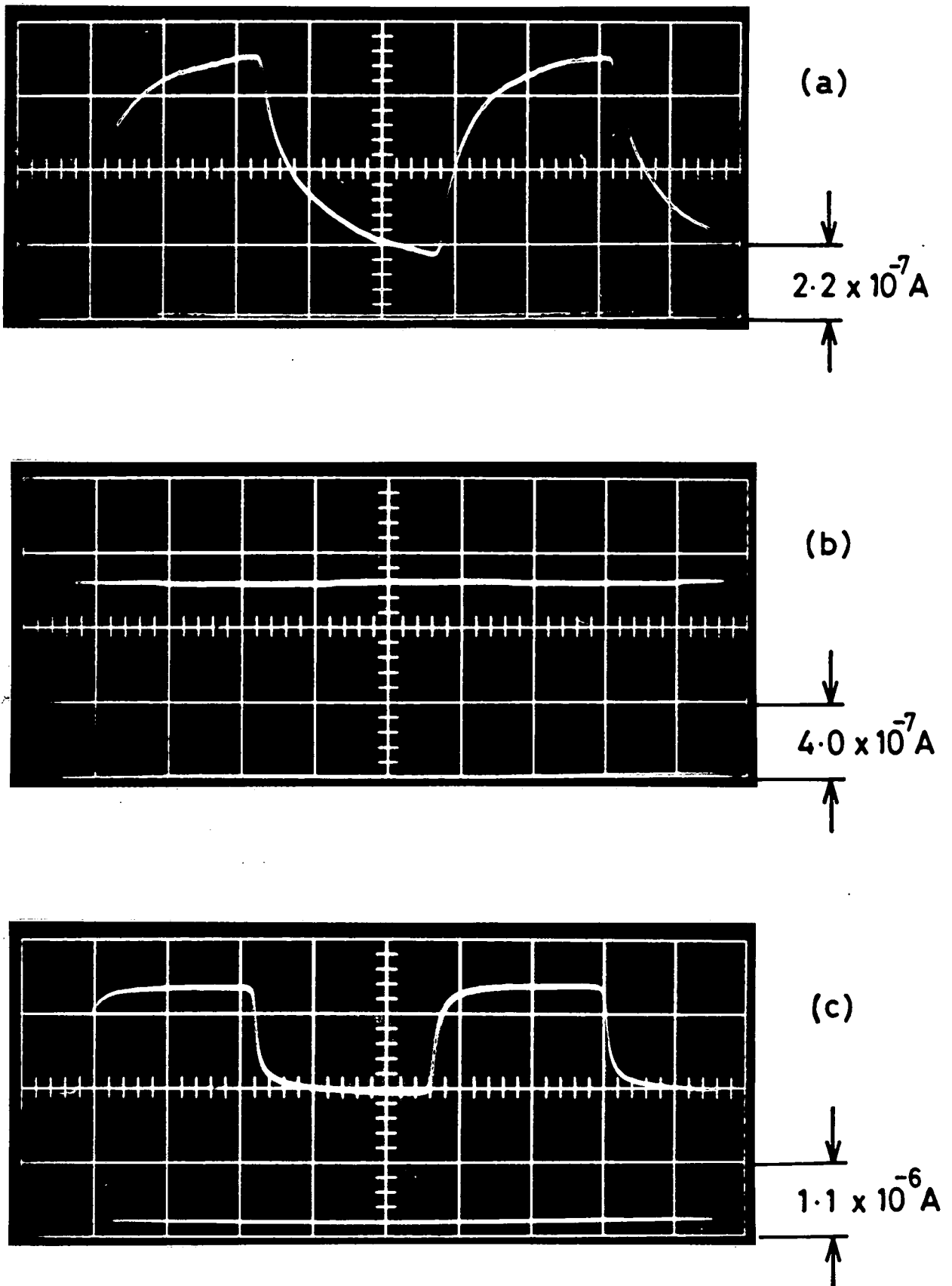


FIG. 7.29 TRANSIENT RESPONSE TO CHOPPED ILLUMINATION FOR :-

(a) I1 , D.C. BIAS = 100V

(b) H3\*, D.C. BIAS = 100V

(c) H3 , D.C. BIAS = 500V

CHOP RATE = 10 Hz . TIMEBASE = 20ms per major division

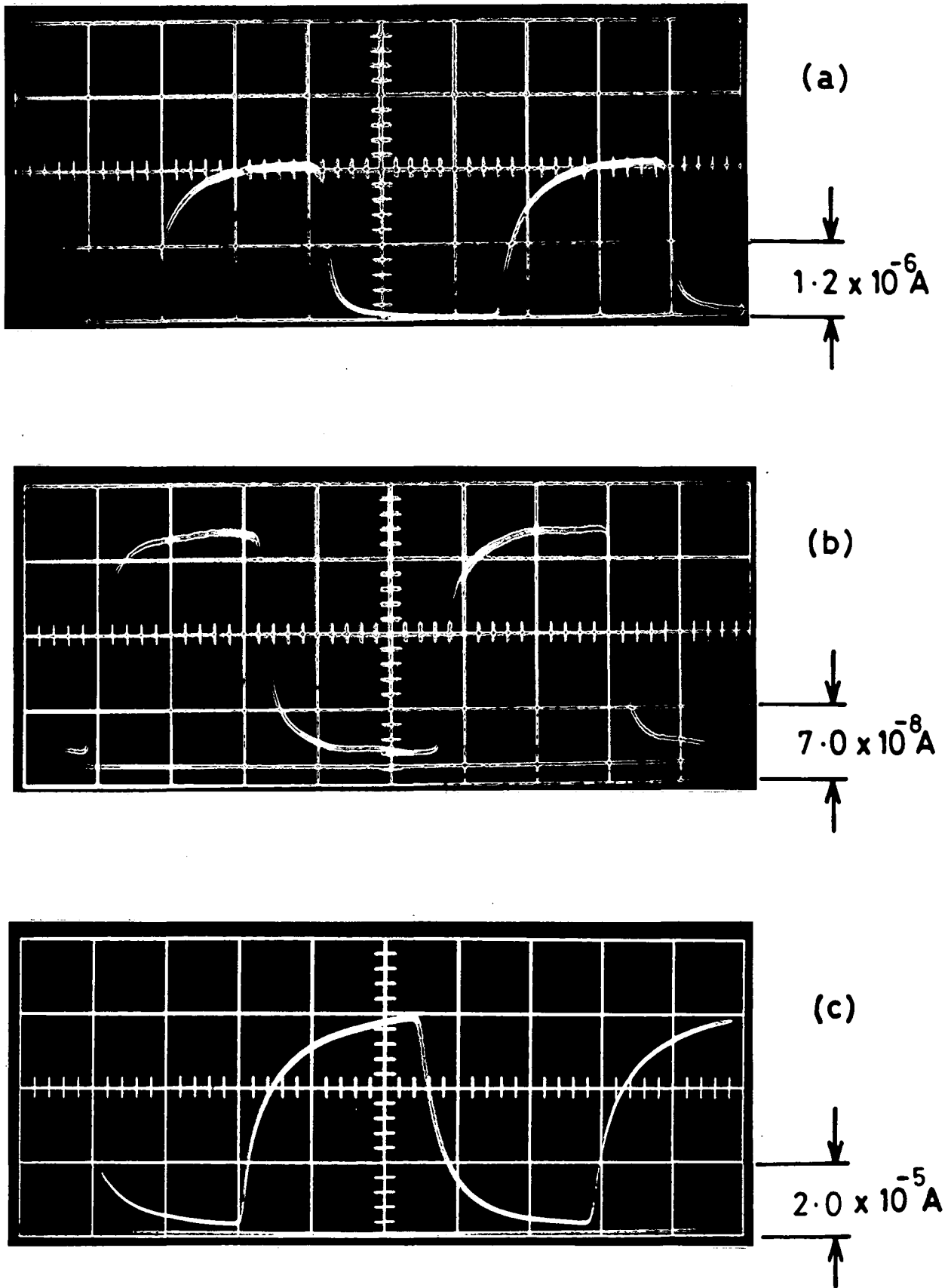


FIG. 7.30 TRANSIENT RESPONSE TO CHOPPED ILLUMINATION FOR :-

- (a) G6\*, D.C. BIAS = 100V
- (b) G6, D.C. BIAS = 100V
- (c) G4, D.C. BIAS = 100V

CHOP RATE = 10 Hz . TIMEBASE = 20ms per major divisor

the powder sample in methanol was found to enhance performance as shown by Fig. 7.29(c). The resultant powder still had a poor (c.2:1) ratio of light to dark current, but exhibited the fastest speed of response observed for a powder sample. Rise and fall time constants are estimated both to be about 2ms. As an example of the many instances of anomalous observed behaviour of powder samples, Fig.7.30(a,b) shows the effects of washing in methanol upon a different sample. Though the speed of response appears to be unchanged (within the limits of resolution of these photographs), the conductivity levels and ratio of light to dark current are larger for the unwashed sample.

In general fast response characteristics and high photosensitivity were found to be mutually exclusive as would be expected from photoconductivity theory. Increased conductivity levels need not be invariably associated with slower response (or reduced light to dark current ratio), however, as may be seen by comparing Fig. 7.29(c) with Fig. 7.30(c). Conductivity levels of the latter are some 2 orders of magnitude higher, yet speeds of response appear to be similar and the ratio of light to dark current is also increased.

#### 7.4 PERFORMANCE OF DEVICES

The first compressed powder pellet, which was prepared from sample F2, exhibited no detectable photosensitivity. At 100v applied bias both dark and light currents were approximately  $1.3 \times 10^{-5}A$ . This represents, however, an increase in

conductivity of 3 orders of magnitude when compared with measured performance of sample F2 in a powder test cell. Recorded current levels in the latter instance were 1 and  $2 \times 10^{-8}$ A in darkness and illumination respectively, also for 100v bias. The second pellet was produced from a mixture of powder samples G4 and G4\*. Current levels recorded for these samples mounted in a powder test cell were  $I_D = 1.8 \times 10^{-8}$ A,  $I_L = 2.3 \times 10^{-7}$ A (G4\*) and  $I_D = 6 \times 10^{-7}$ A,  $I_L = 8.1 \times 10^{-6}$ A (G4) for 90v bias. Photocurrent rise and decay time constants were estimated to be approximately 6ms for both samples. Current levels recorded for the resultant pellet under similar conditions were  $I_D = 5 \times 10^{-7}$ A,  $I_L = 1 \times 10^{-6}$ A. Conductivity levels, therefore, had not increased as much as might have been expected, but comparison is complicated by the fact that the powders were mixed together and simultaneously washed in Propan2ol. Though the light to dark current ratio for this pellet was still only approximately 2:1, estimated photocurrent rise and decay time constants were 2 and 3ms respectively, i.e. substantially faster than those for either of the constituent powders.

Measured performance of the prototype sintered layer was not encouraging. This was prepared from powder sample V2 for which current levels of  $150 \mu\text{A}$  (illuminated) and  $0.6 \mu\text{A}$  (dark) were recorded with 75v bias applied to the powder test cell. In contrast, light and dark current levels for the sintered layer were both below  $0.1 \mu\text{A}$  for 90v bias. These results combined with the poor mechanical resilience of both sintered layers and compressed powder pellets led to the abandonment of these techniques in favour of powder-binder systems for which more

promising results were obtained.

Powder sample V2 was again used to prepare the first powder-binder device in which the applied field was perpendicular to illumination through the substrate, as shown in Fig.4.5(a). At 90v applied fields the dark current was found to be less than  $0.2\mu\text{A}$  yet the light current was approximately  $500\mu\text{A}$ . Comparing these figures with those obtained for sample V2 in powder form reveals an increase in light current by a factor of 3 and a reduction in dark current by a similar factor. Current-voltage characteristics for both the device and the constituent powder under illumination are shown in Fig.7.31.

Use of the same powder-binder mixture to produce sandwich structure devices as shown in Fig. 4.5(b), in which the applied field was parallel to illumination through the substrate, was less successful. Samples were found to be either totally conducting or highly resistive and insensitive to photoexcitation. The former situation was attributed to pinholes in the powder-binder layer through which the deposited electrode made direct contact with the conducting glass substrate. High resistivity and insensitivity to illumination indicated that the powder-binder layer thickness exceeded the penetration depth of the photoexcitation to such an extent that under all light conditions a large series resistance due to non-illuminated material remained. This indication that better layer thickness control was required led to the development of the screen printing technique for depositing powder-binder layers.

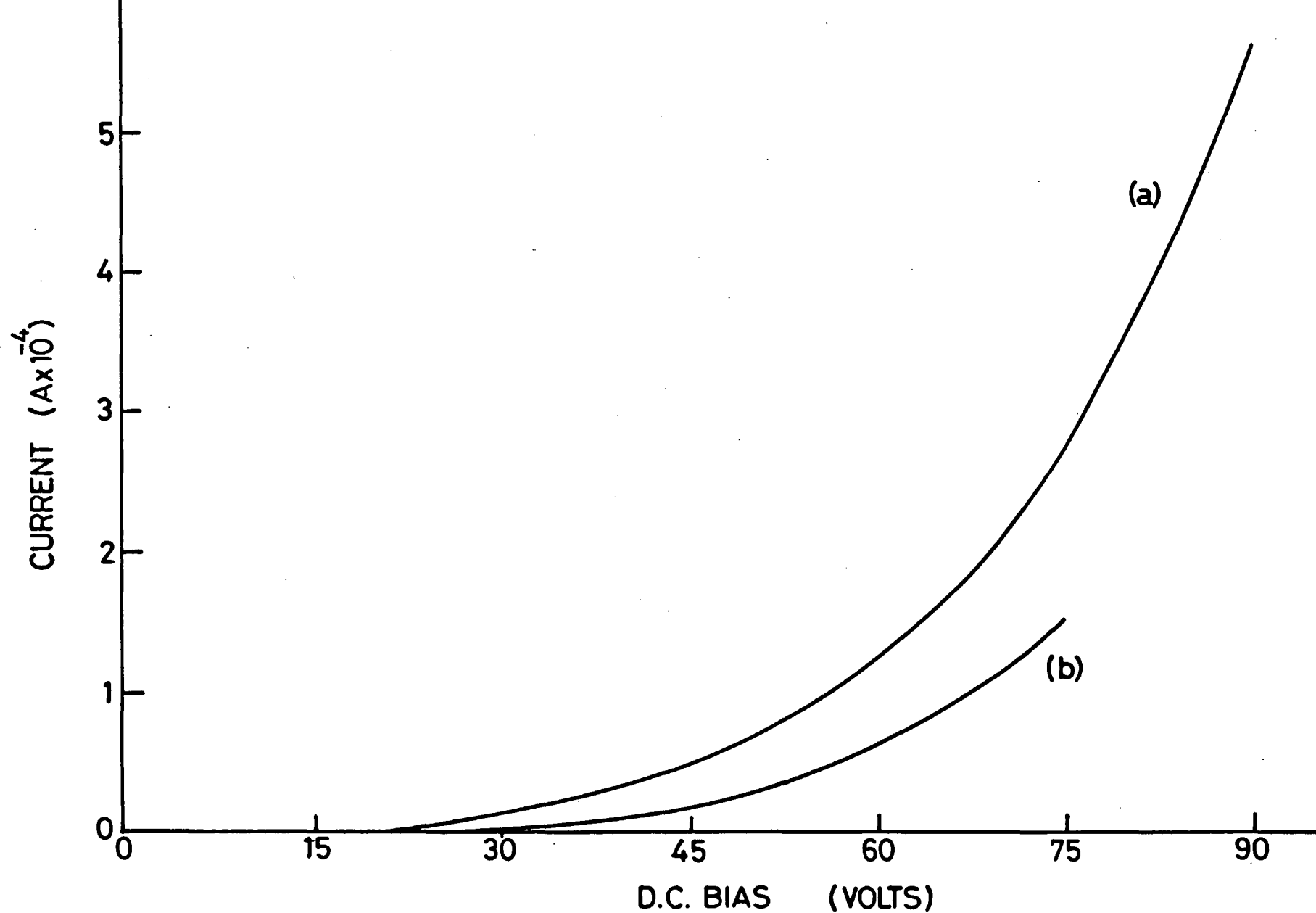


FIG.7-31 I-V CHARACTERISTICS UNDER ILLUMINATION FOR (a) POWDER-BINDER DEVICE  
(b) POWDER ONLY (V2)

Reproducibility of performance of powder binder devices in which the applied field is perpendicular to illumination was investigated by preparing 4 such ostensibly identical devices using powder sample 8 as the starting material. The dark and light current levels recorded for these devices are shown in Fig. 7.32, and the close grouping obtained is clearly visible. Fig. 7.33 shows the variation of  $I_L/I_D$  ratio with voltage for each of the 4 samples. Scatter of data points, especially at low voltages, is due to indeterminacy of  $I_D$  values which were close to the low threshold of detectability. As noted in the case of powder samples the  $I_L/I_D$  ratio was found to increase with applied voltage. Dark current levels were 2 orders of magnitude lower than those recorded for sample 8 in powder form, and light current levels were down by 3 o.m. It should be mentioned, however, that some 2 months elapsed between testing of sample 8 in powder form and preparation of these devices. During this time interval the sample (which was prepared by the partial pressure firing method) was stored in darkness in a normal atmosphere at room temperature.

Consistency of the screen printed powder-binder layers was assessed by investigating the current-voltage characteristics at each of the 10 circular electrodes deposited on each sample. Figs. 7.34-36 show the variation of dark current with voltage for each of the large electrodes on samples 1A, B and C (see Fig. 4.8 for listing of sample preparation conditions). All samples were highly conductive and showed reasonable reproducibility between electrodes indicating an improvement in thickness uniformity. The characteristics of samples 1A and 1C show a strong resemblance to

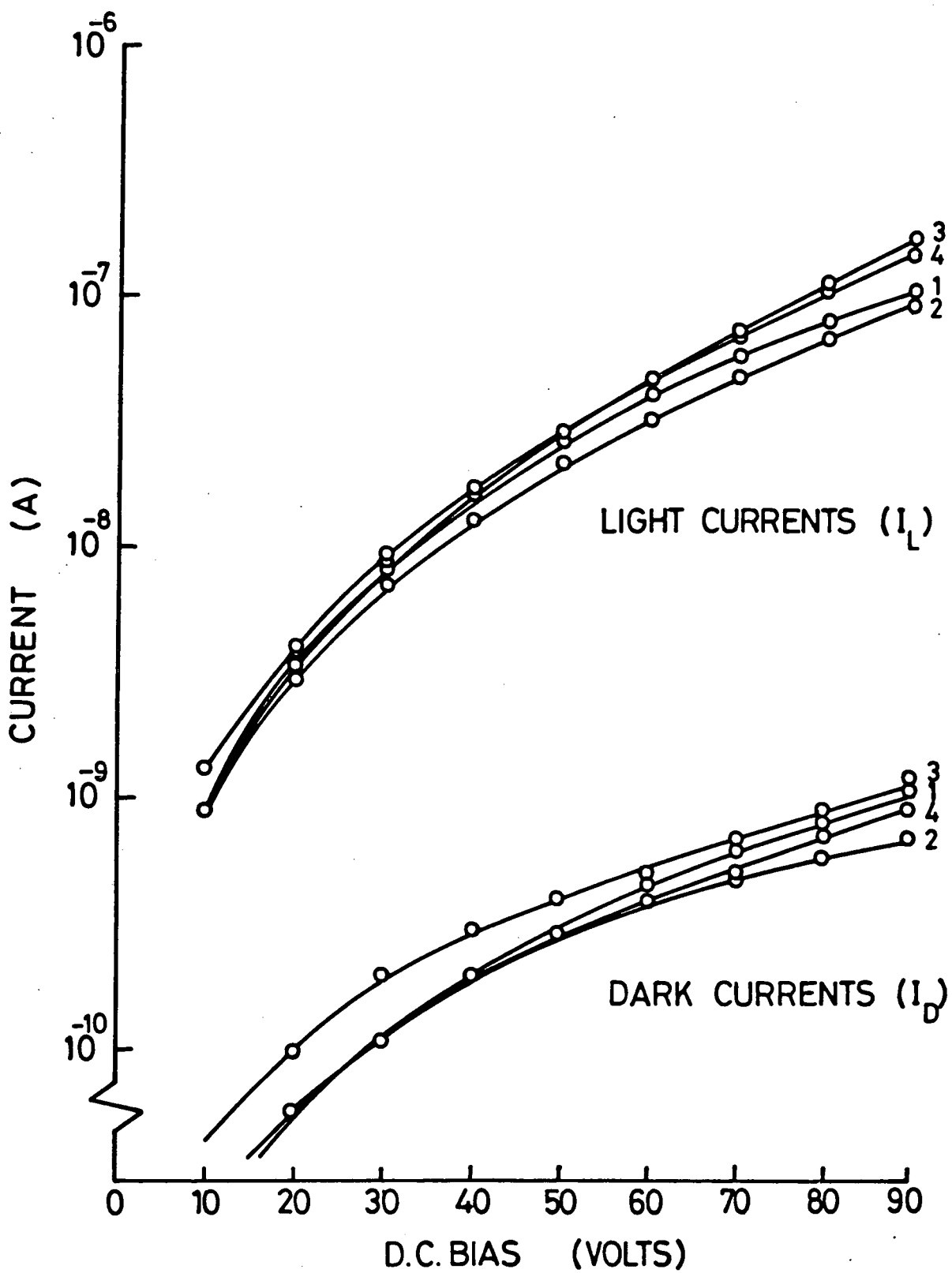


FIG. 7-32 I-V CHARACTERISTICS FOR 4 POWDER-BINDER DEVICES PREPARED USING POWDER SAMPLE 8.

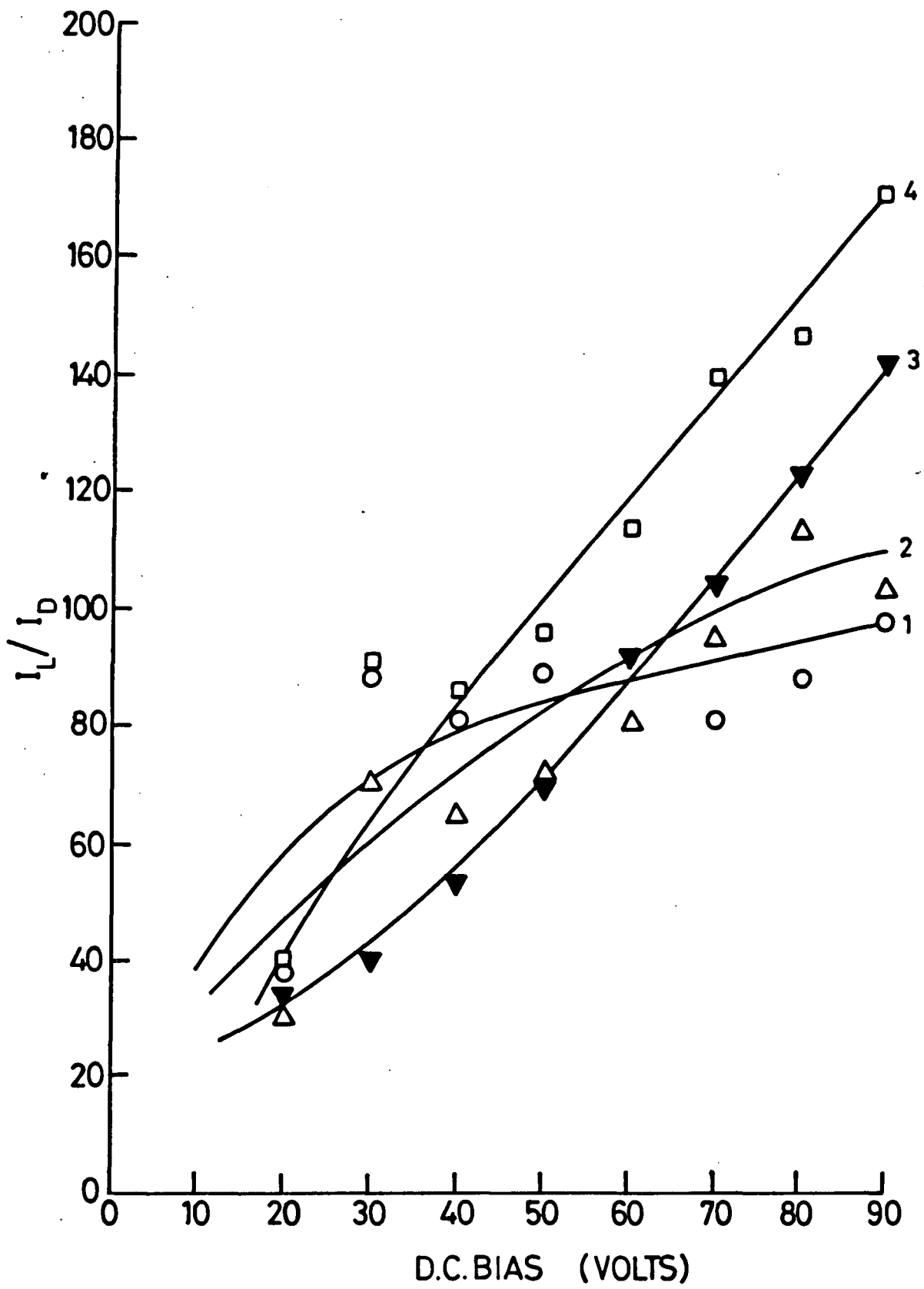


FIG. 7.33  $I_L / I_D$  RATIOS FOR 4 POWDER BINDER DEVICES PREPARED USING POWDER SAMPLE 8

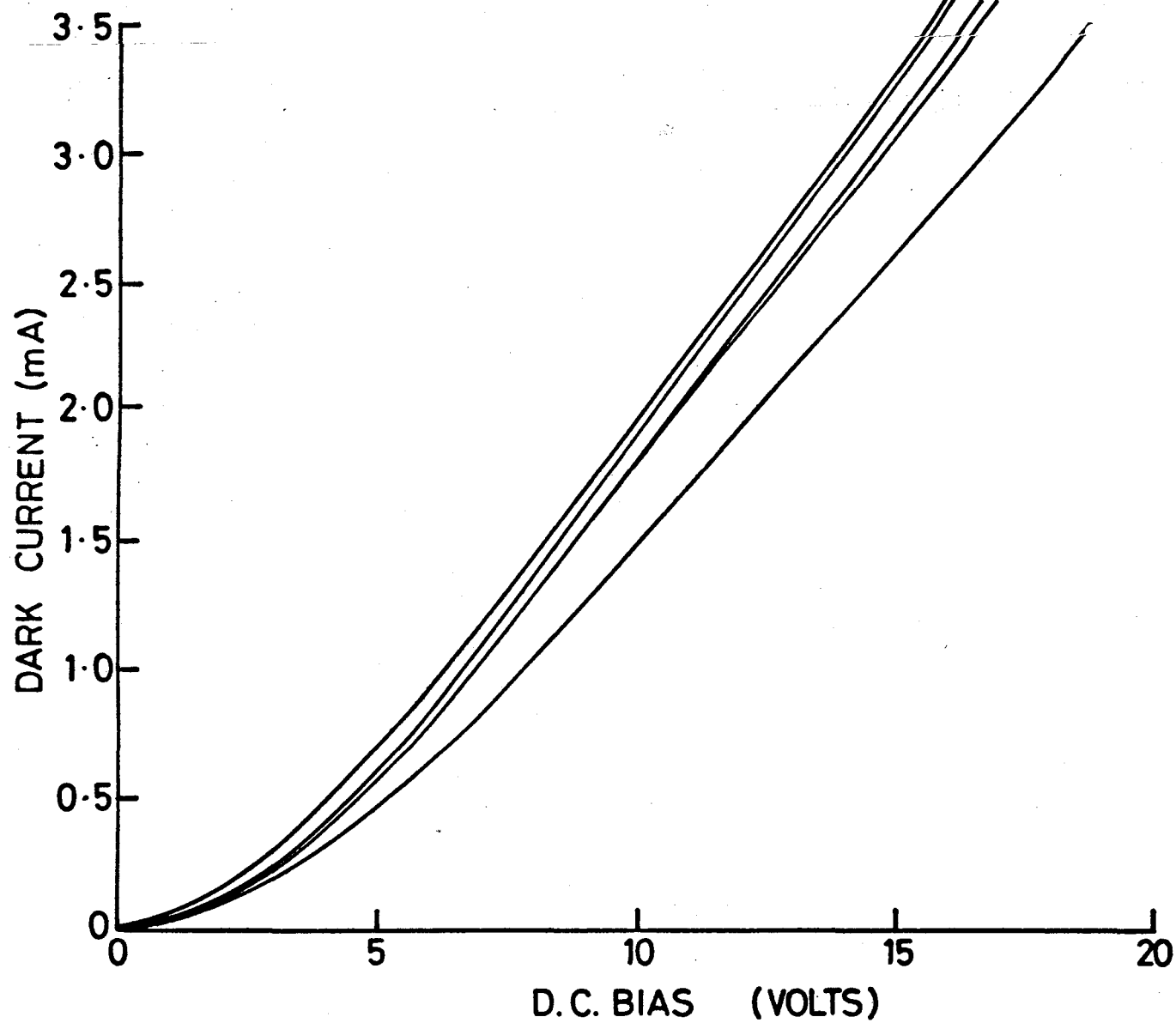


FIG. 7-34  $I_D/V$  CHARACTERISTICS MEASURED AT EACH OF THE 5 LARGE ELECTRODES FOR SAMPLE 1A

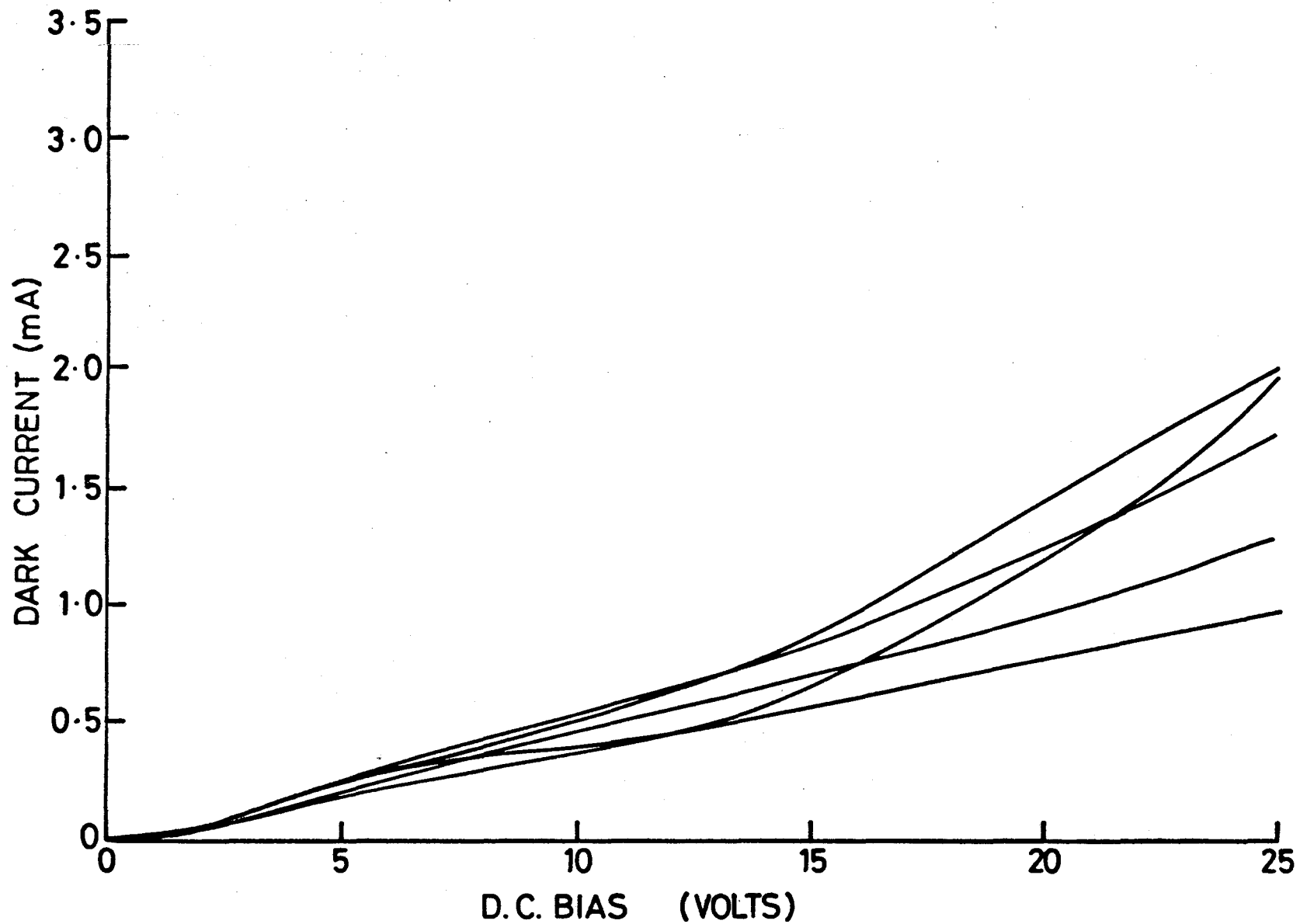


FIG. 7-35  $I_D/V$  CHARACTERISTICS MEASURED AT EACH OF THE 5 LARGE ELECTRODES FOR SAMPLE 1B

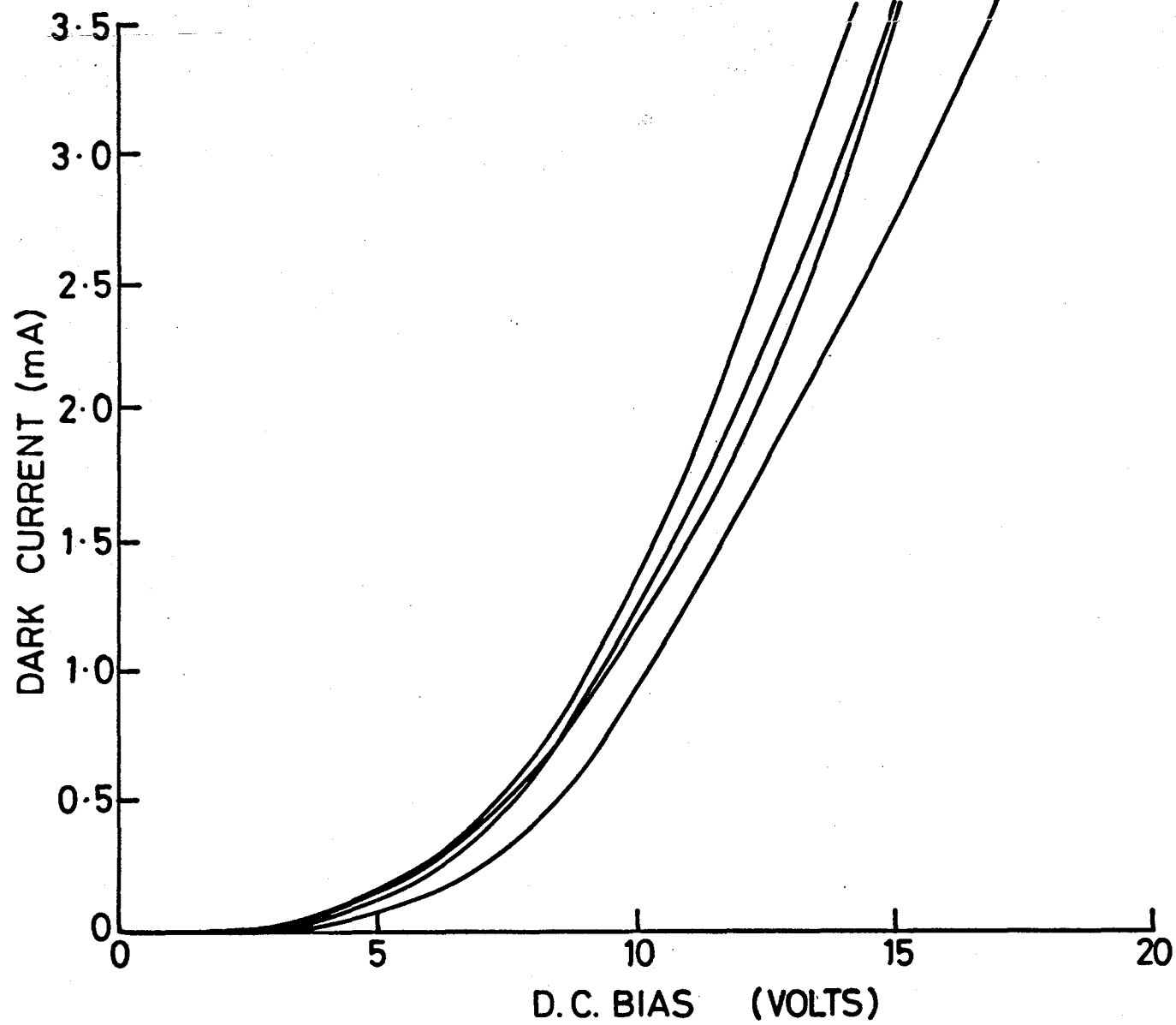


FIG. 7-36  $I_D/V$  CHARACTERISTICS MEASURED AT 4 OF THE 5 LARGE ELECTRODES FOR SAMPLE 1C

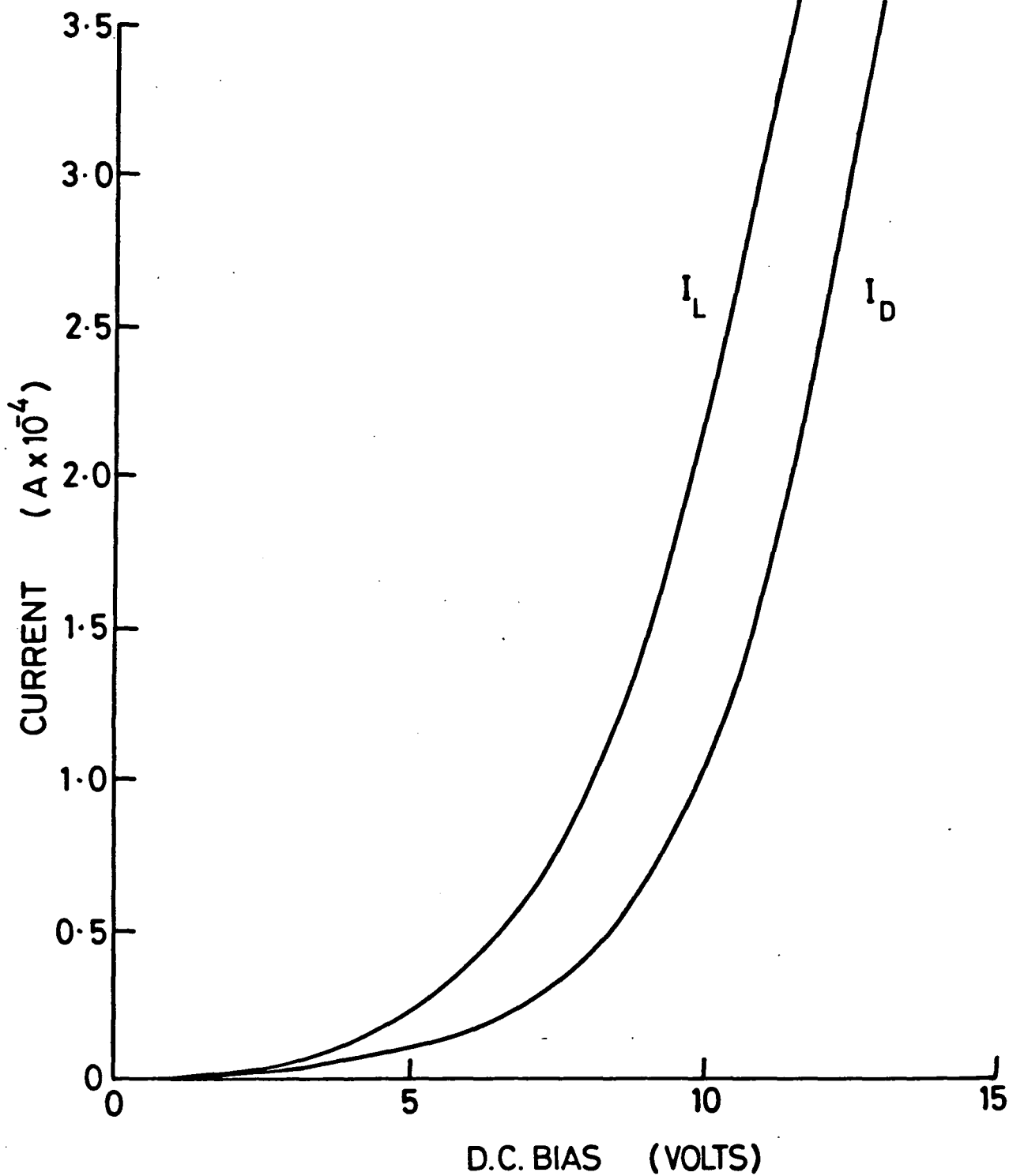


FIG. 7-37 LIGHT AND DARK CURRENTS FOR SCREEN PRINTED POWDER-BINDER DEVICE 1C.

each other; these samples were fired at 550-600°C towards the two ends of the firing tube while the somewhat less conductive sample 1B was at the centre of the furnace (600°C). One of the electrodes on sample 1C had been deposited on a damaged region of the layer caused by clumsy handling and was effectively a short circuit, hence only characteristics obtained at the remaining 4 electrodes have been included in Fig. 7.36.

Investigation of conductivity under illumination was made more than 1 month after the dark current characteristics had been measured. It was found that the dark currents of both samples 1B and 1C had decreased by an order of magnitude while that of sample 1A (which had been stored in vacuum) was unchanged. Samples 1A and 1B exhibited negligible photosensitivity while the ratio of light to dark current recorded for sample 1C was approximately 2. This was the first response to photoexcitation recorded for a sandwich structure device, and is shown in Fig.7.37.

Some of the sensitized powder from which the second series of screen printed powder-binder devices were prepared was evaluated in the powder test cell. It was found to be reasonably conducting but only slightly photosensitive with measured dark and light currents of 1.04 and  $2.10 \times 10^{-5}$ A respectively at 94 volts with a ram supply pressure of 60 p.s.i. Devices 2A and 2C were found to be much more conductive when tested, a dark current of  $6.9 \times 10^{-4}$ A being recorded for 2A at 89 volts. Device 2C which, like its counterpart (1C) in the first series, was stored in air and exposed to daylight, was again the only sample to show

a measurable response to photoexcitation. Though more conductive than the powder from which it was prepared, the ratio of light to dark current had fallen to only approximately 1.1:1 as shown in Fig. 7.38. Furthermore, unlike previous observations (e.g. Fig. 7.32) this ratio appeared to be decreasing as the applied field was increased.

A surprising result was obtained when indium electrodes were deposited on an unfired powder-binder layer (3A), as shown in Fig. 7.39. These characteristics were recorded using two of the smaller circular electrodes, and indicate  $I_L/I_D$  ratios of up to 16:1 over the voltage range recorded. Also the ratio for this device appears to be increasing with applied field. For comparison Fig. 7.40 shows dark and light currents recorded for device 3B. This was fired in the usual way but stored under identical conditions to 3A. Again two of the smaller circular electrodes were used. The effect of firing appears to have been a slight reduction in conductivity under illumination combined with a substantial increase in dark current levels. As a result the  $I_L/I_D$  ratios have fallen to less than 2:1.

An alternative presentation of the results shown in Figs. 7.37, 7.39 and 7.40 is given in Fig. 7.41. This plots the dependence of current density (and hence current, since a constant electrode area was used) upon applied voltage both in darkness and under photoexcitation. As with packed powder samples, close approximations to a general  $I \propto V^m$  law are indicated over the voltage range investigated, with values of  $m$  between about 1.2 and 3. These may be compared with values of  $m$

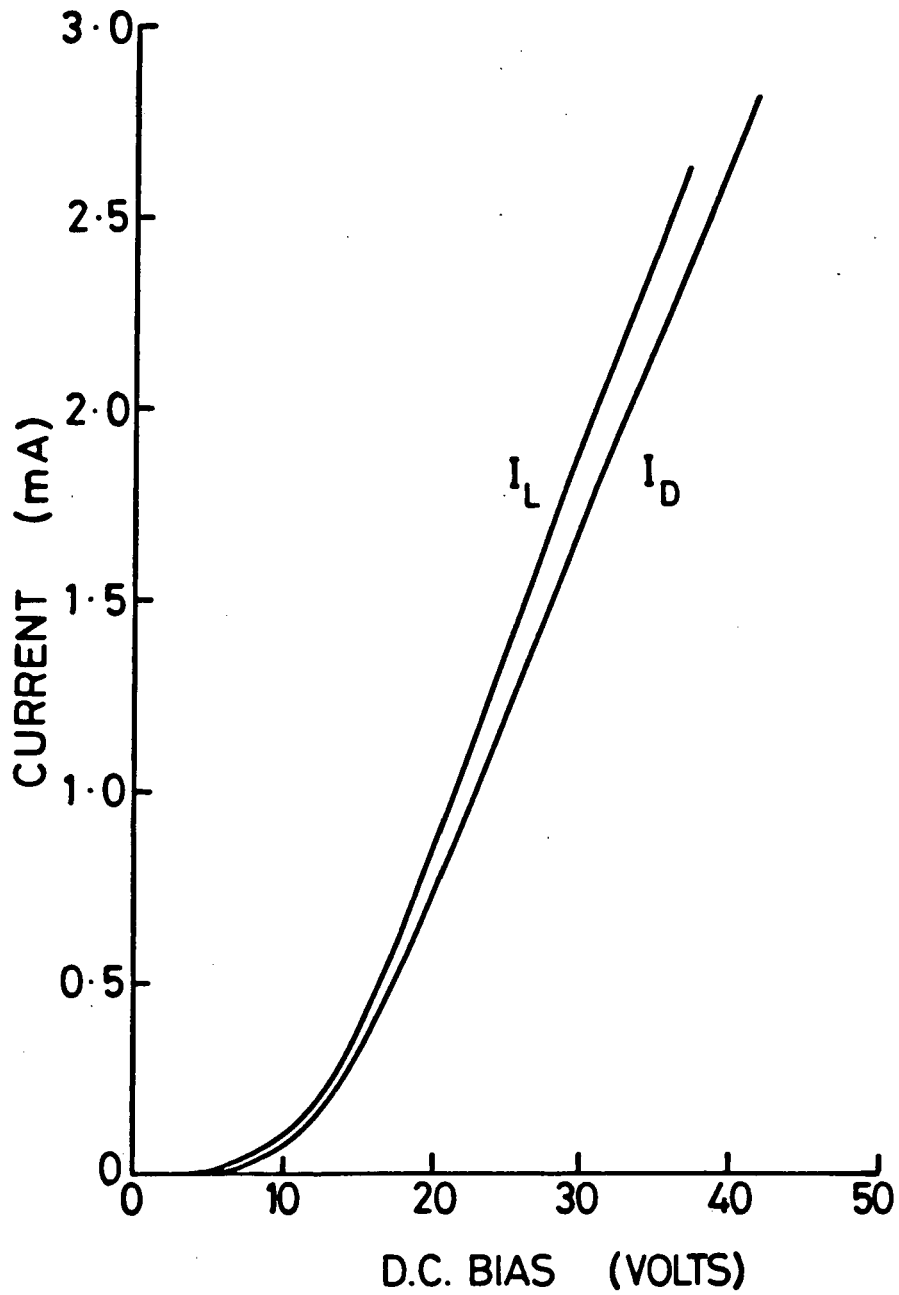


FIG.7-38 LIGHT AND DARK CURRENTS FOR SCREEN PRINTED POWDER-BINDER DEVICE 2C.

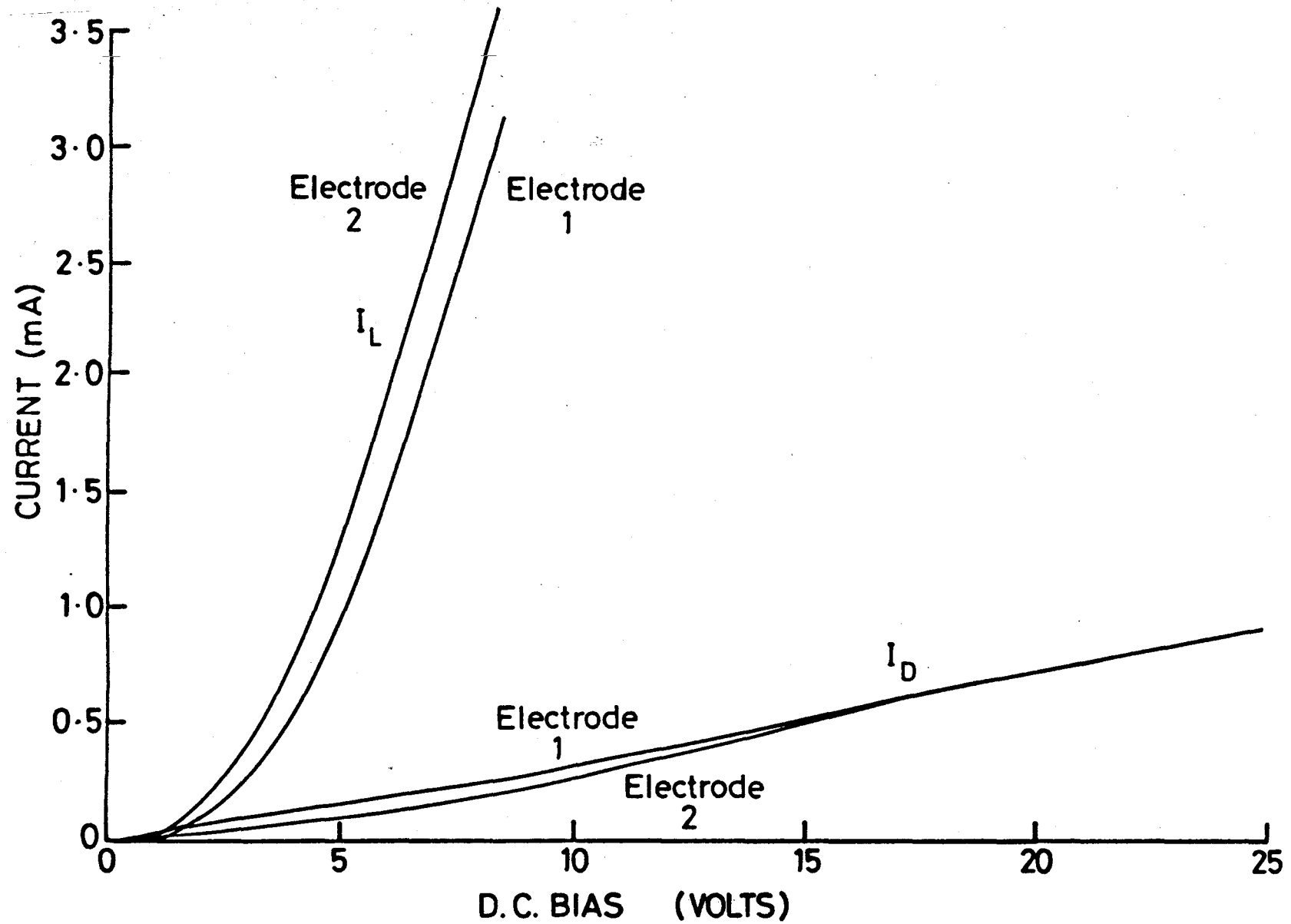


FIG. 7-39 DARK AND LIGHT CURRENTS FOR SCREEN PRINTED POWDER-BINDER DEVICE 3A

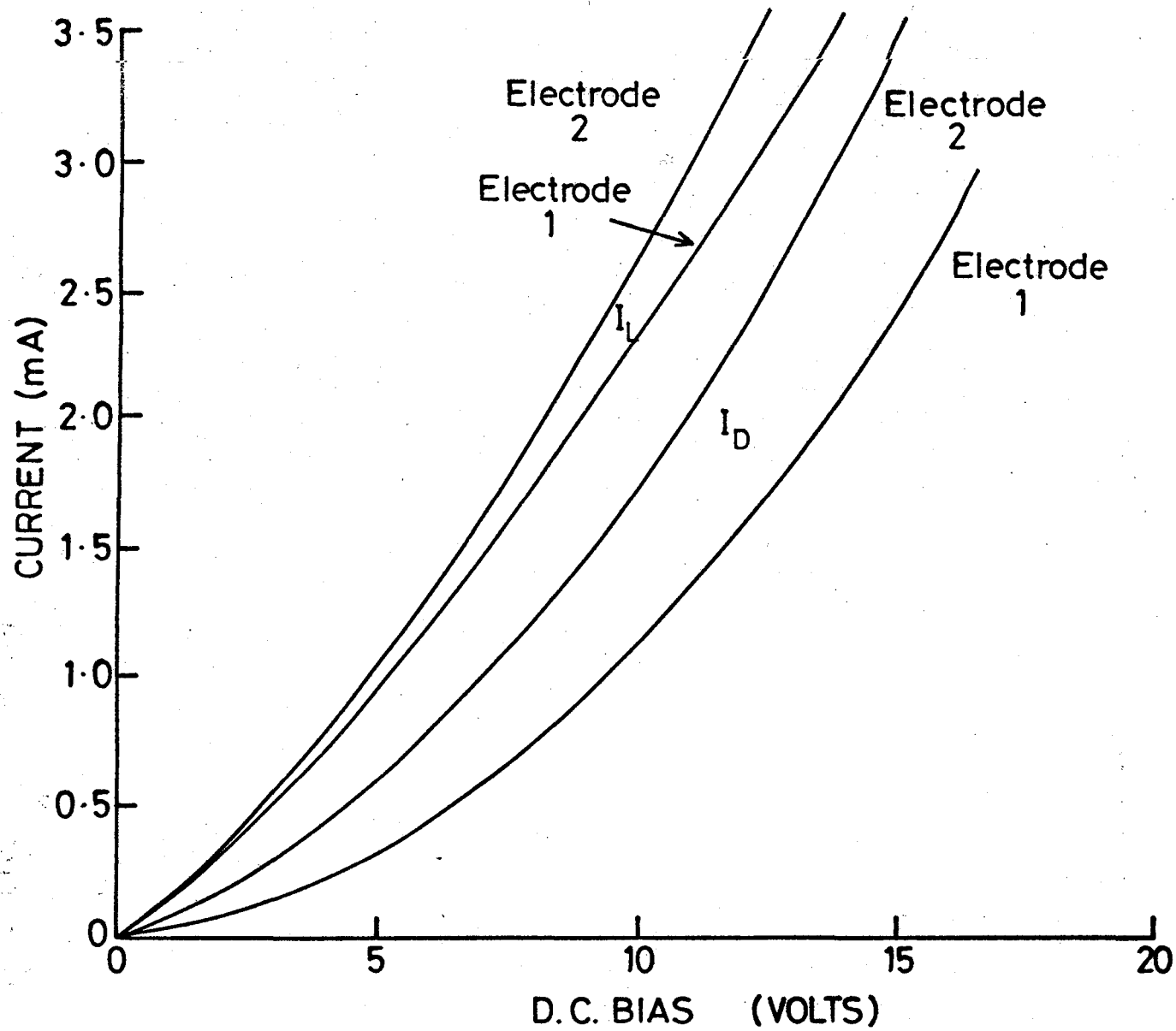


FIG. 7-40 DARK AND LIGHT CURRENTS FOR SCREEN PRINTED POWDER-BINDER DEVICE 3B

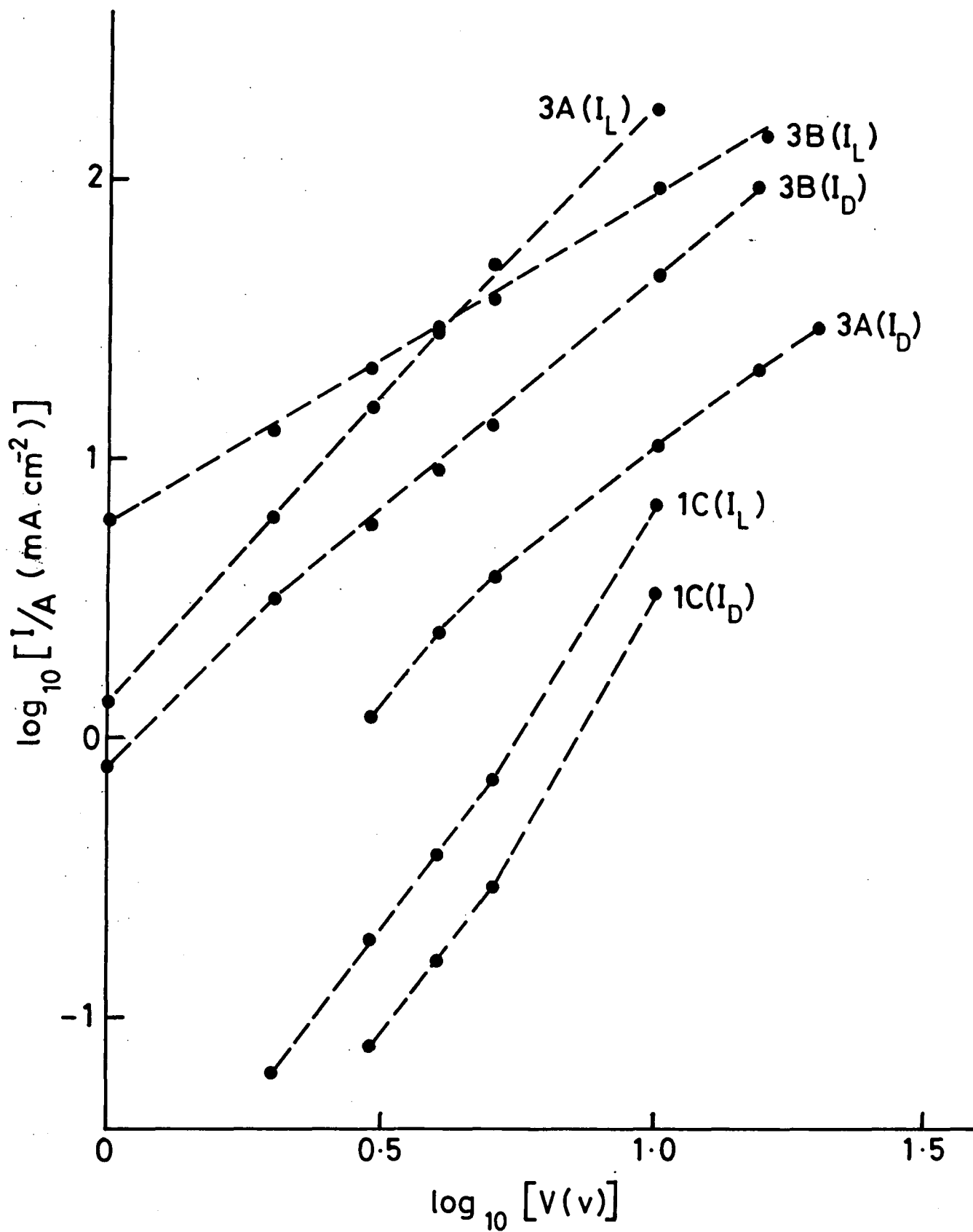


FIG. 7-41 DEPENDENCE OF CURRENT DENSITY UPON APPLIED VOLTAGE FOR SCREEN PRINTED POWDER-BINDER DEVICES 1C, 3A & 3B

of 1 (ohmic) or slightly greater than 1 deduced from results on screen printed, doped CdS powder binder layers produced by Amalnerkar et al (25).

## 7.5 DISCUSSION

It is necessary as a framework for discussion of these numerous and varied results to extend the preliminary theory of Chapter 2 into a review of additional phenomena found to be associated with CdSe. Of overriding importance in this context is the complex surface chemistry of CdSe, especially since the powdered material has such a high surface area to volume ratio. Therefore a brief (chronological) survey of the investigation of CdSe and CdS surface chemistry by other authors will now be presented.

In 1953 Bube (3) found that when CdS crystals were exposed to water vapour both the photosensitivity and time constant for excitation wavelengths shorter than the CdS absorption edge were reduced, while for longer wavelengths they were unaffected. These observations were attributed to an increased recombination rate at the surface. Some 4 years later he turned his attention to the role of oxygen sorption on CdSe crystals (4) and concluded that adsorbed oxygen acts as an acceptor on the n-type surface. A photostimulated, temperature dependent, reversible sorption of oxygen was investigated through its effect on measured dark conductivity levels. Heating samples to temperatures of 100°C or more in flowing helium was found to result in dark conductivity being increased by several orders of magnitude after

illumination. Subsequently it was noted (5) that vacuum annealing of CdSe crystals at 550°C increased conductivity levels by 9 to 10 orders of magnitude and specific sensitivity by 5 o.m. Such vacuum annealed crystals were between 100 and 1000 times more sensitive than CdSe:I:Cu crystals at low light intensities and/or high temperatures. Donor levels at 0.14 and c.0.6eV, and acceptor levels at 0.6 and 1.0eV were reported for the vacuum annealed crystals. Deep acceptor levels were not detected in the CdSe:I:Cu crystals, which also did not exhibit infra-red quenching at room temperature.

Micheletti and Mark (7) reported that thermal desorption of oxygen from CdS:Cl:Cu sintered layers heated to 140°C in flowing nitrogen rendered them useless as photoconductors because the dark conductivity was increased by 6-7 orders of magnitude. Hall effect measurements, however, indicated that oxygen removal was associated with a mobility increase of less than 20%, and it was thus concluded that ambient sensitive current changes should be attributed primarily to changes in conduction electron concentration. Thermal desorption of oxygen from CdSe single crystals was found to require higher temperatures in excess of 300°C (9). Following a 360°C bake out these crystals exhibited photostimulated oxygen adsorption under ultra-violet illumination. This was found to be initially sensitive to the ambient oxygen pressure, and continued at a decreasing rate for many hours. It was suggested that the photoadsorbed oxygen was present on the CdSe surface predominantly in a neutralised state. After successive bake outs above 400°C photoadsorption was still observed but with decreasing rates and amounts. This was

attributed to irreversible surface change caused by a decrease in the concentration of interstitial Cd. Chung and Farnsworth (14) subsequently observed that Cd was indeed evolved from CdSe heated above 400°C.

The difference between physi- and chemi-sorption of oxygen and the associated charge transfer processes have been discussed by several authors. From studies of oxygen sorption on CdS single crystal platelets Weber (10) suggested that the desorption rate was determined by optical excitation of electrons from chemisorbed oxygen ions rather than capture of free holes by chemisorbed oxygen. This hypothesis was contradicted by Tanaka who prepared CdSe films by a "vapour evaporating-reactive sputtering" method using either hydrogen or argon as the carrier gas (12). Firing a sample in vacuo at 150°C caused thermal desorption of oxygen which resulted in a dark conductivity increase of 5 o.m., and hence a reduction of the  $\sigma_L/\sigma_D$  ratio from  $2 \times 10^6$  to 40. This was found to be reversible: dark conductivity decreased again following exposure to the atmosphere at room temperature. Tanaka suggested that photo-adsorption was caused by an increase in the surface electron density under illumination, while photo-desorption was due to an increase of photo-generated holes which were subsequently drawn out of the bulk by the surface Schottky barrier field. Another investigation of CdSe films (11) attributed reduction of conductivity levels by 2 o.m. when heated in vacuo above 70°C following exposure to the atmosphere at room temperature to the conversion of physi- to chemi-sorbed oxygen.

A reversible, thermally stimulated desorption of oxygen from CdS single crystal platelets causing increases of  $\sigma_L$  and  $\sigma_D$  by up to 6 o.m. was reported by Schubert and Böer (13). This change was found, however, to be irreversible if the platelets were heated above 620°C, even if only for a few seconds.

Five discrete acceptor surface levels were detected on CdSe single crystals in vacuo (15). These were responsible for the depletion layer on CdSe surfaces in vacuo, confirming the findings of Consigny and Madigan (8). The presence of oxygen was found to increase this depletion layer slightly due to the appearance of both a donor and acceptor level. This was originally suggested by Somorjai (6). The density of both of these levels was found to approach that of surface elementary cells. Chung and Farnsworth (14) found that oxygen chemisorption on CdSe surfaces was affected by both surface and bulk properties e.g. stoichiometry and the presence of defects or impurities. It was suggested that this was because such properties govern the number of electrons available for transfer between the CdSe surface and the adsorbate.

In a detailed study of the surface chemistry of (11 $\bar{2}$ 0) CdSe Brillson (16) reported that the limiting surface coverage for oxygen was one monolayer. Since the oxygen-adsorbed energy levels distributed across the band gap bore a strong resemblance to those of air-exposed CdSe he concluded that oxygen was more electrically active than the other contaminants detected on the 'real' CdSe surface (by Auger electron spectroscopy). No intrinsic defect states were found on 'clean' (11 $\bar{2}$ 0) CdSe surfaces.

Noticeable by its absence from the literature reviewed is an investigation of sorption effects in CdSe powder. However, Beekmans (17) has constructed an interesting model to explain the observation that oxygen chemisorption and photodesorption can actually increase the photosensitivity of ZnO powder layers. He suggests that contact regions or 'necks' are formed between adjacent grains, and that these necks may be slightly, substantially or totally depleted by oxygen chemisorption depending on their size. Thus large necks will have their conductivity impaired very little by increased depletion layer thickness due to oxygen sorption while smaller necks will exhibit strong dependence of conductivity on depletion layer thickness and consequently on the presence of oxygen which may, in turn, be dictated by photoexcitation conditions. A real powder layer would contain a spread of grain sizes and hence a certain distribution of contact region cross-sectional areas. This model was used to theoretically predict variations of conductivity with time starting in darkness, then under constant illumination and then in darkness again. The variations compared well with empirically derived results for ZnO powder layers, and showed similar characteristics to the current-time curves of Figs. 7.23, 24 and 26. Similar characteristics were presented by Miller (18), including rise and decay of photocurrent in thick samples of ZnO observed by Melnick (19) which could not be fitted in any meaningful way by combinations of first-order and second-order reactions. Furthermore the decay was found to be slower than the rise, both occurring over timescales of hours. Indeed, any variations of current with time observed in this work over timescales of minutes or more were assumed to be due to

photochemical effects. Evidence that the photoconductive processes outlined in Chapter 2 were also occurring was provided by rapid photo-response measurement (e.g. the CRO recordings of Figs. 7.29 and 7.30) of changes occurring over timescales of milliseconds, and by initial and sustained increases in conductivity as a result of photoexcitation. The ratio of the significances of these two general types of effect is considered to have varied between samples, and to have been partially determined by their storage conditions and treatment after preparation. Unfortunately these factors were not fully appreciated until late in the course of this work and therefore extensive data about storage of early samples was not recorded. It is interesting to note, however, that the only screen printed powder-binder samples to exhibit any appreciable photosensitivity were those which had been kept in air and exposed to daylight.

The histograms of Fig.7.6 understate the true discrepancy between porous plug and partial pressure fired powders. Only 9 adequate sets of data for sample pairs out of a possible 24 were available for  $\sigma_D$  comparison, and only 4 for  $\sigma_L$  (and thus  $\sigma_L / \sigma_D$ ). Numerical comparisons could not be made between the remaining sample pairs because the conductivity levels of the partial pressure fired powder of each pair were prohibitively high i.e. either breakdown or current limiting by the ramp generator was occurring.

As shown in Figs. 7.17-27, both rise and decay of photocurrent under constant illumination were observed. If these changes are attributed to photochemical effects the inevitable

conclusion is that photostimulated oxygen adsorption is occurring in some samples, and desorption in others. A similar observation has been made previously (9), and is discussed in "Surface Physics of Phosphors and Semiconductors" (20). This book reviews many other relevant phenomena observed during studies of CdSe. Photoexcitation of CdSe generates electron-hole pairs. Electrons reaching the surface may be lost to any acceptor-type oxygen ions present in which case photoadsorption occurs. If the photogenerated holes, with the assistance of the surface barrier field, reach adsorbed oxygen sites then the transferred charge is regained and photodesorption occurs. The relative magnitudes of these opposite effects are therefore determined by photogenerated electron and hole lifetimes. Thus photodesorption (i.e. increase of photocurrent under constant illumination) occurs in high resistivity samples with relatively long hole lifetimes. It should also be remembered that desorption will reduce the surface barrier field, and may therefore be regarded as a self-limiting process. Conversely, photoadsorption occurs in low resistivity samples in which the majority of carriers reaching the surface are electrons. Again this is a self-limiting process as it causes the surface barrier field to increase. This was the more commonly observed phenomenon resulting in decay of photocurrent under constant illumination. This may be associated with the presence of halogen ions acting as shallow donors, thereby ensuring a plentiful supply of electrons at the sample surface.

It was frequently observed that powder samples which required grinding and sieving after firing exhibited low conductivity levels and very low photosensitivity. This

treatment, rather than the agglomeration which rendered it necessary, is likely to have generated an increased concentration of Class I recombination centres associated with the existence of strains and dislocations caused by mechanical deformation of the powder particles. It does not seem probable, however, in view of the brief grinding times involved, that a significant proportion of the sphalerite phase was produced. Grinding was kept to a minimum, and was certainly less than the 8 minutes minimum ball milling time required to convert a substantial proportion of the powder to the sphalerite phase. From observations of the effect of ball milling on CdS powder Takeuchi (21) suggested that the structural imperfections thus created acted as adsorption sites for oxygen molecules and ambient moisture. If this occurred in ground CdSe powder it would be likely to accelerate the ageing process involving formation of a sphalerite surface layer observed in CdSe single crystals (22), and presumed also to occur in CdSe powder.

## CHAPTER 7: REFERENCES

- 1) SATO K. and YOSHIZAWA M. "Voltage - Current Characteristics of Compressed CdSe Powders" Jap. J. Appl. Phys. 13, No.4, 630-40 (April 1974)
- 2) SATO K. "Non-Ohmic Current Voltage Characteristics of the Compressed CdSe Powder" Jap. J. Appl. Phys. 15, No.6, 1051-8 (June 1976)
- 3) BUBE R.H. "Surface Photoconductivity in Cadmium Sulphide Crystals" J.Chem.Phys. 21, 1409-10 (1953)
- 4) BUBE R.H. "Oxygen Sorption Phenomena on CdSe Crystals" J.Chem. Phys. 21, No.2, 496-500 (Aug. 1957)
- 5) BUBE R.H. and BARTON L.A. "Some Aspects of Photoconductivity in Cadmium Selenide Crystals" J. Chem. Phys. 29, No. 1, 128-37 (July 1958)
- 6) SOMORJAI G.A. "Charge Transfer Controlled Surface Interactions Between Oxygen and CdSe Films" J. Phys.Chem. Solids 24, No.2, 175-86 (Feb.1963)
- 7) MICHELETTI F.B. and MARK P. "Ambient - Sensitive Photoelectronic Behaviour of CdS Sintered Layers" J. Appl. Phys. 39, No.11, 5274-82 (Oct. 1968)

- 8) CONSIGNY R.L. and MADIGAN J.R. "Surface Properties of Cadmium Selenide" Sol.State. Elec. 13, 113-22 (1970)
- 9) KATZ M.J. and HAAS K.J. "The Effect of Adsorbed Oxygen on the Surface Photovoltage of CdSe" Surface Sci. 19, 380-6, (1970)
- 10) WEBER E.H. "Surface Photoconductivity of CdS Influenced By Chemisorption and Desorption of Oxygen" Phys. Stat. Sol. 28, 649-62 (1968)
- 11) WAGNER R.G. and BREITWEISER G.C. "Interface Related Electrical Properties of Cadmium Selenide Films" Sol. State Elec. 12, No. 4, 229-38 (April 1969)
- 12) TANAKA K. "Photoconductivity of CdSe Films Prepared by a Vapor Evaporating - Reactive Sputtering Method" Jap. J. Appl. Phys. 9, No.9, 1070-7 (Sept. 1970)
- 13) SCHUBERT R. and BÖER K.W. "Desorption of Oxygen and its Influence on the Electrical Properties of CdS Single Crystal Platelets" J. Phys. Chem. Sol. 32, 77-92 (1971)
- 14) CHUNG M.F. and FARNSWORTH H.E. "Effect of Bulk Resistivity on Oxygen Sorption on CdSe Surfaces" Surface Sci. 25, 321-31 (1972)

- 15) GUESNE E., SÉBENNE C. and BALKANSKI M. "Electronic Surface Properties of CdSe Single Crystals under Vacuum or Oxygen" Surface Sci. 24, 18-30 (1971)
- 16) BRILLSON L.J. "Surface Electronic and Chemical Structure of ( $11\bar{2}0$ ) CdSe: Comparison with CdS" Surface Sci. 69, 62-84 (1977)
- 17) BEEKMANS NICO M. "Effect of Oxygen Chemisorption and Photodesorption on the Conductivity of ZnO Powder Layers" J. Chem. Soc. Faraday Trans.I, 74, 31-45 (1978)
- 18) MILLER P.H. JR "The Role of Chemisorption in Surface Trapping" Proc. Conf. on Photoconductivity, Atlantic City, 1954, 287-97 Pub: John Wiley and Son (1955)
- 19) MELNICK D. Thesis (Title unknown) University of Pennsylvania, U.S.A. (1954)
- 20) "Surface Physics of Phosphors and Semiconductors" Ed: SCOTT C.G. and REED C.E. Pub: Academic Press (1975)
- 21) TAKEUCHI M., KANEKO F. and NAGASAKA H. "Effects of Grinding on the Photoconductive Properties of CdS Powder" J. Soc. Mater. Sci. (Japan) 24, Pt 262, 613-6 (1975)
- 22) TÜRE I.E., RUSSELL G.J. and WOODS J. "Photoconductivity, Structure and Defect Levels in CdSe Crystals" J. Cryst. Growth. 59, 223-8 (1982)

- 23) BUBE R.H., Chapter 13 "Photoconductivity" 696-7 in "Physics and Chemistry of II-VI Compounds" ed: AVEN M. and PRENER J.S. Pub:North-Holland, Amersterdam (1967)
- 24) NICOLL F.H. and KAZAN B. "Large Area High-Current Photoconductive Cells Using Cadmium Sulfide Powder" J.Opt.Soc.Am. 45, No. 8, 647-50 (Aug.1955)
- 25) AMALNERKAR D.P. et al "Studies on Thick Films of Photoconducting CdS." Bull. Mater. Sci. 2, No.4, 251-64 (Nov.1980).

## CHAPTER 8: CONCLUSION

A large number of sensitized CdSe powder samples and devices have been prepared and their photoelectronic behaviour investigated using a limited range of techniques. Penetration of photoexcitation into powder samples was found to be severely limited by scattering to the extent that less than 0.1% of incident radiation in the wavelength range 0.3-1.0  $\mu\text{m}$  was transmitted through a 150  $\mu\text{m}$  thickness of packed CdSe powder. Current-voltage characteristics for a variety of samples were found to approximately fit the relation  $I \propto V^m$  with values of  $m$  up to 5. Typically the value of  $m$  for photocurrent was greater than that for dark current in the same powder. Dependence of photocurrent upon photoexcitation intensity  $B$  was found to be governed by an equally simple empirical relationship  $I_L \propto B^{0.4}$  representing a sub-linear response. Dark current levels recorded ranged from  $10^{-10}$  to  $10^{-5}$  A for powder samples while photocurrents were between  $10^{-8}$  A and  $10^{-3}$  A. The maximum estimated ratio of photocurrent to dark current was  $5.3 \times 10^4$  for  $600 \mu\text{Wcm}^{-2}$  photoexcitation intensity, yet at the other extreme some samples exhibited negligible photoresponse under the same conditions. Speed of response to change of photoexcitation conditions in samples not exhibiting significant photochemical effects was found to be less varied, and measured rise and fall time constants were typically between 1 and 10 ms.

From comparisons between observed performance of

different samples and concurrent investigations of structural and chemical changes which may occur during sample lifetimes it is concluded that at least five factors determine photoelectronic behaviour.

The first of these factors is the nature and concentration of impurities which are incorporated during sample preparation. Of the dopants used, high purity  $\text{CdI}_2$  and  $\text{CuSO}_4$  appear to be the most suitable sources of halogen and copper ions respectively. Optimum concentrations of these were found to be interrelated. For the usual halogen concentration of 20,000 p.p.m. a copper presence of approximately 1000 p.p.m. generally produced the maximum  $\sigma_L/\sigma_D$  ratio. When the halogen doping level was reduced to 5,000 p.p.m. the optimum copper concentration was found to be around 50 p.p.m., and was as low as 25 p.p.m. when used with 2,000 p.p.m. halogen presence.

The second factor is the physical configuration of the samples under test. Variation of powder sample porosity by externally applied pressure changed both light and dark conductivities by several orders of magnitude, and was generally found to cause proportionally greater change in the latter. Therefore  $\sigma_L/\sigma_D$  ratios typically decreased with increased pressure but this was considered to be attributable simply to mechanical disruption of the photostimulated surface region of powder samples. Again a simple relation  $\sigma_D \propto P^n$  was empirically derived with estimated values of  $n$  between 0.5 and 3.5. It was observed

that the effective conductivity of powder samples could also be increased by mixing with a nitrocellulose binder.

The remaining factors which were found to influence the photoelectronic behaviour of CdSe powder samples and devices are strongly inter-related. The first of these is oxygen adsorption in the presence of water vapour which occurred in all samples following exposure to the atmosphere. The effect of oxygen adsorption upon photoelectronic behaviour is to reduce conductivity levels by several orders of magnitude while generally increasing photosensitivity. Therefore powders prepared in a reducing ambient were initially highly conductive but exhibited minimal response to photoexcitation. The time dependence of photocurrent levels under steady state conditions observed in many samples was attributed to changes in adsorbent concentration. Both photoadsorption and photodesorption were observed, and were attributed to the opposite effects of electrons or holes being the majority carriers reaching the surface of powder particles. Thus the nature of doping in sensitized powder samples affected the type of response to atmospheric exposure. Since the ratio of surface area to bulk volume is extremely high for a powder the effect of surface states is of greater significance than for single crystal specimens.

Grinding of powder samples, even for brief periods, was found to reduce conductivity levels and photosensitivity, in some cases by an order of magnitude or more. This was

attributed in part to the creation of additional Class I recombination centres associated with strains and dislocations generated by mechanical deformation of the powder particles. It is also suspected that such treatment may have created additional sites for oxygen adsorption.

Ball milling of CdSe powder for prolonged periods of time (in excess of 8 minutes) was found to cause a phase change from the usual wurtzite structure to a cubic modification. The lattice parameter of this sphalerite structure was estimated to be  $6.051\text{\AA}$ . The phase change was reversible by firing in air for 2 hours at  $500^{\circ}\text{C}$ . Concurrent investigation of the surface structure of CdSe single crystals revealed that a sphalerite cubic layer was also formed after ageing in air at  $100^{\circ}\text{C}$  for 16 hours or at room temperature for 2 months. This layer had a lower conductivity than the original wurtzite surface and gave rise to photoconductive effects. It was only produced in an ambient containing both oxygen and water vapour.

The consequences of these additional factors governing CdSe powder photoconductive performance diverted effort from the initial objective of producing a photoconductor layer suitable for use in conjunction with d.c. electroluminescent displays. However, considerable progress towards acceptable performance was made. Devices produced by compressing powder samples into pellets or by fabricating sintered layers were found to be both electrically and mechanically unsatisfactory. A prototype powder-binder system exhibited

photoelectronic behaviour which was superior to that of its constituent powder with both increased photocurrent and reduced dark current (by a factor of around 3 in each case). Screen printing provided sufficient powder-binder layer thickness control for photoresponse to be achieved in a sandwich structure. These layers were found to be 40-70  $\mu\text{m}$  thick with excellent mechanical stability; this deposition technique is simple, inexpensive and may easily be extended to cover large areas.

Required properties for a photoconductor layer to be used in flat panel displays may be recalled from Chapter 1. Current density required to drive an electroluminescent panel is around  $5\text{mA cm}^{-2}$  producing about  $200\text{W cm}^{-2}$  radiant emittance i.e. approximately a third of the photoexcitation intensity used throughout this work. Assuming a photoconductor layer thickness of  $50\ \mu\text{m}$ , minimum acceptable  $\sigma_L$  and maximum acceptable  $\sigma_D$  were calculated as approximately  $6 \times 10^{-7}\ \Omega^{-1}\ \text{cm}^{-1}$  and  $2 \times 10^{-9}\ \Omega^{-1}\ \text{cm}^{-1}$  respectively. These conductivity levels were surpassed by several of the powder samples tested, for example sample 8 for which  $\sigma_D = 5.09 \times 10^{-10}\ \Omega^{-1}\ \text{cm}^{-1}$  and  $\sigma_L = 2.54 \times 10^{-6}\ \Omega^{-1}\ \text{cm}^{-1}$  were recorded at 90v with no applied pressure. Sample J1\*, for which the highest  $\sigma_L / \sigma_D$  ratio was recorded, gave  $\sigma_D = 4.5 \times 10^{-12}\ \Omega^{-1}\ \text{cm}^{-1}$  and  $\sigma_L = 2.4 \times 10^{-7}\ \Omega^{-1}\ \text{cm}^{-1}$  at 100v. Speeds of response in powders to changes in photoexcitation intensity were within an order of magnitude of that required. The target response

time was 1ms or less, and values of  $\tau_R$  and  $\tau_F$  of between 2 and 10ms were recorded.

Current density levels recorded for the screen printed powder-binder layers under illumination were as high as  $100\text{mA cm}^{-2}$  at only 10v bias and thus comfortably exceeded the required  $5\text{mA cm}^{-2}$  at up to 40v bias. However, dark current levels were only 2 or 3 times lower than photocurrent levels so pixel latching in the 'off' state would not be achieved by these devices. Improved performance of these layers would be expected to result from increased copper doping which, as was demonstrated with the loose powder samples, causes reduction of dark conductivity and response times.

Of the firing techniques investigated, the porous plug method using a firing temperature of around  $600^\circ\text{C}$  and duration of about 90 minutes gave the most successful results. Merck CdSe was established as the most suitable commercially available starting material, and high purity  $\text{CuSO}_4$  and  $\text{CdI}_2$  as preferred dopants.

Experimental verification of the feasibility of latching with an electroluminescent panel was not obtained. However, the improvement in, and final levels of, photoconductor performance that were achieved are considered to be sufficient to encourage further endeavours in developing this application.

